85

CRANFIELD INSTITUTE OF TECHNOLOGY

SCHOOL OF MECHANICAL ENGINEERING

Ph.D. THESIS

M.T. OLADIRAN

THE EFFECT OF NOZZLE INCLINATION ON HEAT TRANSFER IN JET IMPINGEMENT SYSTEMS

Supervisors: J. Ward (The Open University in Wales, Cardiff)
and
G.P. Hammond

October, 1981

"GO TO THE ANT, THOU SLUGGARD; CONSIDER HER WAYS,

AND BE WISE".

Proverbs 6, Verse 6.

ABSTRACT

Jet impingement heating and cooling techniques are used extensively in industrial applications. In some of these installations, the axis of the jet can be inclined relative to the impingement surface. The impingement flow is then unsymmetrical so that the heat transfer rates are modified. At present, there is a lack of information concerning the effect of inclination on jet impingement heat transfer. Thus, the experimental study reported in this thesis is primarily concerned with the measurement of local and average heat transfer coefficients associated with the impingement of inclined turbulent circular jets onto flat plates. A single free jet exiting into initially stagnant surroundings was considered and the nozzle inclination was varied from 30^{o} to 90^{o} to the surface. The tests covered the range: Z/d (nozzle-target separation) of 6 to 16 and Re (jet Reynolds number based on exit conditions) of 32500 to 65000. The effect of the exit nozzle shape was also determined.

In multiple jet systems, the flow from the upstream jets can significantly affect those situated in the downstream section. Thus, the effect of nozzle inclination on the performance of an impinging jet exiting into a cross flow was also investigated. Thus, as well as the angle of inclination (α), the magnitude of the cross flow (U_c) and the width of the duct (H/d) were also altered in this confined situation. The ranges of these variables were $30^{o} \leqslant \alpha \leqslant 135^{o}$, $5 \leqslant U_j/U_c \leqslant 20.9$ and $8 \leqslant H/d \leqslant 26$.

A 'thin-film' naphthalene sublimation technique was used to measure the variation of the mass transfer rates over the impingement surface and these rates were converted to heat transfer data by invoking the Chilton-Colburn analogy between the two processes. The average heat transfer coefficients quoted in the text were obtained by numerically integrating the local values.

The thin-film naphthalene sublimation technique yielded repeatable results which were generally in good agreement with published data for the limited cases for which comparisons were possible. For the unconfined jets, inclining the nozzle reduced the heat transfer rates. The stagnation point, impingement region and average heat transfer coefficients were correlated by means of simple power law relationships which involved the Reynolds number (Re), the nozzle-target separation (z/d) and the angle of inclination (α). Both circular and elliptical-shaped nozzles produced essentially similar results so that it appears that the shape of the velocity profile at the jet exit can be neglected for the conditions studied in this investigation. For the confined situations, it was found that superimposing a cross flow onto the jet reduced the heat transfer rates and this is in agreement with the results of previous investigators. At low cross flows,

inclining the nozzle further reduced the heat transfer rates. However, at higher cross flows, inclining the nozzle could lead to an increase in heat transfer rates and an angle of inclination of approximately 60° was found to yield optimal results. This optimal appears to result from a balance between two conflicting effects, namely that inclination reduces heat transfer but also simultaneously increases the penetration of the jet upstream into the cross flow.

Limited velocity and turbulence measurements were undertaken for the jets in order to characterise the flow. These measurements were in good agreement with data from previous investigations so that the heat transfer results from this study should be applicable in a fairly general manner. In order to explain the heat transfer results, flow visualization studies were also carried out.

ACKNOWLEDGEMENTS

The author would like to express his deep gratitude to Messrs.John Ward and Geoff Hammond who supervised this research work. He appreciates their sustained interest and constructive criticism most especially during the writing of this thesis.

Special gratitude is extended to the members of staff of the SME Workshops, Library, Photographic Section and Cranfield Computer Centre for their cooperation and services at various stages of this investigation. The willingness of Mr.C.S.Chapman to assist in the laboratory is sincerely appreciated. His thanks go to Mrs.Tricia Forrest-Holden who carefully typed this thesis.

Financial support which was initially provided by the School of Mechanical Engineering and then the Federal Government of Nigeria is gratefully acknowledged.

Finally, the author extends his thanks to friends and members of his family for their sympathy and encouragement after the death of his father. In particular, he is deeply grateful for the support and understanding of his wife during these years at Cranfield. Now that the task is over, he intends to spend more time with his wife and children.

CONTENTS

LIST OF FIGURES

LIST OF PLATES

NOMENCLATURE

Symbol	Description	Page of 1st Appearance
a,A	Area, m^2	17
b	Width of slot nozzle, m	50
C	Degree centigrade	16
	Vapour concentration, Kg/m^3	10
C_b	Ion concentration of the bulk solution	17
C_f	Friction coefficient ($\equiv \tau/\frac{1}{2}\rho U^2$)	11
C_p	Specific heat of air at constant pressure, KJ/KgK	10
C_{30}	Centre line of the jet inclined at 30^o	112
C_6	Centre line of the jet which is 6 nozzle diameters from the impingement surface.	112
d	Diameter of the nozzle, m	6
D	Diameter of the target area over which the mean heat transfer has been measured or integrated, m.	56
E	D.C.output voltage of the hot-wire probe, V.	78
E^1	Fluctuating component of the D.C. voltage, V.	78
E_o	Voltage of the hot-wire probe at zero velocity, V.	78
F	Faradays constant	17
h	Heat transfer coefficient, W/m^2K. 'h_o' is the heat transfer coefficient at the stagnation point. '$\bar{h}$' is the average heat transfer over a surface.	14
h_z	Heat transfer coefficient on a plate located at 'z' nozzle diameters from the exit of the jet. W/m^2K	106
H	Duct width, m	6
H_z	Hertz, cycles per second.	81

Symbol	Description	Page of 1st Appearance
I_L	The limiting current, amps.	17
k	Thermal conductivity, W/mK	53
k_L	Mass transfer coefficient, Kg/m^2s	14
K	degrees Kelvin	23
	Absorption coefficient	100
l	Length of the target area for slot jets, m.	59
L	Length of nozzle or pipe, m.	13
	Thickness of naphthalene coating,m.	100
m	Mass of naphthalene sprayed, mg.	22
M	Jet-cross flow velocity ratio ($\equiv U_j/U_c$)	5
M*	Cross flow-jet mass flow rate ratio ($\equiv \rho_c A_c U_c/\rho_j a_j U_j$)	167
M_c^*	Cross flow mass velocity ($\equiv \rho_c U_c$)	169
M_j^*	Jet mass velocity ($\equiv \rho_j U_j$)	169
n	Valency change in reaction (electro-chemical)	17
N	Mass transfer flux, Kg/m^2s	10
p	Vapour pressure, N/m^2	18
	Static pressure, N/m^2	31
q	Heat flux, W/m^2,	10
r	Radial distance from the axis of the jet, m.	49
r_p	Radial extent of the impingement region	50
r_w	Radial distance from the stagnation point, mm	51
rms	Root mean square of the fluctuating quantity	79
R	Jet-cross flow momentum ratio ($\equiv \rho_j U_j^2/\rho_c U_c^2$)	164

Symbol	Description	Page of 1st Appearance
R_v	Gas constant, J/kgK	247
s	Second	103
	Length of the square area of integration	114
t	Time for clearance of Naphthalene,s.	22
T	Temperature	10
T_u	Turbulence intensity	6
u	Axial velocity, m/s	11
u_l	Velocity at the edge of the laminar layer, m/s	11
u_m	Maximum velocity at a section, m/s	11
u'	Fluctuating value of u, m/s	78
U	Effective cooling velocity, m/s	78
U_c	Velocity of the cross flowing stream, m/s	162
U_j	Velocity of the jet in confined situations, m/s.	162
U_o	Velocity on the jet centre line	49
U_{oo}	Exit velocity of the jet in stagnant surroundings	49
w	Weight of slides, mg	256
	Uncertainty in a variable	262
W	Watts	26
x	Streamwise nozzle pitch, m distance along a flat plate, m	59 36
x_p	Traverse extent ot the impingement region (i.e.for two-dimensional slot jets)	50
y	Spanwise nozzle pitch, m	169
z	Nozzle-to-target spacing (normal to plate), m.	6

Symbol	Description	Page of 1st Appearance
Z'	Nozzle-to-target separation measured along the jet axis, m.	110
Z_c	Length of the potential core, m.	65

Greek Symbols

α	Nozzle inclination, degrees	6
	Thermal diffusivity ($\equiv k/\rho C_p$), m^2s	10
β	Constant	53
δ	Displacement of the stagnation point from the geometrical axis of the nozzle, m.	51
Δ	Distance between the slides and the centre line of the target plate,m.	41
$\mathscr{D}$	Mass diffusivity, m^2/s	55
ε_m	Eddy diffusivity (momentum) m^2/s	10
ε_h	Eddy diffusivity (heat transfer) m^2/s	10
μ	Dynamic viscosity, kg/ms	251
ν	Kinematic viscosity or momentum diffusivity, m^2/s	10
ρ	Density of air, kg/m^3	10
σ	Standard deviation	261
τ	Shear stress, N/m^2	10
	Transmissivity ($\equiv e^{-KL}$)	100
ϕ	Analogy factor ($\equiv St/Stm$)	14
ψ	Constant	51
	Unheated starting length normalised by dividing by the jet diameter	36

Symbol	Description	Page of 1st Appearance
Dimensionless Numbers		
j_H	j-factor for heat transfer ($\equiv StPr^{2/3}$)	13
j_M	j-factor for mass transfer ($\equiv St_m Sc^{2/3}$)	14
Le	Lewis number (≡thermal diffusivity/ mass diffusivity, $\alpha/\mathcal{D}$).	16
Nu	Nusselt number (≡hd/k); similarly, $\bar{Nu}$ is the average Nusselt number corresponding to $\bar{h}$ and Nu_o is the stagnation point Nusselt number corresponding to h_o.	53
Nu_D	Nusselt number based on the target diameter. Similarly $\bar{Nu}_X$ is based on on the nozzle pitch and $\bar{h}$.	56
$\bar{Nu}_y$	Average Nusselt number based on hydraulic diameter and $\bar{h}$.	59
$\bar{Nu}_\alpha/\bar{Nu}_{90}$	Ratio of Nusselt number for a jet inclined at α degrees to that for a corresponding orthogonal jet.	116
Pr	Prandtl number (momentum diffusivity/ thermal diffusivity i.e. ν/α).	11
Pr_t	Turbulent Prandtl number ($\equiv \varepsilon/\varepsilon_h$)	12
Re, Re_d	Reynolds number based on jet diameter and exit velocity ($\rho.U_{oo}.d/\mu$)	6
Re_D	Reynolds number based on target diameter Similarly, Re_Y is based on the hydraulic diameter.	56
Re_X	Reynolds number based on the free stream velocity and the distance 'X'.	36
$Re_{a,d}$	Reynolds number based on arrival velocity, U_a and nozzle diameter ($\equiv\rho.U_a.d/\mu$). Similarly, $Re_{a,x}$ and $Re_{a,D}$ are respectively based on nozzle spacing and target diameter (i.e.$Re_{a,x}=\rho.U_a.X/\mu$ and $Re_{a,D}=\rho.U_a.D/\mu$).	57
Sc	Schmidt number (≡ momentum diffusivity/ mass diffusivity, i.e. $\nu/\mathcal{D}$).	13
Sc_t	Turbulent Schmidt number ($\equiv \varepsilon/\varepsilon_m$)	15

Symbol	Description	Page of 1st Appearance
Sh_d	Sherwood number ($\equiv k_L.d/\mathcal{D}$)	55
St	Stanton number ($\equiv Nu/RePr$)	11
St_m	Mass Stanton number ($\equiv Sh/ReSc$)	13

Subscripts

b	Based on width of the slot nozzle	17
c	For the cross flow	162
d	Based on diameter of the nozzle	6
D	Based on diameter of the target surface	56
j	For the jet	162
max	Maximum	197
n,N	Mass transfer surface (naphthalene)	22
O	At the jet centre line	49
oo	At exit of the jet	49
r	At radial distance 'r' from jet centre line	49
X	At position 'X'	36
∞,b	Bulk fluid or free stream	17

CHAPTER 1

1. INTRODUCTION

1.1 THE PROBLEM IN PERSPECTIVE

Impinging fluid jets are used extensively in industrial processes (heating, cooling and drying) because of the high convective transfer coefficients which can be obtained and also because the flows can be readily controlled. Depending upon the application, either two-dimensional (slot) or axisymmetric (circular) jets can be used singly or as a multiple 'arrangement' which can cover large areas of the transfer surfaces.

Due to the complex nature of the system, very little theoretical analysis has been undertaken. Recently, Wolfshtein (Ref. 1) and Russell and Hatton (Ref. 2) used numerical techniques to respectively predict the heat transfer rates and flow characteristics of single impinging jets. The problem has been extensively studied experimentally and the available data is reasonable for design purposes for many geometries if impingement is orthogonal.

The rate of heat transfer from the jet is affected by factors such as the spacing between the nozzle exit and the transfer surface, the jet exit velocity and profile, the nozzle shape, fluid turbulence and the inclination of the nozzle. In addition, when an array of jets is employed, the exhaust flow from the upstream jets can affect the characteristics of those jets located downstream (i.e. the so called crossflow effect). These crossflows arise in installations such as rapid heating furnaces and turbine blade cooling systems. In these systems, the nozzle spacing also affects the rate of heat transfer.

The present investigation stems from an on-going programme of research at Cranfield aimed at improving the design of these rapid heating furnaces. The effects of nozzle inclination on the rate of impingement heat transfer on a smooth, flat plate are reported. Both 'free' jets and jets in crossflows are examined.

It is relevant at this stage to examine briefly the use of impinging jets in rapid heating furnaces and other important engineering situations.

1.2 JET IMPINGEMENT FURNACES

The conventional type of industrial hydro-carbon fuel fired furnace relies upon the mechanism of thermal radiation to heat the charge to working temperature. Heat is transferred by direct radiation from the flame and also indirectly by re-radiation from the refractory walls. Convection, typically

only accounts for approximately 5% of the total heat transfer. The maximum heating rate in a conventional furnace is, thus, limited by the temperatures which can be withstood by the furnace materials.

In recent years, the so-called rapid heating furnaces (in which convection is the main mode of heat transfer) have been used to heat both ferrous and non-ferrous materials (Ref. 3). The required high rates of convective heat transfer can be obtained either by firing into a chamber which closely surrounds the stock or by utilising impingement of the combustion products. In these latter jet-impingement furnaces, a series of burners is supplied with a pre-mixed, near-stoichiometric mixture of gas and air so that combustion is virtually completed within the burner tunnel. The combustion products issuing from the burners are at temperatures which approach the adiabatic flame temperature and exit at velocities of up to 150 m/s (Ref. 4).

Figure 11.1 depicts the essential features of a typical jet impingement furnace consisting of :

a stock pre-heating zone where heat is recovered from the exhaust gases,

a rapid heating zone which utilises jet impingement,

and a soak zone which reduces the temperature variations within the stock. The mode of heat transfer in this zone is largely by re-radiation from the furnace walls.

The advantages of the convective rapid heating furnace over the more conventional design can include : (see Refs. 3-8).

1. Heating rates are often significantly higher so that the heating period for the charge is greatly reduced. This shorter heating period, in turn, reduces the problems of oxidation, decarburisation and other metallurgical phenomena associated with time spent at elevated temperatures. The high heating rates can also lead to increased throughputs.

2. The high convective heating rates together with a low furnace height (determined by the burner to stock separation distance) result in a compact design for a particular throughput.

3. Concentrated or localised heating of the stock is desirable in certain heat treatment processes, e.g. toughening or hardening of tool blanks. Jet impingement techniques can be readily used for this purpose and burner inclination often makes this easier to perform.

4. As the predominant mode of heat transfer is forced convection from the hot gases, the heating technique does not primarily depend upon re-radiation from the furnace walls. These can then be designed, if required, to have a very low thermal inertia so that rapid start-up and shut-down are feasible. Thus, it is possible to incorporate improved temperature control and plant automation.

5. Installation and maintenance costs are often lower for a rapid heating furnace especially for the smaller installations.

The disadvantages of jet impingement heating include :

1. The available commercial burners only operate with gaseous fuels such as natural gas or liquefied petroleum gas (L.P.G.). Although combustion of gaseous fuels is cleaner, these premium fuels may well become more valuable and scarce in future. The advent of commerical oil-fired burners (still under development) will, of course, significantly reduce the dependence upon premium fuels.

2. The operating cost is primarily dependent on the relative fuel costs. As the premium fuels become more expensive, the overall operating costs for jet impingement furnaces will increase and this trend would continue as the energy resource is depleted.

3. The available commercial jet-impingement burners have relatively small thermal ratings. Technical difficulties (e.g. distribution of the fuel and air supplies) associated with installation of many burners have thus limited the size of jet impingement furnaces.

1.2.1 Other Engineering Applications of the Jet Impingement Technique

The advantages outlined previously for jet impingement make the technique convenient for use in many other industrial processes. Thus, jet impingement is employed to cool the internal walls of turbine blades and discs (Refs. 9 and 10) and as higher turbine operating temperatures are achieved, impingement cooling will become still more important. A recent development is the use of jet impingement to cool the combustion chambers of gas turbines (Ref. 11). It is also used for the 'spot cooling' of temperature sensitive electronic components. Other uses of jet impingement cooling have

included the freezing of tissue in cryosurgery (e.g. cryogenic treatment of tumours).

In the paper and pulp industry, impingement dryers are frequently employed. Jets of hot air are blown either orthogonally or obliquely onto the surface of the drying materials (e.g. paper, veneer, and cardboard). Similar impingement dryers are also employed in the textile industry where a uniform drying of the product is essential and this is achieved by selecting an array of suitably spaced circular or slot jets (see Refs. 12-14).

The high operating speeds of modern equipment coupled with the relatively short length available for the drying operation imply that high rates of heat and mass transfer are needed to dry ink during printing operations. The throughput of the printing process is thus largely dictated by the 'drying' rate rather than by the printing operation itself. The recent adoption of convective jet impingement drying has produced significant improvements (see Refs. 15-18).

Other uses of jet impingement techniques include thermal surface treatment processes, e.g. tempering or toughening of metals and glass, localised heat treatment of plastics and glass plates, de-icing of aircraft wings and windshields, de-misting of car windscreens. It is also used in heating and air conditioning systems.

1.3 THE PURPOSE OF THE PRESENT STUDY

Earlier investigators (e.g. Ref. 19 and 20) concerned themselves almost entirely with measurements of the average heat transfer coefficients beneath an orthogonally impinging jet. However, there is also a need to obtain local heat transfer coefficients (i.e. for oblique jet impingement) which have, hitherto, been almost neglected. Since a heat transfer distribution can help in, reducing variation in heating/cooling over the surface, local overheating of materials can thus be predicted and prevented.

Fluid flow or geometrical constraints dictate that in some systems, fluid jets impinge obliquely upon the target surface. Unfortunately, both the associated fluid mechanics and heat transfer phenomena are only poorly understood. From the work of Perry (Ref. 21), there is evidence that nozzle inclination affects the rate of heat transfer. Perry assumed that the location of the maximum heat transfer coincided with the geometrical axis of the nozzle. Also, the measuring calorimeter and the nozzle were of the same size so that the results were not strictly 'local' in character. Korger and Krizek (Ref. 22) also conducted research with oblique slot jets. In effect, at the start of the present investigation, very little and reliable data was available for oblique jet impingement systems. However, in

1980, Sparrow and Lovell (Ref. 23) published a paper on convective transfer rates under an oblique impinging circular jet although the test conditions are limited.

Furthermore as mentioned previously, in large arrays of jets, the exhaust flow from upstream rows can significantly affect the characteristics of jets near the exit section of the system. The use of an axisymmetric jet in crossflow (in the current research), implies that the flow is three-dimensional. Despite the obvious practical utility of this system geometry, very little attention has been directed to it. This is due not so much to inadequate knowledge of the heat transfer mechanisms alone, but rather to the complexity of the fluid flow. Also, the highly turbulent motion is difficult to model because it requires the solution of the three-dimensional Reynolds equations. Although most previous studies have been concerned with flows and trajectories, a limited literature is available on measurements of both local and average heat transfer coefficients of jets in crossflows (Refs. 24-28). However, the ranges of the ratio of jet velocity to crossflow velocity (M) covered were often rather limited.

For oblique jets in crossflows, experimental and analytical results of jet trajectories have been published (Refs. 29-35). From the programme of research at Cranfield, there is evidence to indicate that inclination of the nozzle into the crossflow is beneficial. Kabari (Ref. 36) obtained flow and heat transfer measurements and noticed that reduction of the maximum heat transfer rate was not as severe for an inclined jet in crossflow as in a comparable unconfined 'stagnant' impingement tests. His test conditions were, however, limited. Jackson (Ref. 37) found that by increasing the angle of nozzle inclination into the crossflow, the heat transfer from the impingement surface was actually increased. The tests were however conducted with a slot jet.

Thus, there appears to be a paucity of information on the effect of jet inclination and the present investigation was undertaken to fillthis gap. The main objectives are thus :

1. To study the influence of nozzle inclination on both local and average heat transfer coefficients so as to provide useful data for designers of rapid heating furnaces and other jet impingement systems. Both unconfined jets discharging into an initially stagnant atmosphere, and confined jets exiting into crossflows are studied.

2. The experimental data can also be used to validate the results emanating from an on-going computer-based numerical study of the effects of crossflows on jets.

1.4 THE SCOPE AND LAYOUT OF THE THESIS

1.4.1 The Scope of the Investigation

The thin film naphthalene mass transfer technique was used in conjunction with the Chilton-Colburn analogy to infer the heat transfer rates. The most important parameters affecting jet impingement heat transfer rates in this study are: the jet Reynolds number (Re_d), the separation distance between the nozzle exit and the impingement surface (z/d), the nozzle inclination (α), the turbulence intensity at the nozzle exit (Tu) and its subsequent variation. In addition, in the presence of crossflows, the velocity ratio between the jet and the crossflow (M) is important as is the width ratio (H/d) of the duct. All these parameters were systematically varied except the turbulence intensities which were, nevertheless, measured in order to 'characterize' the jets.

In the first part of the study which was confined to jets exiting into initially stagnant surroundings, jet velocity profiles were determined. In addition, the variation in turbulence intensity along the jet centre line (for $0 \leqslant z/d \leqslant 40$) was measured. This is to enable comparison to be drawn with the jets used by previous workers. Local heat transfer coefficients were measured for experimental conditions covering the range $6 \leqslant z/d \leqslant 16$, $32500 \leqslant Re_d \leqslant 65000$, $30^o \leqslant \alpha \leqslant 90^o$. Average heat transfer coefficients were determined by numerically integrating over the appropriate area. Both the value and position of the stagnation point heat transfer coefficient are difficult to determine. Thus, a novel technique based on the optical determination of the naphthalene clearance was developed (see Chapter 6).

The flow associated with a jet in crossflow is more complex than that for an unconfined jet. To elucidate the flow mechanisms involved, a smoke visualization study was carried out. The local heat transfer coefficients were measured at $z/d = 6$ for experimental conditions covering the range $30^o \leqslant \alpha \leqslant 135^o$, $5 \leqslant M \leqslant 20.9$ and $8 \leqslant H/d \leqslant 26$. Both the 'circular' jet and the crossflowing streams were characterised by measuring the fluid velocity profiles and turbulence intensities.

1.4.2 The Layout of the Thesis

Following this Introduction, the thesis is divided into four parts as follows :

Part I - Title: Heat and Mass transfer techniques. The chapters deal with the analogy between heat, mass and momentum transfers, and the apparatus and experimental details of the thin film naphthalene technique.

Part II - Title: Heat transfer and fluid flow associated with inclined, unconfined impinging jets.
The experimental investigation carried out with the turbulent jet issuing into a quiescent media (unconfined jet) is reported. A survey of relevant literature on fluid dynamic and heat transfer measurements is also presented.

Part III - Title: Heat and fluid flow associated with an inclined impinging jet in a confined cross flowing stream.
A study of a 'circular' jet in the presence of a cross flowing stream is reported. A brief survey of pertinent papers is also included.

Part IV - Title: Closure
This part covers the conclusion and recommendations for future studies.

Five appendices are also included to provide detailed treatment of some of the material in the main text of the thesis.

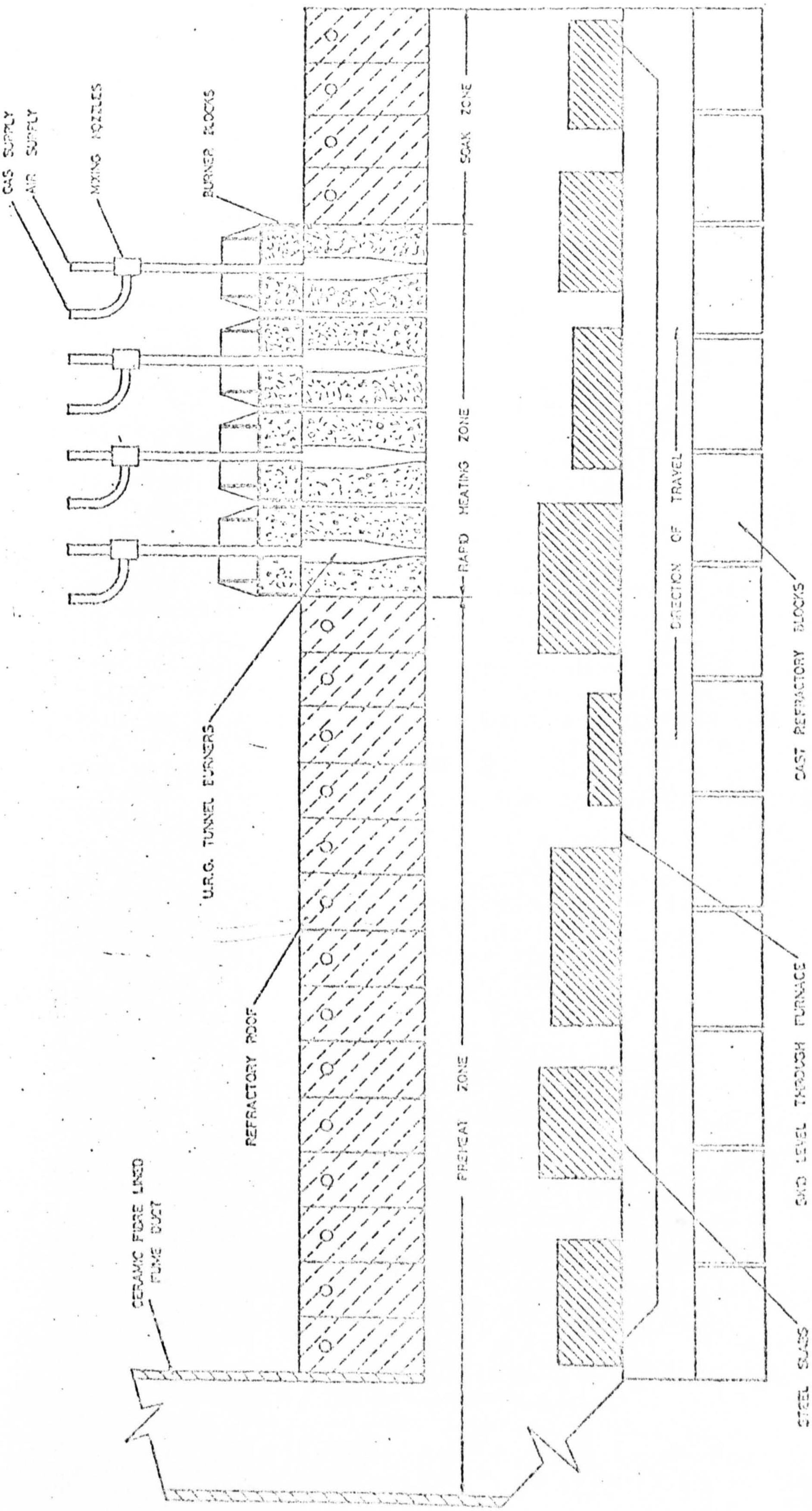

FIG. 1.1.1 TYPICAL JET IMPINGEMENT FURNACE.

CHAPTER 2

2. THE USE OF MASS TRANSFER TECHNIQUES TO ESTIMATE HEAT TRANSFER COEFFICIENTS

2.1 THE NEED FOR AN ANALOGY TO DETERMINE HEAT TRANSFER COEFFICIENTS

Fluid flows in real situations are often turbulent and are consequently so complex that analytical methods cannot be used with confidence to determine the associated convective heat transfer coefficients. This is certainly the case in jet impingement in the presence of a cross-flow where the two or three-dimensional flow (depending on jet geometry) can exhibit a separation bubble and recirculation phenomena. Large scale fluctuating eddies can also be present. It is, thus, customary in these situations to resort to experimental methods to obtain the required heat transfer coefficients.

Direct measurement of local heat transfer coefficients involves determination of both the surface temperature and the heat flux at particular locations. The heat flux can be determined by several methods, e.g. measuring the steady state electrical energy input to a heated section or by measuring the rate of steam condensation over the section (see Ref. 38 for details). Surface temperature measurement can involve the use of many thermocouples embedded in the test surface. The problems which can be encountered with this technique include :

1. If the thermojunctions are located, even slightly above the test surface, errors naturally ensue in the measured temperatures. Such protrusions can also impair the detailed structure of the flow field.

and

2. Similarly, if the thermocouples are located below the test surface, the measured temperatures will again be in error due to the surface temperature gradients.

Combined heat flux and temperature measurements can be obtained with a Gardon gauge which is a small transducer (i.e. .2 mm $\leqslant$ d $\leqslant$ 6 mm) embedded in the test surface (Ref. 39). The test surface and, hence, the gauge can be transvered or alternatively, several gauges can be installed to measure local heat transfer coefficients. Thus, this technique is expensive, tedious and also susceptible to errors.

More recently, the use of liquid crystals to obtain heat transfer coefficients has been developed (Ref. 40). In this technique, liquid crystals embedded in a thin layer of resin can be applied over the test surface. The accuracy of this technique is estimated to be approximately 5% (Ref. 40) and

30% (Ref. 41) respectively for high (Nu >> 100) and low heat transfer situations.

However, all the direct heat transfer techniques are susceptible to thermal conduction within the test surface and this can produce erroneous estimates especially with high heat fluxes. Radiation losses can also be significant particularly for natural convection and flows with low Reynolds numbers.

Nevertheless, some previous workers (e.g. Refs. 5-9 and 21) have used the direct methods although elaborate and costly data logging equipment and instrumentation can be required. Furthermore, these measurements are often time consuming.

Consequently, the use of an analogy to estimate the heat transfer coefficients from measurements of mass or momentum transfer is finding increasing application. These analogies are based on the assumption that the transport phenomena (momentum, heat and mass) are similar both physically and mathematically. These transfer processes can be expressed, in turn, by the following similar gradient type diffusion equations :

τ = f (grad U) for momentum transfer

q = f (grad T) for heat transfer

N = f (grad C) for mass transfer

where

τ, q, N, U, T and C are the shear stress, heat transfer/unit area, mass transfer flux, velocity, temperature and vapour concentration respectively.

2.2 ANALOGIES BETWEEN HEAT AND MOMENTUM TRANSFER

The similarity between the transport of heat and momentum was first pointed out by Osborne Reynolds in 1874 and this led in turn to the formulation of equations relating the friction factor (C_f), to the heat and mass transfer coefficients. The analogies were first developed for laminar boundary layer flows but have also been found valid for turbulent boundary layers.

For a turbulent flow over a flat plate, the two fluxes of momentum and heat can be written in general as :

$$\tau = \rho(\nu + \varepsilon_m) \text{ grad } U \qquad 2.2.1$$

and

$$q = \rho C_p (\alpha + \varepsilon_h) \text{ grad } T \qquad 2.2.2$$

where

ε_m, ε_h, ν, α, ρ and Cp are the turbulent eddy diffusivities of momentum and heat, the kinematic viscosity, molecular diffusivity, density and the specific heat respectively.

Reynold assumed that :

1. The profiles of the time-mean properties (U, T) are similar.

2. The fully turbulent eddy diffusivities are equal

$$\text{i.e. } \varepsilon_m = \varepsilon_h$$

and

3. The molecular diffusivities of momentum and heat are equal, i.e. $\nu = \alpha$ or $Pr = 1$

Dimensional analysis was then applied to equations 2.2.1 and 2.2.2 to yield (see Ref. 42).

$$St = C_f/2 \qquad 2.2.3$$

where

St = Stanton number

C_f = coefficient of friction = $\tau/\frac{1}{2}\rho u^2$

A study of the momentum and energy equations which respectively describe the velocity and temperature fields indicates that a pressure term occurs in the first of these relationships. This implies that exact similarity between momentum and heat transfer is only possible in constant pressure flows (i.e. $\partial p/\partial x = 0$). Furthermore, Reynolds' third assumption is only reasonably true for the common gases (e.g. Pr = 0.7 for air) and does not hold for fluids for which Pr differs significantly from unity. Also, in the laminar sub-layer (which was neglected in the analysis), thermal conductivity and viscosity have an important effect on heat and momentum transfer respectively.

Extensions of Reynolds analogy to allow for the effect of the laminar sub-layer were postulated by Prandtl (Ref. 43) and independently by Taylor (Ref. 44). Their resultant expression is :

$$1/St = \frac{2}{C_f}\left[1 + (Pr - 1)\frac{u_L}{u_m}\right] \qquad 2.2.4$$

where

u_L = velocity at the edge of the laminar layer

u_m = mean velocity in the turbulent core

Some of the restrictions on Pr which were implicit in Reynolds' formulation can now be relaxed. However, equation 2.2.4 still only applies for a limited range of Prandtl number ($0.5 < Pr < 2$).

The simplifying assumptions adopted by Prandtl and Taylor were :

1. Molecular diffusivities are negligible in the turbulent core, i.e. $\nu << \varepsilon_m$

   and $\alpha << \varepsilon_h$

and

2. The turbulent eddy diffusivities of heat and momentum are equal in the turbulent region.

However, the Prandtl-Taylor analysis does not always agree with experimental observations and von-Karman attributed this to the use of only two flow regimes (Refs. 42 and 45). He therefore suggested that the flow should be divided into three regions by incorporating a transition buffer layer where momentum and heat are transferred by both turbulent mixing as well as molecular mechanisms. The relationship he proposed is :

$$1/St = \frac{2}{C_f} + 5\sqrt{2/C_f}\left[(Pr - 1) + \ln(1 + 5/6\ (Pr - 1))\right] \qquad 2.2.5$$

This expression removes the previous serious restrictions on the range of Prandtl numbers for which calculations can be made. In deriving von-Karman's expression, the following were assumed :

1. The turbulent Prandtl number is unity ($Pr_t = 1$) in the turbulent core.

2. The molecular and turbulent diffusivities of heat and momentum are additive in the transition buffer zone.

and

3. The turbulent eddy diffusivities of heat and momentum are negligible in the laminar sub-layer.

i.e. $\varepsilon_m << \nu$

$\varepsilon_h << \alpha$

In 1933, Colburn (Ref. 46) proposed an empirical relationship between heat transfer data and the friction factors for a turbulent flow in a circular pipe so that

$$St(Pr)^{2/3} = C_f/2 = j_H \qquad 2.2.6$$

where

j_H = j factor for heat transfer

This relationship was found to hold for shear layers in which

$Re > 10000$

$0.7 < Pr < 160$

and the length to diameter ratio of the pipe, $L/d > 60$.

To sum up the foregoing discussion, it is apparent that the analogy between heat and momentum transfer can be utilized to determine the heat transfer coefficient from a knowledge of the friction factor or the drag coefficient. All the above analyses hold only when form drag is negligible. The simple analogies are however limited both in accuracy and the fact that they are confined to fluids in which $Pr \simeq 1$. Greater accuracy can be obtained with the more complicated analyses and moreover they are applicable to a wide range of fluids. Fig. 2.2.1 depicts the effects of Reynolds number on heat transfer associated with flows on a flat plate. When Pr = 1, all the analyses reduce to Reynolds equation and the variations at other Prandtl numbers are apparent.

2.3 HEAT/MASS TRANSFER ANALOGIES

Heat and mass transfer are analogous because the former process can be considered as a diffusion process in which the hot molecules diffuse to a 'cold' zone with a corresponding transfer of cold molecules in the reverse direction. Hence, the various analogy relationships of the preceeding section can easily be modified to include mass transfer by replacing Pr, St with Sc and St_m respectively. For example, Chilton and Colburn (Ref. 47) extended the Colburn empirical relationship to include mass transfer by stating that :

$$St_m Sc^{2/3} = C_f/2 = j_M \qquad 2.3.1$$

where

St_m, Sc, and j_M are the mass Stanton number, Schmidt number and the j-factor for mass transfer respectively.

This form of the Chilton-Colburn analogy can be used to relate heat and mass transfer for flows in which form drag is negligible (e.g. flows in pipes and plane surfaces) and has yielded sastisfactory results (Ref. 47). However, for flows around bluff bodies, tube banks, and spheres, the frictional loss is due to both form drag (which was neglected in the original derivation of the analogy) as well as frictional drag. For such situations, it has been found experimentally that, $j_H \simeq j_M$ although neither is equal to $C_f/2$. Thus, more generally it may be concluded that :

$$\frac{St}{St_m} = \left(\frac{Sc}{Pr}\right)^{2/3} = \phi \text{ (analogy factor)}$$

$$= \frac{h}{K_L \rho C_p}$$

$$\text{i.e. } h = K_L \rho C_p \left(\frac{Sc}{Pr}\right)^{2/3} \qquad 2.3.2$$

where K_L and h = mass and heat transfer coefficients respectively.

The relationship expressed in equation 2.3.2 has been verified experimentally by its successful use in obtaining heat transfer coefficients under various flow conditions (Ref. 23, 36, 48-50). Lewis (Ref. 51) has however pointed out the limitations of the analogy. The constant analogy factor, $\left(\frac{Sc}{Pr}\right)^{2/3}$, does not allow for variations in heat and mass diffusivities at different flow velocities. Thus, a rigorous form of the heat and mass transfer analogy must account for the varying contributions of molecular and turbulent diffusivites across the boundary layer. Well-established values of molecular diffusivities exist, but the turbulent values are rather difficult to measure.

In 1969, Jayatilleke (Ref. 52) published an extensive review of the various concepts that can be used to obtain the analogy factor. He subsequently proposed an empirical expression of the form :

$$\frac{1}{St} = \left(\frac{C_f}{2}\right)^{-1/2}\left[Pr_t\left(\frac{2}{C_f}\right)^{1/2} + A\left[\left(\frac{Pr}{Pr_t}\right)^{3/4} - 1\right]\right.$$

$$\left.\left[1 + 0.28\ \exp\left(-0.007\ \frac{Pr}{Pr_t}\right)\right]\right] \qquad 2.3.3$$

where

A is a constant and equal to 8.32 and 9.00 for $Pr_t = 0.9$ and $Pr_t = 1$ respectively.

St_m is obtained by simply substituting Sc for Pr

Figure 2.3.1 shows the analogy factors suggested by previous investigators. The results are for fully developed flow in a tube and the Prandtl number corresponds to that for air (Pr = 0.71) while the Schmidt number is equivalent to that for naphthalene sublimation in air (Sc = 2.44). A considerable difference between the Chilton-Colburn analogy and those of other workers is apparent and this difference increases with Reynolds number. Nevertheless, as discussed in the next section, the employment of the simple $\left(\frac{Sc}{Pr}\right)^{2/3}$ factor often suffices.

2.4 JUSTIFICATION FOR USING A HEAT/MASS TRANSFER ANALOGY FOR JET IMPINGEMENT FLOWS

In confined flows, e.g. duct or pipe flow, friction factors are often easier to obtain than the corresponding heat transfer coefficients. The analogy between skin friction and heat transfer has, thus, been particularly useful in such situations. However, a heat/momentum analogy is not applicable to jet impingement flows because of the difficulty in measuring the friction factors. Also, heat and momentum are not analogous at stagnation points where the heat transfer coefficient is often a maximum whereas the shear stress (and hence the friction factor) is zero. This is also the case at re-attachment points. Furthermore, the analogy can only be accurately applied at stations away from the stagnation point if the relationship between the turbulent diffusivities of heat and momentum (ε_h, ε_m) is known. Most investigators (e.g. Prandtl) have assumed equality of these parameters but recent experimental work has shown that this is not true, i.e. $Pr_t \neq 1$ (Refs. 53, 54).

Thus a heat/mass transfer analogy is employed in the present study. However the complicated analogies of Jayatilleke and von-Karman involve a knowledge of friction factors. In many flow situations (including jet impingement systems) values of this parameter are not often available. Because of this difficulty the simpler Chilton-Colburn heat/mass transfer analogy is employed.

As discussed in section 2.2.2, this analogy between heat and mass transfer has been established theoretically only for boundary layer flows. Thus its application to other situations (e.g. jet impingement) depends on experimental verification. The Chilton-Colburn analogy has previously been used in a wide variety of flow fields with a reasonable degree of success. Moreover, Ward et al (Ref. 48) have demonstrated the suitability of this Chilton-Colburn analogy to infer jet impingement heat transfer coefficients. More recently, Vallis et al (Ref. 49), Kabari (Ref. 36) and Mahmood (Ref. 50) have successfully used the analogy for different jet impingement system geometries. Due to its simplicity and ease of application, it is the most widely used relationship for obtaining heat transfer coefficients from mass transfer data.

The transport of heat and mass can only be completely analogous under the following conditions :

1. Dynamic and geometric similarity must be maintained between the two systems. Dynamic similarity is satisfied when the Reynolds numbers are equal whilst geometric similarity can be fulfilled by proper design of the experimental set up.

2. The diffusivities of heat and mass are equal. The molecular diffusivities are equal if the laminar Prandtl and Schmidt numbers are the same (i.e. Le = 1). None of the mass transfer techniques used to infer convective heat transfer coefficients due to gas flows completely satisfy this condition and in some situations the Lewis number can even be several orders of magnitude greater than unity, e.g. in the electrochemical method, Pr = 0.7 and Sc = 1500 (at 25°C). However with the naphthalene sublimation technique, this criterion is reasonably satisfied since, typically, Sc = 2.44 and Pr = 0.71.

   Available experimental and theoretical data indicate that the turbulent Lewis number is close to unity (Ref. 55 and 56). The condition of equal diffusivities can thus often be reasonably satisfied because the turbulent contribution to the energy and mass fluxes is generally more important than the laminar component.

and

3. The boundary conditions are similar. In mass transfer experiments, the ion concentration (with the electrochemical technique) or vapour concentration (as in the sublimation of naphthalene) generally remains constant over the test surface. Hence, the heat transfer results inferred from such tests correspond to a thermal boundary condition in which the heat transfer surface is at a constant temperature. The 'bare patch' effect which produces a variable boundary condition in the thin film naphthalene technique is discussed in Chapter 3.

2.5 DETERMINATION OF HEAT TRANSFER DATA FROM MASS TRANSFER MEASUREMENTS

2.5.1 Mass Transfer Methods

Mass transfer techniques are often employed to infer heat transfer data and have been used satisfactorily in a wide range of configurations. These techniques are mainly electrolytic in type or involve the sublimation of a volatile solid.

The electrochemical method can be conveniently used for mass transfer investigations which simulate heat transfer in liquids. The aqueous solution used as the test fluid is an electrolyte in which two electrodes (one of which acts as the mass transfer surface) are inserted. Thus, the negatively charged ions move to the anode while the positively charged ions move to the cathode. The movement of the ions is caused by diffusion (neglecting both convective and electric field effects). When the potential difference across the electrodes is sufficiently large, the ions are 'removed' from the solution as quickly as they reach the electrodes and the current reaches a limiting value expressed as :

$$I_L = AnFk_L C_b \qquad 2.5.1$$

where

I_L = the limiting current

A = electrode (mass transfer surface) area

n = valency change in reaction

F = Faradays constant

k_L = convective mass transfer coefficient

C_b = ion concentration of the bulk solution

Thus, the mass transfer coefficient can be calculated from a measurement of the limiting, diffusion-controlled current.

Electrochemical methods have been used extensively by British Gas. For example, Lucas et al (Ref. 57) used nickel electrodes and an alkaline solution of potassium ferro-ferricyanide to determine the mass transfer coefficients in models of various rapid billet heating furnaces. Here at Cranfield, the electrochemical technique has been employed to study tube banks, e.g. Jewad (Ref. 58), Ward and Jewad (Ref. 59), used the method to obtain both local and average heat transfer coefficients in this system geometry. Their results were in good agreement with previous direct heat transfer data (e.g. McAdams (Ref. 60)). Recently, Vallis et al (Ref. 49) have used this technique to study a single free jet impinging on a flat surface.

The electrochemical technique is accurate, speedy and versatile. However, it has certain drawbacks namely: it can only be used with liquids so that high Schmidt numbers (typically Sc = 1500) are enccuntered. Furthermore, only solutions in which a diffusion controlled electrolytic reaction occurs can be employed. An additional consequence of employing liquids is that fluid flow measurements using pitot probes and hot wire anemometry are more difficult.

Mizushina (Ref. 61) has published a detailed review of electrochemical techniques.

Mass transfer investigations using air as the test fluid are usually based on either sublimation or evaporation of the mass transfer substance. Solids that have been used include ice, camphor, naphthalene and parachlorobenzol. Liquids such as water, benzene, toulene, carbon tetrachloride, chlorobenzene and tetrachloroethylene have also been used (although less frequently) as the mass transfer substances.

In 1934, Klein (Ref. 62) used streams of hot air to melt cylinders made of ice and by measuring the weight of the melted ice, he obtained the overall heat transfer coefficients. In his calculations, however, he neglected losses due to radiation and conduction along the length of the cylinder. Also, the effect of air humidity was not considered. Nevertheless, his pioneering work encouraged other researchers to employ mass transfer techniques especially with substances of higher melting points. These solid substances should have a relatively high vapour pressure at ambient temperatures so that the mass transfer coefficients can be obtained after a test of comparatively short duration.

The problems associated with the use of ice were eliminated by Winding and Cheney (Ref. 63) who used naphthalene as the mass transfer substance. This has a vapour pressure of approximately 7.0 N/m^2 at 20^oC and so sublimes (changes from solid to vapour) fairly readily. Split brass moulds

together with plaster of Paris cores were used to cast naphthalene in the form of tubes. By weighing the tubes before and after the tests, the average transfer coefficients were obtained. To obtain the local values, the naphthalene tubes were replaced in the moulds after each test. Changes in the local dimensions were determined with a feeler gauge. The Chilton-Colburn equations enabled them to infer the local and average heat transfer coefficients.

The use of feeler gauges is tedious and inaccurate and Christian and Kezios (Ref. 64) employed a micrometer dial indicator to measure the local sublimation rates. They employed sharp-edged cylinders (cast from naphthalene) in a laminar flow situation. Local values were integrated to obtain average mass transfer coefficients which agreed to within ±3% of the values obtained by direct weight loss measurements.

Houston (Ref. 65) in 1960 used a profilometric method to obtain the local mass losses from a naphthalene nozzle. This nozzle was a scale model of a solid fuel rocket. The profilometric technique he adopted reduced the duration of the measurement period when compared with the methods of previous investigators. Consequently, errors due to natural sublimation of naphthalene were reduced. He also employed a ball-tipped stylus to inhibit scouring of the naphthalene test surface.

More recently, Koopman and Sparrow (Ref. 66) employed a profilometric technique to determine the mass transfer coefficients from a row of impinging circular jets. To simplify the tedium involved in estimating the local naphthalene mass losses they developed a semi-automatic data acquisition system. The local mass transfer coefficients were integrated to obtain the average values which varied by ±6% from those obtained by direct weighing.

Naphthalene sublimation methods using profilometric techniques have thus gradually been improved until it is now a relatively sophisticated technique. However, it is still tedious to employ and very careful experimentation is required to yield accurate and repeatable results. In the jet impingement studies at Cranfield, naphthalene has been frequently used as the mass transfer substance. For example, Mac (Ref. 67) and Al-Mobarek (Ref. 68) measured the space average heat transfer coefficients in a model of a billet reheating furnace. Kabari (Ref. 36) and Oladiran (Ref. 69) determined both the local and average heat transfer coefficients from single and multiple jets respectively. More recently, Dunn (Ref. 70), Mahmood (Ref. 50) and Oladosu (Ref. 71) obtained the average heat transfer coefficients of impinging swirling jets.

However, naphthalene sublimation is not the only mass transfer technique used with air as the working fluid. For example, Todd (Ref. 72), Macleod and Todd (Ref. 73) developed a technique based on the use of a thin coating of natural rubber

which shrank on losing the vapour of an organic swelling agent such as methyl salicylate. The resultant changes in thickness of the coating were obtained by profilometric methods and these can be related to weight changes by calibration. The advantages claimed for this method include :

(i) Once the initial trial run has been completed, the time and effort required for the tests are less than those for methods that require casting of the mass transfer substance,

and

(ii) by using various swelling agents, experiments can be carried out over a wide range of Schmidt numbers so that systematic studies of the effect of this parameter are possible.

However, accurate maximum heat transfer coefficients are sometimes difficult to measure especially at high Reynolds number. Todd (Ref. 72) moreover, indicated that the repeatability of the technique was poorer than that associated with the more common naphthalene sublimation method.

Macleod et al (Ref. 74) also used a profilometric method to obtain the local losses in the thickness of a thin volatile coating. Their probe combined both electromagnetic and pneumatic proximity gauges and was able to measure the local changes in thickness to an accuracy of 1.5 μm. Local heat transfer coefficients were thus obtained on a model of a gas cooled nuclear reactor.

In the present work, the local heat transfer coefficients are measured for an oblique jet both in initially stagnant surroundings and also in the presence of a cross flowing stream. A thin-film napthalene technique is used to obtain the mass transfer measurements which are then converted to the corresponding heat transfer rates by invoking the Chilton-Colburn analogy. It is, thus, appropriate at this point to describe the basic features of the 'thin-film' technique.

2.5.2 The Thin-Film Naphthalene Technique

In the first reported application of this technique, Wilkie and White (Ref. 75) examined the variation of heat transfer coefficients along the ribbed surface of AGR nuclear fuel elements. The ribbed surfaces were coated with a thin layer of naphthalene using a commercial small spray gun held in the tool post of a lathe. The spray gun which was fed with a solution of naphthalene dissolved in acetone, was traversed automatically while the fuel element was rotated between the centres of the lathe. In this manner, an essentially uniform layer of naphthalene (approximately 0.025 mm thick)

was sprayed on to the surface in a single traverse. The naphthalene weight per unit area was not measured, hence absolute values of the mass transfer coefficients could not be obtained. Air was then passed over the coated elements and the mass transfer coefficient was assumed to be inversely proportional to the time required for the napthalene to clear from the surface. Thus, a picture of the heat transfer distribution can be built up by noting the clearance time at various locations. The results of Wilkie and White were in good qualitative agreement with those obtained by direct heat transfer measurements and showed that the thin-film naphthalene technique is an inexpensive, simple and fast method of obtaining qualitative mass transfer data, and can be an aid in predicting hot-spots.

Recently, Neal et al (Ref. 76) at the Central Electricity Research Laboratories (C.E.R.L.), employed a spray rig which coated surfaces with naphthalene in a controlled manner. The coating weight per unit area was determined by using a 'dummy' test piece which was sprayed at the same time and under the same conditions as the test surface. Hence, quantitative values of the mass transfer coefficients can be obtained.

Naphthalene was fed to the central nozzle of a co-axial system while air was supplied under pressure to the annulus. An atomised jet of naphthalene was thus sprayed onto the surfaces. Cylindrical test pieces were sprayed in a similar way to those of Wilkie and White (Ref. 75). Moreoever, an automatic linear motion spraying table was developed to coat flat surfaces. Typically, a spray head speed of 0.8 m/s and a solution flow rate of 60 mm^3/s at a concentration of 1 to 5 parts (by volume) produced an approximate napthalene thickness of 0.015 mm. Figure 2.5.1 shows the experimental results obtained by Neal (Ref. 77) for developing flow in a cylindrical pipe. The data are in good agreement with previously published direct heat transfer results (Refs. 46 and 78). Thus, it may be concluded that the thin-film method together with the simple Chilton-Colburn analogy yielded reliable heat transfer data. The method is relatively cheap, speedy and can, furthermore, easily provide data for the whole field of interest. The growth of the clearance pattern is also visible and can, therefore, be used to investigate various flow phenomena.

At Cranfield, Mahmood (Ref. 50) successfully built a less sophisticated version of the spray rig originally developed at C.E.R.L. He investigated both the local and average heat transfer coefficients associated with swirling impinging jets. He concluded that the thin-film method provided repeatable results which were in reasonable agreement with published data.

The 'thin-film naphthalene device' used by Mahmood was also employed in the current investigation because :

(i) It is difficult to use other techniques to determine whole field data in flow fields as complicated as those associated with oblique jets in cross flows.

(ii) The duration of the tests is much shorter than that for the alternative profilometric method of determining local naphthalene sublimation rates. The time required to prepare and coat the surface is also shorter than the time required for casting naphthalene for profilometric tests.

(iii) The 'thin-film' method has been found to yield heat transfer results which are as reliable as those obtained by other techniques.

(iv) The naphthalene spray rig was readily available.

(v) Visual observation of the clearance patterns can be very useful in checking the experimental set-up, e.g. it is quickly apparent if the cross flow is not uniform over the width of the duct. The clearance patterns can also provide indications of the interaction between the jet and the cross flowing stream.

2.5.3 Calculation of Heat Transfer Coefficients from Naphthalene Sublimation Data

Isothermal models which satisfy the necessary conditions of dynamic and geometric similarity discussed in Section 2.4 can be employed in heat/mass transfer experiments whereby convective heat transfer data may be inferred from mass transfer measurements. If a naphthalene sublimation technique is employed, a mean mass transfer coefficient, K_L may be defined by :

$$m/t = K_L \cdot A_n(C_n - C_\infty) \qquad 2.5.2$$

where

m = sublimation weight loss during the test duration, t.

A_n = the surface area over which sublimation occurs.

C_n, C_∞ = the concentration vapour of the subliming substance at the test surface and in the free stream respectively.

The partial pressure of the naphthalene vapour is negligible so that the vapour can be treated as a perfect gas with a temperature T_n equal to that of the mass transfer surface.

Hence,

$$C_n = P_n/R_n T_n \qquad 2.5.3$$

where

P_n, T_n = the vapour-solid equilibrium values of pressure and temperature respectively.

R_n = the gas constant.

Also, the concentration of the naphthalene vapour in the free stream is often small compared with the concentration at the test surface. The former is, thus, usually neglected, i.e. $C_\infty = 0$.

Combining equations 2.5.2 and 2.5.3, the following is obtained

$$K_L = \frac{m}{A_n t} \cdot \frac{R_n T_n}{P_n} \qquad 2.5.4$$

By invoking the Chilton-Colburn analogy, the heat transfer coefficient can easily be obtained (i.e. substituting equation 2.5.4 into 2.3.2). Thus,

$$h = \frac{m}{A_n t} \rho C_p \cdot \left(\frac{Sc}{Pr}\right)^{2/3} \frac{R_n T_n}{P_n} \qquad 2.5.5$$

Equation 2.5.5 is valid for measurements of both local and average heat transfer coefficients provided that the appropriate values of mass loss/unit area are used in the calculations.

The Schmidt number can be found by using an expression proposed by Sherwood and Trass (Ref. 79) namely :

$$Sc = 7.00(T)^{-0.185} \qquad 2.5.6$$

where

$100^\circ K < T < 500^\circ K$

Sublimation depresses the surface temperature of naphthalene below that of the free stream but this difference is usually small and neglected, i.e. $T_o \approx T_n$ (Ref. 80). Therefore, the saturation vapour pressure, P_n, can be evaluated at the mean free stream temperature. Many empirical correlations (Refs. 79, 81-83) have been proposed for determining the relationship between vapour pressure and temperature. In this present study, the relationship of Sherwood and Bryant (Ref. 81) has been used because this equation yields approximately mean values when compared to the other available correlations, (see Fig. 2.5.2). The general properties of naphthalene are described in Appendix A.1.

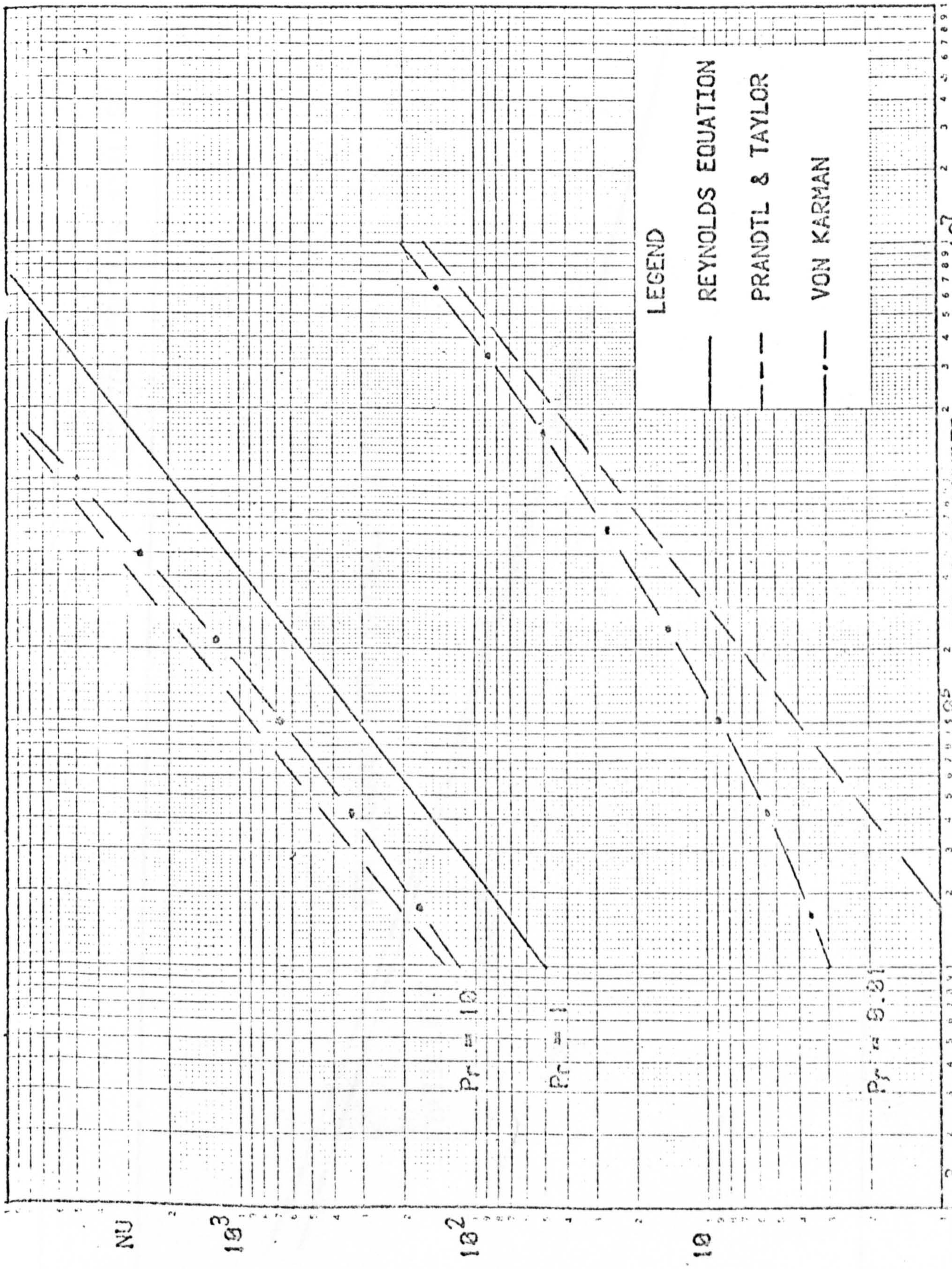

FIG.2.2.1 VARIATION OF NUSSELT NUMBER ON A FLAT PLATE USING DIFFERENT ANALOGY EQUATIONS.

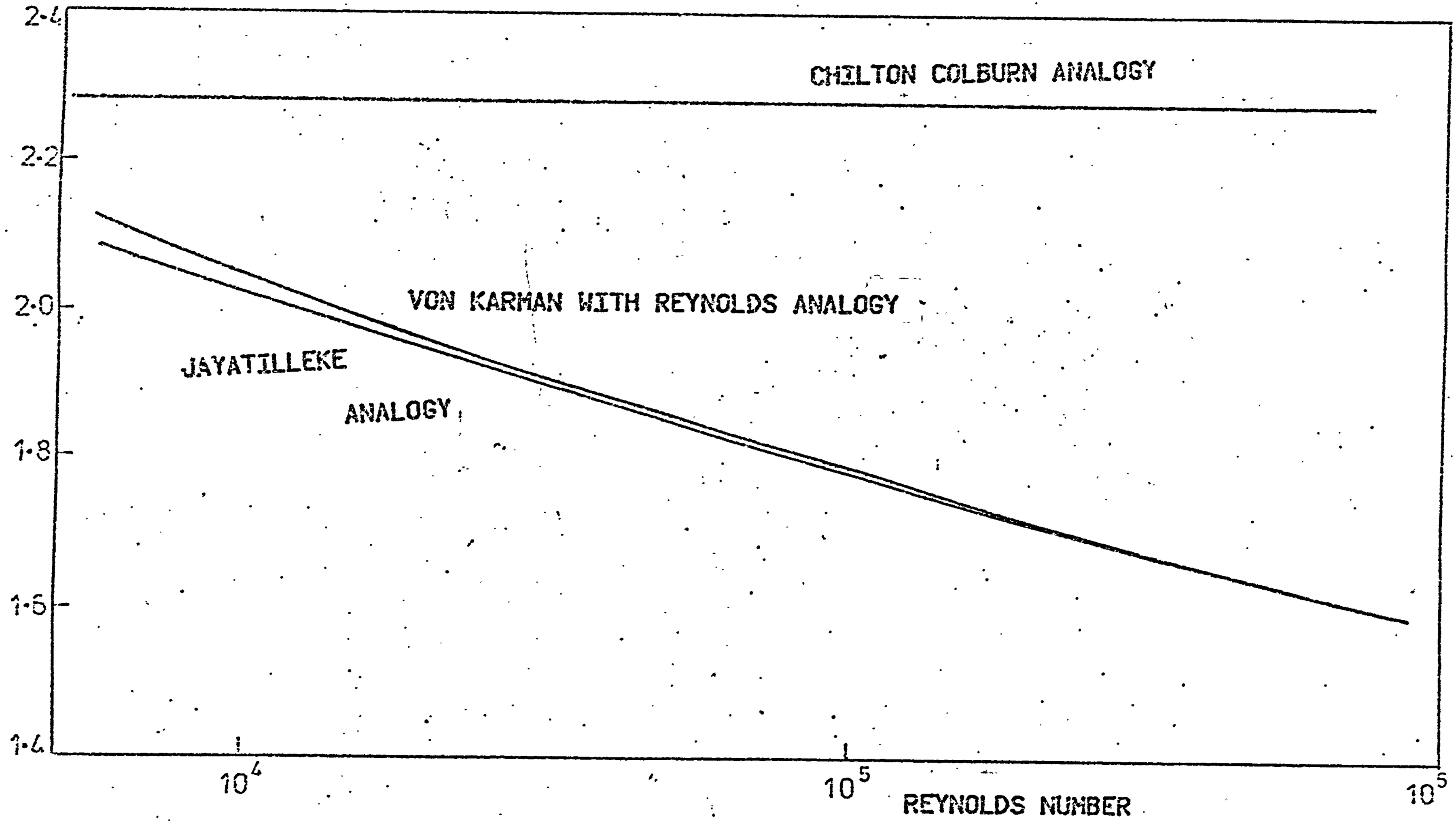

FIG.2.3.1 GRAPH SHOWING MASS/HEAT TRANSFER ANALOGY FACTORS VS REYNOLDS NUMBER.

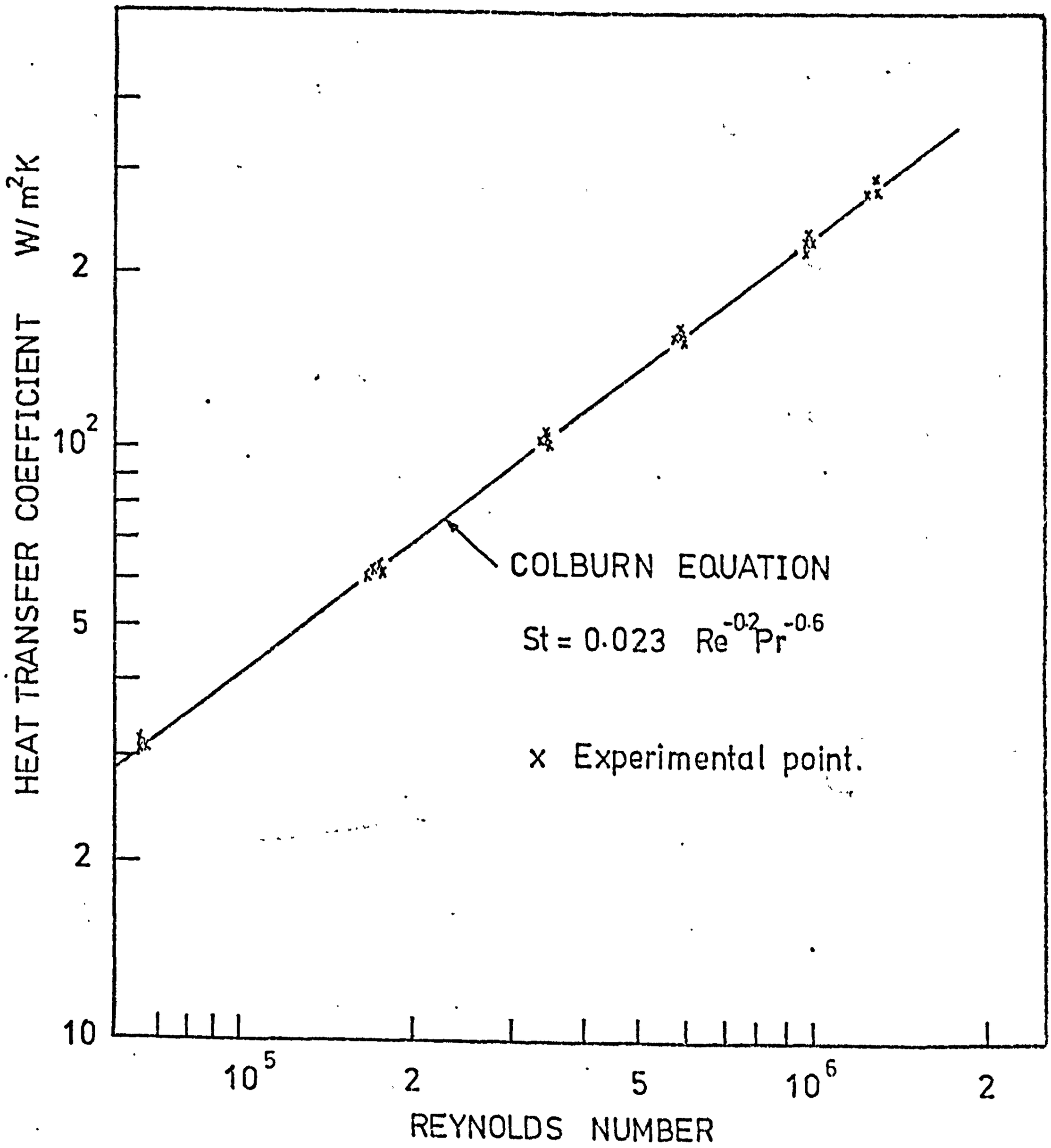

FIG.2.5.1 RESULTS OBTAINED BY NEAL(REF. 77) USING 'THIN-FILM' NAPHTHALENE TECHNIQUE FOR FLOW IN PIPES.

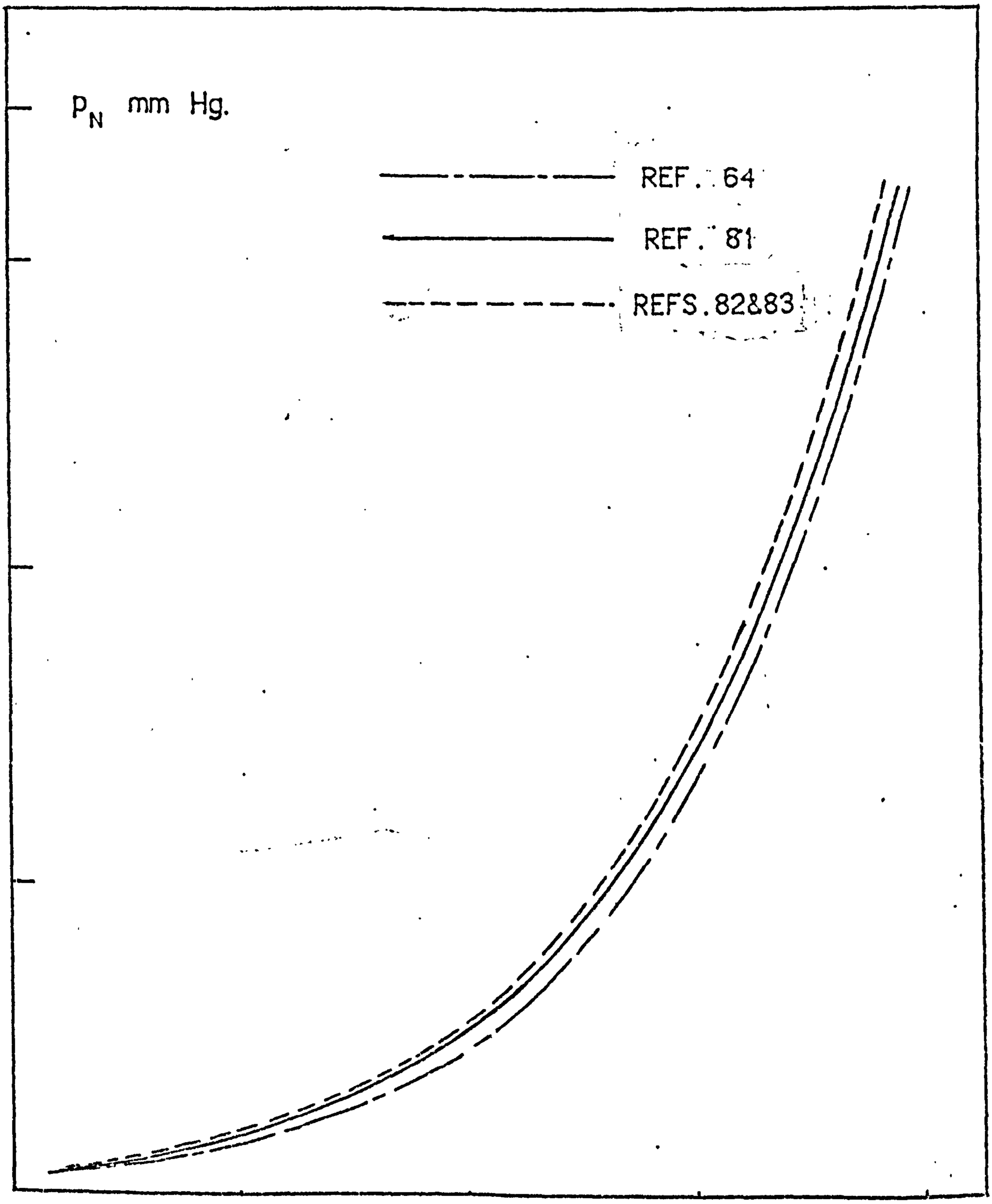

FIG.2.5.2 VARIATION OF NAPHTHALENE VAPOUR PRESSURE WITH TEMPERATURE.

CHAPTER 3

3. THE NAPHTHALENE 'THIN-FILM' MASS TRANSFER TECHNIQUE - APPARATUS AND EXPERIMENTAL DETAILS

3.1 INTRODUCTION

It should be apparent from the previous Chapter that the degree of confidence that can be placed on heat transfer data inferred from mass transfer measurements depends on both the reliability of the analogy which is employed as well as the accuracy of the mass transfer measurements.

The Chilton-Colburn analogy is employed in the present study together with a mass transfer technique based on sublimation of naphthalene in air. Most previous workers who have used this technique have employed accurate weighing of the mass transfer surface to obtain average coefficients. Profilometric techniques (Refs. 36, 65, 66 and 69) have been employed to determine the local values. In the present 'thin-film' naphthalene method, it is necessary to spray the test surface with an essentially 'uniform' film of naphthalene of known specific weight. The time for clearance of the naphthalene film at any station on the surface is then a measure of the local mass transfer coefficients.

The spray rig described in this thesis was originally designed by Mahmood (Ref. 50) and is similar to the one developed by Neal et al (Ref. 76) at the Central Electricity Research Laboratories. The rig is a cheap, semi-automatic device capable of spraying a thin, essentially uniform film of naphthalene over a flat surface.

3.2 THE SPRAY RIG

The spray rig (see Plate 3.2.1) can be divided into three main sections, namely :

the spray mechanism,

the electronic controls and

the flow control systems for the fluids.

3.2.1 The Spray Mechanism

The heart of the spray rig is the nozzle shown in Plate 3.2.2 and in Appendix A.2. This co-axial nozzle was mounted on the front panel of an aluminium carriage block (of dimensions

50.8 mm x 25.4 mm x 22.5 mm) which was carried and guided by two stainless steel guide bars (10 mm dia. x 610 mm long). Two linear roller bearings were employed to reduce sliding friction between the block and the bars. These bars were held parallel by means of two support blocks (one at each end of the spray table).

The required horizontal motion of the carriage on the guide bars was achieved through a motor-driven pulley and wire rope assembly. Changes in the direction of the traverse were obtained by reversing the direction of rotation of the variable speed d.c. motor. Limit switches fixed to the sides of each support block arrested the carriage, thus fixing the length of the traverse. These limit switches were actuated by a striker plate mounted on top of the carriage block.

The reliability of the results from the thin-film naphthalene technique depends on the attainment of a layer of 'uniform' thickness. Two of the most important factors affecting the thickness of the coating are the traverse speed of the nozzle and the flow rate of the solution. With regard to the former variable, it is essential that the spray head travels at a constant speed during the spraying process. This motion was checked by observing the displacement of the carriage with time, by means of a displacement transducer coupled to a cathode ray oscilloscope (CRO). Plate 3.2.3.shows the trace at various d.c. motor speeds. The variation of the carriage position with time is linear for that part of the travel during which the plate was sprayed. Thus, a uniform spray can be obtained provided that the flow rate of the naphthalene solution is maintained constant. For all the tests, a traverse speed of 0.9 m/s was found to be satisfactory.

The test plate to be sprayed was made of perspex so that the naphthalene clearance patters were visible from both sides of the plate. This plate was located on a carrier which lay beneath the spray head. The carrier plate was in turn fixed to a 910 mm long leadscrew (6 threads per cm) which was driven by a stepper motor, type 34PM-C004 (supplied by Astrosyn). This motor can be rotated through an electrically controlled specified number of steps up to a maximum of 1000 with each step being equal to a rotation of 1.8 degrees. Thus, the displacement of the test plate beneath the spray nozzle can be varied in an accurately controlled fashion. In the present spraying operation, a rotation of 200 steps (i.e. one revolution) was found to be adequate.

3.2.2 Electronic Control of the Spraying Operation

The electronic logic circuit which controls the spraying operation was designed and built by the Instrumentation Department at Cranfield. The unit generated signals which were sent to either the d.c. motor or the stepper motor. The logic of this control unit was activated by the two limit switches. The number of steps advanced by the stepper motor was selected on a counter while the rotational speed of the d.c. motor can be set on a dial.

The sequence of the spraying operation, as controlled by the electronic logic circuit, is as follows :

1. The stepper motor rotated through a previously selected number of steps (200 in these tests) to provide the necessary feed of the test plate. This movement was at right angles to the direction of traverse of the spray head.

2. The 12-v d.c. motor was then energised to drive the carriage and spray head assembly over the test plate so that a thin strip of naphthalene was sprayed on to the plate.

3. The horizontal travel of the carriage was arrested by one of the limit switches and the rotation of the d.c. motor reversed. The carriage thus travelled back to its initial position where it was again brought to rest by actuation of the other limit switch. A second layer of naphthalene was, thus, sprayed on top of the initial strip.

4. The signal from this second limit switch de-energised the d.c. motor and re-started the stepper motor to advance the test plate again. This whole sequence was repeated continually until the required length of the test plate was completely sprayed with a uniform film of naphthalene. Typically, the specific weights of the naphthalene coatings varied from 1.9 to 3.3 mg/cm^2.

Figure 3.2.1 shows a schematic layout of the electronic control system and also illustrates the sequence of the spraying operation. It may be seen that the actual spraying time is only a fraction (approximately 20%) of the complete cycle. The period during which the spray head assembly is stationary at the end of each traverse is sufficiently long for the solvent to evaporate so that the film of naphthalene 'dries out' before further deposition.

3.2.3 Control of the Flow of Fluids

Figure 3.2.2 depicts a diagrammatic layout of the flow circuit. The naphthalene solution consisting of solid naphthalene dissolved in 'Inhibisol' was contained in a pressurised steel bottle having a capacity of five litres. This naphthalene solution was fed through a plastic tube to the central nozzle of the co-axial spray head. Mahmood (Ref. 50) initially used a naphthalene concentration of 200 gms/litre of solvent but encountered problems with clogging of the nozzle. Hence, he resorted to a concentration of 100 gms/litre so as to avoid this problem. In the present series of tests, a concentration of 150 gms/litre was successfully used and a thicker film of naphthalene was obviously obtained.

During initial tests, it was found that fluctuations of air pressure in the naphthalene storage container resulted in an uneven delivery., To overcome this problem, nitrogen (from a portable storage cylinder) maintained at 276 KN/m^2 was used to pressurise the naphthalene solution. A sintered brass filter was included in the naphthalene feed line to prevent blocking of the nozzle by foreign particles. A Rotameter (Fisher Porter FP 1/8 20-G-5/81) was also incorporated to monitor the flow rate. A needle valve (Edwards High vacuum Type EUCO 3) was used to make fine adjustments to the flow of naphthalene solution.

Compressed air at 552 KN/m^2 was supplied through a nylon tube to the annulus of the spray head and once again, a needle valve was used to set and control this flow. The shearing of the liquid 'naphthalene' jet by this blast of air produced a finely atomised conical spray.

3.3 DETERMINATION AND CONTROL OF THE NAPHTHALENE FILM THICKNESS

3.3.1 Measurement of the Naphthalene Film Weight

It is not possible to calculate the specific weight of naphthalene film from a knowledge of the concentration and flow rate of the naphthalene solution because of end effects, i.e. at the end of each traverse, there is a dwell period during which naphthalene is not sprayed onto the plate.

In order to determine the average naphthalene mass concentration over the test surface, four polished plastic thin slides each of 76 mm x 25.4 mm were employed as flush fitting removable plugs. These slides were mounted in-line on an axis parallel to the movement of the spray head (see Fig. 3.3.1). From the weight gained by these slides during the spraying process the naphthalene mass/unit area of the coated surface could be obtained. A sensitive balance with a

resolution of 10^{-4} gms was used to weigh the slides. The variation in the weight of naphthalene sprayed onto the calibration slides during a test was always less than 3% (see Appendix A.5 for a detailed error analysis).

The average 'film weight' or density over the coated surface must be corrected to allow for 'free' convective losses before the mass transfer test. These losses may be split into two components for convenience :

1. A free convective loss occurs throughout the spraying operation and varies linearly over the test plate. This variation of the naphthalene weight/unit area between the first and last layer of sprayed naphthalene was always less than 5%. (A typical variation is shown in Fig. 3.3.2).

and

2. The losses that occur during the period between the completion of spraying and the commencement of the impingement test. This loss applies equally to both the whole test surface and the calibration slides.

These convective losses were found to be temperature dependent and can be estimated from a knowledge of the spray period and the time between the end of spraying and the beginning of the test. The slides were always weighed on two separate occasions separated by an interval of at least 3000 secs to establish the free mass loss rate pertinent to the particular test.

3.3.2 Control of Coating Thickness and Uniformity

The factors which affect the quality and specific weight of the deposited film include :

1. Concentration of the Solution

   The higher the concentration of naphthalene in the solvent, the thicker is the layer of the film on the test plate. As previously mentioned, a concentration of 150 gms/litre of the solvent was found to be satisfactory and did not result in undue blockage of the nozzle.

2. The Solution Flow Rate

   The first consideration when choosing a flow rate is that the solution reaching the test plate should not flow freely over the surface. Even when the solution dries quickly on the plate, the choosen flow rate should not produce a rough surface as this may lead to erosion

instead of sublimation of the naphthalene. A flow rate of approximately 0.2ml/s was found adequate for the present tests.

3. Air Pressure

The pressure of the air supply can affect the fineness of atomisation and inadequate pressure can also result in clogging of the nozzle. Air pressures of 414-552 KN/m^2 produced satisfactory results.

4. Test Surface

Before spraying, the test plate was thoroughly cleaned and polished to remove any dirt or grease which can affect the quality of the film.

5. The Nozzle Geometry

The nozzle was mounted at least 25 mm (i.e. 25 spray nozzle diameters) above the test plate and inclined at 45-60 degrees to the horizontal. This arrangement resulted in a sprayed strip which was considerably wider than the pitch between the adjacent spray passes so that each station was subject to about six passes. In this fashion, an essentially even coating of napthalene was produced on the test surface.

6. Traverse Speed

The effect of various traverse speeds on the displacement of the nozzle assembly is illustrated in Plate 3.2.3. The traverse speed used for the tests was 0.9 m/s. At lower speeds, an excessively thick naphthalene coating or free flow of the solution over the test plate was produced. At higher speeds, inertia effects resulted in a non-uniform motion of the spray head.

7. Stepper Motor Feed Rate

The spread of the naphthalene jet was relatively wide so that the low test plate feed rates resulted in each location on the test plate being subject to numerous spray passes. However, very low feed rates lead to exceptionally long spraying periods with consequent greater variations in the free convective losses that occur during the spraying process. Furthermore, the likelihood of nozzle blockage increases with spraying period. As mentioned earlier, a stepper motor feed of 200 steps was used in all the tests. This stepping rate was equivalent to a linear displacement of 1.6 mm so that a length of 305 mm could be sprayed in 45 minutes.

It should be mentioned that the above factors are not independent, e.g. the delivery rate of the solution cannot be chosen in isolation from the available air pressure, if satisfactory atomisation is to be achieved. Initial trial tests were carried out to establish suitable combinations of these variables to produce the required surface smoothness and thickness of the naphthalene on the test plate.

The consistency of this naphthalene coating was checked by direct measurement. Three rows of calibration slides were fixed on the test surface, as shown in Fig. 3.3.3 and were subsequently coated with a film of naphthalene during a normal spraying operation in which the flow rate of the solution was maintained constant. The free convective loss rate from these slides was determined by weighing them before and after an interval of 3000 secs. The first of these measurements (corrected for free convective losses) was then employed to determine the specific coating referred to a datum position. The difference between the corrected weights is less than · 2% so that the thin film naphthalene is reasonably uniform, see Table 3.3.1

Also, the uniformity of the film was confirmed during initial tests in which the coated surface was exposed to impingement from an unconfined circular air jet placed at z/d of 6. The sprayed plate cleared uniformly starting at the stagnation point, see Fig. 3.3.4. Any inconsistencies in the coating would have produced an uneven naphthalene clearance, see Fig. 3.3.5.

3.4 RECORDING OF THE CLEARANCE PATTERNS

To evaluate the mass transfer coefficients over the sprayed surface, it is essential to record the growth of naphthalene clearance as the mass transfer test progresses. Three different recording techniques were developed, namely :

(i) a photographic method

(ii) tracing of the patterns by hand, and

(iii) measurement of the periods required for clearance to occur at specified locations.

In the photographic method, photographs were taken at suitable intervals during the test. The variation in mass transfer coefficient over the surface was then built up from successive photographs. To reduce costs, clearance patterns were also traced by hand on the rear of the plate and the respective clearance times were noted. Results obtained with this simple technique were compared with those achieved 'photographically' and were found to be in good agreement.

These two recording methods were used for the unconfined inclined jet tests and for the tests involving a circular jet in the presence of a cross flowing stream, since the flow is three-dimensional and the variation in mass transfer is complicated.

Finally, the third method is suitable for either a slot jet (the clearance is a progressive straight line) or an unconfined circular jet. In the latter, clearance is essentially axy-symmetric.

3.5 VARIATION IN THE BOUNDARY CONDITIONS

Wilkie and White (Ref. 75) pointed out that the boundary condition (initially constant naphthalene vapour concentration which is equivalent to constant surface temperature) is modified during a naphthalene thin-film test by the appearance of bare patches. It was concluded that this phenomenon led to an over estimation of the heat/mass transfer coefficients. Neal (Ref. 77) found the bare patch effect to be negligible since it is time dependent and influences any local position for only a relatively short time. This conclusion was partly arrived at because of the good agreement of Neal's results with previously published heat transfer data. In addition Stephenson et al (Ref. 84) modelled the bare patch effect whilst using a finite difference numerical technique to predict tube entrance region heat transfer rates. These calculations indicated that the error introduced by the effect is about 1% and that the heat transfer rate at any station is only substantially affected when naphthalene clearance has moved to within about one tube diameter of that station, see Fig. 3.5.1. The results of Stephenson et al were in good agreement with the measurements of Neal (Ref. 77).

A further numerical calculation was carried out in the present study to check that heat/mass transfer results inferred from the thin film technique are not significantly affected by the movement of the cleared area. The wall jet region is, somewhat, analogous to turbulent flow over a flat plate. Thus, attention was paid to this latter situation since the available heat transfer correlations include the effect of initial unheated portions of the plate. A flat plate with an unheated starting length was thus assumed to be analogous to a partly cleared surface coated with naphthalene provided that the cleared section and the unheated length were of the same dimensions. The heat transfer distribution for turbulent flow over a flat plate with an unheated initial length can be calculated from the expression (Ref. 85) :

$$h = .0287\ Pr^{.6}\ Re_x^{.8} \left[1 - \left(\frac{\Psi}{x/d}\right)^{.9}\right]^{-1/9} \qquad 3.5.1$$

where

Re_x = Reynolds number based on the free stream velocity and the distance 'x'

x = distance downstream of the point of maximum heat transfer

Ψ = Dimensionless length of the unheated portion

When Ψ = 0 in equation 3.5.1, the heat transfer distribution on a completely heated flat plate is obtained.

The effect of a gradual clearance of the naphthalene film on heat/mass transfer at any station can then be assessed as follows :

A time interval (typically, 600 secs for the current mass transfer tests) is chosen to correspond to initial clearance and during this period, the mass transfer coefficient at any station is unaffected by the bare patch. The heat transfer distribution over the flat plate is, thus calculated for this condition. A small time step (50 seconds) is then assumed and the extent of the cleared length calculated. This length is then used to estimate the new heat transfer coefficients at various stations downstream of the cleared portion. Successive repetition of this procedure (until clearance reaches the point being considered) can be used to calculate a 'time-weighted' actual value of the heat/mass transfer coefficient at the particular station. A typical calculation procedure is presented in Appendix A.3.

Figure 3.5.2. shows the effect of bare patch on heat transfer coefficients at various stations. It was found that gradual movement of the clearance boundary only affected the convective transfer coefficient by approximately 2%. Also, this phenomenon was found to be highly localised. See Table 3.5.1. Hence, this bare patch effect was neglected in this current investigation.

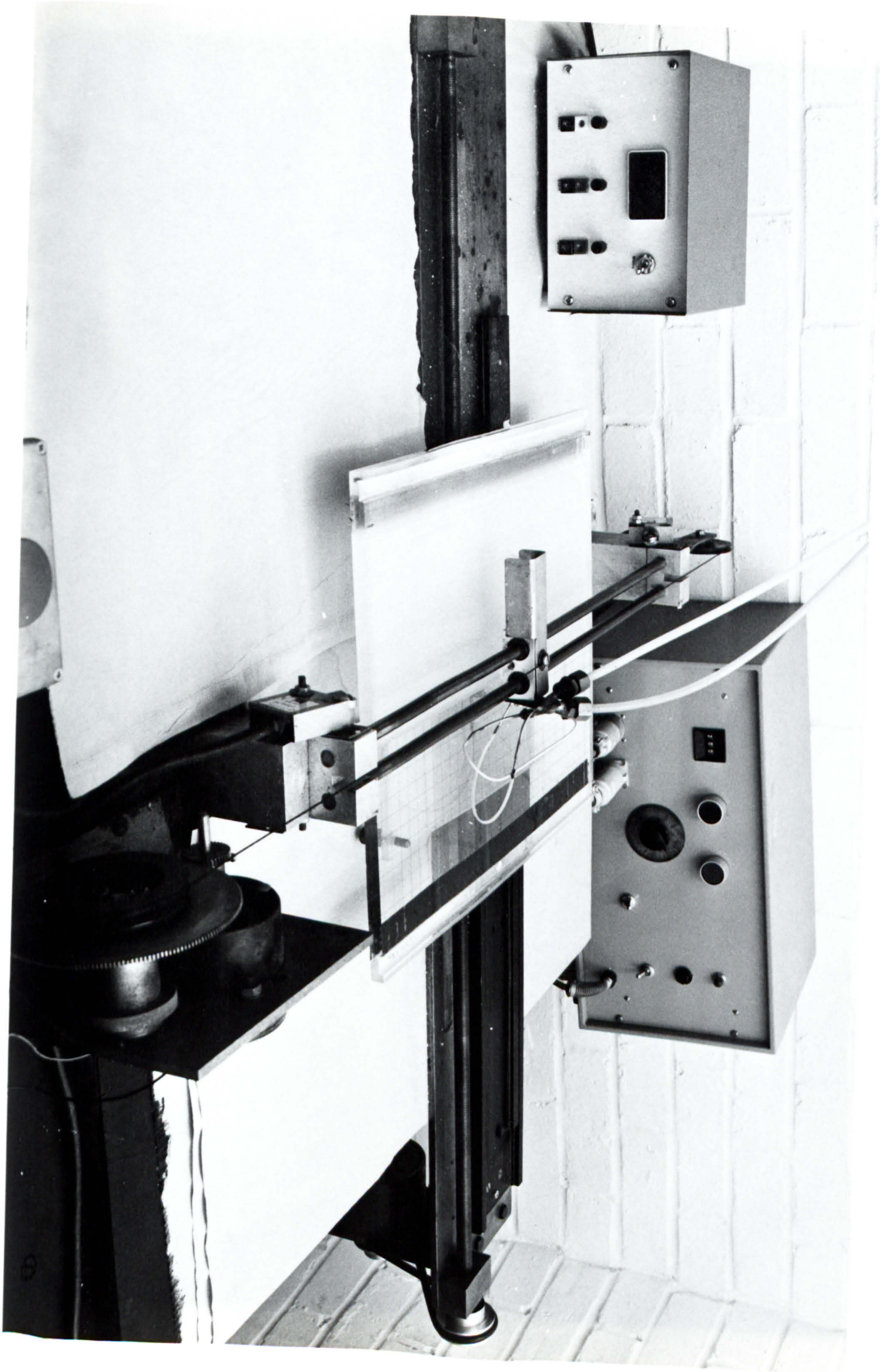

PLATE 3.2.1 THE SPRAY RIG

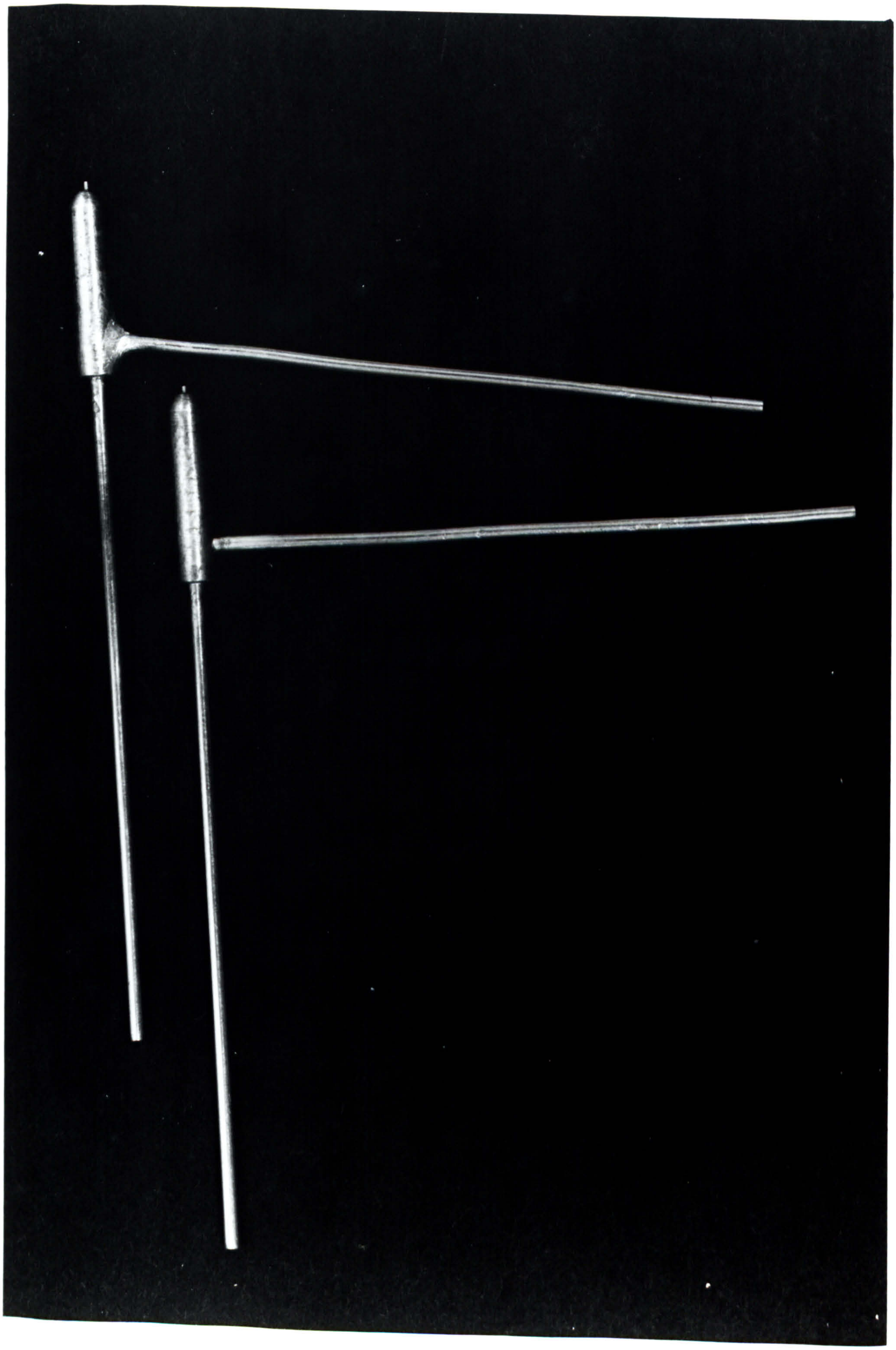

PLATE 3.2.2 THE SPRAY NOZZLE

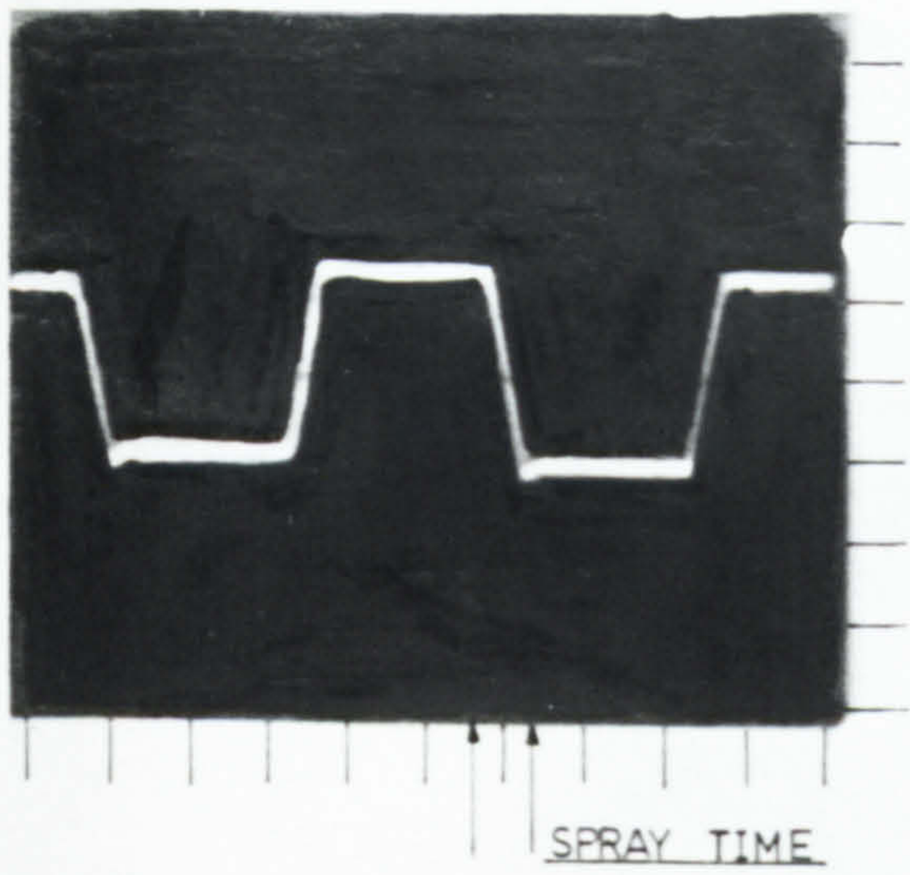

1·0 s / div

SPRAY-HEAD VELOCITY = 0·9 m / s

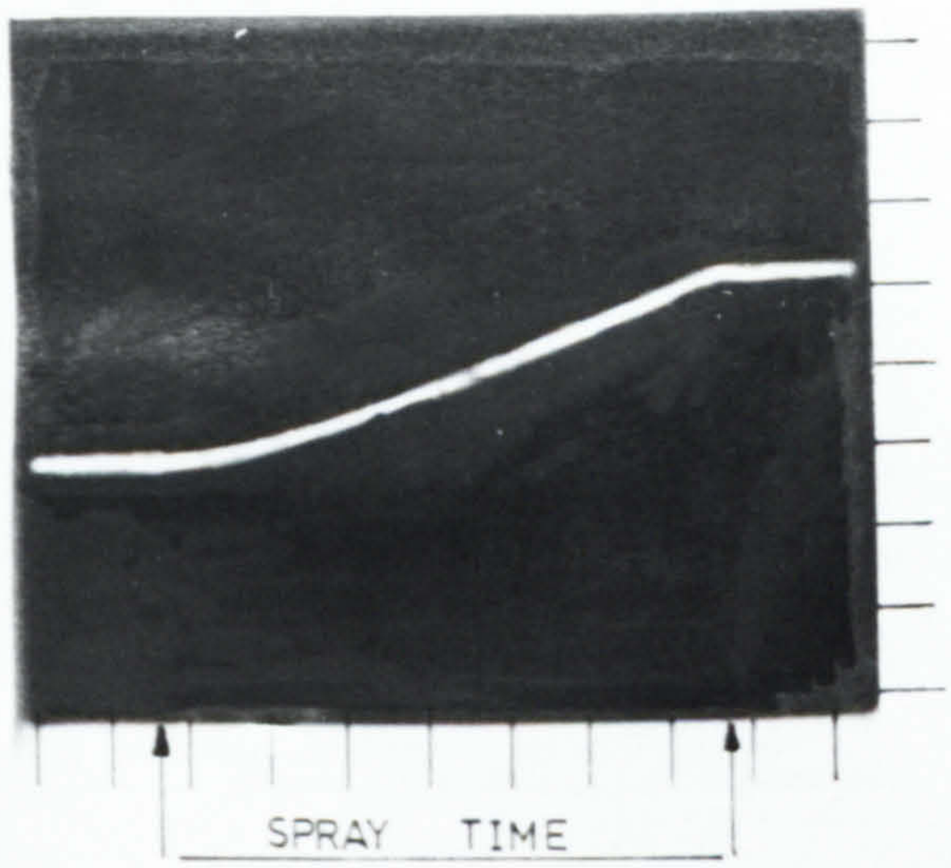

0·1 s / div

SPRAY-HEAD VELOCITY = 0·9 m / s

[NOTE LINEAR TRACE DURING SPRAY]

SPRAY-HEAD VELOCITY OF 0·9 m/s USED FOR ALL TESTS

0·1 s/div

SPRAY-HEAD VELOCITY = 1·2 m / s

[NOTE NON-LINEARITY DURING SPRAY]

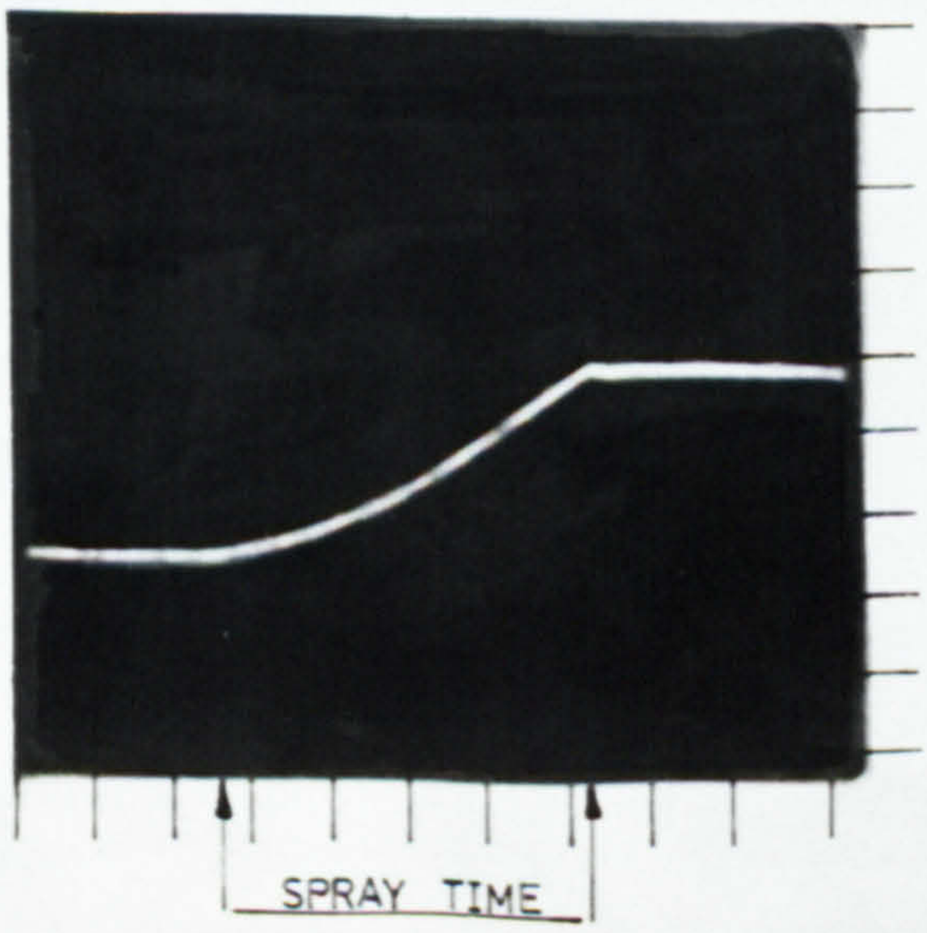

0·1 s / div

SPRAY-HEAD VELOCITY = 0·8 m / s

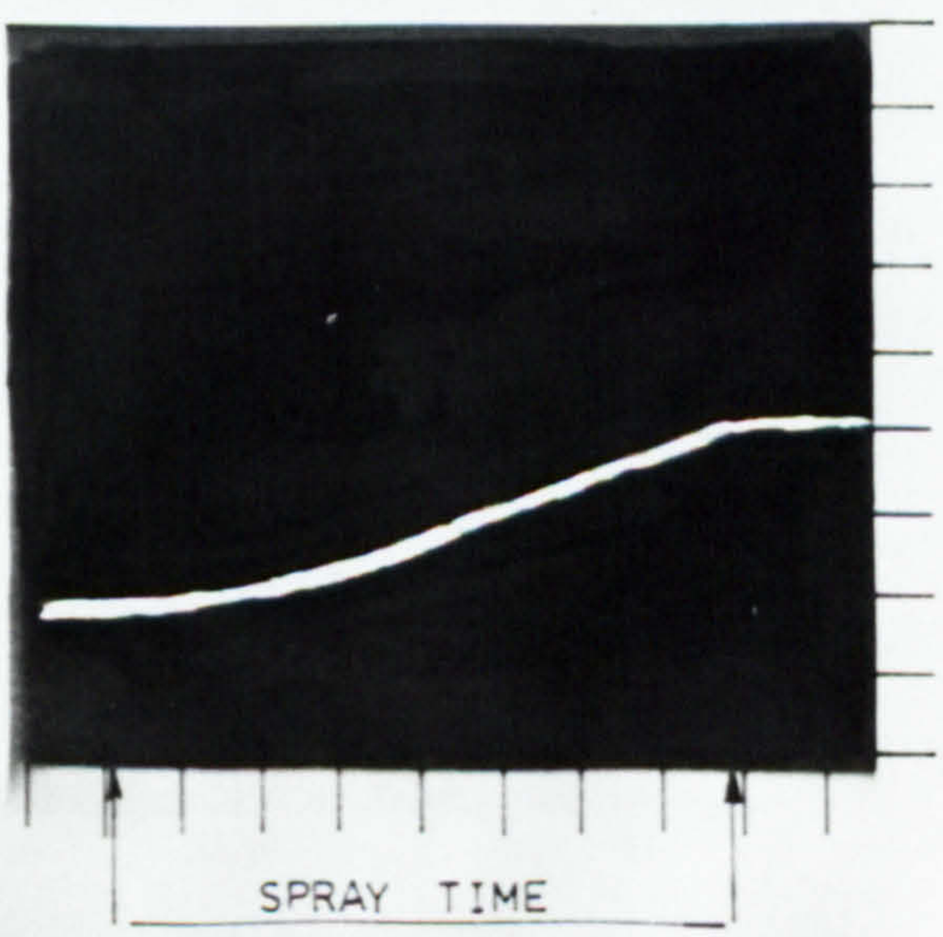

PLATE 3.2.3 DISPLACEMENT TRACES OF THE SPRAY HEAD HEAD AT VARIOUS VELOCITIES.

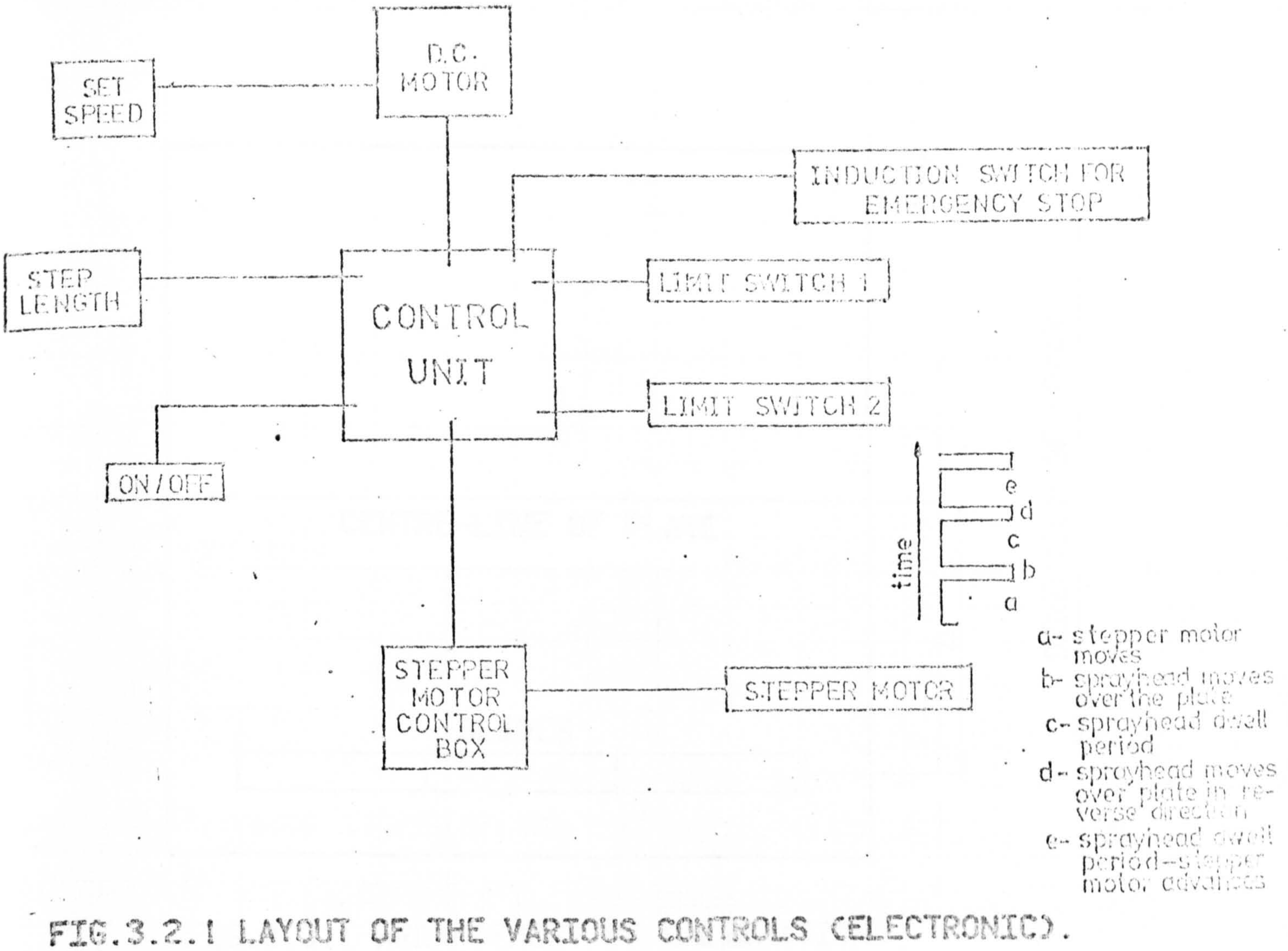

FIG.3.2.1 LAYOUT OF THE VARIOUS CONTROLS (ELECTRONIC).

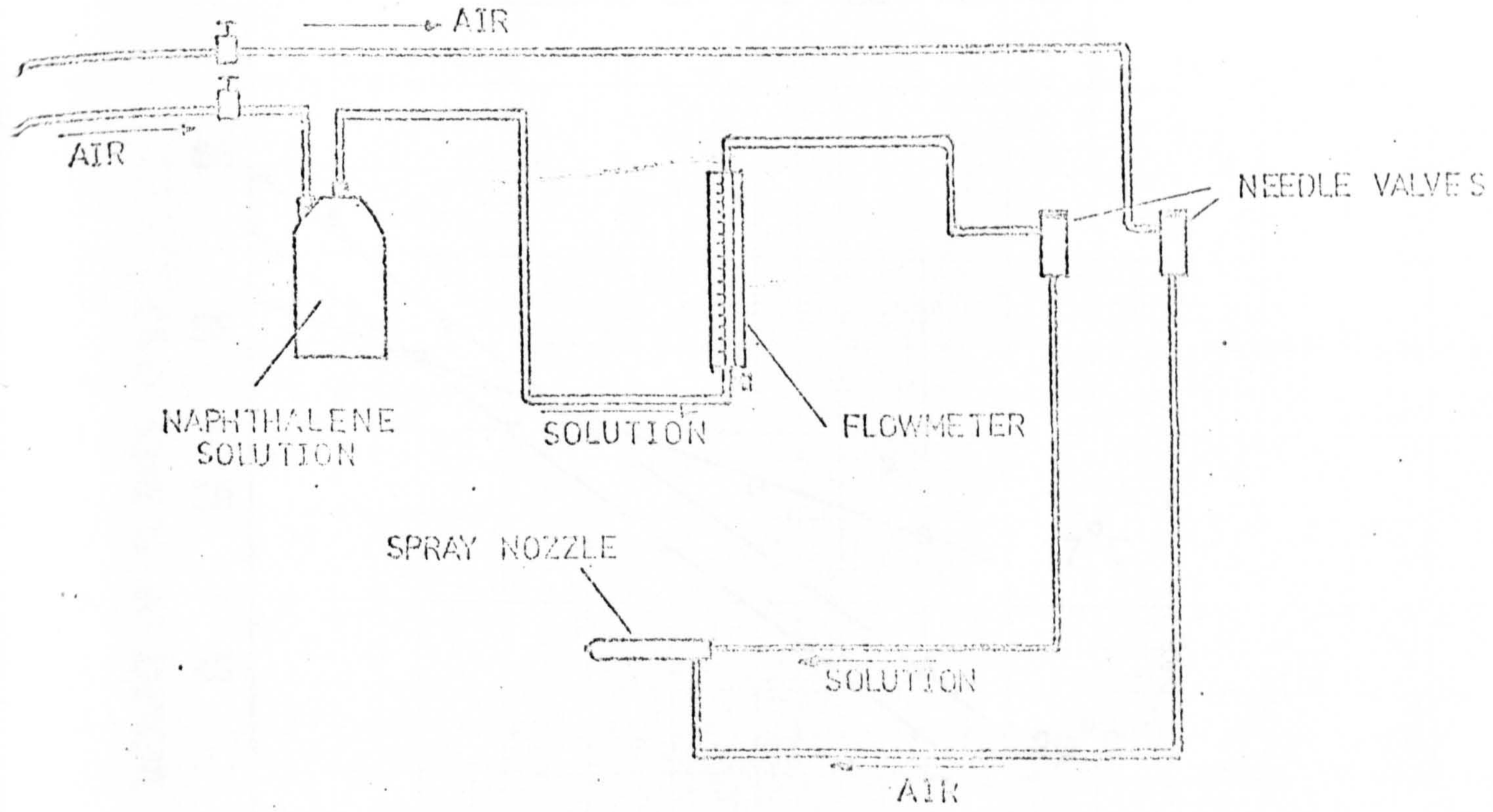

FIG.3.2.2 NAPHTHALENE SOLUTION FLOW CIRCUIT.

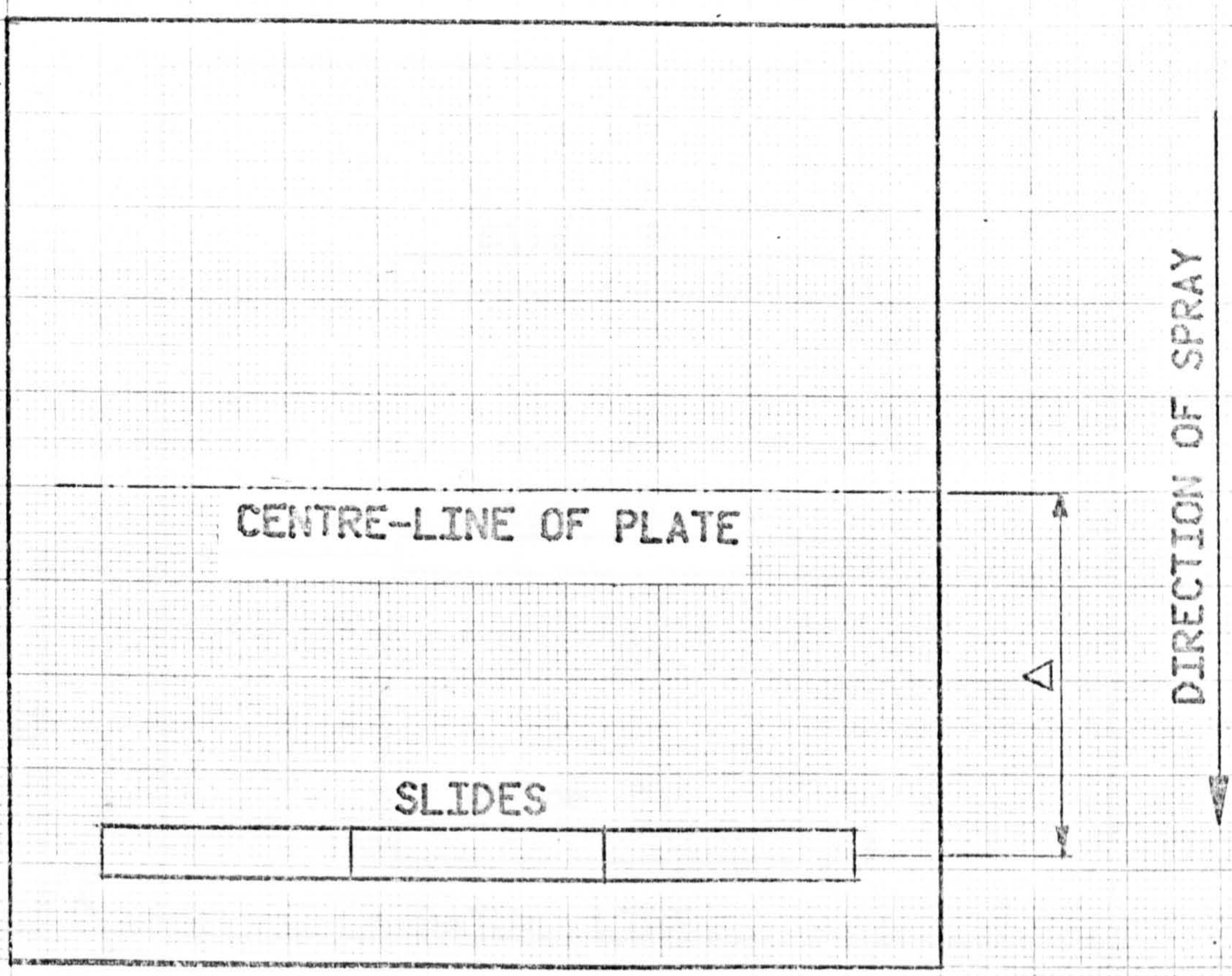

FIG.3.3.1 ARRANGEMENT OF CALIBRATION SLIDES ON THE TEST PLATE.

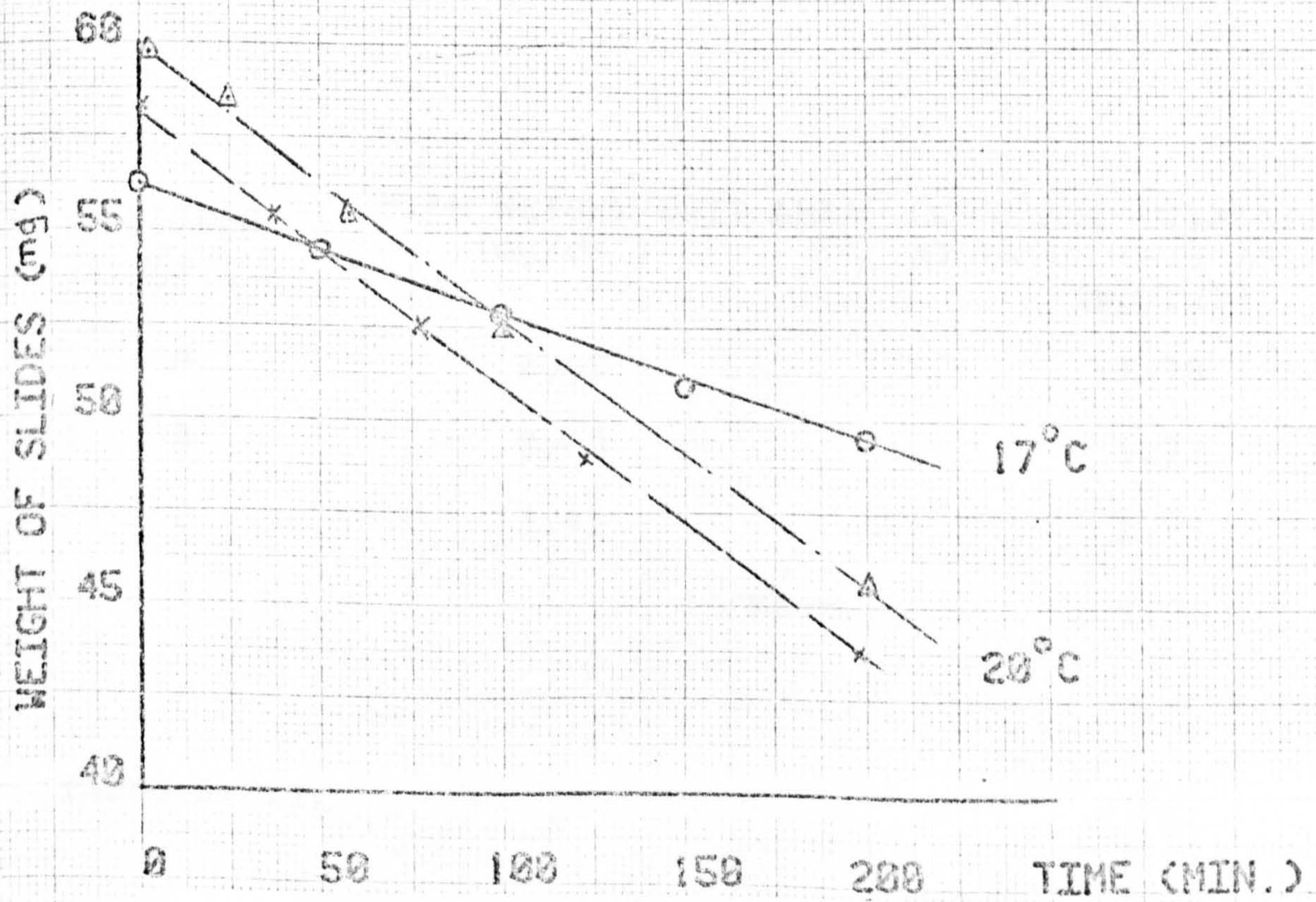

FIG.3.3.2 LOSS OF NAPHTHALENE FROM THE SLIDES DUE TO NATURAL CONVECTION.

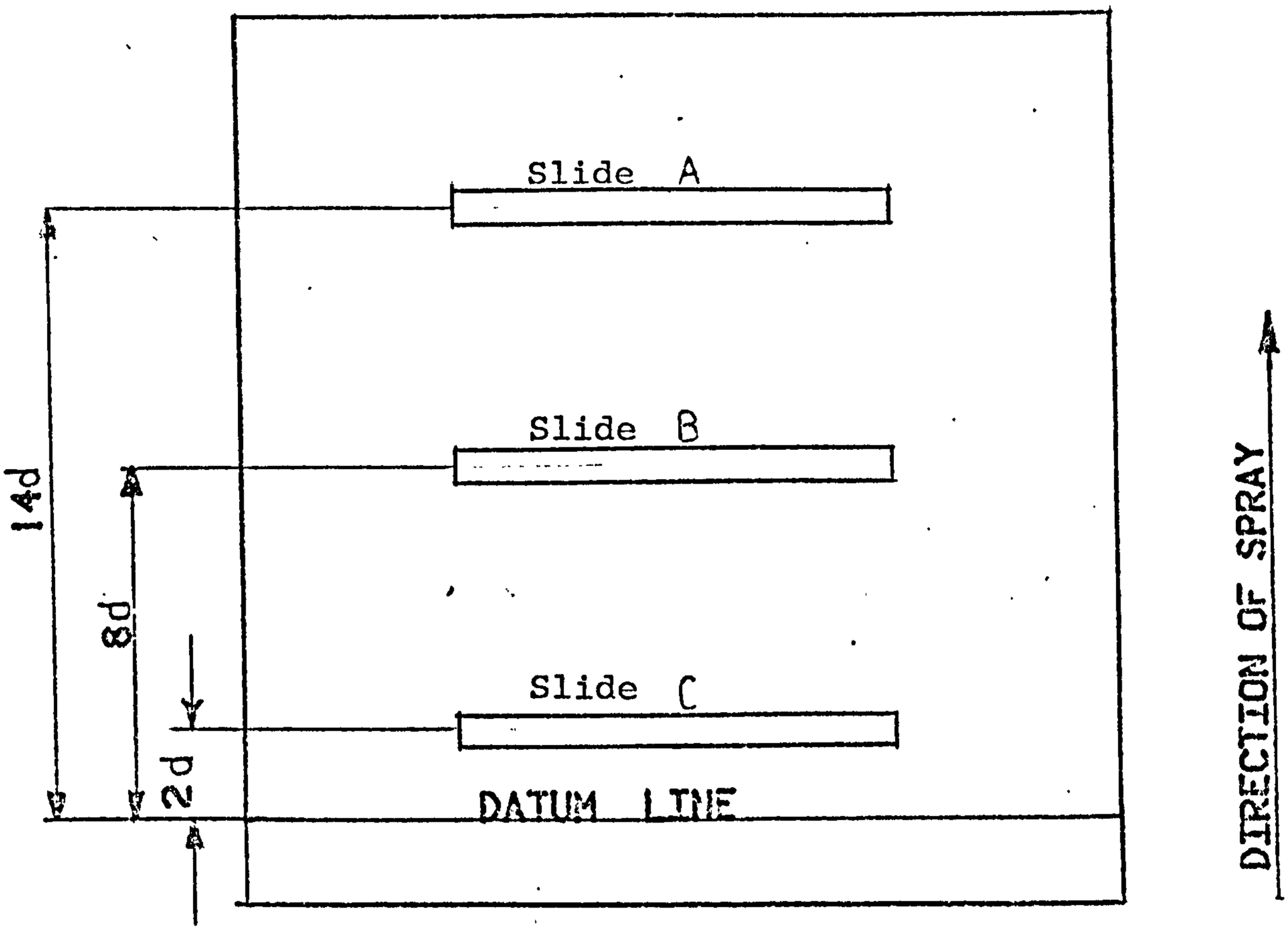

FIG.3.3.3. ARRANGEMENTS OF SLIDES TO CHECK CONSISTENCY OF SPRAYING

SLIDES	FILM WEIGHT/UNIT AREA (mg/cm)	CORRECTED FILM WEIGHT AT DATUM/UNIT AREA (mg/cm)
A	2.63	1.78
B	2.08	1.73
C	1.91	1.75
	Mean	1.76

TABLE 3.3.1.

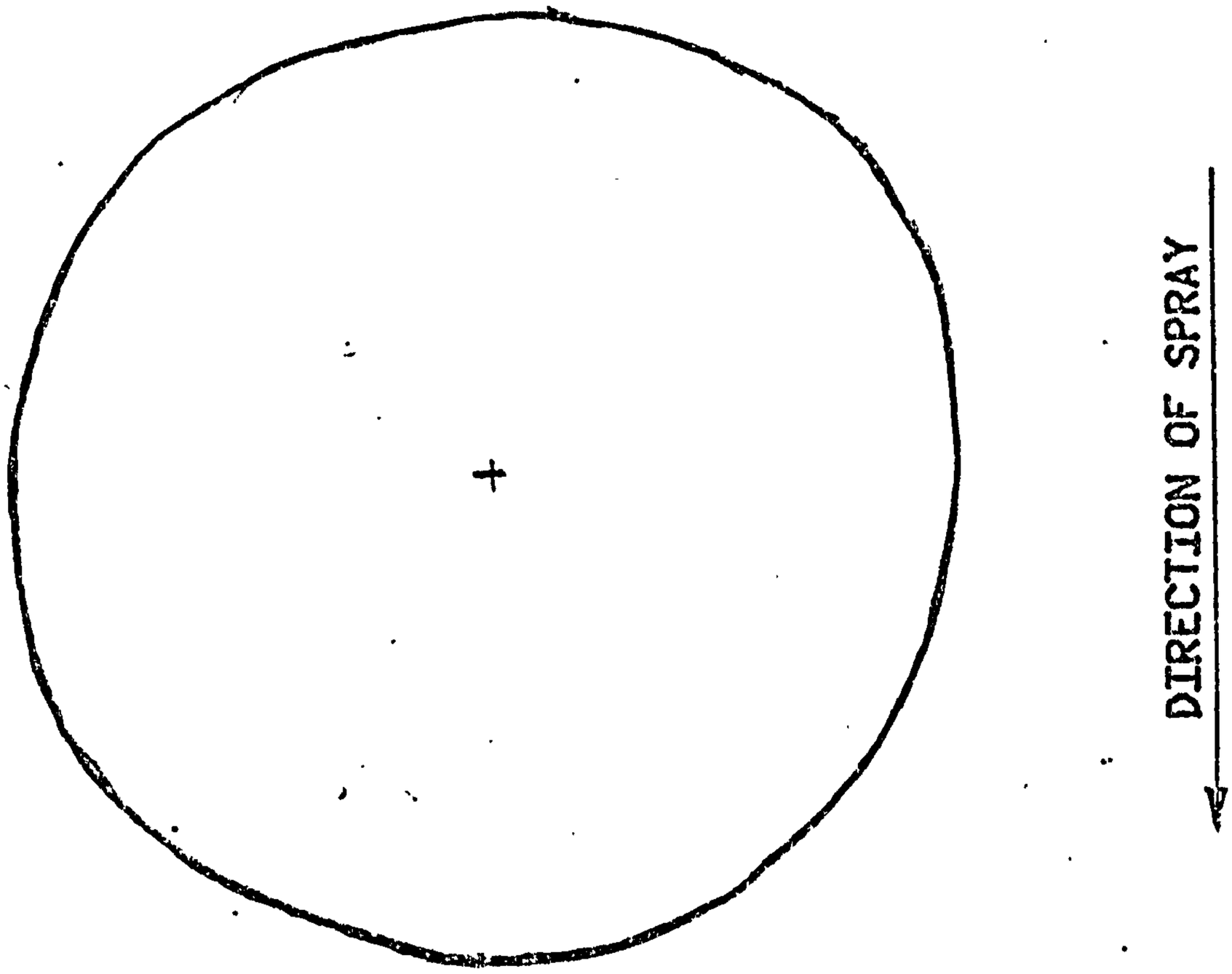

FIG.3.3.4. CLEARANCE PATTERN FOR A UNIFORM SPRAY

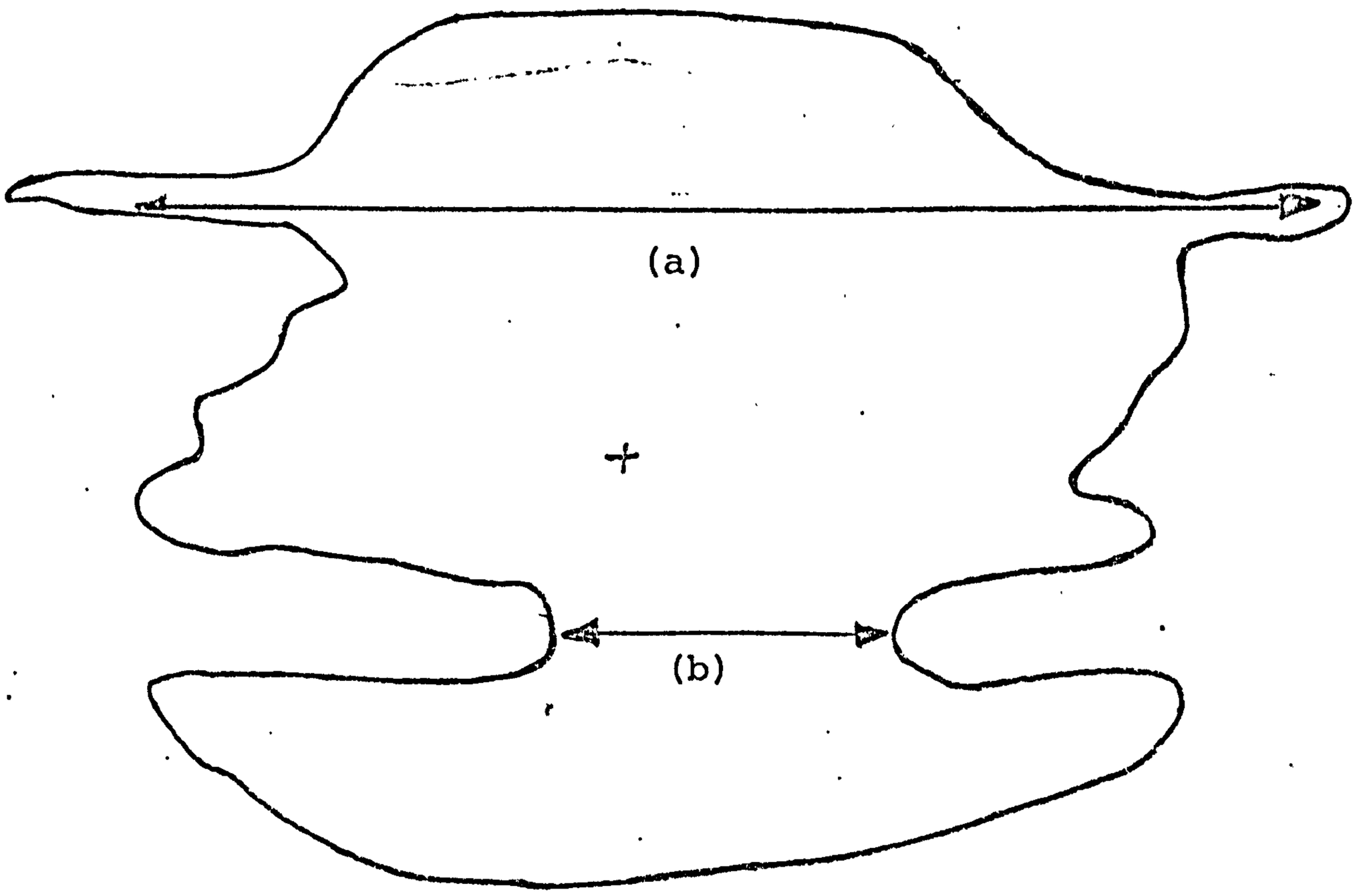

FIG.3.3.5. CLEARANCE PATTERN FOR AN UNEVEN SPRAY
(a) LESS THAN AVERAGE SPRAY
(b) GREATER THAN AVERAGE SPRAY

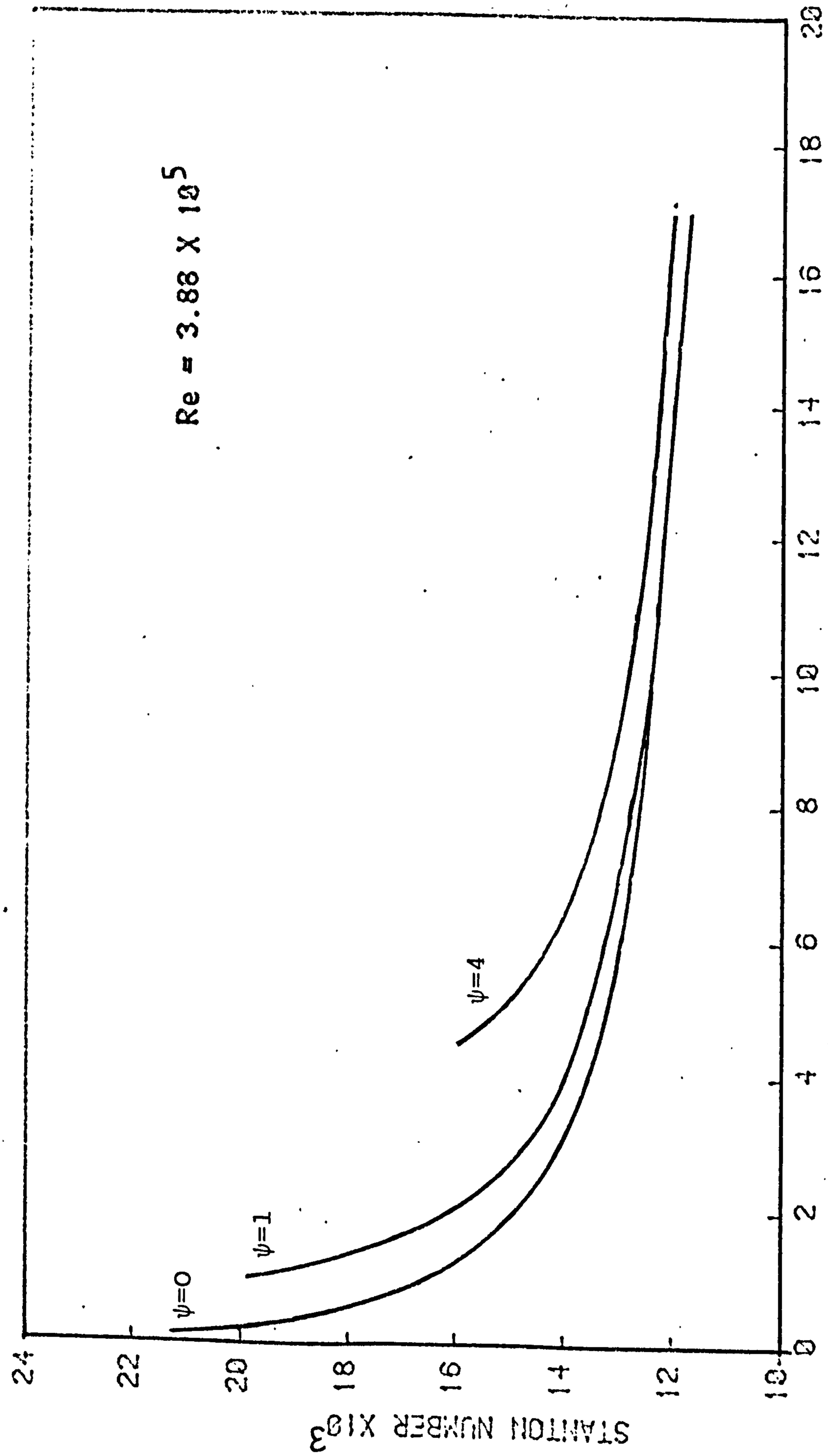

FIG.3.5.1 VARIATION OF MASS STANTON NUMBER FOR A CIRCULAR TUBE WITH VARIOUS UNHEATED STARTING LENGTHS (REF. 64).

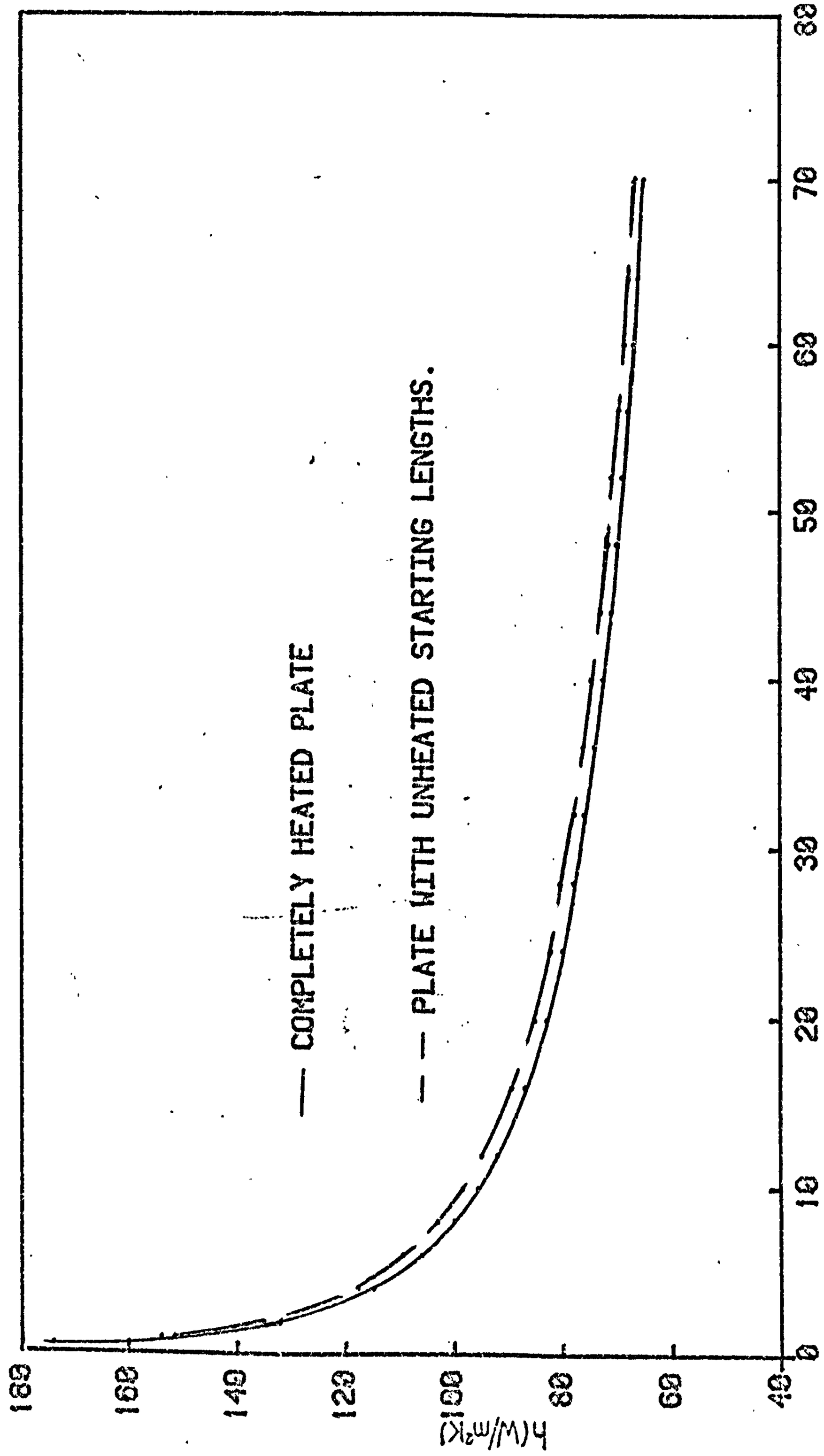

FIG.3.5.2 THE EFFECT OF VARYING NAPHTHALENE BOUNDARY ON HEAT TRANSFER COEFFICIENTS.

x/d	Ψ = 0	0.8	1.6	3.0	5.2	6.6
1	151.8 w/m^{2}K	154.2*				
2	131.9	132.6	135.1*			
4	114.8	115.1	115.8	117.6*		
6	105.9	106.1	106.5	107.3	109.4*	
8	100.0	100.1	100.4	101.0	102.1	103.1*
10	95.6	95.7	95.9	96.3	97.1	97.2
12	92.0	92.1	92.2	92.6	93.1	93.5
16	87.0	87.0	87.2	87.4	87.8	88.0

* Local station most affected by clearance

TABLE 3.5.1 EFFECT OF BARE PATCH ON HEAT TRANSFER COEFFICIENTS

CHAPTER 4

4. FLOW AND HEAT TRANSFER CHARACTERISTICS OF TURBULENT IMPINGING JETS IN 'STAGNANT SURROUNDINGS'

4.1 INTRODUCTION

The fluid dynamic behaviour of impinging jets (and hence their heat transfer characteristics) are complicated and not always completely understood. These jets can be conveniently classified according to :

1. their geometry: jets are usually either circular in cross section, i.e. axisymmetric or are of the long, narrow slot type, i.e. two-dimensional.

2. their surroundings: jets can be unconfined or alternatively they can exit into a restricted space, i.e. they are of the confined type.

and

3. the type of flow: the flow regime can either be laminar or turbulent. Most jets in practical situations are turbulent or alternatively, the initially laminar jet soon becomes turbulent due to mixing and entrainment with the surrounding fluid. The critical Reynolds number (based on jet exit velocity and nozzle diameter or width) for "transition" is approximately 50 (Ref. 86), i.e. jets with Re < 50 always remain laminar. The mixing layers of jets with exit Reynolds number of 50 - 2000, are initially laminar but become unstable and degenerate into turbulence. A jet with a Reynolds number of 2000 - 3000 has a fully developed turbulent core flow whereas at high Reynolds number (i.e. > 14000), the jet may be considered to have a self-preserving far-field.

4.2 THE FLUID DYNAMICS OF ORTHOGONAL TURBULENT IMPINGING JETS

Most previous investigations have dealt with orthogonal impinging jets emerging from either a slot or circular nozzle into an essentially stagnant fluid. The following description deals with (unless otherwise stated) an orthogonal circular jet since this is the type of jet employed in the experimental investigation. The behaviour of two-dimensional slot jets is qualitatively similar in most respects. Fig. 4.2.1 presents schematically the flow field associated with such an orthogonal axisymmetric impinging jet. It is clear that the flow can be divided into the following three main regions :

1. the initial free jet region which is unaffected by the presence of a target surface,

2. the impingement region where the strong, essentially inviscid, interaction of the jet with the target plate produces a change in flow direction,

and

3. the wall jet region which consists of an essentially radial flow over the surface with a gradually thickening boundary layer.

The Free Jet Region

This region can be further sub-divided into flow development, transitional and established flow regimes. On leaving the nozzle, the jet immediately begins to entrain the surrounding stationary fluid. The resultant mixing causes the jet to spread although the intensive turbulent activity at the edges of the mixing layer occurs intermittently. The central core of the jet is not initially affected by these entrainment processes so that the static pressure and velocity remain constant. However, the diameter of this core (referred to as the potential core) continuously decreases along the length of the jet as entrainment proceeds. Eventually, at the end of the potential core, the turbulence generated at the edge of the jet has penetrated to the centre-line and the axial velocity throughout the jet then subsequently gradually decays. The region between the exit of the jet and the end of potential core is known as the flow establishment or development region. Previous workers (Ref. 87 and 88) have found that the length of the potential core varies from 4 to 7.7 nozzle diameters (5 - 12 nozzle widths for slot jets) and that it is independent of jet Reynolds number for fully developed turbulent jets. The discrepancies in the length of the potential core have been attributed to differences in the jet initial conditions (e.g. the exit velocity profile) and turbulence characteristics rather than experimental error.

Beyond the potential core, free shear mixing continues to cause entrainment of the still surroundings with consequent increase in the mass of flow. Since no external forces act on the jet, the momentum of the jet is conserved at all sections downstream of the exit plane. Hence, there is a continual increase in the diameter of the jet and a rapid decay in the axial velocity.

The flow development zone is immediately followed by the transitional region which extends up to a maximum distance of 10 - 12 nozzle diameters from the nozzle exit (for circular jets). In this region, there is a gradual change from the flow development zone to the fully developed turbulent region. It has been found that as the jet Reynolds number is increased, the extent of the transition region decreases.

An established (fully developed) flow region then ensues and exists until the effect of the impingement surface becomes apparent. In the established region, velocity profiles are similar and can be described by relatively simple relationships. For example, the relationship between the local velocity (u) at a radial distance (r) from the axis of the axisymmetric jet, and the maximum velocity (u_m) at that plane is given by (Ref. 89) :

$$\frac{u}{u_m} = \exp\left[-C\left(\frac{r}{z}\right)^2\right] \qquad 4.2.1$$

where c is a constant and varies between 82 and 92 and z is the axial distance from the nozzle exit.

Figure 4.2.2 presents the decay of centre-line velocity for both circular and slot jets. Turbulent mixing is less intense in slot jets than with circular jets and this results in a more rapid decay of velocity in the latter case. The centre line velocity at any downstream location has been found to be given by :

$$u_o \propto z^{-0.5} \quad \text{for slot jets}$$

and

$$u_o \propto z^{-1.0} \quad \text{for circular jets}$$

Thus, for circular jets, Trupel (Ref. 90) experimentally obtained :

$$\frac{u_o}{U_{oo}} = \frac{7.32}{z/d} \qquad 4.2.2$$

and Rajaratnam (Ref. 88) recommended

$$\frac{u_o}{U_{oo}} = \frac{6.3}{z/d} \qquad 4.2.3$$

where

u_o = local centre-line velocity

U_{oo} = jet exit velocity

z/d = non-dimensional distance from the nozzle exit to the particular local point along the jet axis.

The flow characteristics in the free jet region of an impinging jet thus depend on the location of the target surface relative to the jet exit. For example, if the target surface is placed within the potential core length, then the characteristics of the transitional and fully developed flow zones will obviously not be encountered. Thus, the heat transfer characteristics of jets with close nozzle-to-plate separations are especially complicated, although such geometries frequently occur in practice.

The Impingement Region

The jet eventually experiences the influence of the impingement surface at a distance of approximately 1.1 nozzle diameters or widths upstream of the surface. In the so-called impingement region which then ensues, the static pressure rises above the ambient value. Significant pressure gradients are set up and these cause the flow stream lines to turn through 90° to a direction almost parallel to the target surface. The jet centre-line velocity finally falls to zero at the impingement point where the pressure attains the maximum stagnation value. In 1964, Schauer (Ref. 91) calculated the width (x_p) of the surface area associated with the impingement region for a two-dimensional jet to be equal to

$$x_p/b = 0.308\ z/b \qquad 4.2.4$$

where

b = width of the nozzle

x_p = transverse extent of the impingement region with centre at the stagnation point.

More recently, Dawson and Trass (Ref. 92) used a similar technique and suggested that the radial extent (also usually loosely called "the impingement region") of the impingement region of an axisymmetric circular jet can be empirically described by :

$$r_p/d = 0.284\ z/d \qquad 4.2.5$$

where

r_p = radial extent of the impingement region

The Wall Jet

At the end of the impingement region, the static pressure drops back to the ambient value and a radial wall jet region (in the case of circular impingement) ensues. A boundary layer builds on the impingement surface and this can be divided into two parts: the outer and inner layers. The outer layer resembles half a free turbulent jet flow while the inner layer grows from the stagnation point beneath this outer layer. Over a near stagnation region of 1.2 nozzle diameters, the inner boundary layer has a constant thickness (Ref. 93) before growth occurs over the impingement surface. The boundary between the two layers is associated with the maximum or peak velocity in the wall jet. It has been found by Bakke (Ref. 94) that this maximum velocity can be deduced from :

$$u_m = \frac{\psi}{(r_w)^n}, \qquad 4.2.6$$

where

r_w = radial distance (mm) from the stagnation point.

n = a constant and lies between 1.1 and 1.14

ψ = a constant (9.33 approximately)

4.3 OBLIQUE JET IMPINGEMENT

The cross section of a jet at the exit plane of an oblique nozzle can be either axisymmetric or elliptical. The latter shape is obtained when the initially circular nozzle is cut off flush with the nozzle carrier plate. See Fig. 4.3.1.

The flow regions described in the last section also exist in the case of an obliquely impinging jet. However, whilst for the orthogonal impingement of a circular jet the fluid flow is completely symmetrical, this is not entirely so in the 'oblique' case, where symmetry has been found to exist only in the free jet zone (Ref. 95). Near the impingement surface, the fluid streamlines divide unequally so that the stagnation point is shifted away from the geometric axis of the nozzle (see the schematic representation in Fig. 4.3.2). Schauer (Ref. 91) obtained an expression for this displacement of the stagnation point for a two-dimensional slot jet, thus :

$$\frac{\delta}{b} = 0.154 \cot(\alpha)\, z/b \qquad 4.3.1$$

where

δ = the displacement of the stagnation point.

α = the nozzle inclination (see Fig. 4.3.2)

Although, a similar displacement has been found to occur with circular jets (Ref. 23), a similar expression to equation 4.3.1 does not exist.

Understandably, the flow associated with impingement of a jet of elliptical cross section is unsymmetrical. However the flow regimes discussed above can be expected.

It should also be obvious that the flows in both the impingement and wall jet zones associated with oblique nozzles vary with circumferential position.

4.4 TURBULENCE

It has been established that the magnitude of the turbulence intensity in the flow can significantly affect heat transfer characteristics of impinging jets (especially over the area associated with the impingement region). The earliest centre-line turbulence measurements were probably published by Corrsin (Ref. 96). Some of the results for tests carried out at a jet Reynolds number of 17500 are presented in Fig. 4.4.1. It is apparent that the turbulence intensity (based on the maximum jet velocity at exit, U_{oo}) gradually increases up to an axial distance, z/d, of approximately 8 and then subsequently decreases. However, when the local maximum velocity, u_o, at the measuring station is used as the reference, the turbulence intensity increases sharply in the jet initial region ($z/d < 10$). Beyond this distance, the turbulence intensity continues to increase but only at a moderate rate. See Fig. 4.4.1. Thus, it is important that the reference velocity must be specified in any data quoted for turbulence intensity.

More recently, Boguslawski and Popiel (Ref. 97), Donaldson et al (Ref. 98) and Rodi (Ref. 99) have published details of both radial and axial distributions of mean velocity, and turbulence intensities of free circular turbulent jets. Their results are broadly in agreement with those of Corrsin. These authors may be consulted for more details on this subject.

4.5 JET IMPINGEMENT HEAT TRANSFER

4.5.1 Introduction

The results of a comparatively large number of experimental investigations of both local and average heat transfer in jet impingement systems have been published. The geometries studied have included both circular, and two-dimensional slot jets and these have been employed in single and multiple jet systems. Normal impingement has received most attention although a few publications have dealt with inclined jets. Jet impingement heat transfer results can usually be correlated in the form :

$$Nu = hd/k = \beta\, Re^{m}\, Pr^{1/3}\, G(\text{geometry})^{n} \qquad 4.5.1$$

where

β, m and n are constants whose values depend on the particular experimental results. The geometrical function is also non-dimensionalised for homogeneity of the expression 4.5.1

Nu = the Nusselt number

The complicated flow phenomena of impinging jets usually produce considerable variations in the associated convective transport coefficients. Generally, high heat transfer is obtained in the near stagnation region and this subsequently decreases in the radial direction. In general the magnitude of the heat transfer rates decrease with increasing z/d. Furthermore, at low z/d's ($z/d < 4$), the location of the maximum heat transfer is displaced from the nozzle centre line. Typical heat transfer plots are reproduced in Fig. 4.5.1

Since this thesis is mainly concerned with heat transfer rather than fluid flow aspects of jet impingement, it is now relevant to include a review of the more important publications dealing with jet impingement. The papers reviewed in this section are chosen for either their relevance to the present investigation or their contribution to the understanding of the characteristics of impinging jets. In the main, only single circular jets are discussed so that two-dimensional slot jets and multiple jets are only included when they add to the basic understanding of jet impingement. More comprehensive reviews can be found in Arganbright and Resch (Ref. 13), Becko (Ref. 100) and Martin (Ref. 101).

4.5.2 Orthogonal Jet Impingement Heat Transfer

1. Local Heat Transfer

Gardon and Cobonpue (Ref. 102) studied the heat transfer coefficients beneath single turbulent circular jets and varied the following parameters: $0.25 \leqslant z/d \leqslant 50$, $7 \times 10^3 \leqslant Re_d \leqslant 1.12 \times 10^3$ and 2.3 mm $\leqslant d \leqslant$ 9 mm. Local heat transfer rates were measured with a heat-flow transducer (i.e. a so-called Gardon gauge, see Ref. 39 for details). For their fully developed turbulent jet, the stagnation point Nusselt numbers were found to depend on Reynolds number, nozzle to target distance and nozzle size, see Fig. 4.5.2. It may be anticipated that any effect of nozzle size on heat transfer coefficients will disappear by presenting the data in the form of Nusselt numbers but this is contrary to the experimental results especially at $z/d < 20$. Though Gardon and Cobonpue could not explain why nozzle diameter affected the variation of Nusselt number, later studies (e.g. Ref. 103) suggest that it may be due to changes in the initial turbulence levels in the jets. The stagnation point heat transfer coefficients exhibited minima at z/d of 0.5 and maxima at a z/d of between 6 and 7. When $z/d < 0.5$, a wall jet (Ref. 104) is formed with a corresponding general increase in heat transfer. Thus, z/d of 0.5 represents the minimum separation distance to obtain an impinging jet. The location of maximum heat transfer can be associated with the region of high turbulence intensity on the jet axis.

The results (at $z/d > 20$) were correlated by :

$$Nu_o = \frac{hd}{k} = 13\, Re_d^{0.5}\, (z/d)^{-1} \qquad 4.5.2$$

where

Nu_o = stagnation point Nusselt number and

Re_d = Reynolds number based on exit velocity and nozzle diameter.

and is valid for $Re_d > 14000$

Generally, local heat transfer coefficients decreased rapidly as the radial distance increased. For low values of separation distances (i.e. $z/d < 4$), well defined secondary peaks occurred (at $r/d = 2$ approximately) in the radial variations of heat transfer. These were originally attributed to a transition from laminar to turbulent flow in the wall jet region. Subsequently, however, it is considered that other influences such as laminarisation, or streamwise curvature may also be important. It is pertinent to mention here that secondary peaks are also found in multiple jet systems. In the latter situation, however, the secondary peaks occur mid-

way between adjacent nozzles and have been attributed to the interaction of the wall jets. See Gardon and Akfirat (Ref. 103)..

Rao and Trass (Ref. 105) employed a profilometric mass transfer technique to determine local mass transfer coefficients beneath an impinging turbulent jet of water. The jet Reynolds number and the separation distance (z/d) were respectively varied from 2.5×10^4 to 1.25×10^5 and 0.2 to 19.23. A coating of trans-cinnamic acid was obtained by pouring molten liquid uniformly over the target plate. The surface was finally smoothened with emery paper. A thickness gauge (with an accuracy of 0.0025 mm) was used to obtain four different profile measurements (the scatter was about 10%) at each radial station. The difference between the readings obtained before and after each test was used to calculate local mass transfer coefficients.

Figure 4.5.3 shows a typical variation of mass transfer and it is obvious that for r/d > 4.5, the local Sherwood number is independent of the separation distance, z/d. Their results were correlated by :

$$Sh_d = \frac{k_L d}{\mathfrak{D}} = 1.3\ Re_d^{0.84}\ \left(\frac{r}{d}\right)^{-1.27} \qquad 4.5.3$$

where

Sh_d = local Sherwood number

k_L = local mass transfer coefficient

$\mathfrak{D}$ = mass diffusivity

and is valid for r/d > 4.5 and Schmidt number, Sc, = 900

Equation 4.5.3 can be converted to heat transfer by invoking the Chilton-Colburn analogy discussed in Chapter 2. Although, the location of maximum convective transfer is quantitatively similar to that of Gardon and Cobonpue (Ref. 102), secondary peaks reported in the latter studies were not, however, observed by Rao and Trass.

Recently, Vallis et al (Ref. 49) used an electrochemical technique to infer the heat transfer coefficients from submerged liquid jets. Three different nozzle diameters (3 mm, 6 mm and 9 mm) were employed. The stagnation point heat transfer results were correlated by :

$$Nu_o = 1.93\ Re_d^{0.58}\ (z/d)^{-0.74}\ Pr^{1/3} \qquad 4.5.4$$

valid for $3880 < Re_d < 23000$

and $10 < z/d < 20$

The values of the stagnation point Nusselt numbers obtained with expression 4.5.4 fall between the results of other workers, see Fig. 4.5.4. However, the exponents for Re and z/d are somewhat different. For example, the exponents on z/d are respectively -1.0 and -0.74 for Gardon and Cobonpue (Ref. 102) and Vallis et al. The variations were attributed to differences in the test conditions.

The difficulties associated with the measurement of stagnation point heat transfer rates can lead to large errors. It is thus often more convenient to report the heat transfer over an "impingement region" which can be defined by equation 4.2.5. Vallis et al thus obtained a correlation for this region so that :

$$\overline{Nu}_D = 0.225\ Re_D^{0.68}\ Pr^{1/3} \qquad 4.5.5$$

and is valid for $2 < D/d < 16$

$$5675 < Re_d < 20680$$

and $12 < z/d < 20$

where the characteristic dimension in $\overline{Nu}_D$ is the target diameter, D

Re_D = Reynolds number based on arrival velocity and the target diameter

D/d = the diametral ratio between the effective target surface and the nozzle.

For the same range of validity, these results were, however, lower than those of Gardon and Cobonpue.

To summarise the foregoing discussion, the main heat transfer characteristics of impinging jets have been identified. The variations in different studies are, however, large (±35% approximately), see Fig. 4.5.4. Heat/mass transfer correlations have been obtained for near-stagnation, impingement and wall jet regions by using different experimental techniques.

2. Effect of Turbulence on Heat Transfer Rates

Gardon and Akfirat (Ref. 106) studied the influence of different levels of turbulence on heat transfer from slot jet systems. The test conditions were: 1.58 mm $\leqslant$ b $\leqslant$ 6.35 mm, $2 \leqslant z/b \leqslant 32$ and $450 \leqslant Re_b \leqslant 11000$. Various levels of turbulence were obtained by altering the axial position of a mesh screen placed in front of the nozzle. It was found that

up to z/b = 8, the stagnation point heat transfer increased considerably (by a maximum of 41%) as the turbulence at the nozzle exit increased from 2.5% to 18%. The effects of artificially promoted turbulence were especially significant at low nozzle to impingement surface spacings, see Fig. 4.5.5.

Hoogendorn (Ref. 107) also studied the effect of different levels of jet turbulence on convective transfer coefficients at the near stagnation zone. Liquid crystals were employed to determine local heat transfer coefficients due to the impingement of a circular jet onto a plane surface. The nozzle diameter was fixed at 57 mm and wire grids were employed to increase the fluid jet primary turbulence level at the exit plane. It was concluded that when turbulence effects are considered, then the stagnation point heat transfer could be expressed as :

$$Nu_o \, Re_{a,d}^{-0.5} = 0.65 + 2.03 \left(\frac{Tu \, Re_{a,d}^{0.5}}{100}\right) - 2.46 \left(\frac{Tu \, Re_{a,d}^{0.5}}{100}\right)^2 \qquad 4.5.6$$

and is valid for

$$Pr = 0.71$$

$$1 < z/d < 10$$

$$2 \times 10^4 < Re_{a,d} < 9 \times 10^4$$

and $9\% \leq Tu < 20\%$

where

$Re_{a,d}$ = Reynolds number based on arrival velocity and nozzle diameter.

Tu = turbulent intensity based on the main velocity component.

The scatter of the data around the recommended equation is however appreciable (i.e. < 20%).

Similar effects were observed by Kataoka and Mizushina (Ref. 108) who employed an electrochemical technique and a submerged jet which issued from a 10 mm diameter nozzle. The jet Reynolds number and nozzle to target spacing were varied from 2×10^3 to 3.6×10^4 and 3.86 to 8.5 respectively.

The location of the secondary peaks differs from that found by earlier investigators (e.g. Gardon and Cobonpue). For example, at z/d = 3.86, the secondary peak occurs respectively at r/d = 4 and 2 for Kataoka and Mizushina and Gardon and

Cobonpue respectively. The variations were essentially attributed to differences in the measuring techniques.

3. Average Heat Transfer

The mean heat transfer coefficient can be obtained either by direct measurement or alternatively by integrating measured local values over a specified region. Thus,

$$\bar{h} = \frac{1}{A} \int_A h dA \qquad 4.5.7$$

Thus the area of integration can markedly affect the value of the mean convective transfer coefficients. It is, therefore, important that the target area must be specified or is, at least, implicit in any experimental correlation. For example, Vallis et al (Ref. 49) published expressions for different target areas,

$$\overline{Nu} = 0.81\ Re_d^{0.68}\ (\frac{d}{D})^{0.32}\ (z/d)^{-0.68}\ Pr^{1/3} \qquad 4.5.8$$

valid for $2d < D < 16d$

and

$$\overline{Nu} = 85.5\ Re_d^{0.68}\ (\frac{d}{D})^{2}\ (z/d)^{-0.68}\ Pr^{1/3}$$

$$+ 0.27\ Re_d^{0.82}\ (\frac{d}{D})^{2}\ \left[D/d - 16\right]\ Pr^{1/3} \qquad 4.5.9$$

valid for $16d < D < 34d$

$12 < z/d < 20$

and $5675 < Re_d < 20682$

Metzger (Ref. 109) who was interested in localised cooling of electronic components determined the average impingement heat transfer coefficients from a slot jet for the following test conditions: $3 \leqslant z/b \leqslant 20$, $3000 \leqslant Re_y \leqslant 10000$ and $0.25\ mm \leqslant b \leqslant 2.03\ mm$. A direct heat transfer technique was employed and this consisted of measurement of the transient variation in plate temperature due to the impinging jets. It was observed that the average heat transfer coefficients reached a peak at $z/b = 8$ and that they also decreased monotonically

with increasing target surface area. The data were correlated by :

$$\overline{Nu}_y = 0.74\ Re_y^{0.566}\ Pr^{0.37}\ (l/2b)^{-0.434} \qquad 4.5.10$$

and this is valid for $7 < z/b < 10$

and $3 < l/b < 50$

where the characteristic dimension in $\overline{Nu}_y$ and Re_y is the hydraulic diameter and

l = length of the rectangular target

The effect of changes in the nozzle exit velocity profile was found to be rather small. Tests were also carried out with circular nozzles (5 mm in diameter) and the average heat transfer characteristics were similar to those of two-dimensional slot jets.

Gardon and Akfirat (Ref. 103) measured the heat transport coefficients for both single and multiple slot jet impingement systems. The range of variables investigated included : $0 \leqslant z/b \leqslant 60$, $6 \times 10^3 \leqslant Re_{a,x} \leqslant 6 \times 10^5$ and $16 \leqslant x/b \leqslant 64$.
The direct heat transfer technique employed earlier by Gardon and Cobonpue (Ref. 102) was used and the results for the jet arrays were correlated by :

$$\overline{Nu}_x = 0.36\ Re_{a,x}^{0.62} \qquad 4.5.11$$

valid for $Re_b > 2000$ and $z/b > 8$

where the characteristic dimension in $\overline{Nu}_x$ is the nozzle pitch.

$Re_{a,x}$ is based on arrival velocity and the nozzle pitch.

Re_b is Reynolds number based on nozzle exit conditions.

Interaction of the wall jets in multiple system was discussed previously and it is obvious that the value of nozzle pitch and separation distance affect the variation of local, and, hence, average heat transfer coefficients. For example, at $z/b > 4$ and $x/b > 32$, the jets maintain their essential individual identity so that the average heat transfer is comparable to that obtained for single jet impingement. At $x/b = 16$ and $z/b > 40$, jet interaction prior to impingement is severe (i.e. the jets join together and completely loose their individual identity). There is a corresponding reduction in the mean heat transfer although the local distribution at such geometries is virtually uniform over the test surface.

The average heat transfer coefficients for a single slot jet were found to be less dependent on the separation distance as the target surface area increased. Furthermore, distinct maxima were obtained for this system geometry. Tests were also carried out with circular jets (12.5 mm in diameter) at a Reynolds number of 20600. Average heat transfer results for this single circular jet impinging on to a round target plate were expressed as :

$$\overline{Nu}_d = 0.78\ Re_{a,d}^{0.55}\ \left(\frac{d}{D}\right)^{0.45} \qquad 4.5.12$$

valid for $Re_d > 2000$, $z/d > 12$

$Re_{a,D} > 10^4$ and $1 > D/d > 24$

where

the characteristic dimension in $\overline{Nu}_d$ is the nozzle diameter.

$Re_{a,d}$ is based on arrival velocity and nozzle diameter.

$Re_{a,D}$ is based on arrival velocity and target diameter, D.

Equation 4.5.12 agrees with the data of other workers (e.g. Metzger (Ref. 109)). The average heat transfer coefficients did not, however, exhibit any maxima corresponding to those found for slot jets. Although Gardon and Akfirat did not explain these phenomena, the variations in the two jets may be attributed to differences in their turbulence characteristics. Turbulence is less severe in two dimensional slot jets so that the lateral variation of heat transfer reduces only gradually when compared to the circular jets.

Huang (Ref. 110) investigated orthogonal impingement of single axisymmetric jets onto flat surfaces. A direct heat transfer technique was used and the measurements covered $10^3 \leqslant Re_{a,d} \leqslant 10^4$, $1 \leqslant z/d \leqslant 12$ and 3.2 mm $\leqslant d \leqslant$ 6.35 mm. Average convective transfer coefficients were measured and the results were expressed as :

$$\overline{Nu}_d = 0.018\ Re_{a,d}^{0.87}\ Pr^{1/3} \qquad 4.5.13$$

This was considered to be valid for $1 < z/d < 10$ and D/d of 0 to 40. It must, however, be mentioned that Huangs' measurements were obtained on large target areas and thus the effect of 'd/D' was not included in the correlation equation. It was found that the average heat transfer coefficients were about 25% less than the corresponding local centreline values in the range of validity of the expression.

More recently, Koopman and Sparrow (Ref. 66) employed the sublimation of naphthalene to investigate the convective transport coefficients due to the impingement of a row of circular jets on a plane target surface. The tests were conducted for the following variables : $2 \leqslant z/d \leqslant 10$, $4 \leqslant x/d \leqslant 6.67$ and $2.4 \times 10^3 \leqslant Re_d \leqslant 10^4$. The averaging area was systematically varied and the mean heat transfer coefficient was found to decrease as the impingement area increased.

To summarise the above discussion, the average heat transfer coefficients from single jets can be calculated by integrating the local values. However, in multiple systems, the presence of other jets can modify the distribution of heat transfer (depending on system geometry). The target surface area as well as the turbulence level in the jet can also affect the values of the mean convective transport coefficients and it is important therefore, to include details of the transfer area in any correlation.

4.5.3 Review of Heat Transfer Rates in an Oblique Jet Impingement System

As discussed in Chapter 1, the number of investigations into the characteristics and performance of orthogonal jets are much higher than those into obliquely impinging jets. Even the excellent review by Martin (Ref. 101) in 1978 contained only two references namely: those of Perry (Ref. 21) and Korger and Krizek (Ref. 22). The present study has therefore concentrated on inclined geometries.

Perry was probably the first investigator to obtain jet impingement heat transfer coefficients with an inclined jet. The inclination of the plate to the jet axis was varied between 15° and 90° in steps of 15°. Single air jets were used with nozzle diameters of 16.5 mm or 21.6 mm and the other parameters in the tests covered the range : $1.1 \times 10^4 \leqslant Re_D \leqslant 3.8 \times 10^4$ and $11 \leqslant z/d \leqslant 19$. A 16.5 mm diameter calorimeter was embedded in the target plate to measure the direct heat transfer rates and "quasi-local" values were obtained by moving the impingement surface relative to the jet.

It was observed that the "quasi-stagnation" heat transfer coefficient decreased rapidly with decreasing target plate inclination. For example, at an angle of 15° to the vertical, the heat transfer rate was 43% lower than that for normal impingement. The experimental data at the stagnation point were correlated by :

$$Nu_o = \psi Re_D^{0.7} Pr^{0.33} \qquad 4.5.14$$

and is valid for all test conditions

where the characteristic dimension in both the Nusselt and Reynolds numbers is the diameter of the measuring calorimeter. The constant 'ψ' is a function of the plate inclination and varies between 0.104 and 0.181 for 15^o and 90^o respectively.

In a published discussion of Perrys paper, Thurlow (Ref. 111) reported his experimental measurements of both local and average impingement heat transfer rates for inclined jets. A direct heat transfer technique was used and the tests were conducted for :

$2.2 \times 10^4 \leqslant Re_d \leqslant 5.7 \times 10^4$, 12.7 mm $\leqslant d \leqslant$ 25.4 mm and $z/d < 10$.

It was observed that the maximum local heat transfer coefficient was almost independent of the nozzle inclination (up to $\alpha = 60^o$). It was suggested that natural convection had an appreciable effect on local heat transfer variations at large radii from the nozzle centre. The values of r/d at which natural convection was important were not however reported.

Thurlow found the average heat transfer coefficients over the target plate to be a maximum with normal impingement and this observation corroborated the earlier study of Perry.

Smirnov et al (Ref. 112) measured the heat transfer coefficients from a submerged liquid jet. The test conditions were : $50 \leqslant Re_d \leqslant 31000$ and 2.5 mm $\leqslant d \leqslant$ 36.6 mm. A 48 mm diameter copper calorimeter was used for the direct measurements and equations were proposed for three different regions of z/d. For example, the stagnation point heat transfer coefficients were correlated by :

$$Nu_o = 0.034 d^{0.9} Re_d^{0.64} Pr^{1/3} \exp(-0.037\ (z/d)) \qquad 4.5.15$$

valid for $0.5 < z/d < 10$

and

$$Nu_o = 0.034 d^{1.3} Re_d^{1/3} Pr^{1/3} \exp(-0.037\ (z/d)) \qquad 4.5.16$$

and is valid for $z/d > 10$

The inclusion of nozzle diameter as a separate variable in these correlations corroborates the observation of Gardon and Cobonpue that Nu is affected by nozzle diameter as discussed in section 4.5.2. The equation for $z/d < 0.5$ is

not presented here because of its very limited practical application. A degradation factor (ψ) which was used to multiply these values was suggested as a means of accounting for nozzle inclination. The predictions then agreed with Perrys measurements. Typical values of ψ are 0.88, 0.69 and 0.58 for 60°, 30° and 15° respectively. It must be pointed out, however, that the degradation factors were obtained at only one separation distance (i.e. $z/d = 8$) so that the modified equations should be used with caution. Furthermore, Smirnov et al used a comparatively large calorimeter (of diameter = 48 mm) which means that the measurements were, in effect, average heat transfer coefficients over a finite area around the stagnation point.

Korger and Krizek (Ref. 22) used the sublimation of naphthalene to obtain heat/mass transfer coefficients for impinging slot jets. For the inclined jets, it was found that the location of the stagnation point did not coincide with the point of intersection of the nozzle axis and the impingement surface. The stagnation point shifted as shown in Fig. 4.3.2. It was also found that local convective coefficients 'downhill' of the stagnation point were higher than those at the corresponding 'uphill' locations. From the integrated results, it was observed that for a constant z/d, the mean convective transport coefficients were nearly independent of nozzle inclination. The integration area was not, however, specified.

More recently, since the start of the present study Sparrow and Lovell (Ref. 23) reported both the local and mean heat/mass transfer coefficients due to an oblique circular impinging air jet. Because of its relevance to the present investigation, it is pertinent to review it in detail. They cast naphthalene in a metallic mould to produce a 76 mm x 152 mm impingement test surface and employed a nozzle diameter of 6.35 mm. The test conditions covered a range of :

$7 \leqslant z/d \leqslant 15$, $2.5 \times 10^3 \leqslant Re_d \leqslant 10^4$ and $30^\circ \leqslant \alpha \leqslant 90^\circ$

(in steps of 15°). A profilometric technique was used to derive the sublimation rates of the naphthalene.

It was observed that the location of the stagnation point was displaced from the intersection of the geometrical axis of the nozzle and the test surface. This displacement continually increased as the angle of inclination decreased, see Fig. 4.5.6. These findings corroborated those of Korger and Krizek (Ref. 22) which applied to slot jets. Figure 4.5.7 is reproduced from Sparrow and Lovell and the usual characteristic bell shape associated with jet impingement heat transfer is evident. The variation of heat transfer becomes increasingly asymmetrical as the nozzle inclination is reduced. Also, the convective transfer coefficients decay more rapidly on the 'uphill' side because the jet momentum in this direction is much lower than that on the 'downhill' side.

Local heat transfer coefficients were numerically integrated to obtain mean values over specified surface areas (usually a square of length = 4d and 8d centred around the geometrical axis). Both the maximum and mean heat/mass transfer coefficients were found to be moderately sensitive to inclination of the jet. The difference between the values for orthogonal impingement and for $\alpha = 30^{o}$ was about 20%. However, they did not attempt to correlate their results and even the data for orthogonal jet impingement were not compared with those of previous studies.

To summarise the discussion in this section, various experimental techniques have been employed to determine the heat transfer capabilities of impinging jets. The behaviour of these jets are thus relatively well-established for certain geometries especially for orthogonal impingement. However, only limited data exist for obliquely impinging jets and correlations for 'true' local values have not been reported. The investigations and conditions discussed in this review are summarised in Table 4.5.1

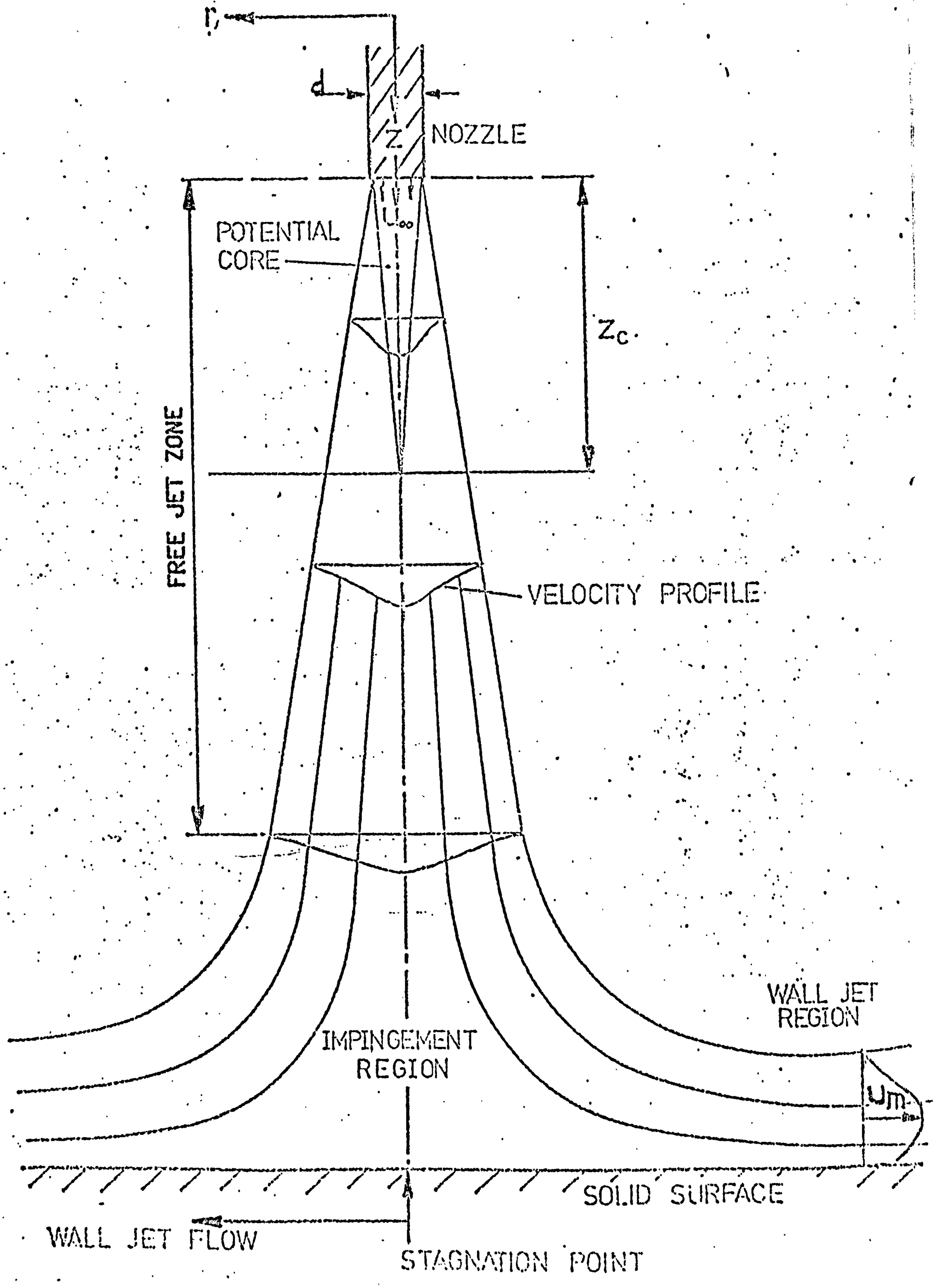

FIG. 4.2.1 FLOW CHARACTERISTICS OF A FREE JET IMPINGING ON A FLAT PLATE.

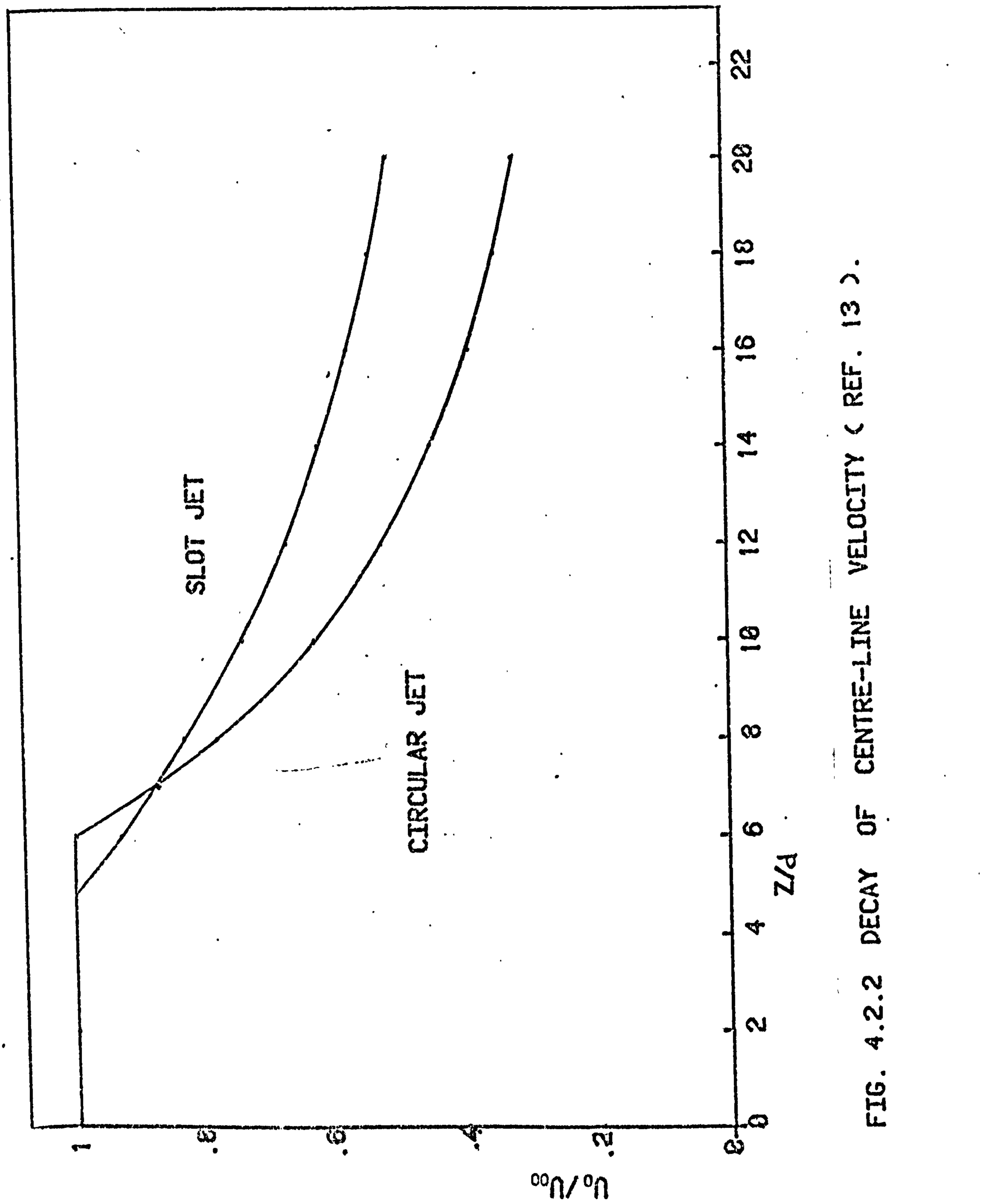
U_o/U_∞
1.0
0.8
0.6
0.4
0.2
0.0
4
6
8
10
12
14
16
18
20
22
Z/d
CIRCULAR JET
SLOT JET
DECAY OF CENTRE-LINE VELOCITY (REF. 13).

FIG. 4.2.2

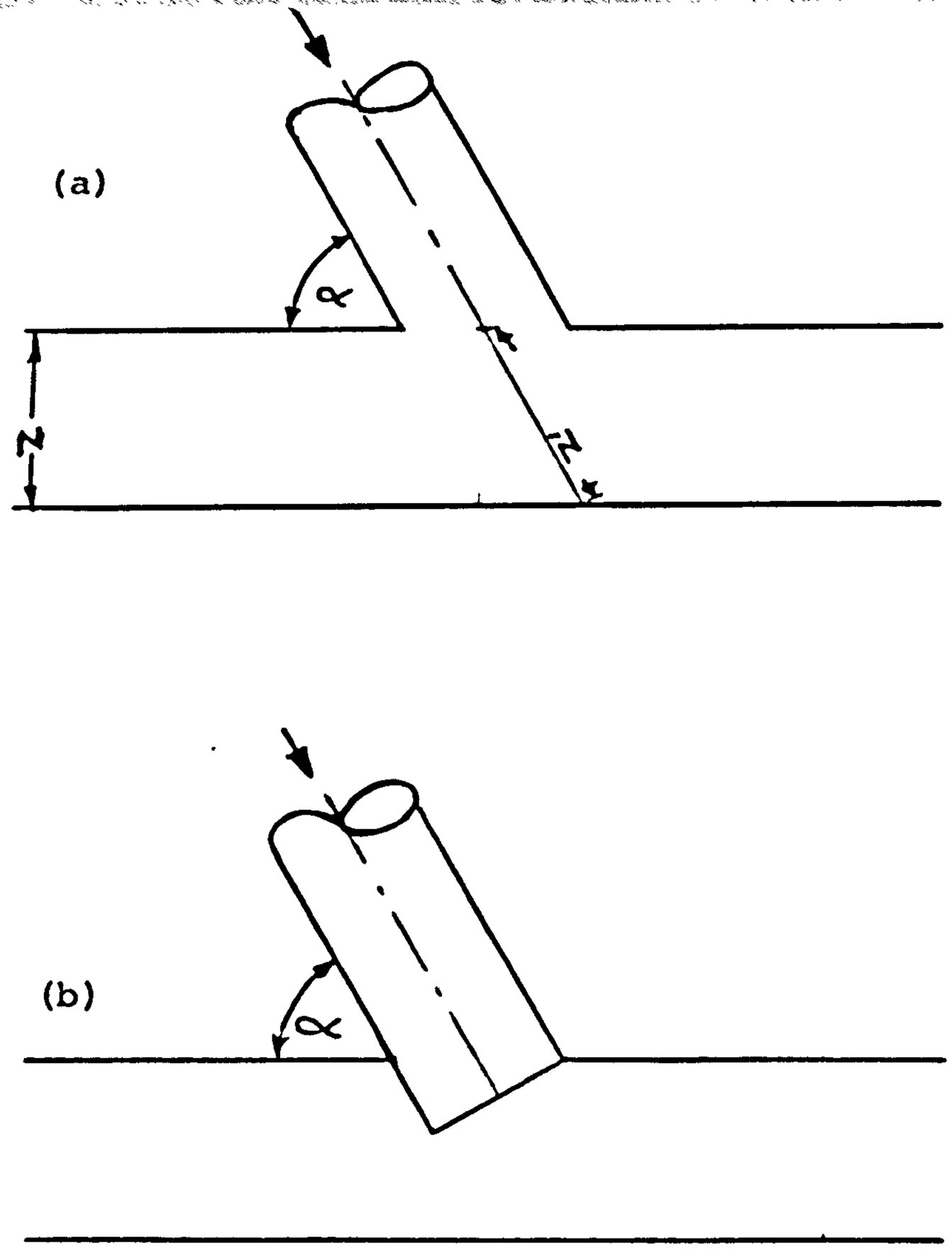

FIG.4.3.1. SCHEMATIC REPRESENTATION OF OBLIQUE JETS - (a) ELLIPTICAL SHAPE
(b) CIRCULAR SHAPE

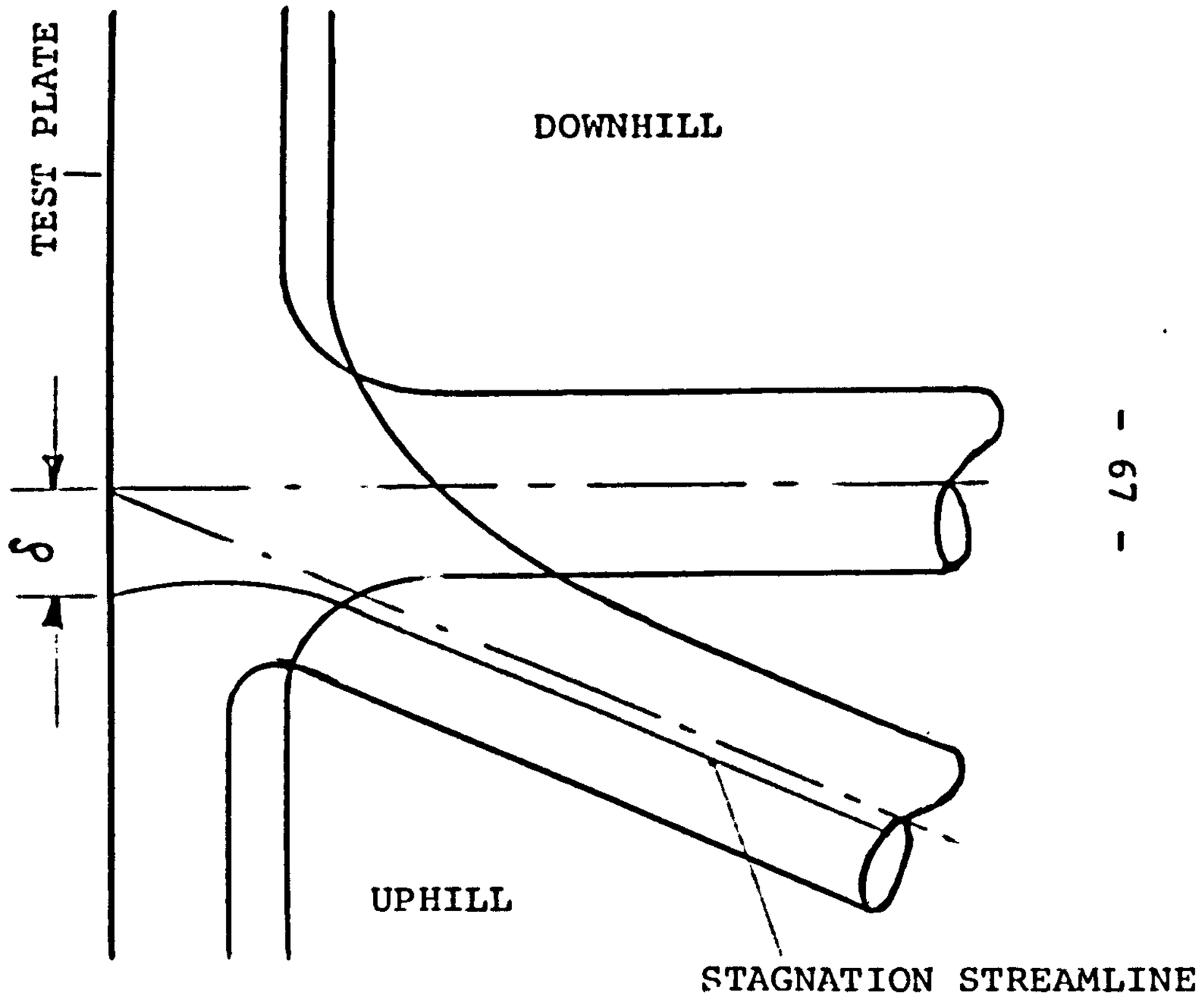

FIG.4.3.2. DISPLACEMENT OF THE STAGNATION POINT IN OBLIQUE JETS.

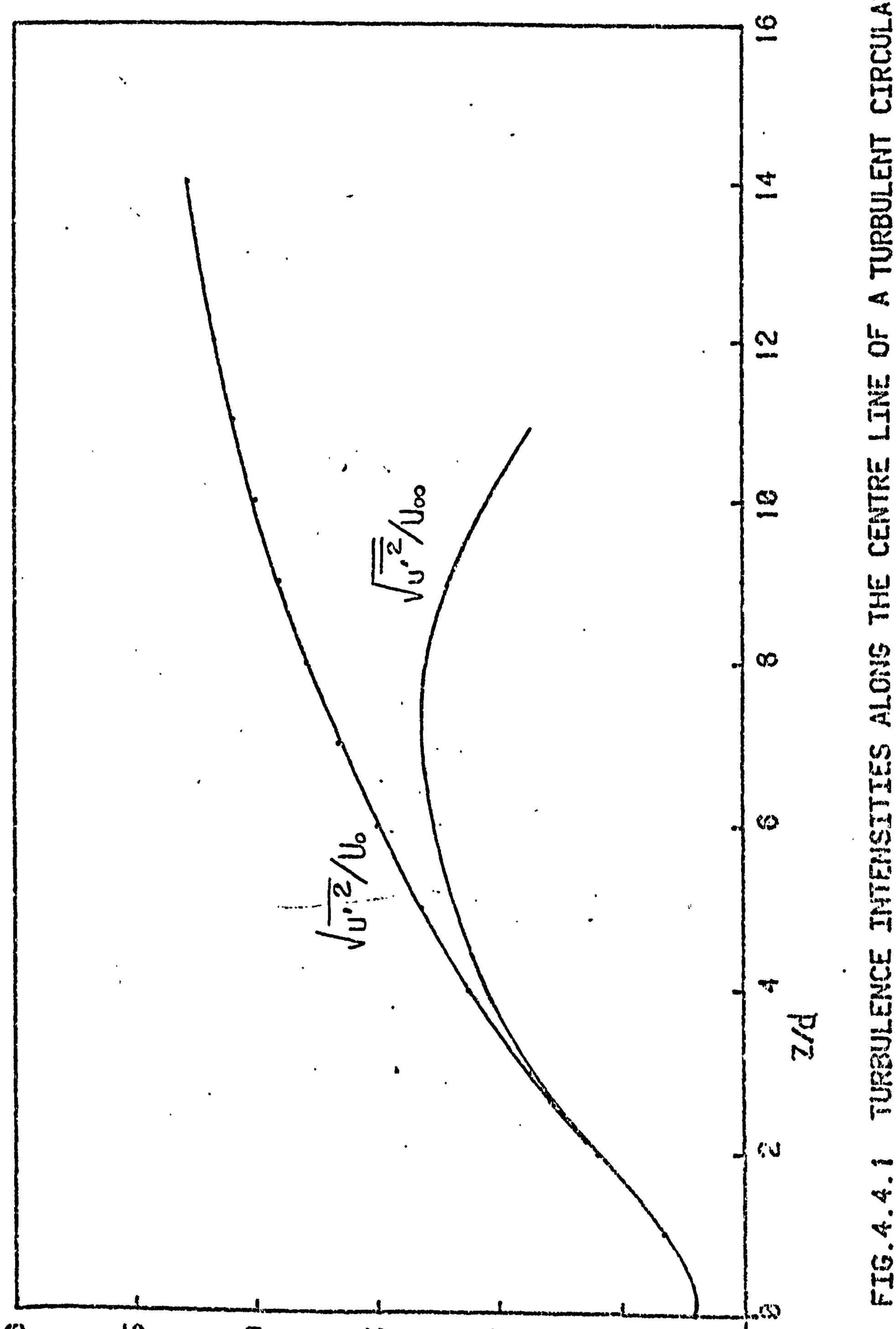

FIG. 4.4.1 TURBULENCE INTENSITIES ALONG THE CENTRE LINE OF A TURBULENT CIRCULAR JET - REF 96.

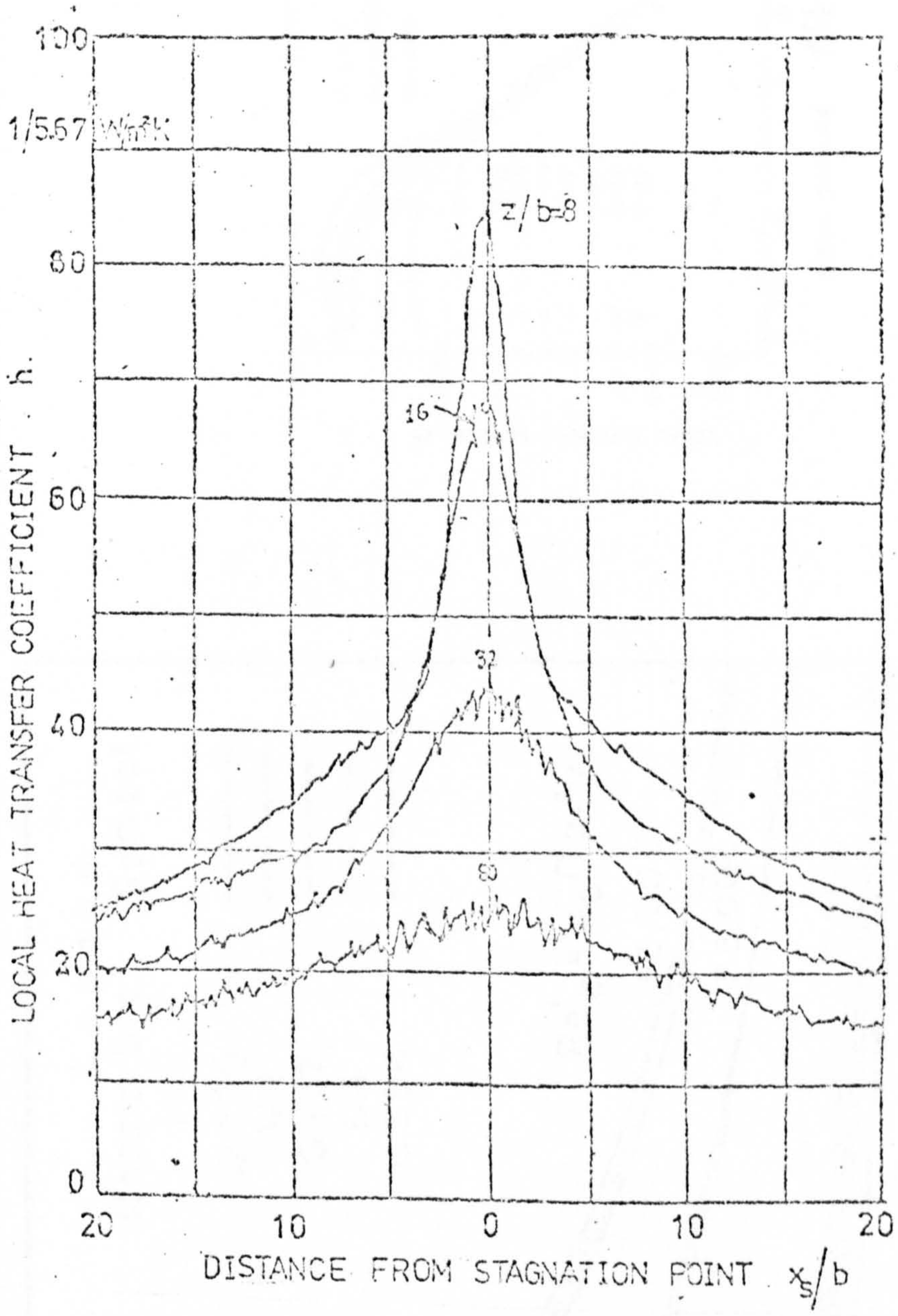

(a)

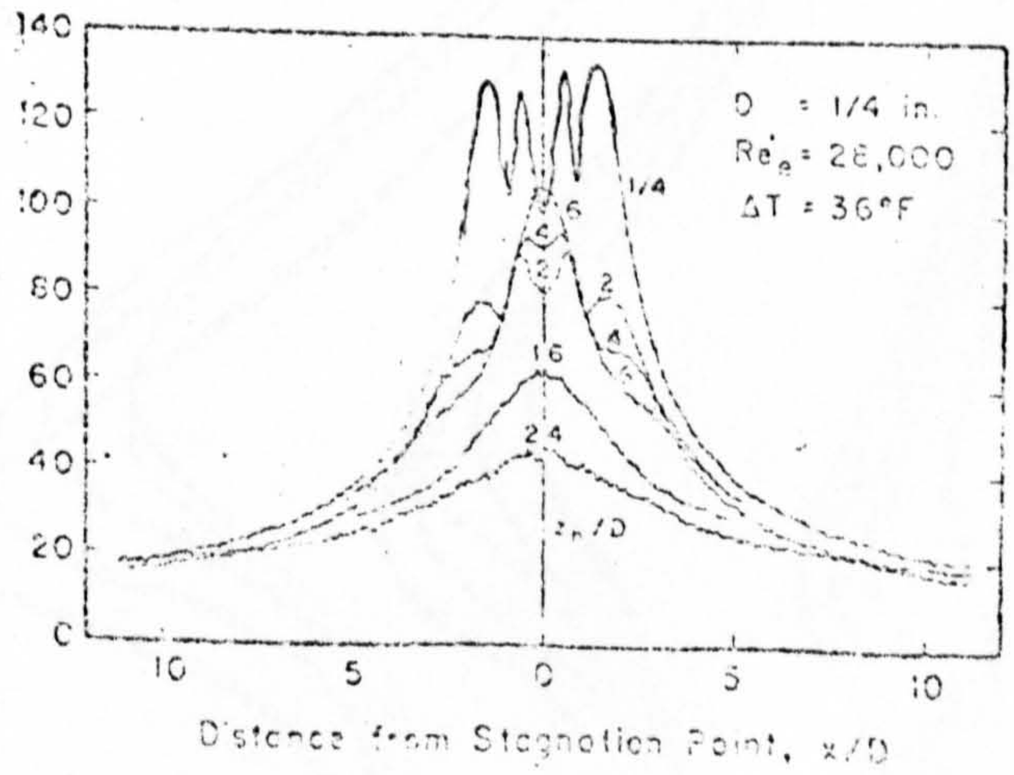

(b)

FIG.4.5.1. VARIATION OF HEAT TRANSFER COEFFICIENTS ASSOCIATED WITH AN IMPINGING JET
(a) REF.103
(b) REF.102.

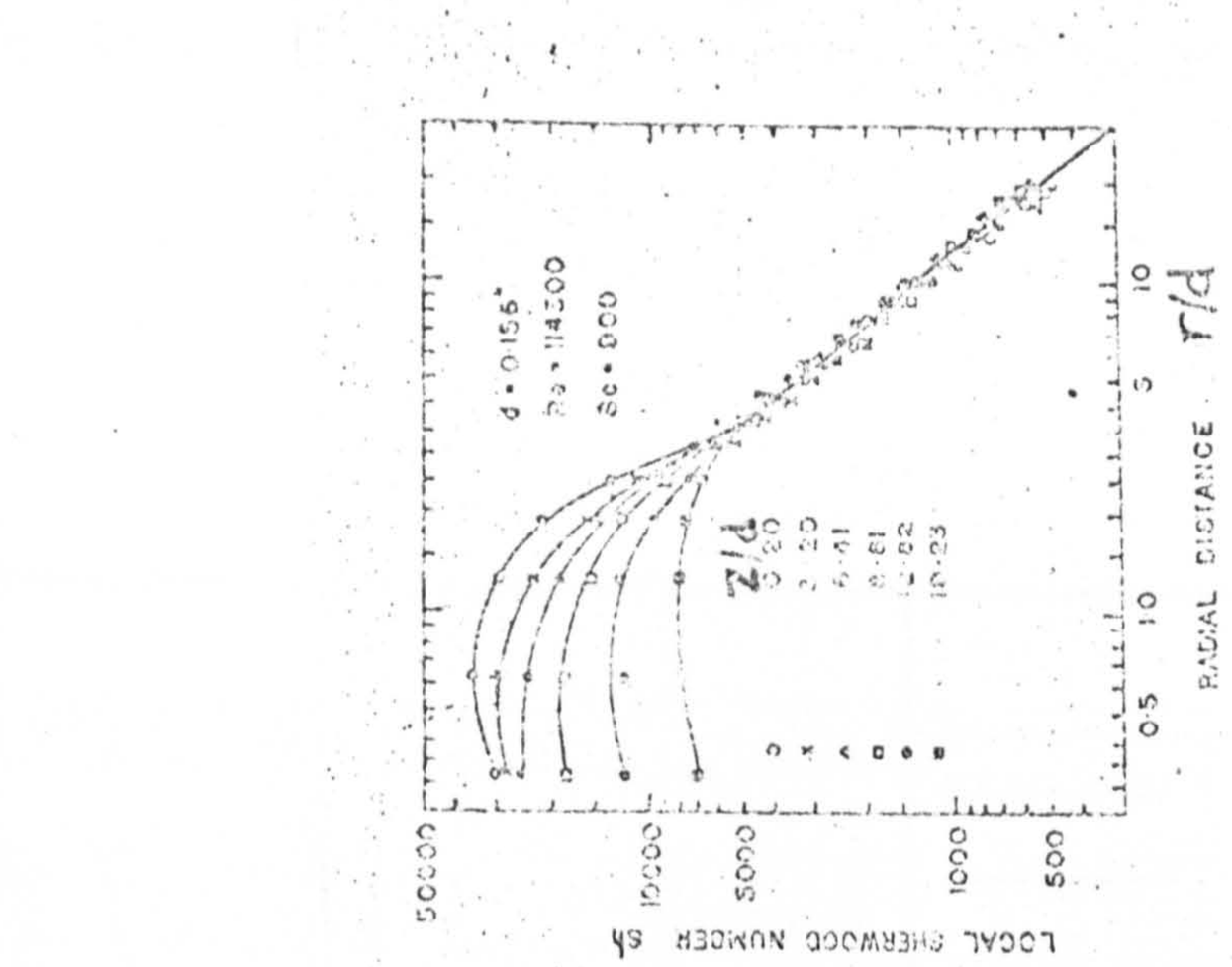

FIG.4.5.3. RADIAL VARIATION OF HEAT TRANSFER (Ref.105).

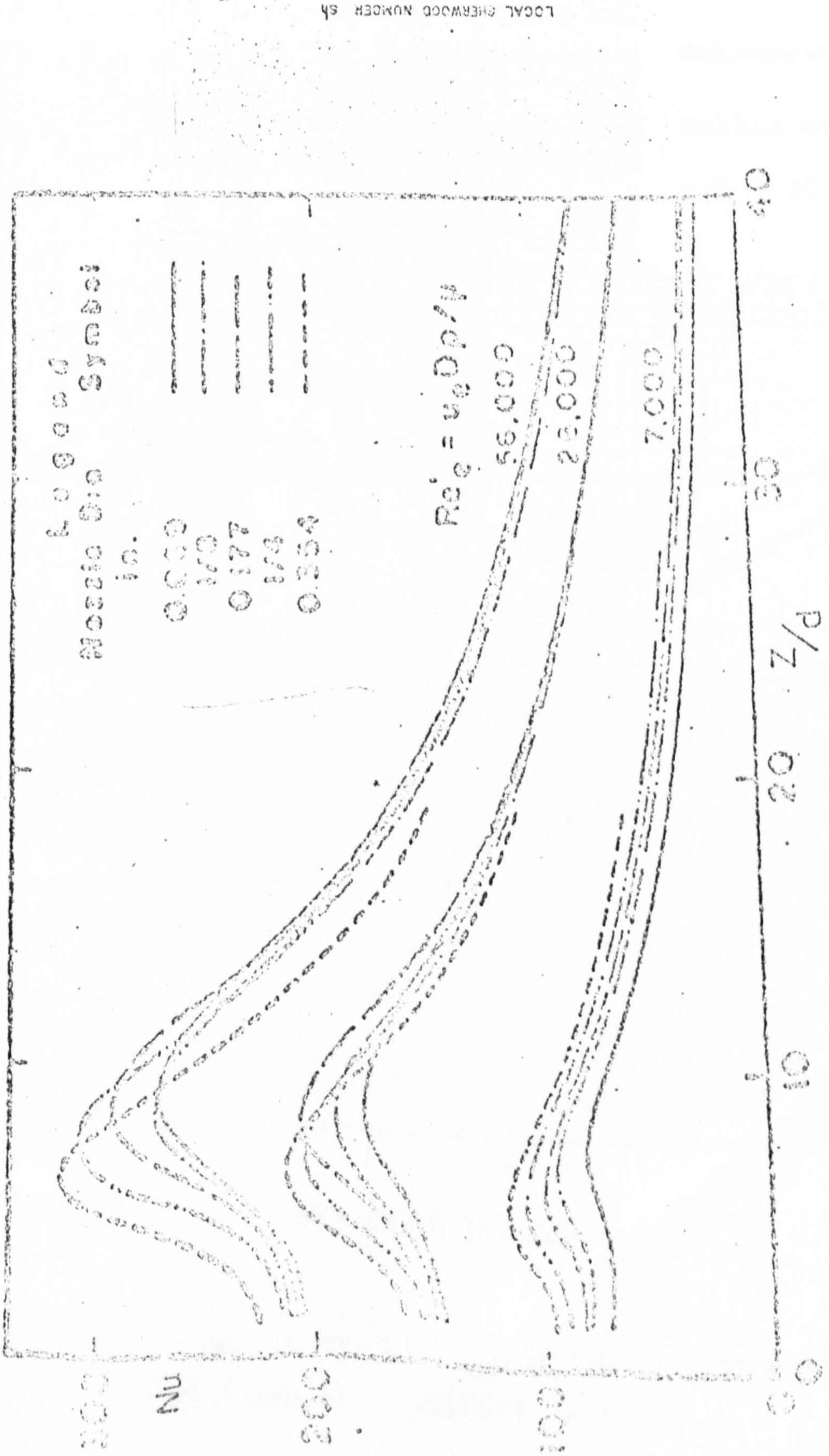

FIG.4.5.2. EFFECT OF z/d ON HEAT TRANSFER (Ref.102)

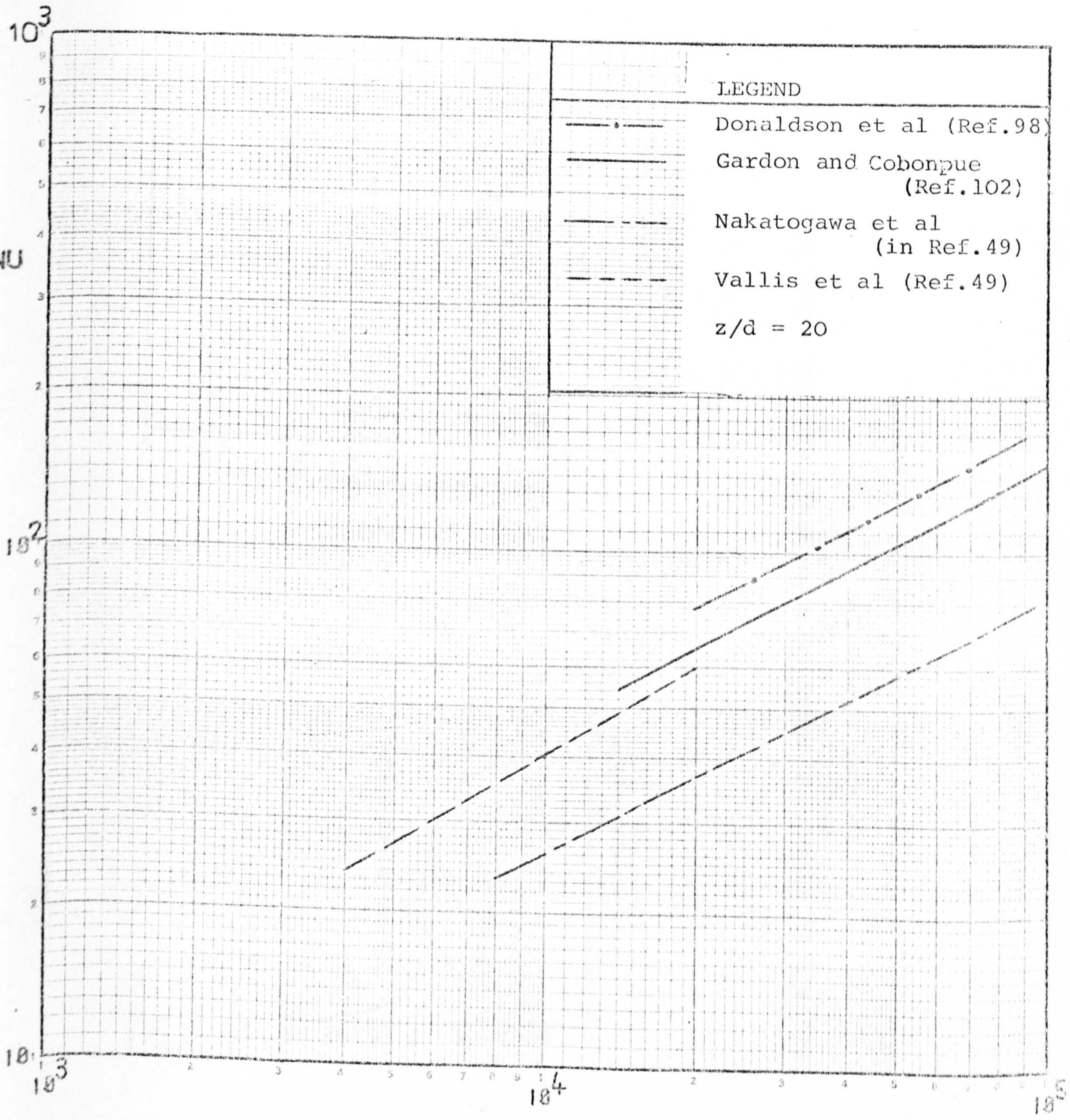

FIG.4.5.4 VARIATION OF STAGNATION POINT NUSSELT NUMBER FOR PREVIOUS WORKERS(REF.49).

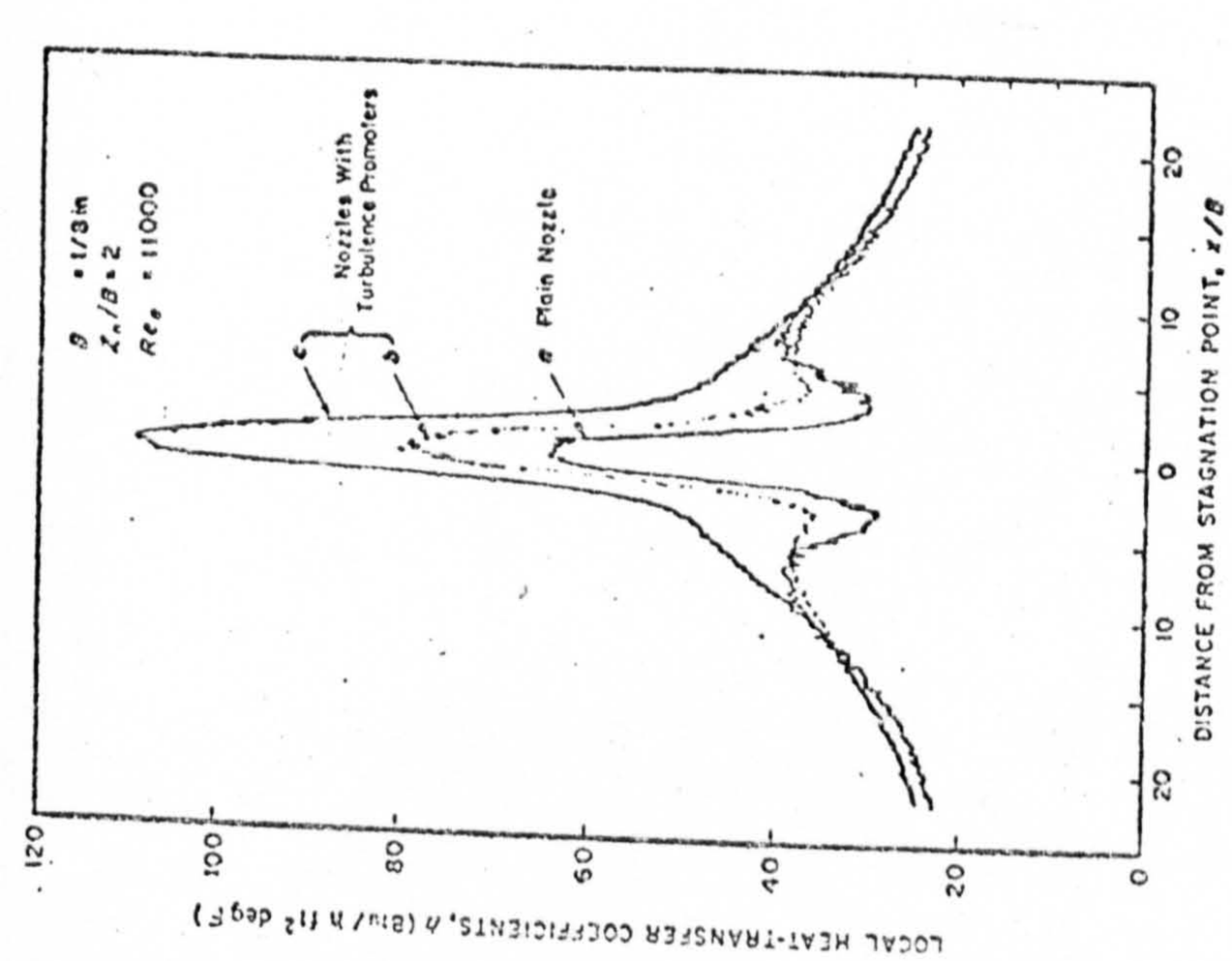

FIG.4.5.5. EFFECT OF TURBULENCE ON HEAT TRANSFER - REF.106.
(a) STAGNATION POINT VALUES
(b) LATERAL VARIATION

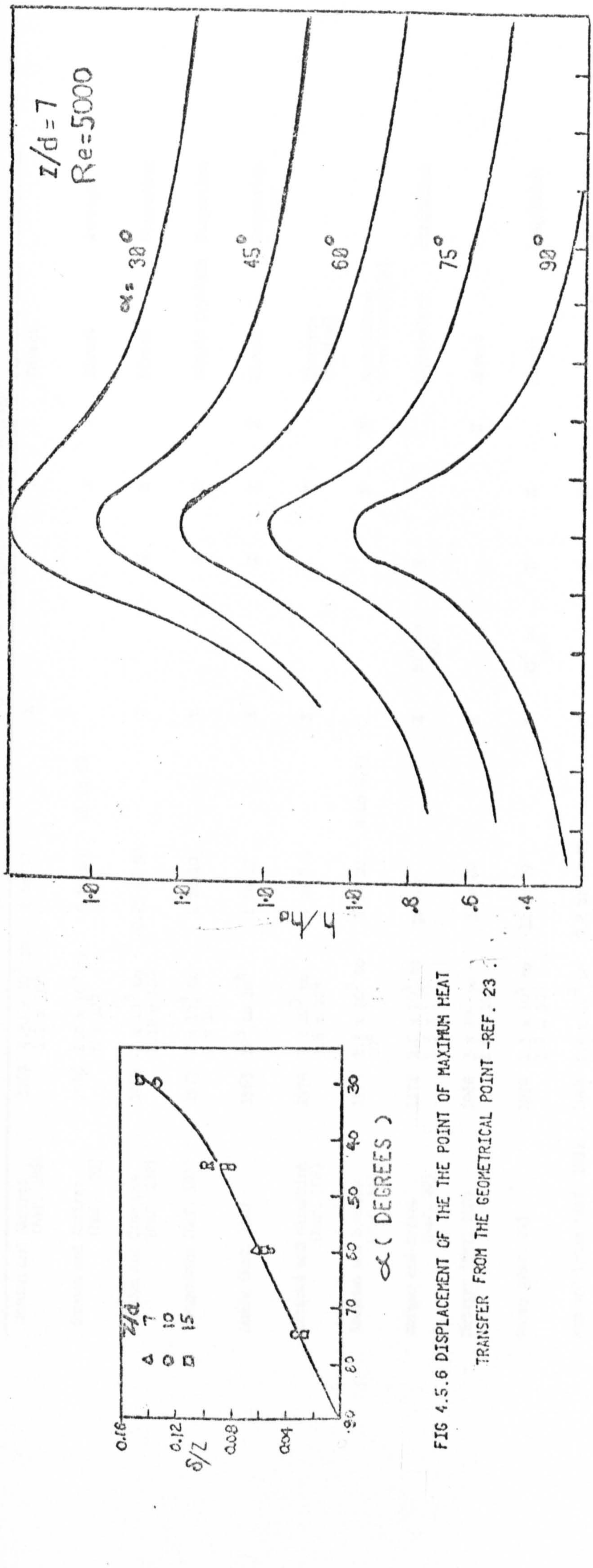

FIG. 4.5.7 VARIATION OF LOCAL HEAT TRANSFER COEFFICIENTS ALONG THE LINE OF SYMMETRY (REF 23).

FIG 4.5.6 DISPLACEMENT OF THE POINT OF MAXIMUM HEAT TRANSFER FROM THE GEOMETRICAL POINT -REF. 23 .

TABLE 4.5.1

AUTHOR	YEAR	RANGE OF TEST CONDITIONS					TYPE OF HEAT TRANSFER COEFF. REPORTED			TECHNIQUE	PUBLISHED CORRELATION
		Re	z/b or z/d	x/d or x/b	Single	α	Stagnation	Local	Average		
Gardon and Akfirat (Ref. 106)	1965	4.50×10^2 to 1.1×10^4	2 to 32		X		X	X		Direct	
Gardon and Akfirat (Ref. 103)	1966	6.0×10^3 to 6×10^5	0 to 60	16 to 64				X	X	Direct	Average
Gardon and Cobonpue (Ref. 102)	1962	7×10^3 to 1.12×10^5	0.25 to 50		X		X	X		Direct	Stagnation
Hoogerdorn (Ref. 107)	1977	2×10^4 to 9×10^4	1 to 10		X		X	X		Liquid Crystals	Stagnation
Huang (Ref. 110)	1963	10^3 to 10^4	1 to 12		X		X	X	X	Direct	Stagnation Average
Kataoka and Mizushina (Ref. 108)	1974	2×10^3 to 3.6×10^4	4 to 8.5		X			X		Electro-Chemical	
Koopman and Sparrow (Ref. 66)	1976	2.4×10^3 to 10^4	2 to 10	4 to 6.67				X	X	Naphthalene (Profilometric)	
Korger and Krizek (Ref. 22)	1972	1.6×10^4 to 1.5×10^5	≥ 8.5		X	30° to 90°	X			Naphthalene	Stagnation
Metzger (Ref. 109)	1962	3×10^3 to 1.0×10^4	3 to 20		X				X	Direct	
Perry (Ref. 21)	1954	1.1×10^4 to 3.8×10^4	11 to 19		X	15° to 90°	X	X		Direct	Stagnation
Rao and Trass (Ref. 105)	1964	2.5×10^4 to 1.25×10^5	0.2 to 19.23		X		X	X		Mass Transfer	Local Wall Jet
Smirnov (Ref. 112)	1961	50 to 3.1×10^4	≥ 0.5		X	15° to 90°	X			Direct	Stagnation
Sparrow and Lovell (Ref. 23)	1980	2.5×10^3 to 10^4	7 to 15		X	30° to 90°	X	X	X	Naphthalene (Profilometric)	
Thurlow (Ref. 111)	1954	2.2×10^4 to 5.7×10^4	< 10		X	30° to 90°		X	X	Direct	
Vallis et al (Ref. 49)	1978	3.88×10^3 to 2.3×10^4	5 to 20		X		X	X	X	Electro-Chemical	Impingement Average

CHAPTER 5

5. JET CHARACTERISATION

5.1 INTRODUCTION

As outlined in Chapter 1 the primary objective of the present research programme is to obtain heat and mass transfer coefficients for obliquely impinging jets. However, the rate of heat transfer, especially in the impingement region of a jet, is particularly dependent on the velocity and turbulence characteristics of the flow. Thus, a knowledge of these properties facilitates comparison of the heat transfer results from various jet impingement investigations.

Limited measurements of turbulence intensities were thus undertaken using a hot-wire anemometer and the results are subsequently employed in Chapter 7 to explain the variation of heat transfer. The use of this instrument also enables the local flow velocities to be measured. Consequently, profiles of these properties were measured for the jet initial region.

A hot-wire anemometer has been used at Cranfield to study various turbulent flows (e.g. Ref. 50, 113 and 114) and these theses may be consulted for details of the technique. However, for completeness, both the basic principles and the method of operation of a hot-wire anemometer are briefly presented in this Chapter.

5.2 THE TEST RIG

A schematic layout of the test rig is shown in Fig. 5.2.1. The 1.5 kW variable speed centrifugal blower (Sturtevant type 525130) which was used in the tests had a delivery rate of 3.07 m^3/sec at a maximum pressure of 7.46 KN/m^2. The air was fed through a water cooler (i.e. a counter flow heat exchanger) which was used to maintain the jet temperature at or very close to the ambient value.

Orifice plates (44 mm to 64 mm in diameter) designed according to BS 1042 (Ref. 115) were mounted in the supply line to measure the air flow rates. The speed of the blower was adjusted to control the flow rate so as to obtain the required jet Reynolds number.

A pitot tube constructed from hypodermic tubing of 1.2 mm inside diameter was used in conjunction with a micromanometer (Furness Controls type MCD F001) to calibrate the hot wire anemometer.

The jet nozzle was 508 mm (i.e. 32 jet diameters) long and was machined from a copper tube of 16 mm inside diameter. This nozzle was fixed into a carrier plate and the unit was mounted on a four-wheel carriage which in turn was mounted on a mild steel frame. The position of this carriage could be adjusted to give the required axial distance between the nozzle exit and the hot wire sensor. This sensor was fixed onto a traverse so that the variation in turbulence properties across the jet can be measured.

5.3 HOT-WIRE ANEMOMETRY

5.3.1 Basic Principles of a Hot-Wire Anemometer

The alternative techniques which are available for measuring the turbulence characteristics of a free jet include hot-wire anemometry which is widely used and also hot-film and more recently, laser-doppler anemometry. In the present study, a hot-wire method was used not only because of its well proven ability but also because it was readily available at Cranfield.

The basic sensor or transducer used in the present experiments consists of a small (5 μm diameter) electrically heated tungsten wire which is fixed at each end to ceramic supports. The probe (i.e. the wire and its supports) is necessarily small because of theneed to respond quickly to rapid fluctuations in flow. Also, very little interference with the flow is essential. As the operating temperature of the wire is normally higher than that of the flowing stream, it loses heat to the main fluid.. The rate of heat dissipation from the wire to the fluid is assumed to be a function of the velocity i.e.

$$Nu = \phi(u) \qquad 5.3.1$$

The changes in the hot-wire temperature (dictated by the changes in the fluid velocity) result in changes in the electrical resistance of the wire. The anemometer can be operated either in a constant current (CCA) or a constant temperature (CTA)mode.

In the CCA mode, the variation in the wire resistance produces a fluctuating voltage. However. if large fluctuations in wire temperature occur (e.g. in highly turbulent flows), the original calibration can be adversely affected and manual adjustments are required. The frequency response is relatively poor in this mode due to thermal inertia effects of the wire. In the CTA mode, a feedback circuit is incorporated to maintain an invariant wire temperature. The fluctuations in

current necessary to maintain constant temperature produce voltage variations as the anemometer output. Thermal inertia effects are reduced so that a high frequency response can be obtained. For example, an upper frequency limit of 100 Hz in a system without a feedback can be increased to 400 KHz (for a 5 μm tungsten wire) by including a feedback circuit. This constant temperature mode was employed in the current investigation.

Figure 5.3.1 is a schematic layout of the anemometer and the circuit consists of a Wheatstone bridge which has the sensing wire as one of its arms. The probe resistance, and hence its temperature is maintained constant by keeping the bridge in balance. Any change in the fluid velocity will immediately throw the bridge out of balance and this out-of-balance signal is amplified and fed back to restore the balance condition. The amplifier output current or an equivalent voltage drop is a measure of the rate of heat dissipation from the sensing wire. Both the mean and the root-mean-square (r.m.s.) of the fluctuating rates of heat transfer are, thus, obtained in the form of two separate voltages.

Equation 5.3.1 implies that the convective heat loss to the fluid from the hot-wire depends on the fluid velocity. This is only true if both the density and temperature of the fluid are kept constant. In the present tests, temperature stratification and compressible effects are negligible so that a relationship similar to equation 5.3.1 holds. The theoretical relationship between the convective heat loss and the flow velocity can, in principle, be established by solving the energy and momentum equations for an infinitely long circular wire (Ref. 56). Such an analytical approach is not usually employed however because (Ref. 116) :

i) the probe geometry is highly sensitive to slight changes in manufacturing conditions so that probes even from the same batch do not always possess identical characteristics.

ii) the actual rate of heat loss is affected by conduction through the prong supports. Natural convection and radiation losses can also occur.

and

iii) the length to diameter ratio of an actual wire is finite.

Hence, a universal calibration (based on a theoretical analysis) cannot be employed and in practice, an empirical calibration (relating heat loss to the fluid velocity) is determined.

Probably, the earliest form of a semi-empirical relationship is that known as Kings law (Ref. 117). It states that :

$$Nu = A + Bu^{0.5} \qquad 5.3.2$$

where :

A and B = experimentally determined constants for a particular probe.

u = effective cooling velocity normal to the wire.

Nu = Nusselt number

The heat loss from the hot-wire is reflected as a bridge output voltage. Hence, equation 5.3.2 can be re-written as :

$$E^2 = E_o^2 + Bu^{0.5} \qquad 5.3.3$$

The use of 0.5 as the exponent of the cooling velocity has, recently been criticised (Ref. 116). In a more general form, equation 5.3.3 can, therefore, be expressed as :

$$E^2 = E_o^2 + bu^n \qquad 5.3.4$$

where :

$0.45 \leq n \leq 0.5$ and is also determined by experiment.

By differentiating and re-arranging equation 5.3.4, the following expressions for turbulence intensity and mean velocity can be obtained :

$$\frac{\sqrt{\overline{u'^2}}}{\bar{U}} = \frac{2}{n} \frac{(\overline{E'^2})^{\frac{1}{2}} E}{(E^2 - E_o^2)} \qquad 5.3.5$$

and

$$\bar{U} = \frac{(E^2 - E_o^2)^{1/n}}{b} \qquad 5.3.6$$

where :

$\bar{U}$ = the mean flow velocity

E = the probe d.c. voltage

E_o = the voltage at zero flow velocity

$\overline{(u'^2)}^{\frac{1}{2}}$, $\overline{(E'^2)}^{\frac{1}{2}}$ = rms components of the fluctuating velocity and voltage respectively

With n = 0.5, equations 5.3.5 and 5.3.6 yield the turbulence intensity and mean velocity from a Kings law relationship.

Sidall and Davies (Ref. 118) have proposed a three term equations, namely

$$E^2 = c + du^{0.5} + eu \qquad 5.3.7$$

where :

c, d and e are empirical constants.

They found that over a wide range of fluid velocities (0 - 160 m/s) the addition of an extra term to Kings law produced a significant improvement in accuracy. The expressions for turbulence intensity and mean velocity are then respectively :

$$\frac{\sqrt{\overline{u'^2}}}{U} = \frac{4E\ \overline{(E'^2)}^{\frac{1}{2}}}{\frac{D - dD^{\frac{1}{2}}}{2e}} \qquad 5.3.8$$

and

$$\bar{U} = \frac{D^{\frac{1}{2}} - d}{2e}^2 \qquad 5.3.9$$

where

$$D = d^2 + 4e\left[(E)^2 - c\right] \qquad 5.3.10$$

It is pertinent to mention here that these relationships (e.g. Kings law) are accurate for low turbulence intensities

(i.e. Tu < 25 to 30%). Beyond this limit, other sophisticated analyses (e.g. Rodi (Ref. 99)) may be required. Only the King's law and Sidall-Davies, three-term equations were employed in analysing the hot-wire measurements in the present study, because of their relative simplicity and also because high turbulence intensities were not measured. However, very little difference was observed in the turbulence data calculated using the two relationships. Results in this Chapter are based on a three-term equation.

5.3.2 The Present Hot-Wire Anemometer

The equipment used in the present series of tests is shown in Plate 5.3.1. The probe was a DISA type 55P14 with a single, straight, 5 μm diameter, tungsten wire. The output from the probe was fed into a DISA measuring unit which consisted of :

1. a 55D01 constant temperature anemometer,
2. a 55H30 shorting probe
3. a 55D31 DC digital voltmeter,
4. a 55D35 r.m.s. voltmeter,
5. a 55D25 axuiliary unit which was employed as the square wave generator,

and

6. a 55D10 linearizer.

The details of each of these units are available in the DISA operating manual (Ref. 119).

5.3.3 Calibration and Test Procedure

Prior to calibration of thehot-wire anemometer, the stability and frequency response of the system was checked by means of a square wave test signal. This was fed to the probe and the system output was displayed on a cathode ray oscilloscope (Tektronix type 516). Any slight bridge off-balance or the choice of an unsuitable amplifier bandwidth can generate oscillations in the output signal (see the two top responses in Plate 5.3.2). When proper adjustments of both the amplifier gain and bridge balance are effected, a smooth pattern is obtained (see for example the lower response of Plate

5.3.2 which was obtained during the present study). An upper frequency limit of approximately 36 kHz was thus measured.

Calibration of the wire is essential to determine the constants in equations 5.3.2 to 5.3.10. The air velocity was varied to cover the range of Reynolds number in the heat transfer tests. A pitot tube which was connected to a micromanometer was mounted adjacent to the hot-wire to measure the air velocity in the potential core of the jet. The corresponding mean wire output voltage was recorded and its square was plotted against the mean velocity. By also displaying the output of the wire on the oscilloscope, it was possible to monitor the physical state of the wire, e.g. one can determine if the wire was damaged. A typical resultant calibration curve for the hot-wire is shown in Fig. 5.3.2.

A least squares curve fitting technique was used to evaluate the constants in Kings law as A = 7.02 and B = 2.61. For the three-term equation (e.g. 5.3.7), measurements of the mean velocity, the square of the d.c. voltage and the square root of the mean velocity were used as the input data in a multiple regression procedure. The constants c, d and e were found to be 6.79, 2.85 and -0.035 respectively. Sidall and Davies also found the value of 'e' to be negative. Differences in the two calibration results are discussed in the next section.

Velocity and turbulence intensities within the jet (for $0 \leqslant z/d \leqslant 8$) were obtained by traversing the calibrated hot-wire probe across the jet at right angles to the longitudinal axis. Both the mean bridge voltage and its fluctuating rms component were recorded at each measuring station. This procedure was repeated for all of the "orthogonal" jet flow conditions. Most jet turbulence measurements previously reported in the literature were found to be applicable to the self-preserving region of the flow. Hence, centre-line turbulence intensities and velocity decay were obtained for the range $8 \leqslant z/d \leqslant 40$ to enable comparisons to be made with these published data. Because of the fragility of the hot-wire, the air supply to the jet was filtered to remove any harmful particles.

5.4 RESULTS AND DISCUSSION

5.4.1 Introduction

Tests were conducted on symmetrical circular jets and, hence, results are only presented for one half of the flow field. Fig. 5.4.1 depicts the calibration data obtained by using both King's law and a Sidall-Davies three-term equation.

The standard errors of estimate are respectively 0.32 and 0.75. It can be seen from the results that agreement is generally good, even at high velocities (>50 m/s) where a difference of about 3% is apparent. The present results are qualitatively similar to those of Sidall and Davies (Ref. 118), see Fig. 5.4.2. The maximum velocity employed in this study was approximately 61 m/s so that either of the two relationships can be employed with little error.

5.4.2 Velocity Measurements

Figure 5.4.3 presents the radial distributions of axial velocity at various downstream locations. These velocity distributions were normalised by dividing by the maximum jet velocity. The velocity profiles can be conventiently divided into two sections, namely: inner and outer sections.

The inner section (the core of the jet) can be bounded by r/d = 0.375. At low z/d's, the non-dimensionalized velocity remains virtually unchanged until r/d = 0.25. Whereas the velocity profiles become more bell-shaped at larger downstream distances. See, for example, the profiles at z/d = 2 and 8 in Fig. 5.4.3(a).

The outer section contains the mixing layers. It can be seen from Fig. 5.4.3(a) that the non-dimensionalised velocity decays faster at lower z/d. For example, u/u_o which is respectively 0.80 and 0.70 for z/d = 2 and 6 at r/d = 0.375 becomes 0.18 and 0.33 at r/d = 0.75. The spread of the jets is also apparent in this diagram. (For example, u/u_o = 0.01 occurs at r/d = 0.94 for z/d = 1 and r/d = 2.44 for z/d = 8).

This behaviour can be attributed to turbulent mixing with, and entrainment of, the surrounding stationary fluid so that the jet spreads continuously.

The velocity profiles obtained in this study are self-consistent at various Reynolds numbers.

Figure 5.4.4 depicts the decay in the centre line velocity. It can be noticed that up to z/d $\simeq$ 6, the velocity is virtually invariant and this corresponds to the potential core or flow development region. Beyond this zone, the centreline velocity gradually decreases. This can be attributed to entrainment which increases the mass of the fluid and because the jet exit momentum is conserved, the velocity is reduced. The data of Donaldson et al (Ref. 98) are shown in the figure and agreement is generally good especially in the initial region of the jet.

5.4.3 Measurements of Turbulence Intensities

Figure 5.4.5 presents the variations in centreline turbulence intensity (based on the local velocity) at various Reynolds numbers. These results can be conveniently divided into three different regimes, namely: low, medium and high turbulence intensity regions.

For $z/d \leqslant 6$, the turbulence intensities are usually low (i.e. < 10%). This zone contains the potential core so that any variations in turbulence intensity are due mainly to increases in the velocity fluctuations rather than to changes in the mean velocity. It can be seen that for $6 \leqslant z/d \leqslant 12$, the turbulence intensity increases very rapidly and this zone can be associated with the transition region. The turbulence generated at the edges of the jet has penetrated to the centre causing a decrease in the local velocity. For $z/d \geqslant 12$, the turbulence intensity still grows slowly and this is the fully developed jet zone.

The results are qualitatively similar with those of Corrsin (Ref. 96) and Boguslawski and Popiel (Ref. 97), which were obtained for turbulent circular jets at Reynolds numbers of 17500 and 125000 respectively.

In Fig. 5.4.6 the velocity fluctuations are normalised by the exit velocity of thejet. It is noticeable that the turbulence intensities which are initially low at exit rapidly increase to maxima around a z/d of 8 and subsequently decrease. Presentation of the data in the present form thus reveals that the velocity fluctuation on the jet centreline continues to increase even beyond the potential core region before subsequently decreasing. The locations of these maxima are similar to those found by Gardon and Akfirat (Ref. 106) and Corrsin for slot and circular jets respectively.

A comparison of Fig. 5.4.5 and 5.4.6 shows that the turbulence intensities in the former diagram are usually larger in magnitude. For example, at z/d = 12, the turbulence intensities are respectively 17% and 7.5% (at a jet Reynolds number of 32500). Moreover, totally different trends are apparent. Thus, it is important that any data for turbulence intensity should quote the velocity on which the measurements are based. The values in the ensuing discussions are expressed in terms of the maximum velocity at a particular plane.

Figure 5.4.7 present the radial variation in turbulence intensity at various stations downstream of the nozzle exit. For the range of z/d investigated, the turbulence intensity increases from the centreline value to a maximum at r/d = 0.5 (approximately) and then it subsequently decreases. This position is in the mixing layer zone where the velocity gradient is high and the flow is usually contorted. Although

turbulence starts to penetrate the potential core as soon as the jet exits from the nozzle, it can be observed that even at z/d = 8, the maximum turbulence intensity does not occur at the centre line. However, it is obvious in Fig. 5.4.7(a) that the variations of turbulence intensity appear to be lifted up in the inner region as z/d increases. For example, between r/d = 0 and 0.37, the turbulence intensity increases by approximately 2.5 and 1.24 for z/d of 1 and 8 respectively. It may be expected, therefore, that further downstream (i.e. z/d > 8), the turbulence intensities at the jet center-line will be maxima.

Figures 5.4.8 and 5.4.9 present the turbulence intensity data at various Reynolds numbers. It can be observed that near the jet centre-line ($r/d \leq 0.5$), the turbulence intensity increases slightly as the Reynolds number is reduced. However, the reverse effect seems to be true at higher r/d's. It is also apparent that the jet spreads more as z/d increases. (For example, a turbulence intensity of 0.4% occurs at r/d = 2.37, 1.87 and 1.37 for z/d = 8, 6 and 4 respectively). It is interesting to note that even at z/d = 1 (Fig. 5.4.9), the mixing layers have extended beyond r/d = 1 and this shows how rapidly the turbulent activity ensues.

To summarise the above discussions, the turbulent characteristics of the free jet used in the present study are in good agreement with those of other jets used in previous investigations. Consequently, it can be expected that the impingement heat transfer measurements presented in Chapters 7 and 10 will be typical of those that can be expected for fully developed turbulent jets.

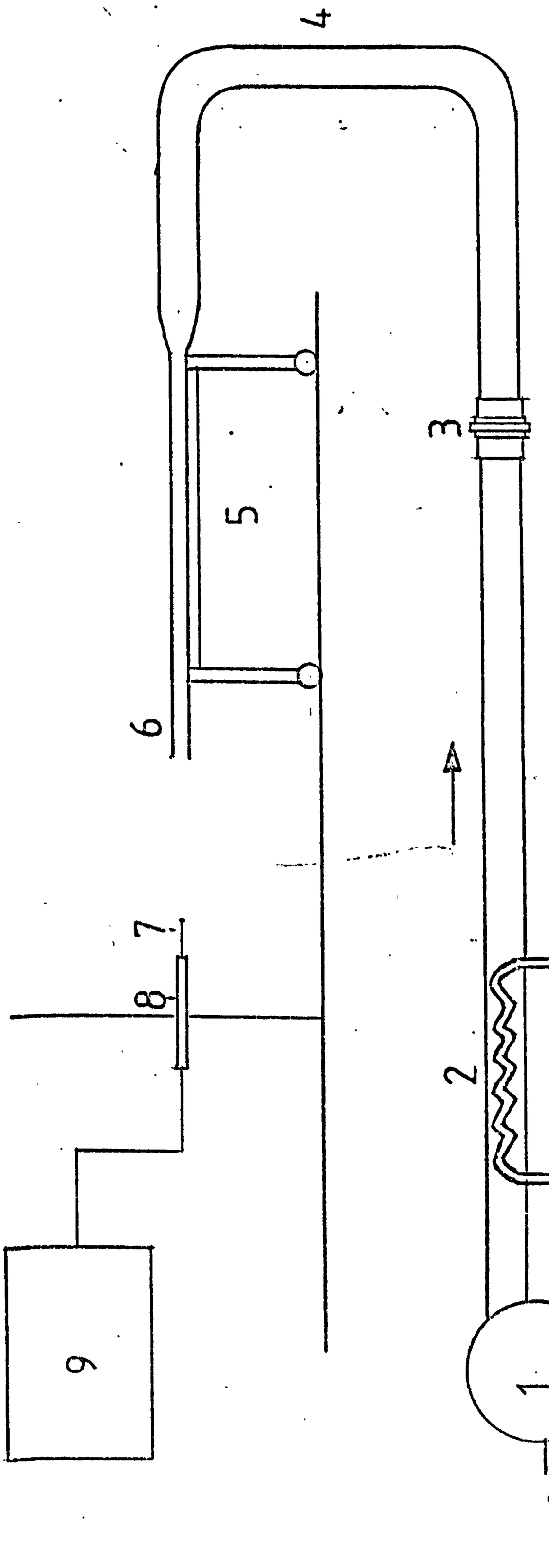

1.Centrifugal Fan (Variable Speed)
2.Water Cooler
3.Orifice Meter
4.Flexible Pipe
5.Carriage
6.Nozzle
7.Hot Wire
8.Probe Holder
9.Anemometer Unit

FIG.5.2.1. SCHEMATIC REPRESENTATION OF THE TEST RIG.

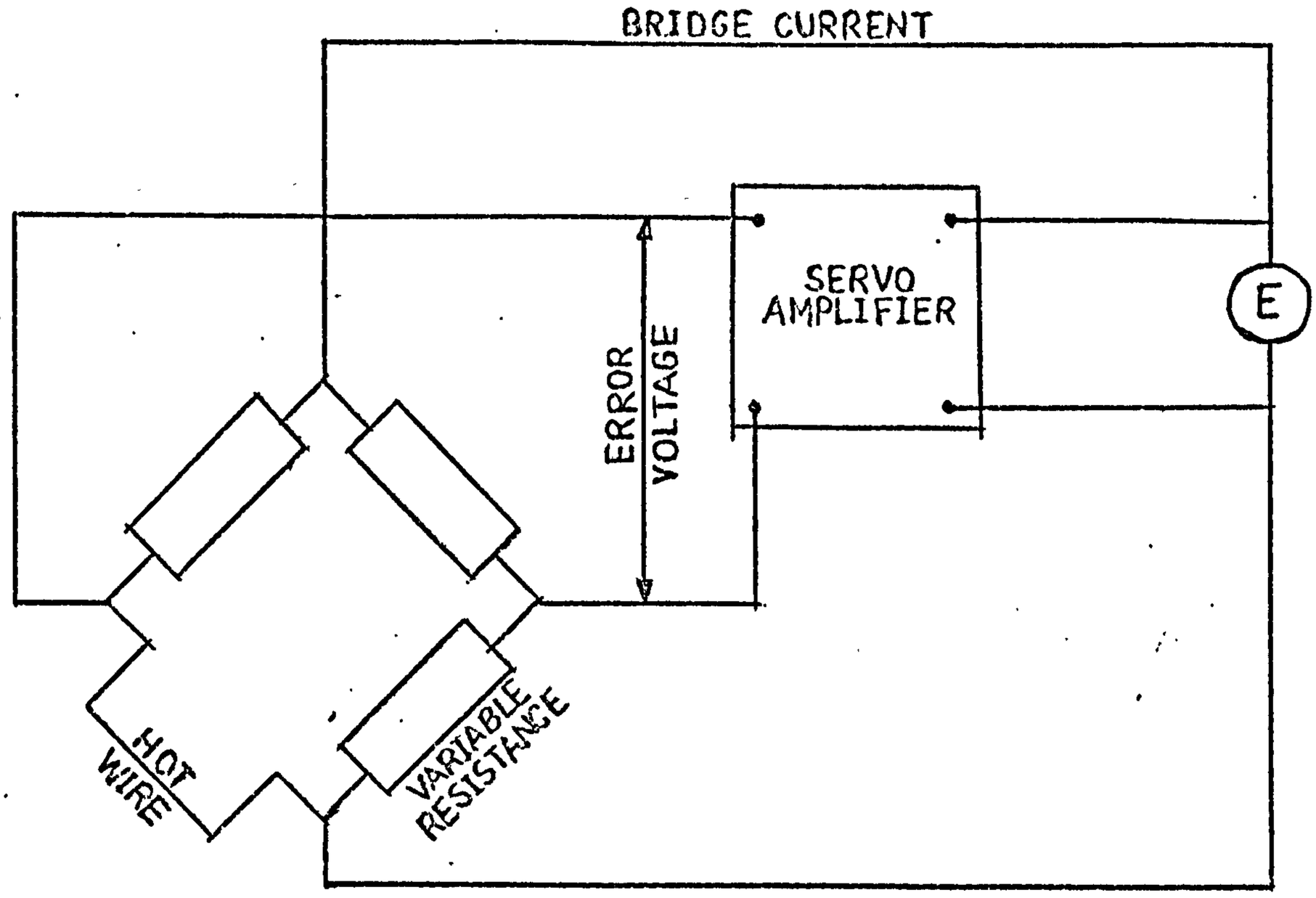

(a)

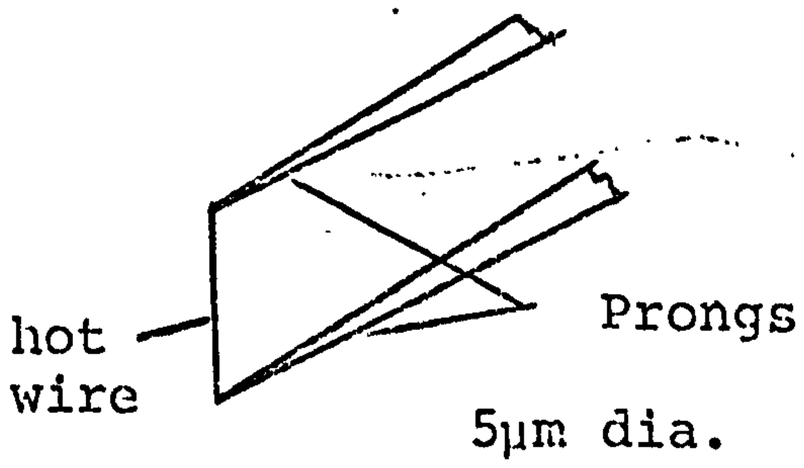

(i) General purpose type

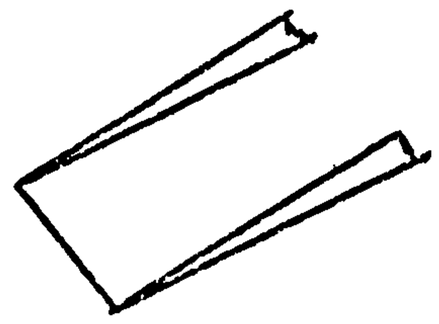

(ii) 45° Slanting sensor type

(b)

FIG.5.3.1. SCHEMATIC LAYOUT OF THE CONSTANT TEMPERATURE ANEMOMETER

(a) CONNECTION OF THE PROBE
(b) TYPICAL HOT-WIRE PROBES.

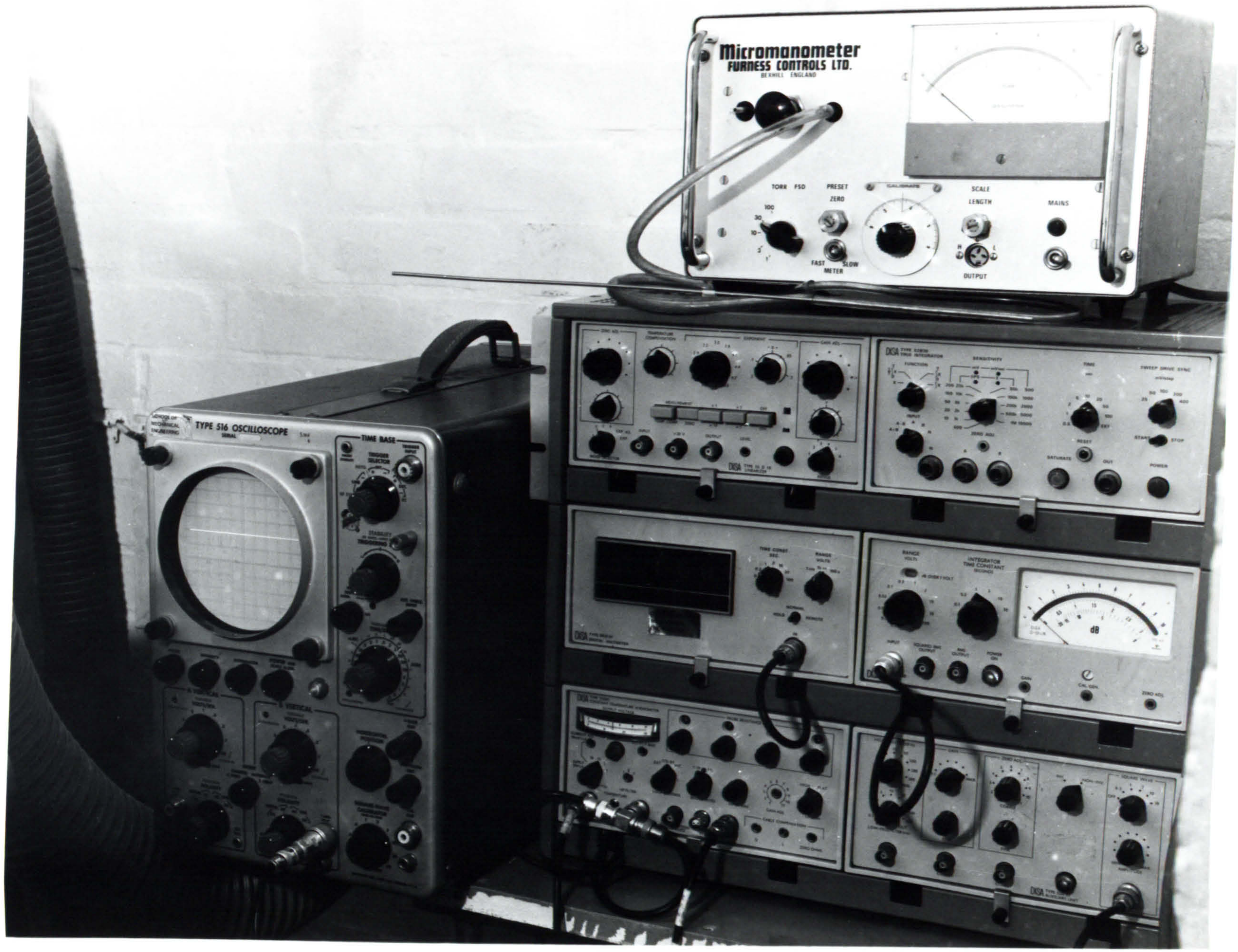

PLATE 5.3.1 A DISA UNIT FOR TURBULENCE MEASUREMENTS.

OSCILLATION CAUSED BY POOR BRIDGE BALANCE.

OSCILLATION CAUSED BY UNSUITABLE AMPLIFIER BAND WIDTH.

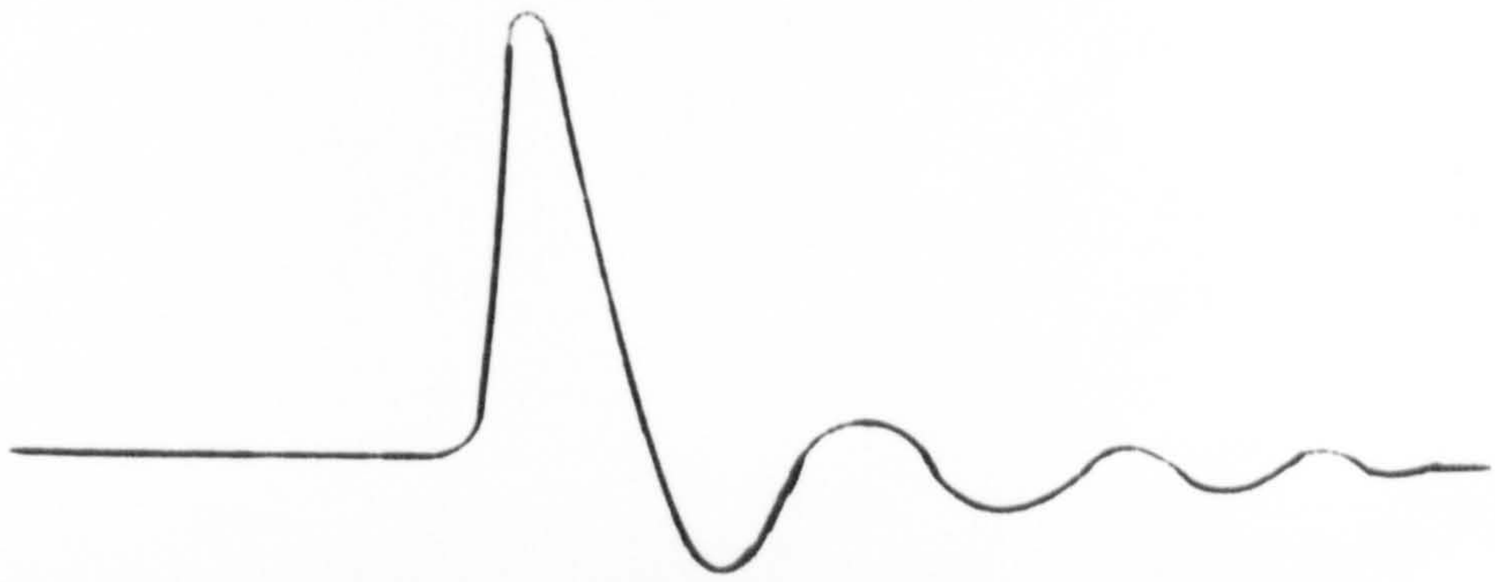

RESPONSE FROM A BALANCED SYSTEM.

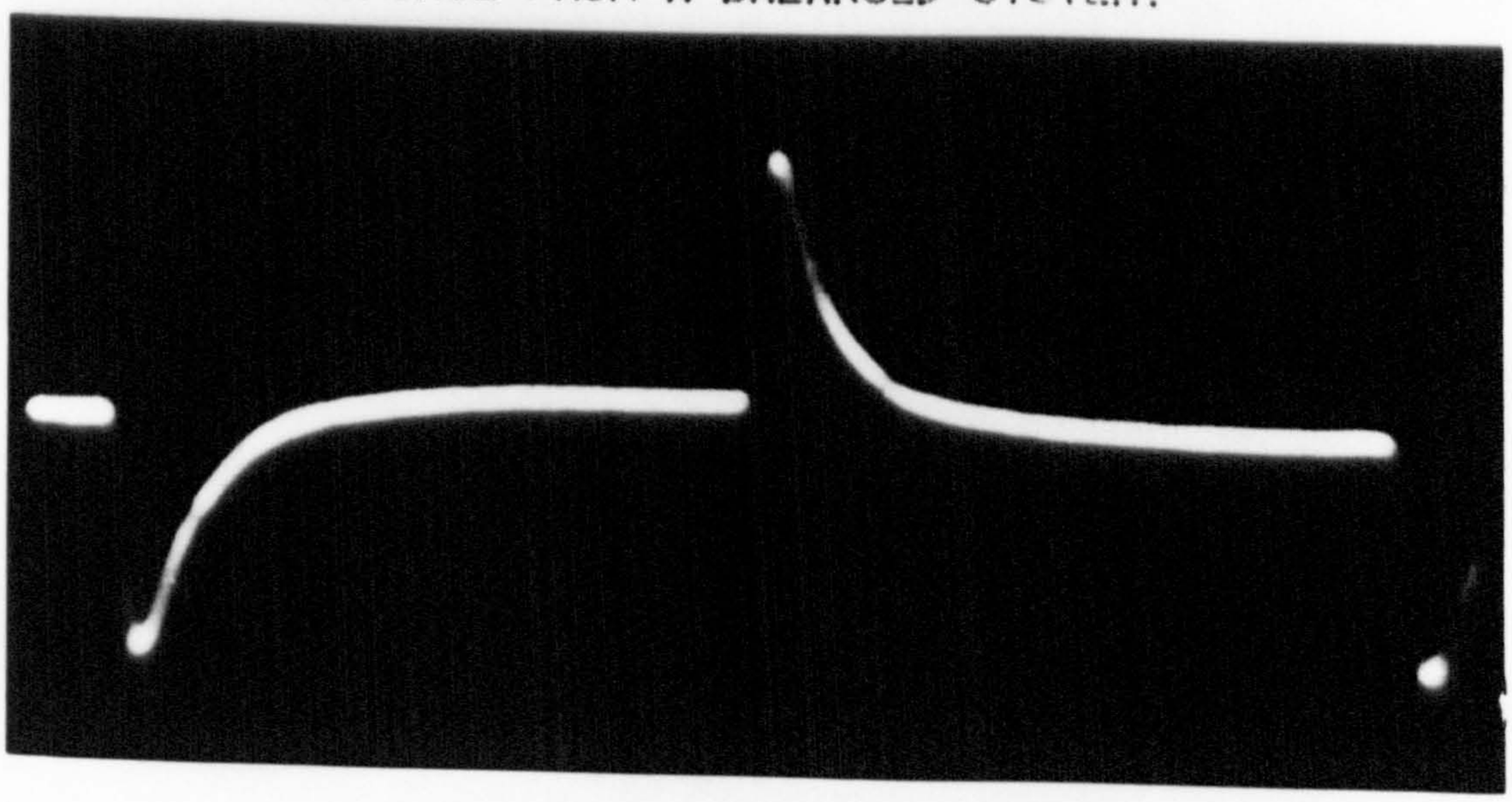

PLATE 5.3.2 TYPICAL RESPONSES DURING A SQUARE WAVE TEST.

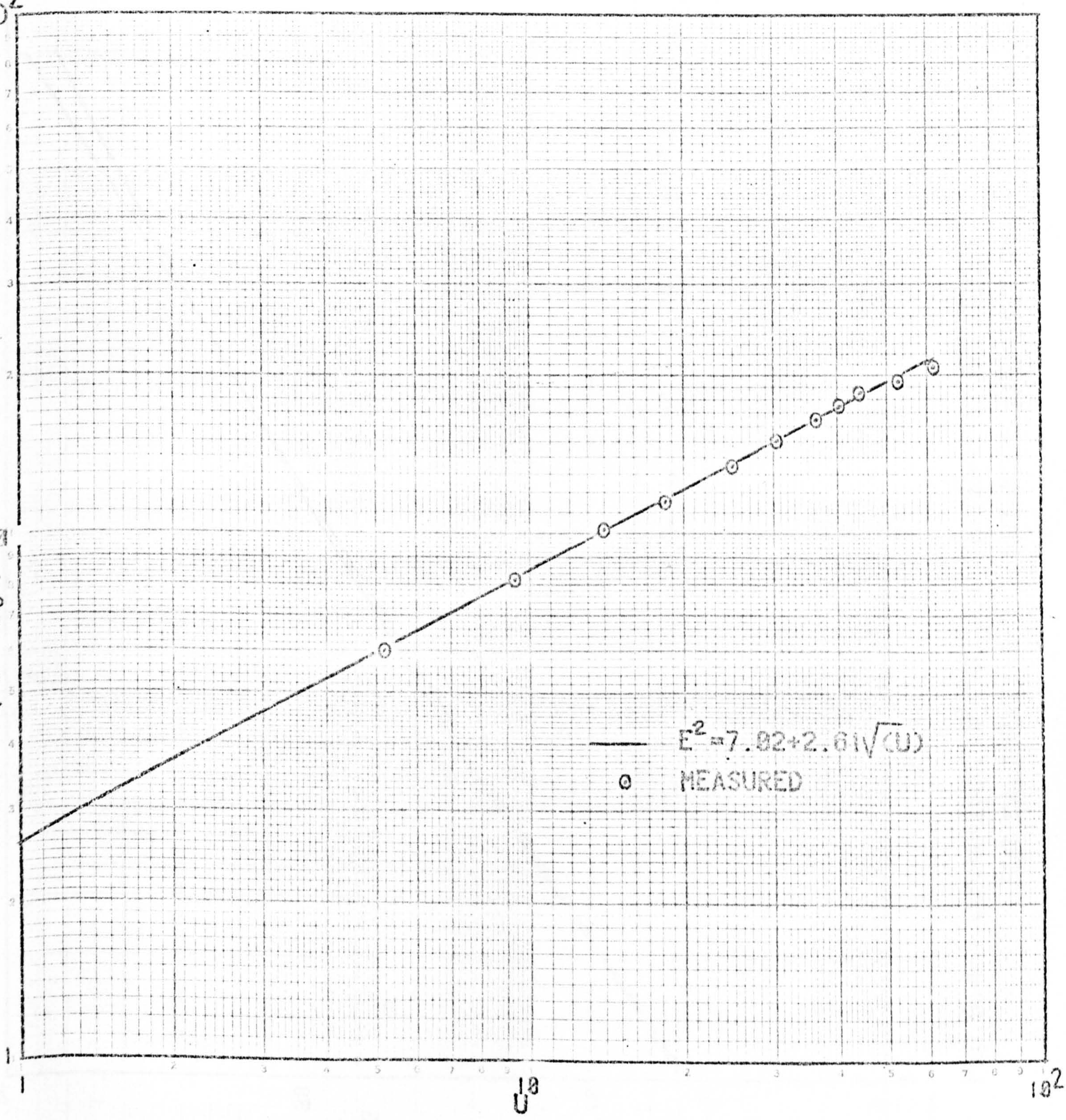

FIG.5.3.2 CALIBRATION CURVE OF THE HOT-WIRE ANEMOMETER.

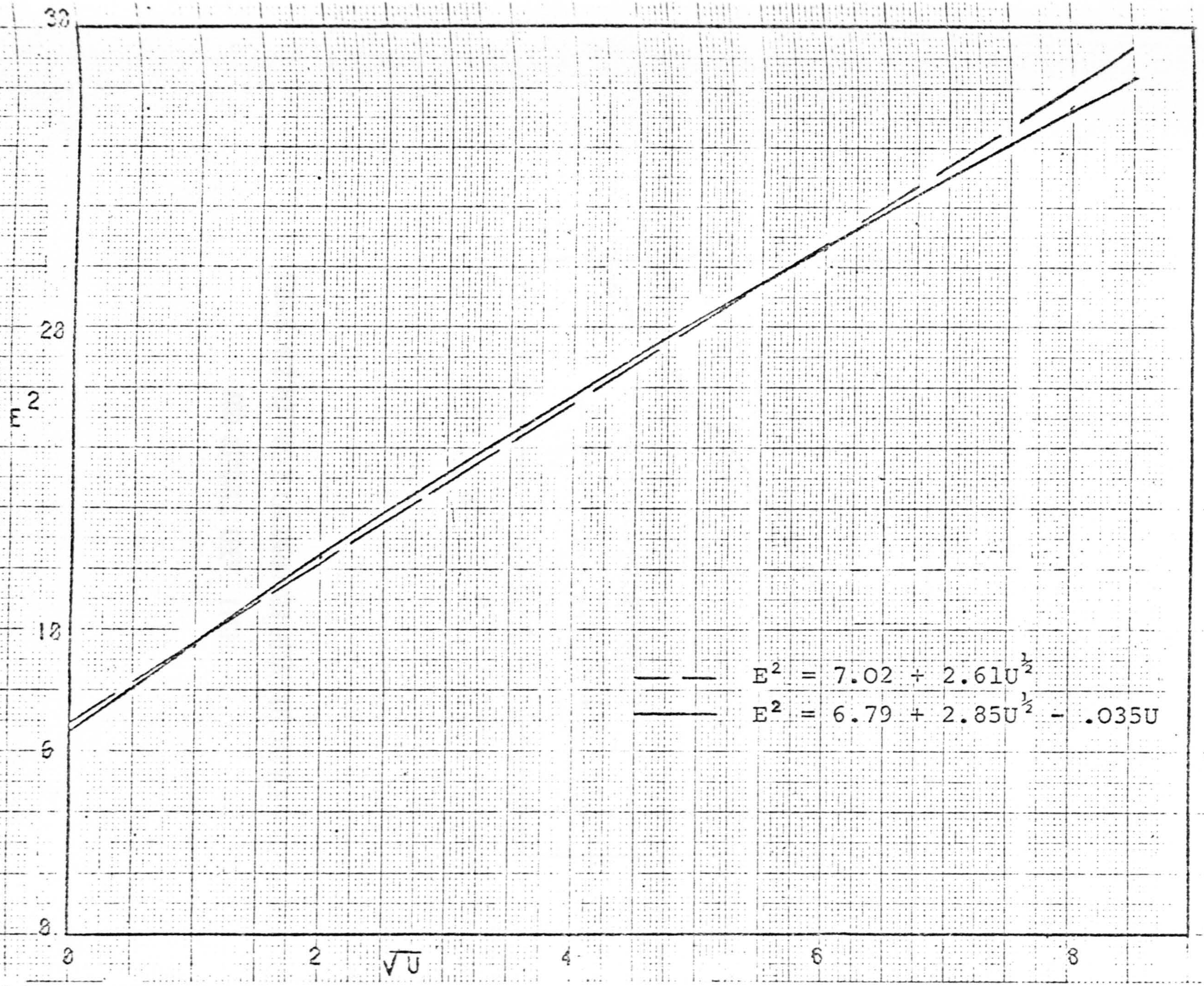

FIG.5.4.1 COMPARISON OF TWO AND THREE-TERM EQUATIONS FOR CALIBRATING THE HOT-WIRE ANEMOMETER.

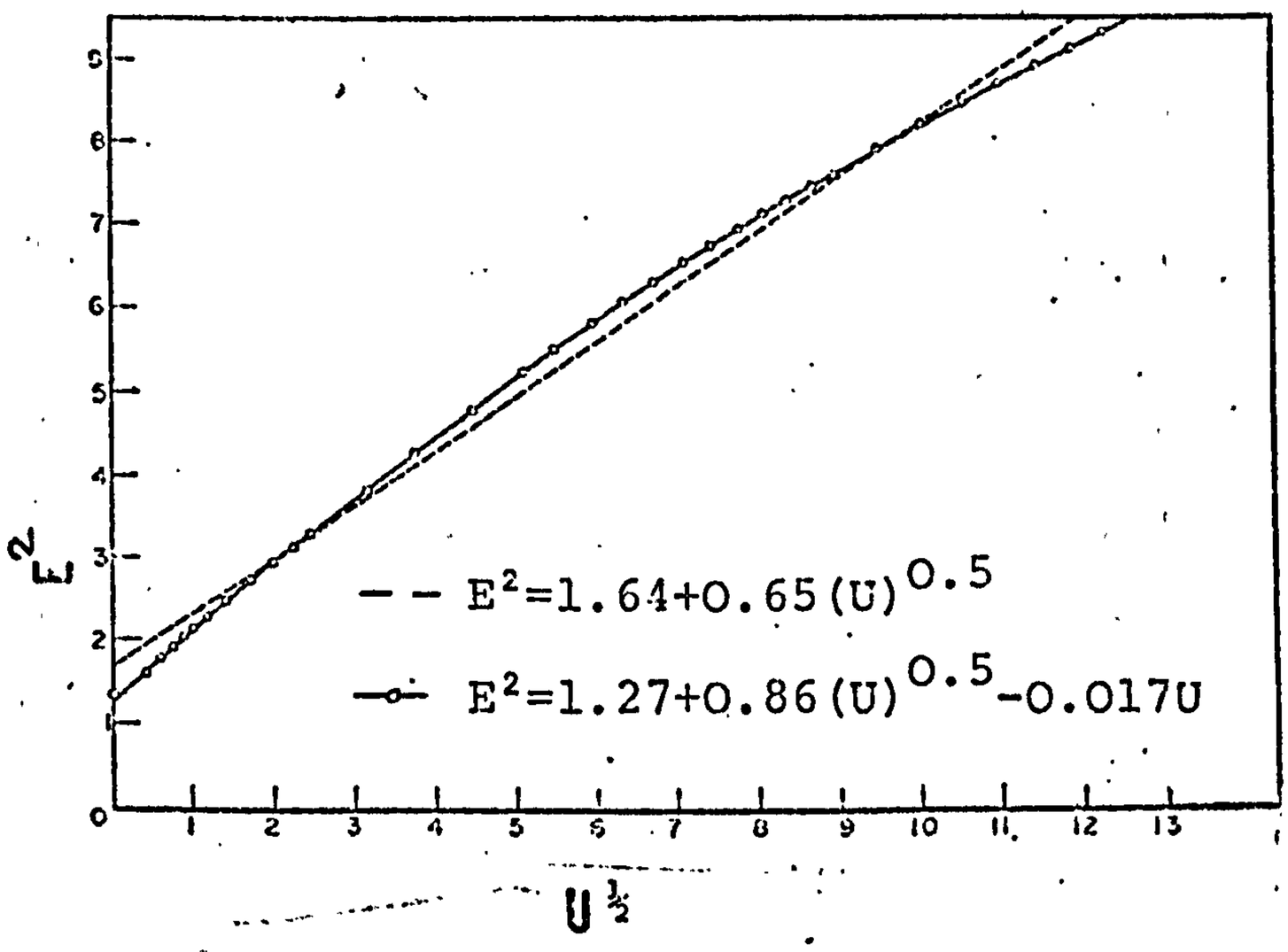

FIG.5.4.2 HOT-WIRE CALIBRATION DATA OF DAVIES AND SIDDALL (REF. 118).

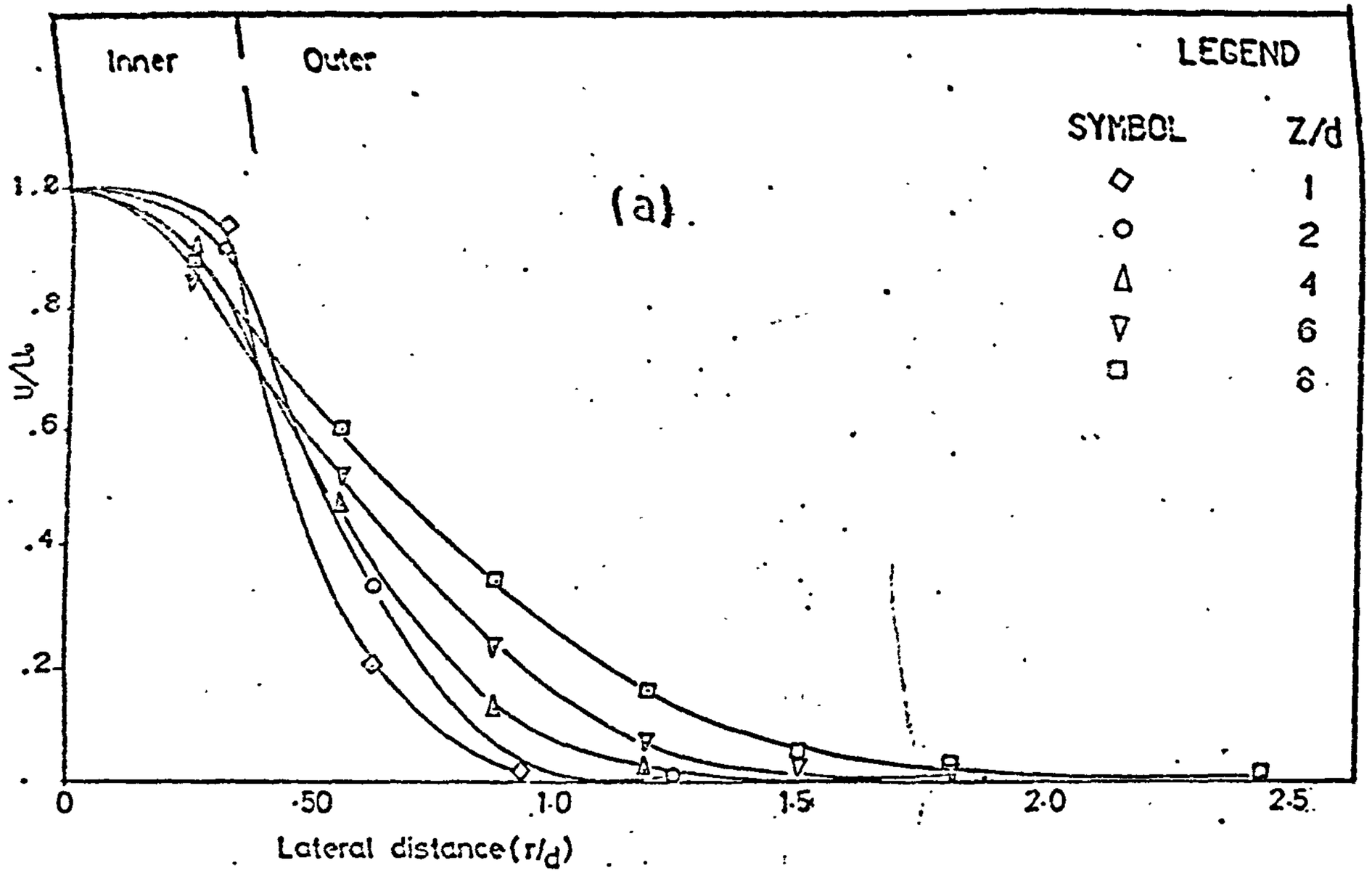

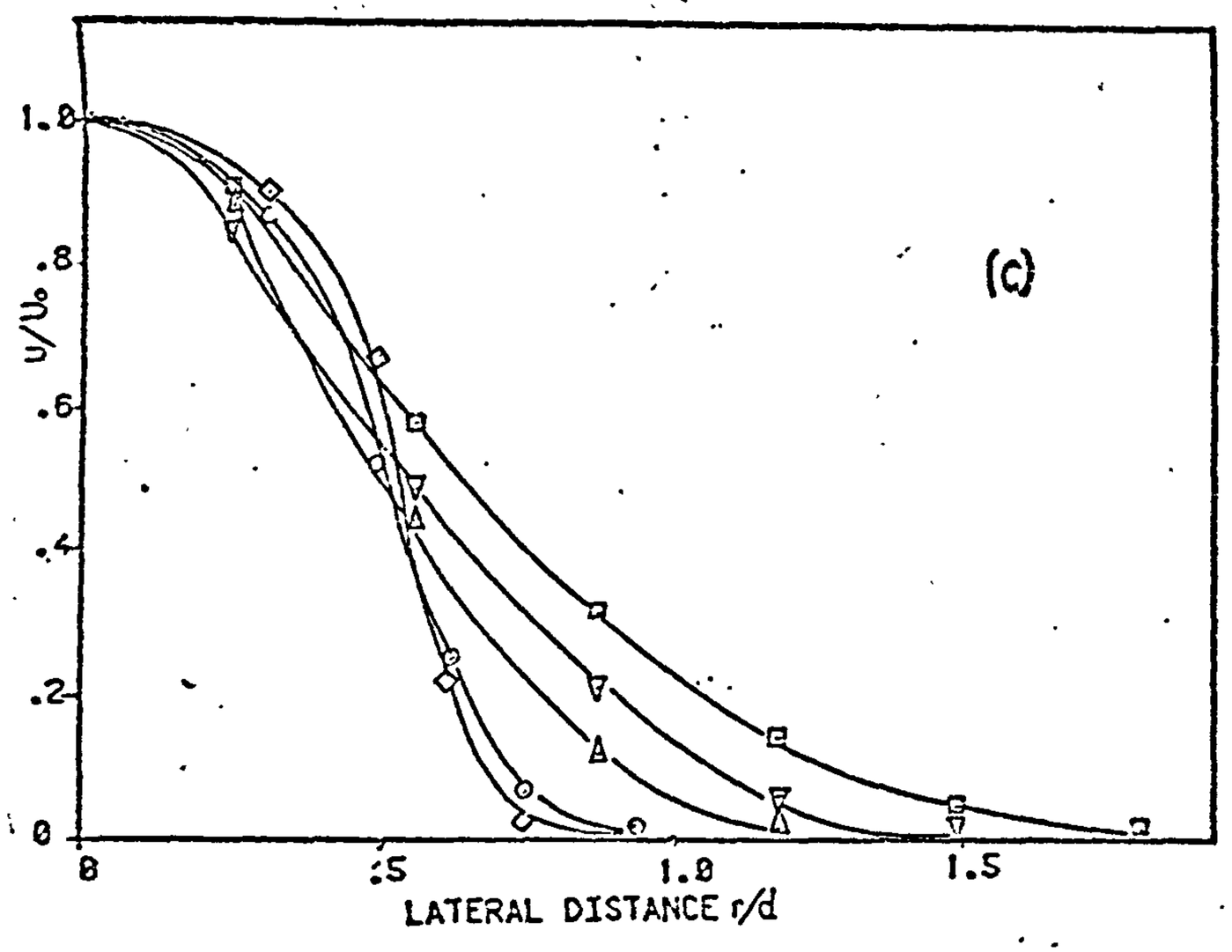

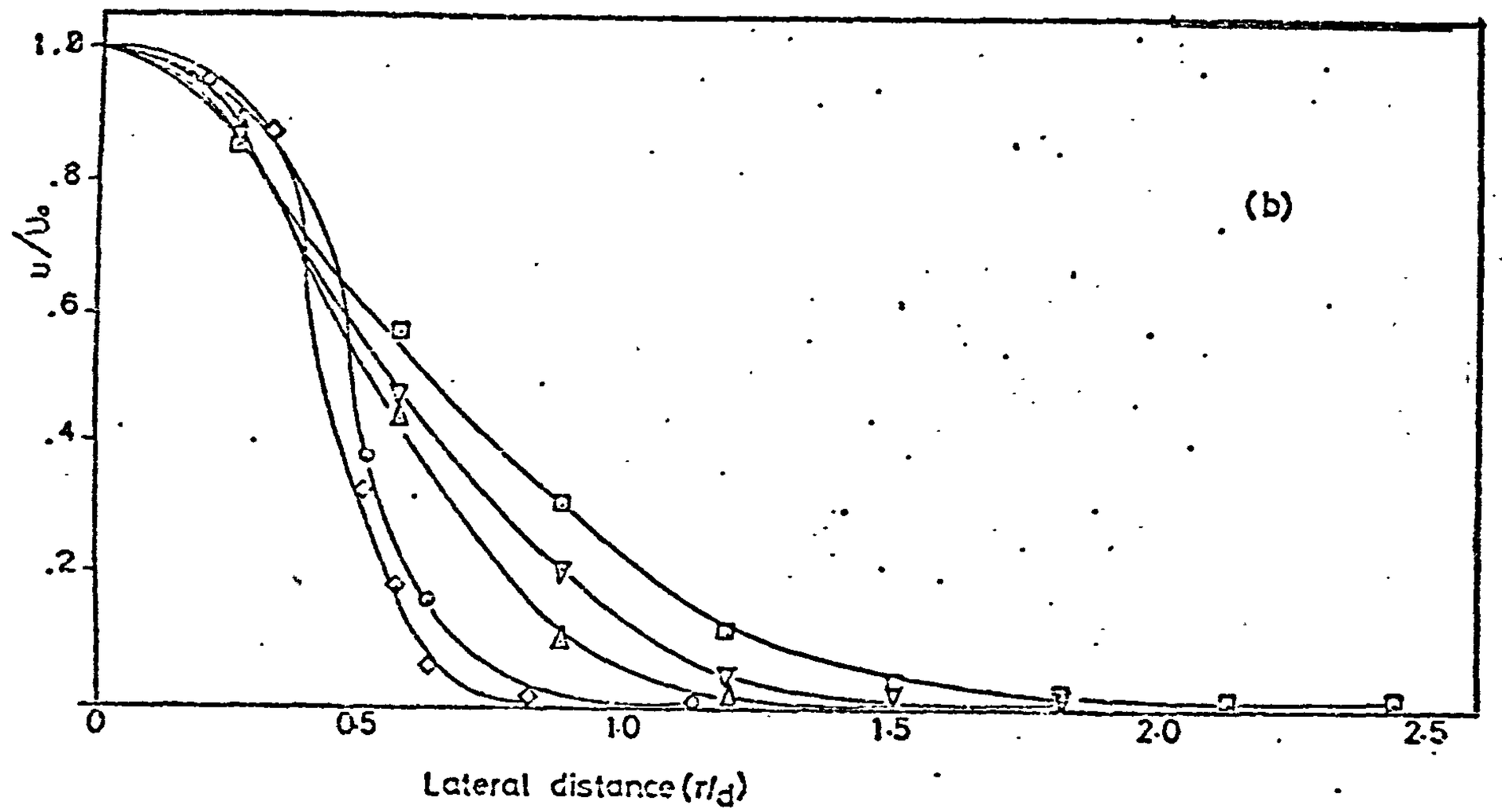

FIG. 5.4.3 RADIAL VARIATIONS OF AXIAL VELOCITY

(a) Re = 56000

(b) Re = 46000

(c) Re = 32500

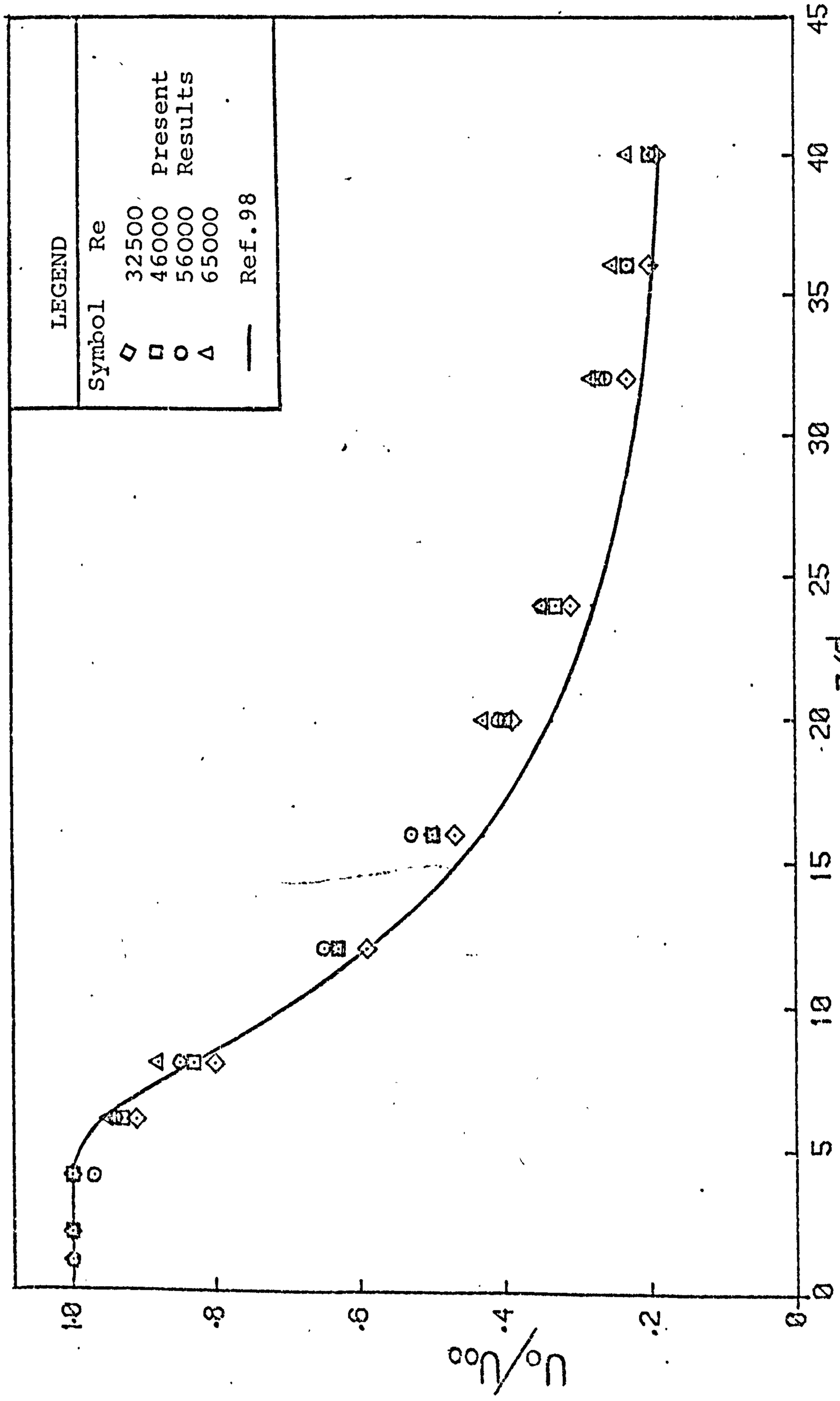

FIG. 5.4.4 DECAY OF CENTRE-LINE VELOCITY.

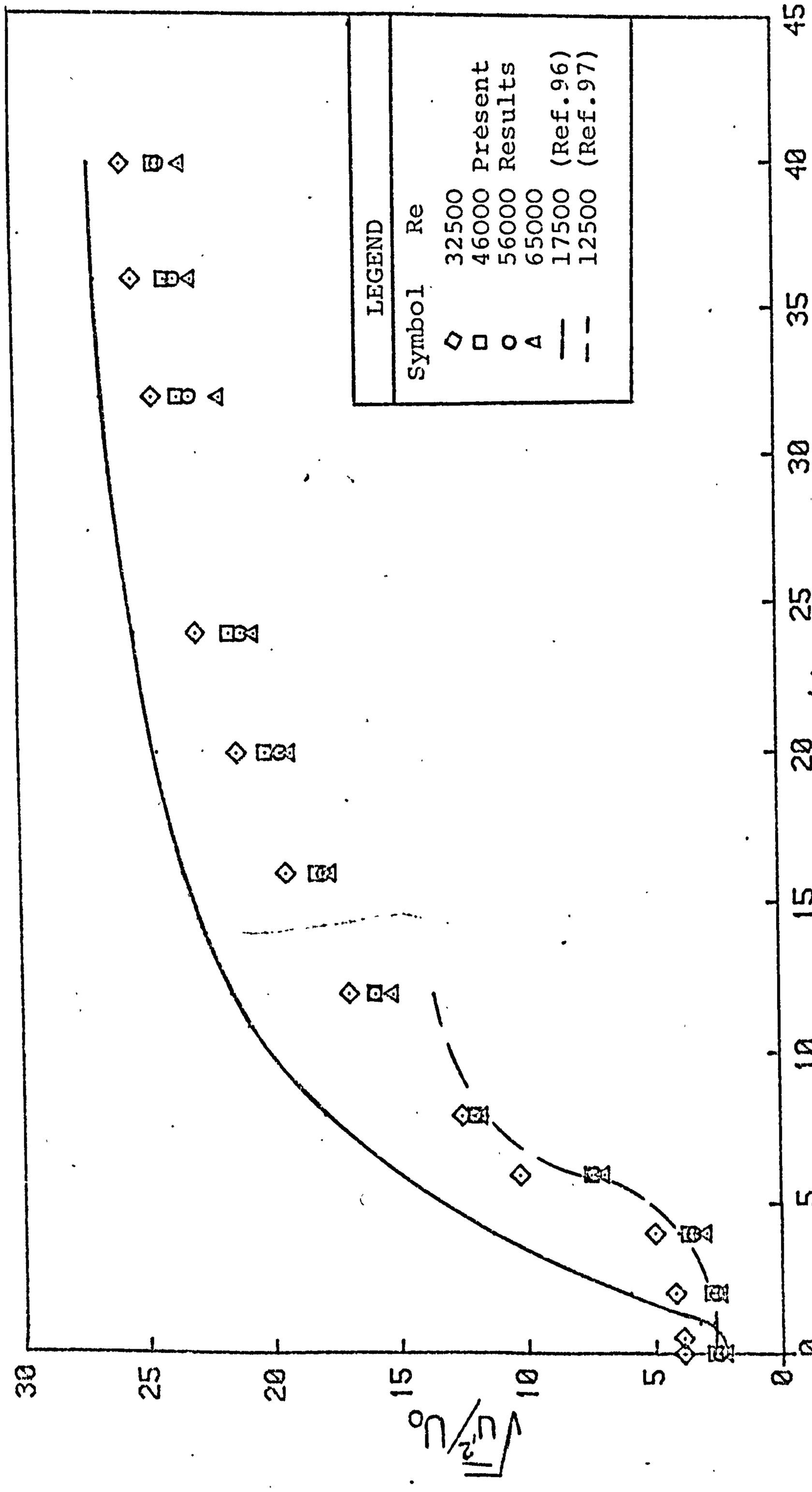

FIG. 5.4.5 COMPARISON OF PRESENT CENTRE-LINE TURBULENCE INTENSITY RESULTS WITH THOSE OF PREVIOUS WORKERS.

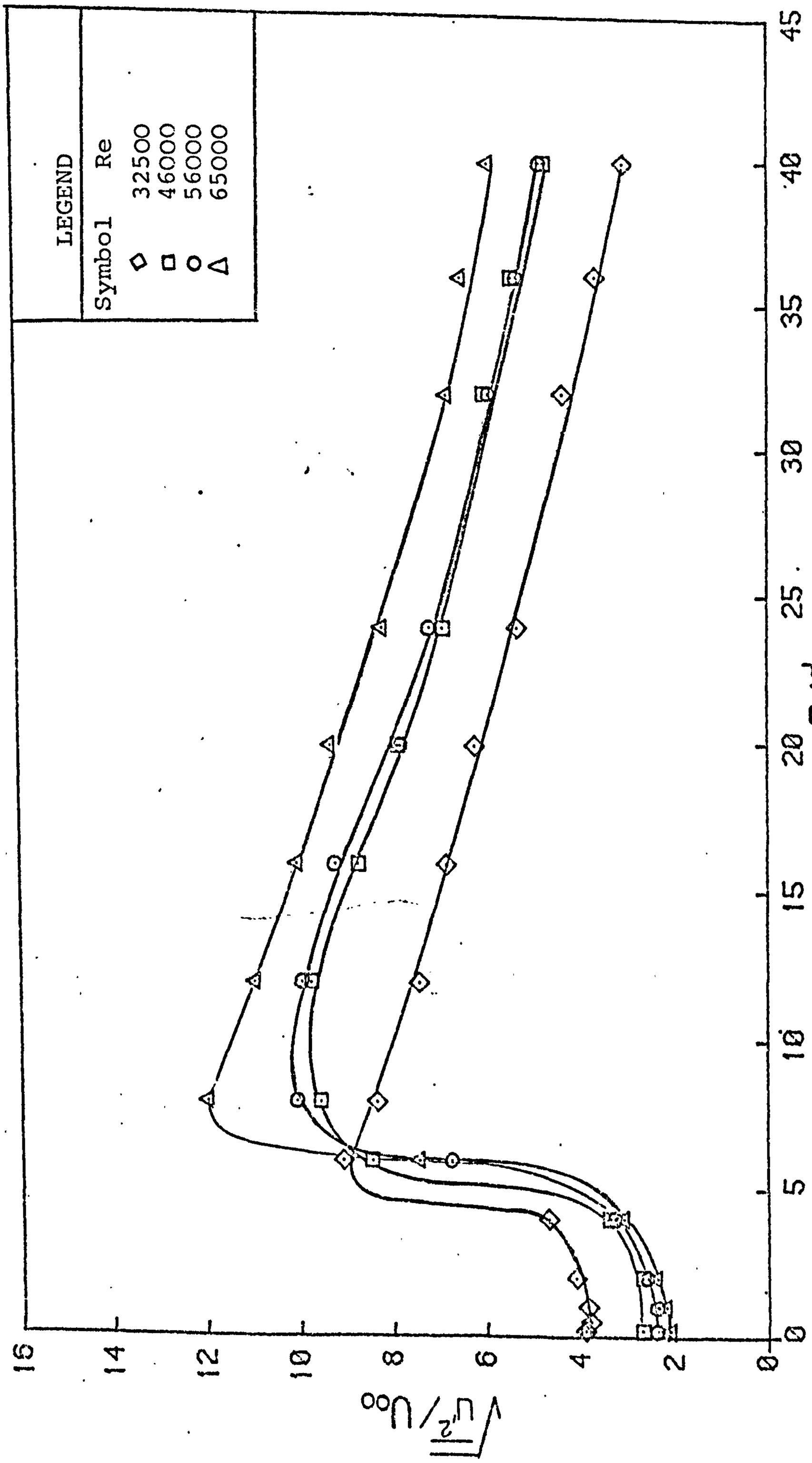

FIG. 5.4.6 VARIATION OF TURBULENT VELOCITY FLUCTUATION ON THE JET CENTRE-LINE.

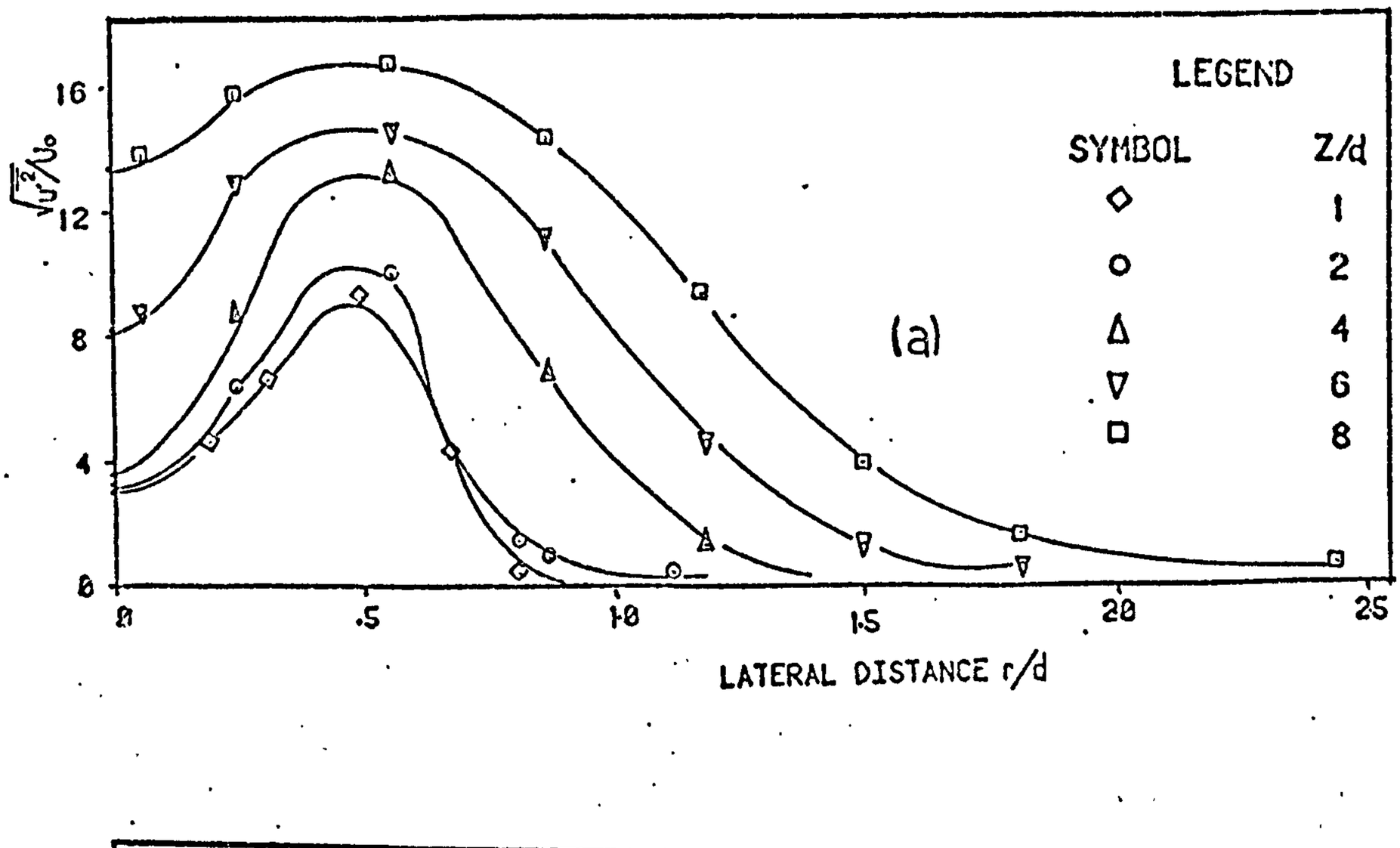

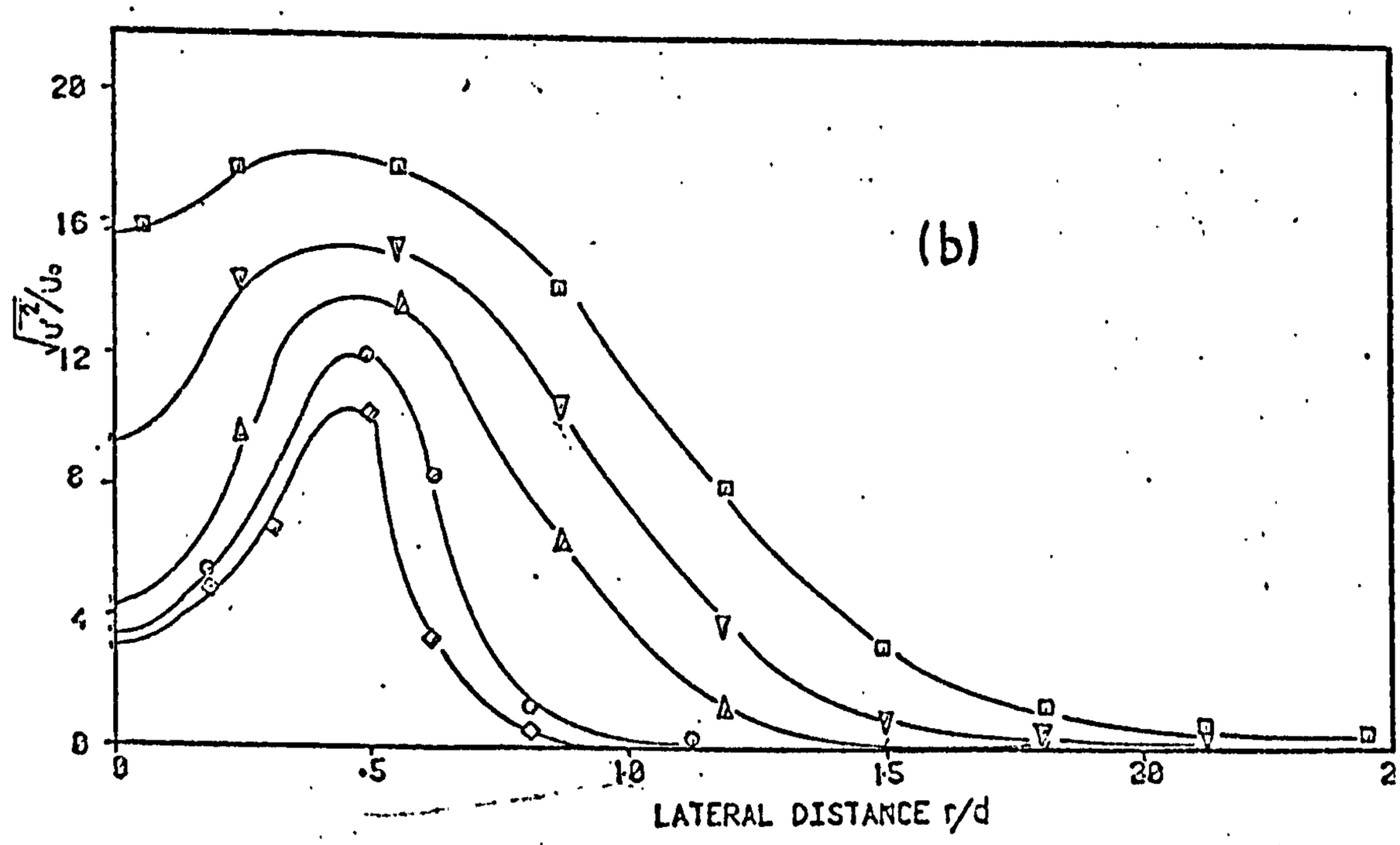

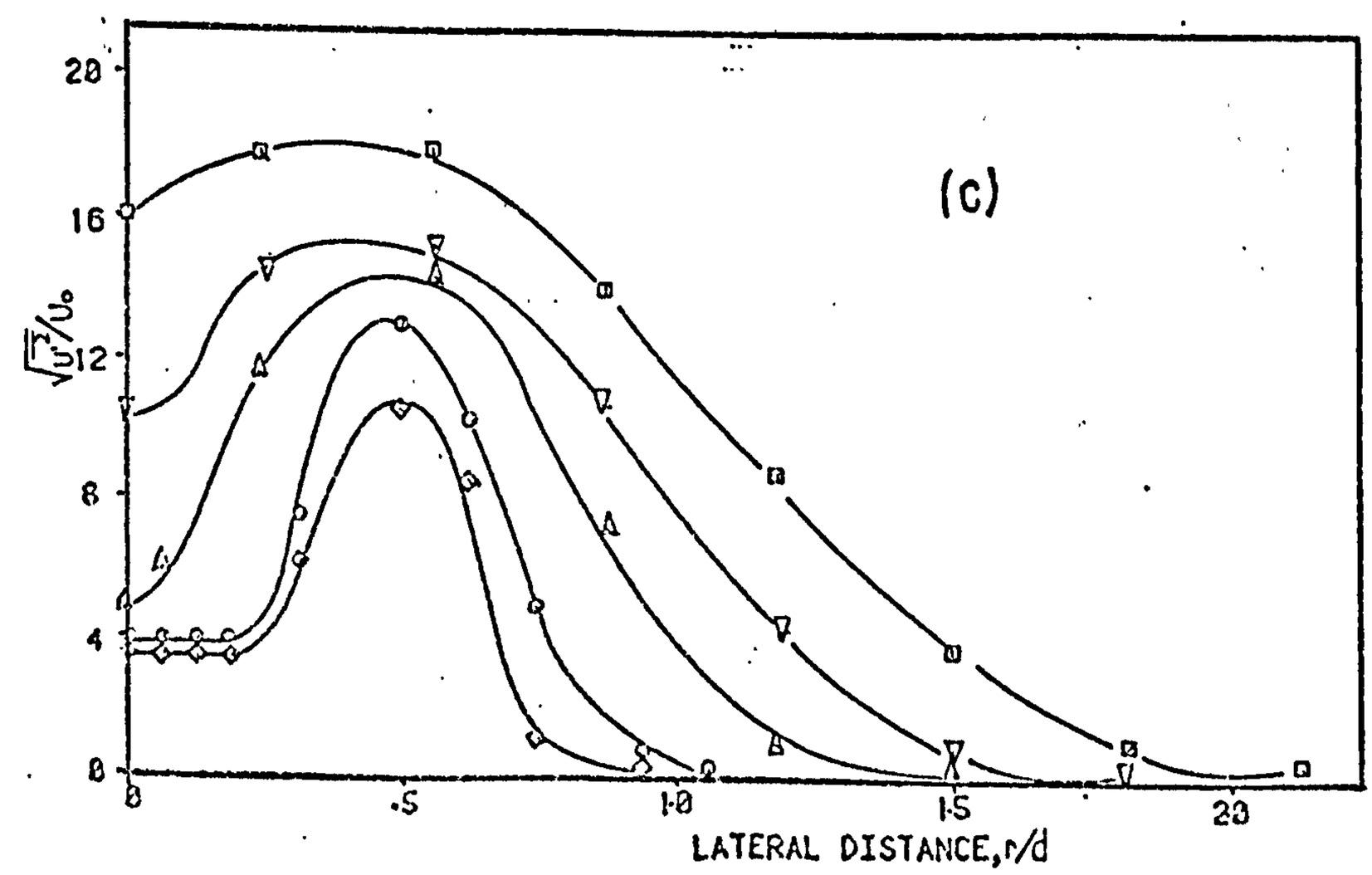

FIG.5.4.7 RADIAL VARIATIONS OF TURBULENCE INTENSITY

(a) Re = 50000

(b) Re = 40000

(c) Re = 32500

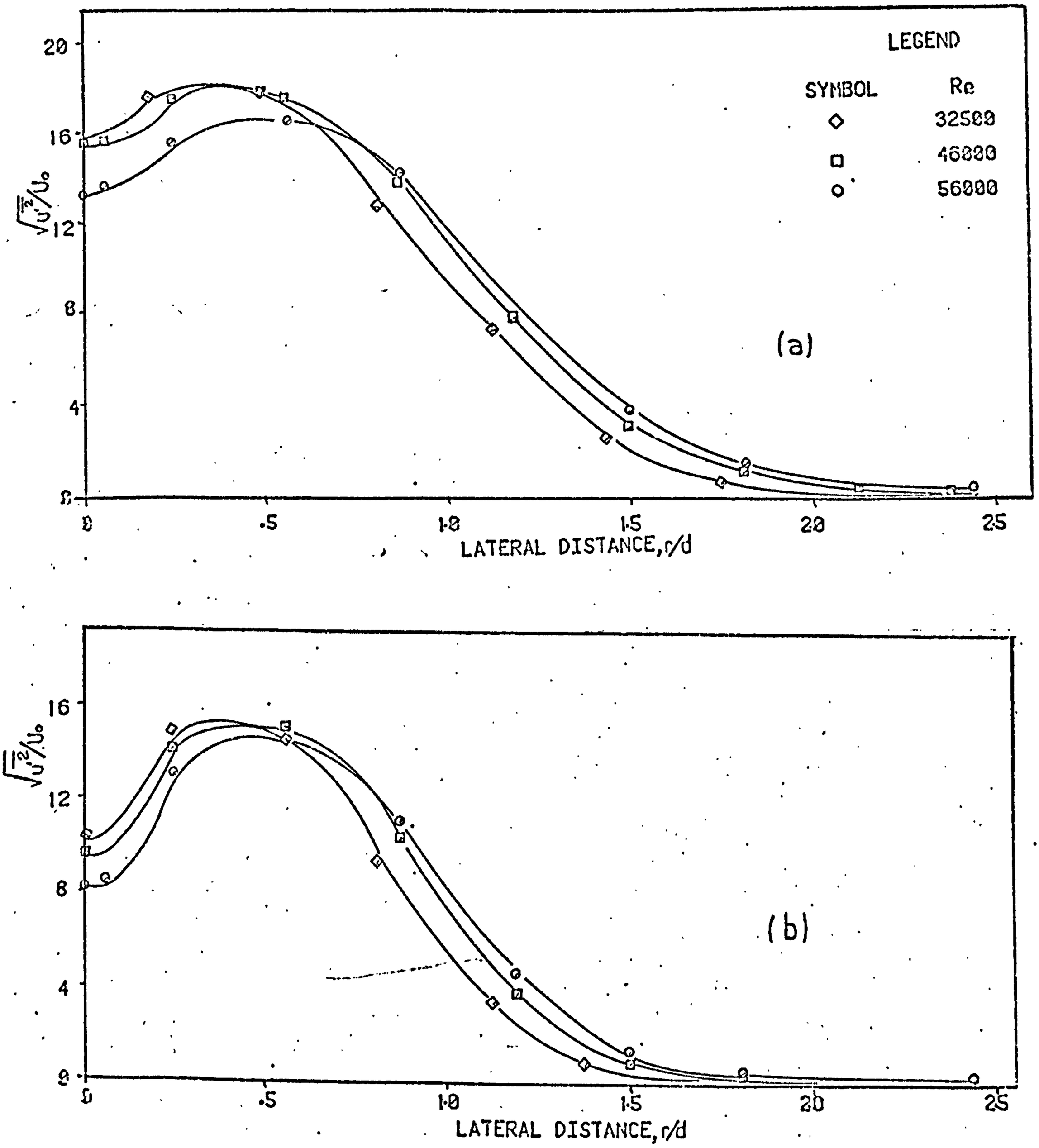

FIG. 5.4.8 RADIAL VARIATIONS OF TURBULENCE INTENSITIES
(a) Z/d = 8 (b) Z/d = 6

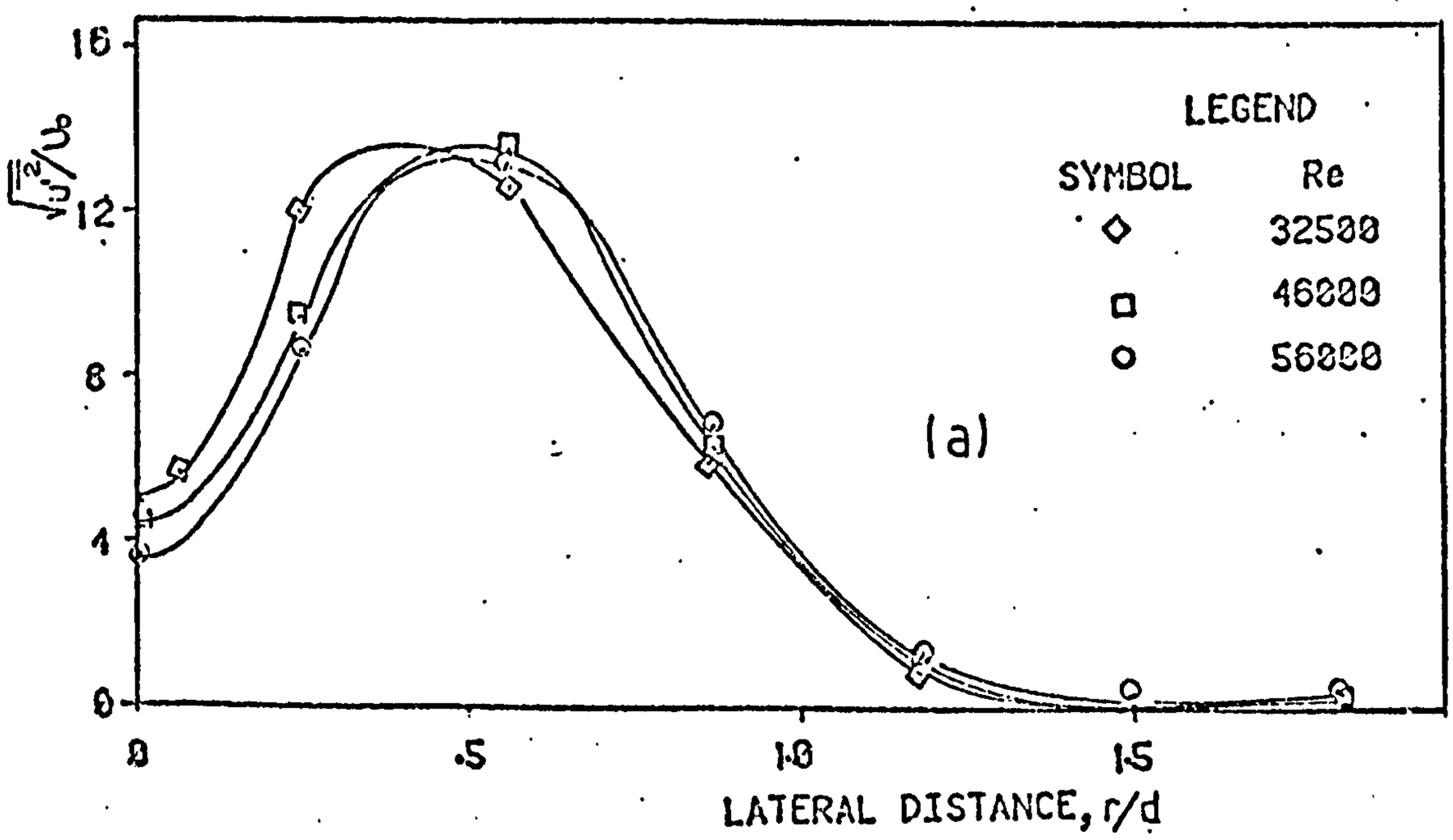

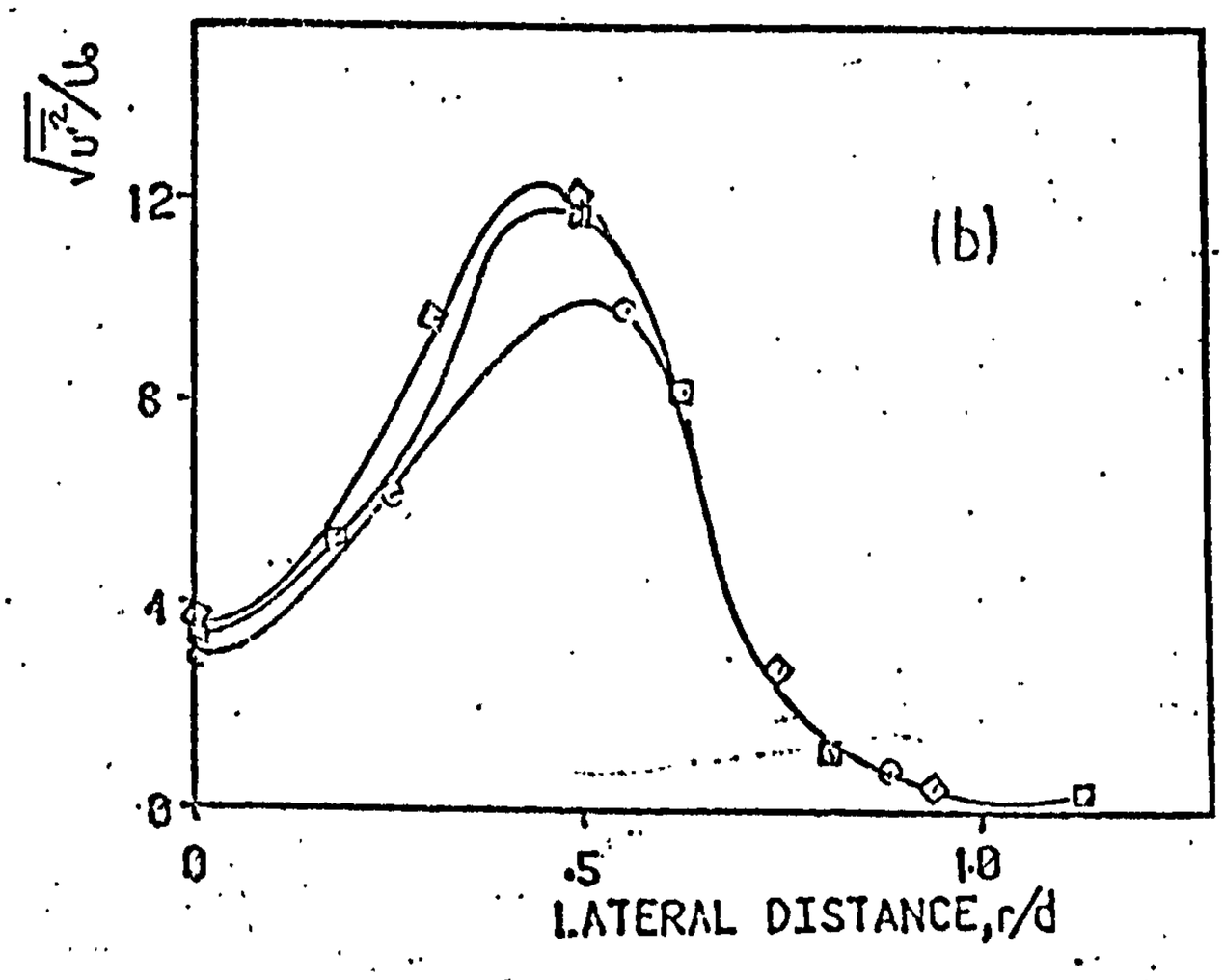

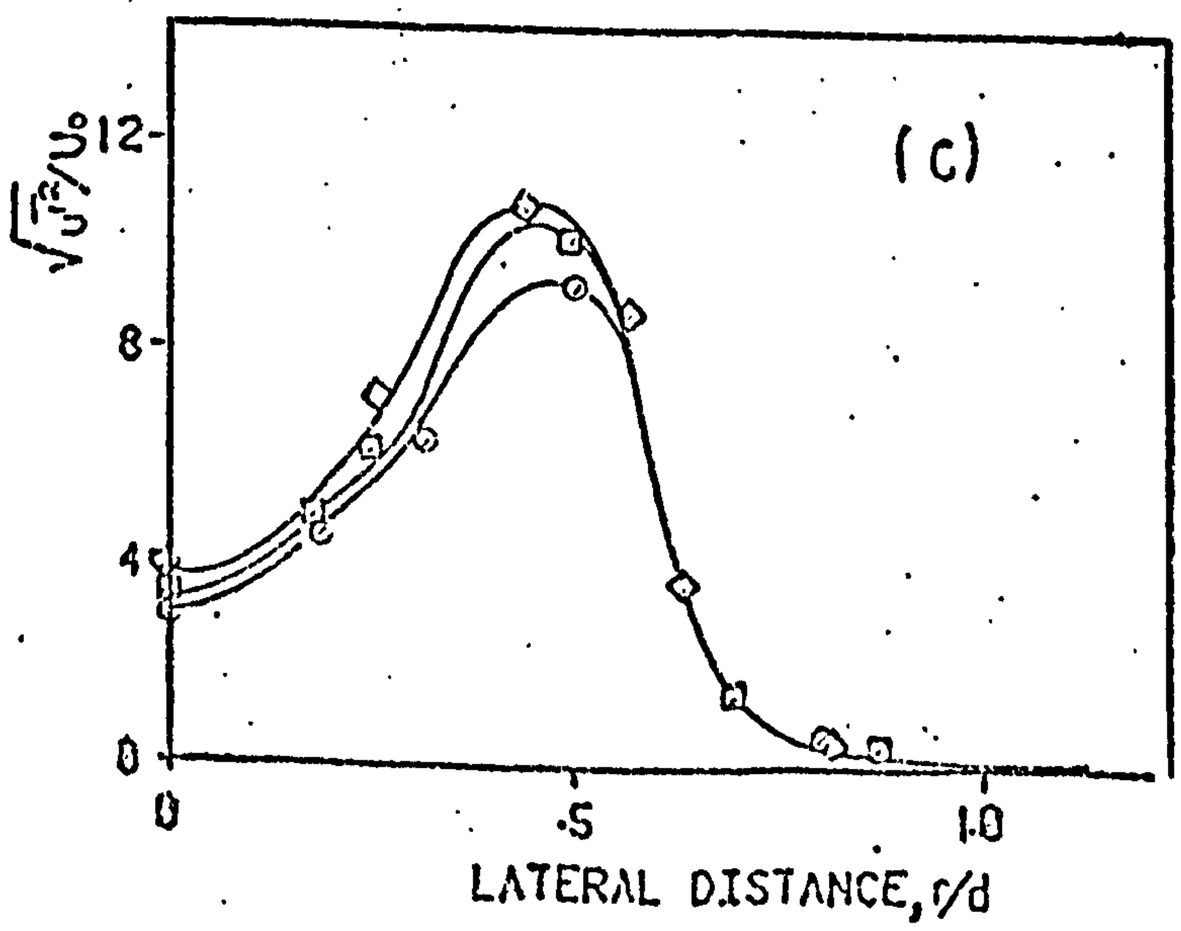

FIG. 5.4.9 RADIAL VARIATIONS OF TURBULENCE INTENSITIES
(a) Z/d ≈ 4 (b) Z/d ≈ 2 (c) Z/d ≈ 1

CHAPTER 6

6. HEAT TRANSFER - APPARATUS AND PROCEDURE

6.1 INTRODUCTION

The procedure employed in the mass transfer tests is presented in this Chapter. However, stagnation point values can be difficult to measure so that their reproducibility is poor. In this study, repeatable stagnation point heat transfer coefficients were obtained by employing an optical technique to determine the time for initial clearance of the naphthalene. Details of this technique are also discussed in this Chapter.

6.2 THE TEST RIG

The mass transfer spraying equipment was described in Chapter 3, whilst details of the test rig were presented in Chapter 5.

6.3 STAGNATION POINT MEASURING EQUIPMENT

As discussed in Chapter 4, the available results for stagnation point heat transfer vary widely (±35%, see Fig. 4.5.4). This scatter is probably due to differences not only in the jet characteristics but also due to errors inherent in the measuring techniques. For example, Perry (Ref. 21) used a transducer of 16.25 mm diameter so that the stagnation point heat transfer was in effect a mean value over the area of the transducer.

In the thin-film naphthalene technique, the clearance pattern is visible so that in principle stagnation point mass transfer rates can be readily estimated. This procedure was found to be relatively reliable at lower z/d's ($z/d \lesssim 6$) but at higher z/d's, initial clearance is difficult to detect and errors may be introduced. Photographic records cannot be analysed until the clearance pattern has spread to $r/d = 1$. In general the estimation of the time for initial clearance is rather subjective and depends upon the experience of the investigator.

In this study, the stagnation point values can be determined by extrapolation of the radial variation in heat/mass transfer coefficients or by taking the mean of two "stagnation times" or by an optical method.

When the first of these techniques is adopted, frequent estimates of the extent of clearance are made near the stagnation point so that the radial variation of heat transfer can be extrapolated to the "actual stagnation point". The repeatability of this procedure is however poor because of the difficulty in obtaining a consistent shape of the heat transfer curve near the stagnation point. In the second method, two readings are taken, the first estimate corresponds to when clearance appears to have just commenced whilst the other indicates definite clearance. Mahmood (Ref. 50) found that these two stagnation times varied by between 5 to 10% and the mean was used as the actual stagnation value. This technique was found to be usually more satisfactory than the extrapolation procedure.

To reduce the problems in the methods described above, an optical system was designed and used to determine the time for clearance at the stagnation point. It is pertinent to describe the system fully. It consisted of :

(a) A helium-neon gas laser (Spectra-Physics Model 120) together with an exciter (Spectra-Physics Model 256)

and

(b) A silicon photo-voltaic cell (Ferranti Model MS 11 AE)

A schematic diagram of the system is shown in Fig. 6.3.1. The location of the stagnation point was determined visually in a previous test. The coherent, bright and extremely narrow parallel beam of light from the laser tube was focussed onto the location of this stagnation point. The silicon detector was mounted in line with the laser beam on the other side of the perspex test plate. This detector has an active area of 22.2 mm in diameter so that any laser light transmitted through the test surface as the thin film of naphthalene sublimed was readily detected. The output signal from the detector was fed to an X-Y recorder (Bryans Auto Plotter 22000 series) and a typical plot is shown in Fig. 6.3.2.

It can be observed that very little transmission occured during most of the time prior to clearance. However, as the naphthalene clearance began, the output of the detector then increased. The variation in output appears to follow an 'S' saturation curve. This is characteristic of transmission through a layer of gradually decreasing thickness. (The transmissivity of a layer of uniform thickness is expressed by $\tau = e^{-KL}$ where τ = transmissivity, K = absorption coefficient of the layer and L = thickness). Final clearance was assumed to occur at point B on the trace.

6.4 MASS TRANSFER TEST PROCEDURES

The procedure adopted for the mass transfer measurements on the single free jet was as follows :

1) The target plate was selected and cleaned with a suitable solvent, such as acetone. "Brasso" was used for final cleaning and polishing. The calibration slides were also cleaned, weighed and fixed at the appropriate locations on the test surface employing double-sided adhesive tape.

2) The operation of the spray mechanism, in particular the spray nozzle, was checked and the nitrogen and air supply pressures were adjusted to required levels.

3) The nozzle of the air jet was fitted into the appropriate carrier plate and fixed onto the mounting frame. The inclination of the nozzle was checked and adjusted with a combination set. The distance between the target and nozzle exit (z/d) was then set. Finally, the laser and optical arrangement was aligned with the pre-determined stagnation point.

4) The air supply flow rate to the jet was adjusted to the required value. This early start-up of the rig stabilised the air temperature prior to commencement of the mass transfer measurements. The air temperature was measured with a digital thermometer (Kane and May digitherm MK.III) and the cooling water was adjusted so as to maintain the jet temperature at or very near to the ambient value. The time required for temperature stabilization depended on the jet Reynolds number (40 minutes was found to be adequate in all cases).

5) The target plate which was to be sprayed was mounted on the carrier in the spray rig as depicted in Plate 6.4.1. This plate was levelled (if necessary) by means of the adjusting screws.

6) The target plate was sprayed as discussed in Chapter 3. A narrow width was sprayed initially to allow the spray mechanism to stabilise and after stabilization, the test surface proper was sprayed. The digital clock was started upon commencement of spraying of this test surface. Both the length of the sprayed portion and the total "spraying time" were recorded.

7) All the calibration slides were carefully removed from the sprayed surface and re-weighed to evaluate the initial coating density. Preliminary tests were carried out to determine the effect on the coating density of mounting the calibration slides on top of the test plate. The details are presented in Appendix A.5. This effect was however found to be negligible (i.e. < 0.5%).

8) The sprayed target plate was mounted in the test rig whilst the naphthalene surface was shielded from the jet. The shield was removed upon commencement of the mass transfer test and the time was recorded.

9) The laser and the X-Y recorder were switched on.

10) If photographic recording was to be employed, the equipment was set up at the rear side of the impingement surface.

11) After stagnation point clearance was recorded the optical system was switched off. If the laser was not used, then the "two stagnation times" procedure was employed to obtain the 'actual' initial clearance of the thin film of naphthalene.

12) Photographs were taken at times which corresponded to clearance proceeding to pre-determined radial positions. Typically, ten photographs were taken during a test. Alternatively, the progress of the clearance pattern was noted at regular intervals.

13) The surface temperature was measured with a digital thermometer (Kane and May) which has a resolution of 0.1^{o}C and a cylindrical tip of 0.8 mm diameter.

14) The calibration slides were finally re-weighed after at least 3000 seconds had elapsed since the previous weighing. These two weighings enabled the rate of naphthalene loss due to natural convection to be estimated.

15) A typical calculation procedure for the local heat transfer coefficients is presented in Appendix A.4.

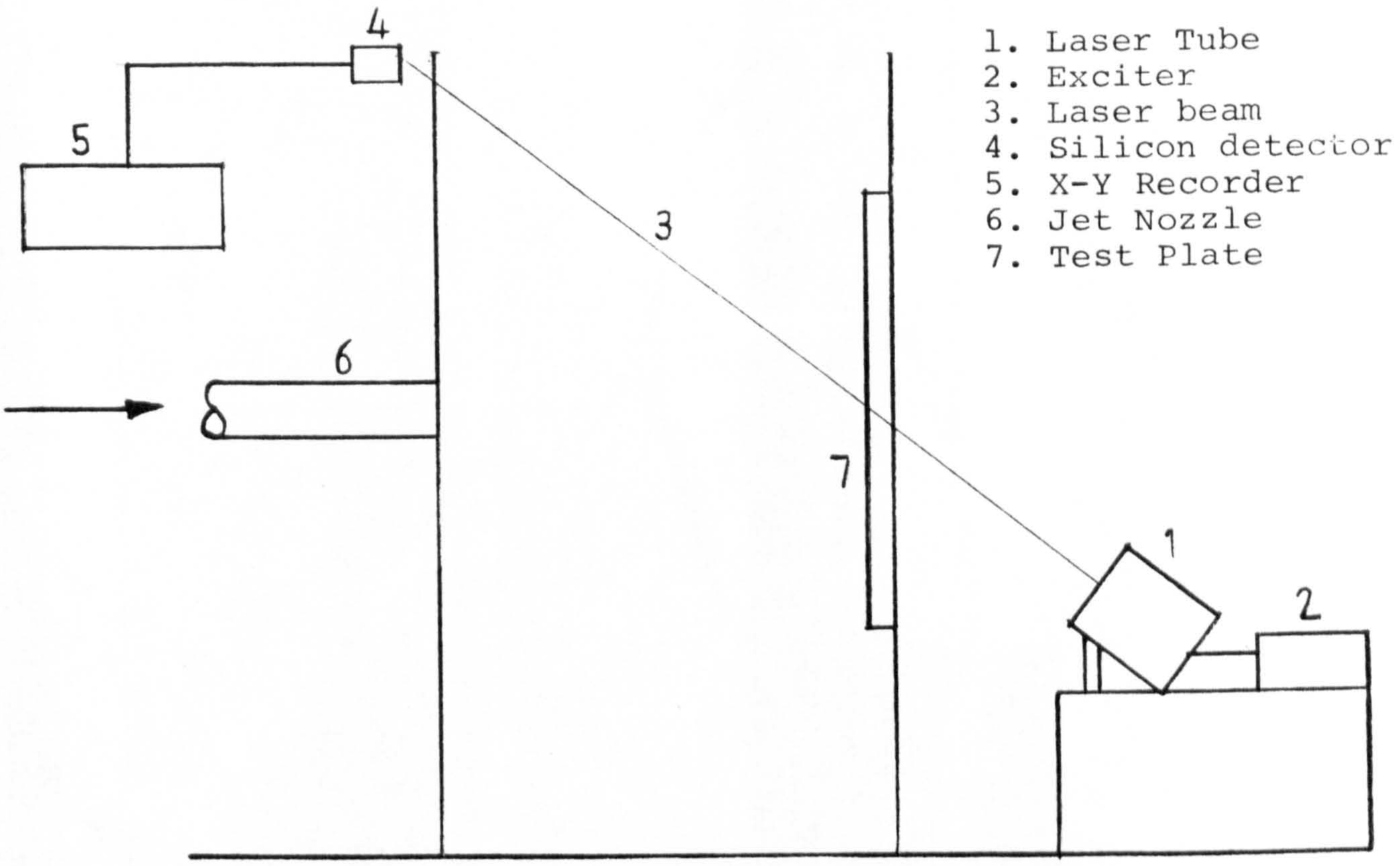

FIG.6.3.1 SCHEMATIC LAYOUT OF AN OPTICAL SYSTEM FOR OBTAINING THE STAGNATION POINT.

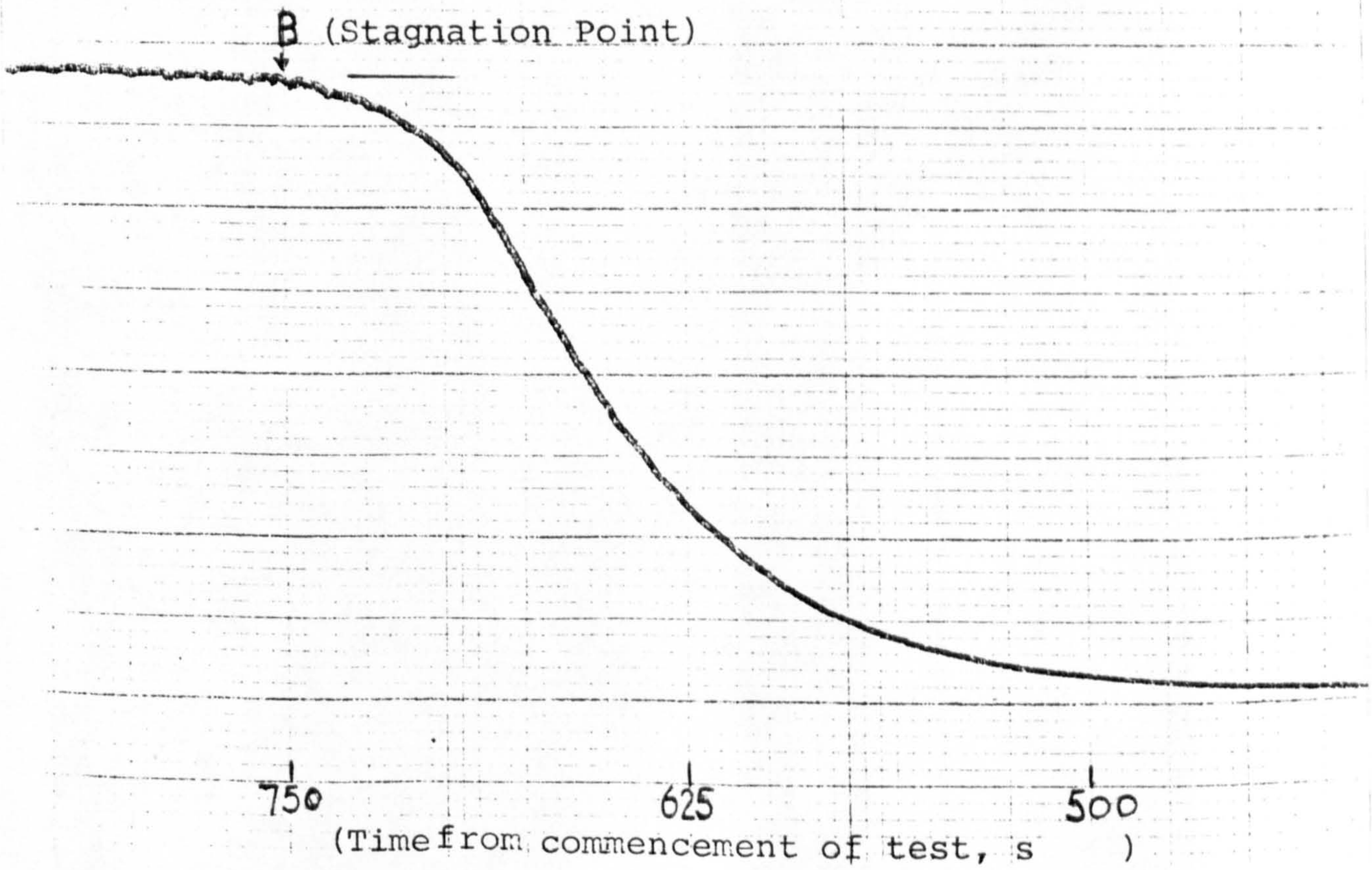

FIG.6.3.2 A TYPICAL SUBLIMATION CURVE FROM THE X-Y RECORDER.

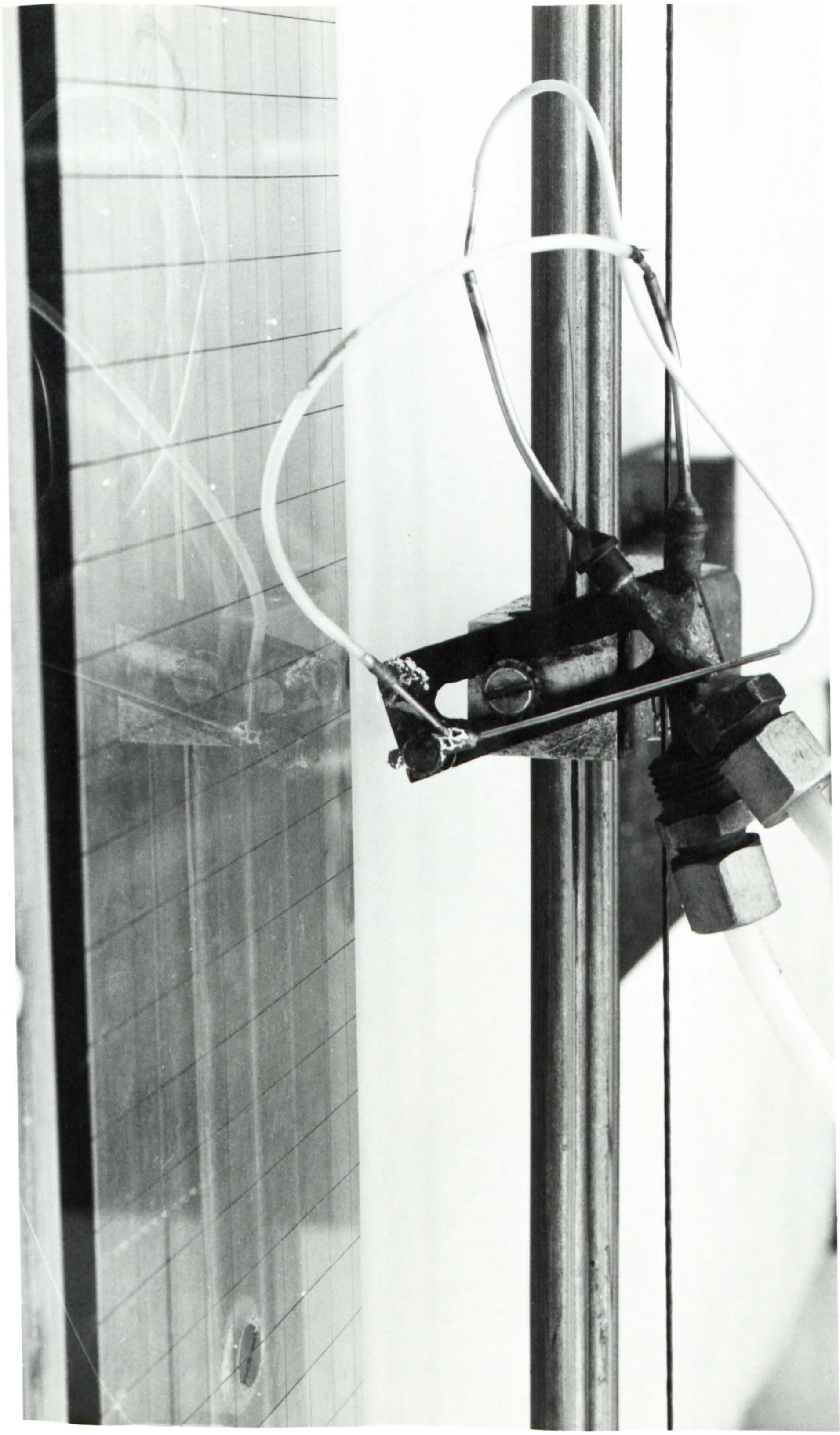

PLATE 6.4.1 THE TEST PLATE DURING A SPRAYING OPERATION.

CHAPTER 7

7. HEAT TRANSFER IN FREE IMPINGING JETS - RESULTS AND DISCUSSION

7.1 INTRODUCTION

The heat/mass transfer results determined as described in the preceeding chapter are now presented and discussed. The main purpose of this experimental investigation was to determine the effect of nozzle inclination on heat transfer. However, the effects of jet Reynolds number (Re) and nozzle-to-target separation (z/d) were also determined for turbulent jets issuing into nominally stagnant surroundings. A total of 44 tests are reported for z/d of 6, 8, 12 and 16 and Re of 3.25×10^4, 4.6×10^4, 5.6×10^4 and 6.5×10^4. The nozzle inclination (α) was varied in steps of 15^o from 30^o to 90^o to the plane of the test surface. Tests were also carried out to establish both the repeatability and validity of the experimental technique.

A set of typical photographs obtained during a thin-film naphthalene mass transfer test is presented in Plate 7.1.1 (carried out at Re = 32500, z/d = 6 and $\alpha = 60^o$). It can be seen from the set of photographs that an oval shaped clearance pattern was initially obtained. However, this pattern soon became slightly distorted because of the variation of the naphthalene coating over the test surface prior to the mass transfer test. However, a correction was included in the calculation procedure to account for this variation which was due to free convective losses. The local convective transport coefficients were then estimated by susbstituting the local naphthalene mass density in equation 2.5.2 and the corrected pattern was virtually oval-shaped. The variation of local heat transfer coefficients along the axis of symmetry is also shown in Plate 7.1.1. A typical calculation procedure is presented in Appendix A.4.

7.2 REPEATABILITY TESTS

Three different orthogonal jet impingement tests were carried out at a Reynolds number of 65000 and a nozzle-to-surface spacing of 12 to determine the repeatability of the heat/mass transfer measurements. To ensure the integrity of the results, these tests were carried out on different days. Fig. 7.2.1 depicts the radial variations of the local heat transfer coefficients in these tests. The results are in close agreement even at the stagnation point where the napthalene clearance time was determined with the "laser technique". The thin-film naphthalene mass transfer technique, thus, appears

to yield repeatable results. An estimation of the errors involved in the experiments is presented in Appendix B.1.

As discussed previously, an optical system can be used to reduce the scatter in the measurements at the stagnation point. The benefits, however, appear to depend on the nozzle-to-surface spacing, see Fig. 7.2.2 which compares results obtained by using the optical method and by visual observation of naphthalene clearance. At a z/d of 6, the results of the two techniques are in very good agreement but at z/d = 16, a scatter of >10% was obtained with visual observation. It therefore appears that convective transfer coefficients in the near stagnation region can be determined visually (i.e. noting the time of naphthalene clearance) provided that the nozzle-target distance is small (i.e. $z/d \leq 6$).

7.3 ORTHOGONAL JET IMPINGEMENT HEAT TRANSFER

7.3.1 Heat Transfer at the Stagnation Point

The effect of the nozzle-to-target separation on the stagnation point heat transfer coefficients for orthogonally impinging jets is presented in Fig. 7.3.1(a). For the current test conditions, the maximum heat transfer generally occurs at a z/d of between 6 and 8. The values of maximum heat transfer are of practical importance as they indicate the maximum heating/cooling capabilities of impinging jets. It is interesting to note that the axial locations of maximum heat transfer found by previous workers vary significantly, see Table 7.3.1. The variations in the results may be attributed to differences in either the flow structures of the jet or the nozzle geometry. The results of other workers are presented in Fig. 7.3.1(b) and the data of Gardon and Cobonpue (Ref. 102) are in good agreement with those of the present study. The variations between the present results and those of Mahmood (Ref. 50) can be attributed to differences in the experimental technique to determine the time of initial clearance of the film of naphthalene and to the use of short nozzles ($\ell < 4d$) by Mahmood.

Figure 7.3.2 relates the turbulence intensity and velocity decay to the heat transfer, h_z/h_6 (the subscript denotes nozzle-to-target separation). It is apparent that the separation which corresponds to the maximum heat transfer virtually coincides with the position of greatest turbulence intensity. This corroborates Gauntner et al (Ref.87), who suggested that the location of maximum heat transfer occurs where there is an increase in jet turbulence along the centre line. It is, thus, plausible in the present situation to assume that the maximum heat transfer occurs near the end of the potential core.

Figure 7.3.3 compares the present heat transfer data at stagnation with those of Huang (Ref. 110) and Gardon and Cobonpue (Ref. 102) at a separation of 6 nozzle diameters. The results of the latter study are in good agreement with those of the present investigation especially at jet Reynolds numbers $\leq$ 56000. The difference at higher Re is about 8%. Huang's data are however somewhat lower and the maximum difference of about 15% occurs at the lowest Re (i.e. Re = 32500). However, Huang made his "stagnation" measurements over a comparatively large area of the test surface so that the data are really average heat transfer coefficients in a region around the stagnation point. This procedure thus somewhat reduces the stagnation point heat transfer coefficients.

TABLE 7.3.1: LOCATION OF MAXIMUM HEAT TRANSFER

Author	Posistion of Maximum Heat Transfer (z/d)
Kabari, (Ref. 36)	3
Mahmood (Ref. 50)	5
Gardon and Cobonpue (Ref. 102)	6 to 7
Vallis et al (Ref. 49)	8
Present Study	6 to 8

7.3.2 Variation of Local Heat Transfer Coefficients

The variations in the local heat/mass transfer coefficients for an orthogonally impinging jet are essentially axially-symmetric. Figs. 7.3.4 to 7.3.7 present the local Nusselt numbers obtained at various z/d's. It can be observed that the variation of heat transfer is similar at the different Reynolds numbers investigated. Thus, the ensuing discussion is based only on one Reynolds number (i.e. Re = 32500).

In Fig. 7.3.7., it is apparent that the heat transfer reaches a maximum at the stagnation point and subsequently decreases along the radial axis. The presence of strong negative pressure gradients and high turbulence levels in the near stagnation zone probably produce the high heat transfer in this zone. In the wall jet region, the negative pressure gradient disappears as the pressure returns to the ambient value and hence the heat/mass transfer decreases. Also, any secondary

peaks (which have been previously attributed to transition from laminar to turbulent boundary layer flows) are absent at $z/d \geqslant 8$. This indicates that the wall jet flow is completely turbulent and that there is no 'relaminarisation' at these separations. At $z/d = 6$ however, a small inflection is noticeable at $r/d = 2$ (approximately) and this may possibly develop into a secondary peak at lower nozzle-to-target surface separations. These results corroborate the data of Gardon and Cobonpue (Ref. 102) and Mahmood (Ref. 50).

It can also be observed that the variation of heat transfer produces a bell-shaped curve which decays rapidly at z/d of 6 and 8 whilst at z/d of 12 and 16, the decrease is more gradual. At $r/d = 11$ (approximately), the heat transfer coefficients at all z/ds approach a common value. This region may be associated with the fully developed radial wall jet zone where the radial distribution of velocity (and hence, heat transfer) is relatively independent of nozzle-to-plate distance. The heat transfer data of Gardon and Cobonpue assumed a common value at approximately $r/d = 10$. Vallis et al indicate that this region starts when $r/d > 8$. Thus, the present local heat transfer results possess similar qualitative and quantitative characteristics to those of previous studies and this further validates the reliability of the naphthalene thin film technique.

Figure 7.3.8 depicts the radial heat transfer distribution, normalised by dividing by the stagnation value (this is a form suggested by Gardon and Cobonpue). This form of correlation indicates that the normalized Nussett number (or heat transfer coefficient) strongly depends on the dimensionalised radial position (r/z). Quantitative agreement of the present data and those of Ref. 102 is shown by their juxtaposition in Fig. 7.3.8.

7.4 INCLINED JET IMPINGEMENT HEAT TRANSFER

7.4.1 Effect of Nozzle Shape

When a circular nozzle is inclined, the exit profile can be either circular or elliptical. This latter shape, for example is produced when the end of the jet tube is machined parallel to the plane of the impingement surface. Preliminary tests were carried out to investigate the effects of these nozzle shapes on the impingement heat transfer coefficients. Fig. 7.4.1 shows the maximum heat transfer at various Reynolds numbers for both these shapes. It is apparent that the results obtained with the two nozzles are in very good agreement (e.g. a maximum data variation of about 5% is noticeable). Fig. 7.4.2 presents the lateral variation of local heat transfer coefficients and there is again good agreement

especially in the "downhill" direction.

Metzger (Ref. 109) observed that heat transfer is practically insensitive to changes in the exit velocity profile of the jet. It thus seems that impingement heat transfer is more dependent on the turbulence level at the nozzle exit (see Ref. 106) rather than the velocity profile so that either of the two shapes may be employed in the present situation. The current tests were thus carried out with inclined nozzles of circular exit profile.

7.4.2 Heat Transfer at the Stagnation Point

General Discussion

As can be seen from Fig. 7.3.1, the stagnation point heat transfer is dependent on Reynolds number. However, the effects of altering the system geometry (i.e. z/d and nozzle inclination) are virtually independent of Re. For example, Fig. 7.4.3 indicates that the effect of nozzle inclination is practically identical at all Reynolds numbers. Thus, when discussing the effects of system geometry it is only necessary to consider a single value of Reynolds number.

Figure 7.4.4 shows the effect of nozzle-to-target separation, z/d, on the heat transfer coefficients. The trends are similar at all nozzle inclinations and are also similar to that described in the previous section for orthogonal jet impingement (i.e. the highest heat transfer occurs at z/d = 6 and subsequently decreases at greater spacings). Fig. 7.4.5(a) depicts the effect of nozzle inclination on the stagnation point Nusselt numbers (non-dimensionalised by dividing by the value associated with orthogonal jet impingement). It can be seen that at all z/d's, the heat transfer rate is virtually insensitive to inclination for angles $\geqslant 60^{\circ}$ (a reduction of only about 10% is apparent at 60°). Nozzle inclinations, α, $< 60^{\circ}$ however bring about a sharp reduction. This observation agrees with the previsouly reported results of Thurlow (Ref. 111). It seems also that for a particular nozzle inclination, the reduction in heat transfer increases with z/d. For example, at an inclination of 30°, the reductions at z/d's of 6 and 16 are 23% and 38% respectively.

The present results are in reasonable agreement with those of Sparrow and Lovell (Ref. 23) and Perry (Ref. 21), see Fig. 7.4.5(b). The variations between Perry's data and those of this current study can be attributed to differences in the measuring techniques. Perry inadvertently assumed that the maximum heat transfer always occurs on the nozzle axis. However, Schauer (Ref. 91) found that the position of maximum heat transfer is usually displaced from the geometrical axis of the jet and that this displacement increases as the nozzle inclination is reduced. Thus, Perry's technique inevitably failed to measure the maximum heat transfer.

Figure 7.4.6 presents the effect of 'apparent' nozzle-to-target separation, z'/d (i.e. the separation distance measured along the jet axis) on the Nusselt numbers. It is interesting to note that the variation of heat transfer rate appears to be dependent on z'/d and hence virtually independent of nozzle inclination except for $\alpha = 30^{o}$. This observation is similar to that of Korger and Krizek (Ref. 22) for 2-dimensional slot jets. Thus, it appears that the maximum heat transfer rates associated with inclined jets may be assessed by means of the nozzle-to-plate separation measured along the nozzle axis i.e. the behaviour of inclined jets may be explained purely in terms of the corresponding increased nozzle-to-plate spacings (see Fig. 7.4.6). It is thus important for inclined jets to stipulate the particular datum employed for the nozzle-to-plate separations.

For all nozzle inclinations, the location of the maximum heat transfer is shifted from the geometrical axis of the nozzle. This observation corroborates the results of Korger and Krizek for slot jets and Sparrow and Lovell for circular impinging jets. Fig. 7.4.7 shows the displacement of the position of maximum heat transfer at various separation distances. For a particular nozzle inclination, the displacement increases with z/d. For example, at 30^{o}, the displacements are 1.2 and 2.6 nozzle diameters at z/d = 6 and 16 respectively. This difference may be attributed to the 'kinematics' of the fluid flow. In inclined jets, the stagnation streamline is not coincident with the jet axis (see Fig.4.3.2.) and as the jet entrains more of its surrounding fluid, this displacement increases.

The present results are in good agreement with those of Sparrow and Lovell, see Fig. 7.4.7.

Correlation of the Maximum Heat Transfer Data

As discussed in Chapter 4, the dimensionless parameters normally associated with jet impingement heat transfer can be correlated in the form :

$$Nu/Pr^{1/3} = f(Re, z/d)$$

However, in this present investigation, the angle of inclination will also be important so that the relationship may be assumed to be of the form :

$$Nu/Pr^{1/3} = \beta(\sin \alpha)^{n} Re^{m}(z/d)^{\ell} \qquad 7.4.1$$

where β, n, m and ℓ are empirical constants

These constants were evaluated simultaneously by employing a non-linear optimisation technique (multiple regression) so that :

$$Nu/Pr^{1/3} = 0.22\ (\sin\alpha)^{0.84} Re^{0.81} (z/d)^{-0.69} \qquad 7.4.2$$

Approximately, 95% of the present measurements lie in a ± 10% limit on equation 7.4.2, see Fig. 7.4.8.

This relationship cannot be compared directly with earlier studies because other correlations have not been published previously. However, the exponents on the Reynolds number and z/d are close to those obtained for orthogonal jet impingement by Perry (Ref. 21) and Vallis et al (Ref.49) respectively.

It can be observed from Fig.4.3.1. that

$$z/d = z'/d \sin\alpha \qquad 7.4.3$$

where z'/d = the nozzle-to-plate separation measured along the jet axis.

By substituting equation 7.4.3 into 7.4.2, the following relationship may be obtained :

$$Nu/Pr^{1/3} = 0.22\ (\sin\alpha)^{0.15} Re^{0.81} (z'/d)^{-0.69} \qquad 7.4.4$$

This correlation corroborates Fig. 7.4.6 and suggests that the maximum heat transfer from inclined jets can be explained almost entirely by the increased jet-to-targetseparation and that any additional effects due to inclination are weak (i.e. $(\sin\alpha)^{0.15}$).

It is thus relevant to produce a correlation solely in terms of z'/d, namely :

$$Nu/Pr^{1/3} = 0.21\ Re^{0.81} (z'/d)^{-0.69} \qquad 7.4.5$$

However, the data points exhibit a greater scatter about this correlation, e.g. 95% fall within ± 15%, see Fig. 7.4.9.

7.4.3 Local Variation of Heat Transfer

The local heat transfer distribution associated with an inclined impinging jet is only symmetrical about a single axis referred to in the ensuing discussion as the 'symmetry line'. Figs. 7.4.10 and 7.4.11 present the heat transfer rates along this line for nozzle inclinations, α, of 90°, 75°, 60°, 45° and 30° and at different Reynolds numbers. It is apparent that at all nozzle inclinations, the magnitude of the local heat transfer rates are reduced as the Reynolds number is decreased. Also, the heat transfer distributions become more 'peaked' and steeper as the Reynolds number is increased. For example, the heat transfer, h_x (normalised by dividing by the maximum heat transfer, h_o) at $x/d = 4$ is 0.19, 0.24 and 0.27 for Re = 65000, 50000 and 32500 respectively for $\alpha = 60°$. Similar behaviour was reported by Gardon and Akfirat (Ref. 103) and Sparrow and Lovell (Ref. 23) for orthogonal and inclined jets respectively. The location of maximum heat transfer is, however, constant at all jet Reynolds numbers. Because of the generally qualitative similar behaviour at different Reynolds numbers, only the results at Re = 32500 are now discussed.

In Fig. 7.4.11(b) the geometric axes of the jets are indicated by C_{30}, C_{45} etc. (the subscript denotes the nozzle inclination α), so that these locations can be compared with the positions of maximum heat transfer. The displacements of the maxima are apparent and these have already been discussed. It can also be seen that inclining the nozzle reduces the heat transfer capabilities of impinging jets. Moreover, as the angle of incidence is decreased, the heat transfer distribution becomes more "skew". This skewness may be attributed to an imbalance of the air flows on the impingement surface. As α is reduced more of the flow is directed to the "downhill" side with a consequent reduction in the "uphill" flow.

These heat transfer distributions are replotted in Figs. 7.4.12 and 7.4.13 which present the heat transfer for oblique jet impingement systems at various z/d's. The centre lines of the nozzles are depicted by C_6, C_{16}, etc. (the subscript denoting the separation distance z/d). It can be observed that for a particular nozzle inclination, the maximum heat transfer decreases as the separation distance increases in a similar fashion to that for orthogonal jet impingement. It is again noticeable in Figs. 7.4.12 and 7.4.13 that the heat transfer is skewed with the higher heat transfer rates occurring in the "downhill" side. Increasing asymmetry and skewness of the heat transfer are apparent as α is decreased. (Compare, for example, Fig. 7.4.12(a) and (b) for 75° and 60° respectively).

The heat transfer rate decays faster on the "uphill" direction. For example, at $x/d = \pm 4$ (measured about the stagnation point) and for z/d = 16 and $\alpha = 75°$, the local Nusselt numbers are 68 and 56 for the 'downhill' and 'uphill' directions respectively. These effects, as mentioned earlier, are caused by the higher

momentum flux in the downhill direction which is in turn, due to a greater mass flow of fluid in the wall jet. This imbalance is illustrated in Plate 7.4.1 which applies for confined jets at Re = 32500 and z/d = 6. Symmetry is apparent in the case of orthogonal impingement whilst the greater part of the fluid flow ensues in the downhill direction for oblique impingement.

As α is reduced (i.e. the angle of incidence is decreased) and z/d is increased, the heat transfer rates become uniformly distributed. Some of the benefits of jet impingement are virtually lost and the heat transfer characteristics ultimately approach those associated with parallel flow over a flat plate.

7.4.4 Heat Transfer Contour Plots

The variations of local heat transfer distributions (partially described in the preceeding section) can only be fully represented as contour plots and these are thus presented in Figs. 7.4.14 to 7.4.16. A plot of this form provides information over the whole field of interest. These contour plots are presented as normalised heat transfer coefficients, h_r/h_o (i.e. in terms of the maximum stagnation point value). Figure 7.4.14 shows the effect of nozzle inclination on the heat transfer at z/d = 6 and Re = 32500. It can be observed that the plots change from concentric circles to oval-shaped contours as the nozzle is inclined. Also, for the inclined situations, the contour lines are very close together in the uphill direction, and that conversely, they become more spread out in the downhill direction. (Compare, for example, the plots for 30^o and 90^o in Fig. 7.4.14). It is, thus, apparent that a larger area on the downhill side experiences some impingement effects so that there is an imbalance in the heating/cooling capabilities of the oblique impinging jets. However, the uniformity in the lateral direction is relatively unaltered by nozzle inclination.

Figure 7.4.15 depicts the effect of varying z/d on the heat transfer plots at various nozzle inclinations. Generally, an increase in nozzle-to-target spacing causes the contour plots to spread and become more uniform (usually, less lines on a plot indicate a more uniform variation of heat transfer coefficient). Fig. 7.4.16 shows the effect of Reynolds number on the contour plots at various nozzle inclinations. It can be observed that these plots become more uniform as the Reynolds number is reduced.

7.5 AVERAGE HEAT TRANSFER COEFFICIENTS

7.5.1 Introduction

A knowledge of the spatailly averaged heat/mass transfer rates is often required for design purposes. Hence, average convective coefficients were evaluated by numerically integrating the local distributions. This was achieved by first of all defining the surface area over which the integration was required. This area was centred around the stagnation point since this will always produce the maximum average heat transfer. The area was normally a square with a side length, s, (≡ 2d, 4d, 6d, 8d or 16d) and this was further divided into a number of elements. It was found that the number of elements affected the accuracy of the results so that a minimum of 49 grid points was used. The local heat transfer coefficient at each of the grid points was determined by interpolation and substituted into equation 4.5.7. The average value was obtained by successive use of "Simpson's rule".

To facilitate comparison of the present results with those of previous studies, circular integration areas were used for the orthogonal jet impingement data. Values of 'hr' (where h is the local heat transfer coefficient at a radial distance, r, from the stagnation point) were plotted against 'r' and the area under this curve was determined by employing Simpsons rule. Average heat transfer coefficients were, thus, obtained for various circular areas.

7.5.2 Effect of the Area of Integration

Figure 7.5.1 shows the effect of integration area on the average Nusselt numbers for orthogonal jet impingement at Re = 32500 and z/d = 6, 8, 12 and 16. It can be observed that the average heat transfer decreases as the integration area is increased. This variation follows since the high local heat transfer rates near the stagnation point become less important as the impingement surface area increases. Vallis et al (Ref. 49) Gardon and Akfirat (Ref. 103) and Mahmood (Ref. 50) have all found that average heat transfer is highly dependent on the target size. From Fig. 7.5.1, it is plausible to expect that at large integration areas (> 16d), the average heat transfer becomes relatively less sensitive to the separation distance.

A similar decrease in $\overline{Nu}$ as the integration area is increased is apparent in Fig. 7.5.2 which presents data at various Reynolds numbers. It appears that the rate of decrease in the average Nusselt number is greatest at high Re. Also from Fig. 7.5.2, it can be expected that at large integration areas (> 16d), the variation of the mean heat transfer becomes relatively less sensitive to changes in the jet Reynolds number.

It is thus important that the impingement surface area should be defined whenever average heat transfer rates are quoted.

The mean heat/mass transfer coefficients for the orthogonal jet impingement situations were also determined by averaging over circular areas centred on the stagnation point. The results for various nozzle-to-target surface separations and a Reynolds number of 32500 are presented in Fig. 7.5.3(a). $\overline{Nu}$ obviously decreases as the area of integration increases because of the reduction in local heat transfer rates as the radial distance from the stagnation point is increased. It can be observed in Fig. 7.5.3(a) that at large integration areas (i.e. $r/d \geq 10$), the mean heat transfer is less sensitive to the separation distance. Earlier workers (e.g. Gardon and Cobonpue (Ref. 102) and Huang (Ref. 110)) found similar variations of the average heat transfer.

The data of Vallis et al (Ref. 49) and Mahmood (Ref. 50) obtained at $z/d = 12$ and $Re = 32000$ are shown in Fig. 7.5.3(b). The current results are in good agreement with those of Vallis et al especially at $r/d \geq 2$. The results of Mahmood are, however, lower and this can be attributed to the difference in the nozzle geometries. Mahmood used a short nozzle (i.e. $\ell < 4d$) whilst Vallis et al ($\ell = 50d$) and the present study ($\ell = 32d$) employed much longer nozzles.

7.5.3 Heat Transfer in the Impingement Region

Heat transfer rates at the stagnation point are difficult to measure (as discussed in Chapter 4). Furthermore, the values are highly dependent on the nozzle geometry and the local fluid flow structure. These problems can be reduced by evaluating the heat transfer coefficient over an impingement region around the stagnation point. This region is associated with strong negative pressure gradients and high streamline curvature. Its radial extent has been defined by equation 4.2.5 and it is obvious that the surface area of the impingement region increases with z/d.

Figure 7.5.4 presents the effect of z/d on the heat transfer in the impingement region for the present "orthogonal" jets. At a particular Re, there is a sharp decay in heat transfer especially at the lower z/d's. This initial rapid degradation appears to be due to both the sharp peak in heat transfer which occurs at these geometries and also to the smaller impingement areas at low separations.

In Fig. 7.5.5, the "impingement region" results are compared with those of Vallis et al (Ref. 49) and Gardon and Akfirat (Ref. 103). Reasonable agreement exists between the current data and those of Ref. (49) although Gardon and Akfirat's results are lower. The present heat transfer data over the impingement region associated with orthogonal jet impingement can be correlated in the form :

$$\overline{Nu} = 0.45\ Re^{0.78}\ (z/d)^{-1}\ Pr^{-1/3} \qquad 7.5.1$$

and all the evaluation points fall within ± 10% of this equation, see Fig. 7.5.6.

7.5.4 The Effect of Nozzle Inclination on Average Heat/Mass Transfer

The average heat transfer coefficients for non-orthogonal impingement also decrease as the impingement surface area increases, see Fig. 7.5.7. This diagram presents the average heat transfer rates for nozzle inclination of 30° and it is apparent that up to an integration area of length, s = 4d, the mean heat transfer decreases sharply. However, the average heat transfer seems to become less dependent on the size of the integration areas at large s/d's and this observation is in agreement with previous studies (e.g. Ref. 103) concerning orthogonal jets.

Figure 7.5.8 shows the effect of nozzle inclination on the average Nusselt numbers for various integration areas. It can be observed that the variation of the average heat transfer is essentially self-consistent especially for integration areas of 4d and 8d. Thus, only the values for the latter size of area are employed in the remainder of the discussion. It is noticeable in Fig. 7.5.8 that the variation of stagnation point Nusselt number is somewhat greater than that for integrated mean values. These diffiferences can be attributed to the complicated flows associated with jet inclination as discussed in Section 4.3

Figure 7.5.9 depicts the effect of nozzle-to-surface spacing, z/d, on the average heat transfer for oblique jet impingement. For all nozzle inclinations, the mean convective transfer coefficient decreases as z/d increases. A comparison of this figure with the corresponding stagnation data reveals that the average heat transfer data do not exhibit maxima between z/d of 6 and 8. Fig. 7.5.10 is reproduced from Ref. (103) and the trend of the average heat transfer is apparent especially at z/d = 6 and 8 where the well-defined maximum associated with stagnation values disappears.

Fig. 7.5.11 presents the overall effect of nozzle inclination on the normalised average Nusselt number, $\bar{Nu}_\alpha/\bar{Nu}_{90}$, (i.e. the ratio of average heat transfer for oblique impingement to that for orthogonal flows). It can be observed that inclining the nozzle generally decreases the mean heat/mass transfer. In this figure, two curves are drawn which encompass the data points so that a mean line can be used for practical situations. It is apparent from Fig. 7.5.11 that there is only a moderate reduction (about 10%) in the average heat transfer for $\alpha \geqslant 60^\circ$. However, any further reduction of the nozzle inclination produces a sharp decrease in the mean heat transfer. For example, at 30° the average heat transfer is approximately 67% of the corresponding value for orthogonal jet impingement.

There is also some evidence that the reduction in average heat transfer is greater at $z/d \geq 12$.

Published information concerning heat transfer rates associated with inclined nozzles is scanty and only the work of Sparrow and Lovell (Ref. 25) appears to be pertinent to the present investigation. Fig. 7.5.12 presents data from the two studies. Sparrow and Lovell conducted their tests at Re = 5000 whereas the present study employed a minimum Reynolds number of 32500. Consequently, the magnitudes of the average values in the two investigations are vastly different. Furthermore, Sparrow and Lovell's jets exited through an orifice which was located in relatively thin wall whilst in this study, the jet exited from a long circular nozzle. It is, therefore, probable that these differing arrangements yielded variations in the exit conditions, e.g. in the form of velocity profile and turbulence level in the jets. Nevertheless, good agreement exists when the results are compared on a normalised basis, $\bar{Nu}_\alpha/\bar{Nu}_{90}$.

7.5.5 Correlation of the Average Heat Transfer Results

The following equation was assumed to correlate the mean convective transport coefficients :

$$\bar{Nu}/Pr^{1/3} = \beta(\sin(\alpha))^n Re^m (z/d)^\ell \qquad 7.5.2$$

A multiple regression technique was again employed and yielded :

$$\bar{Nu}/Pr^{1/3} = C(\sin\alpha)^{0.71} Re^{0.66} (z/d)^{-0.66} \qquad 7.5.3$$

where C is a degradation factor whose value depends on the area of integration. For example C = 0.71 and 0.48 for s/d = 4 and 8 respectively.

Approximately 95% of the data points fall within a limit of ±10% of the proposed equation, see Fig. 7.5.13. The average heat/mass transfer rates for oblique jet impingement geometries have not been correlated previously so that this present expression cannot be compared with published data. However, a comparison of equation 7.5.3 with the equation (4.5.8) obtained by Vallis et al for orthogonal jet impingement reveals good agreement in the exponents on both the Reynolds number and z/d.

By substituting equation 7.4.3 into equation 7.5.3, the following expression can be obtained.

$$\overline{Nu}/Pr^{1/3} = C\ (\sin(\alpha))^{0.05}\ Re^{0.66}\ (z'/d)^{-0.66} \qquad 7.5.4$$

This equation indicates that the average Nusselt numbers for obliquely impinging jets are virtually independent of the angle of inclination provided that the nozzle-to-target separation is measured along the axis of the jet. A further regression analysis indicates that :

$$\frac{\overline{Nu}}{Pr^{1/3}} = C\ Re^{0.66}\ (z'/d)^{-0.66} \qquad 7.5.5$$

can describe the average heat transfer.

The average heat transfer is less sensitive to "angle" effects (as opposed to purely separation effects) than in the stagnation heat transfer, e.g. exponents of 0.05 and 0.15 on sin α in the two cases.

7.5.6 Summary

To summarise the main points in the foregoing discussions, it has been found that :

(1) The thin-film napthalene technique produces repeatable heat transfer results for jet impingement situations. Furthermore, the results for the "orthogonally" impinging jets are in good agreement with those of previous studies.

(2) Inclining the jet nozzle reduces both stagnation point and average heat transfer rates. The location of the maximum heat transfer also shifts away from the geometric position as the nozzle is inclined.

(3) Nozzle inclination produces an "imbalance" in the heating/cooling capabilities of turbulent impinging jets. As the angle of incidence is reduced, a proportionately greater flow occurs "downhill" in comparison with "uphill" direction.

(4) For both orthogonal and oblique impingement, the average heat transfer is highly dependent on the impingement surface area although this effect becomes reduced at $s/d > 16$.

(5) The results for inclined jets can be correlated by :

$$Nu/Pr^{1/3} = 0.22\ (\sin\alpha)^{0.84}\ Re^{0.81}\ (z/d)^{-0.69}$$

for stagnation point value.

and

$$\overline{Nu}/Pr^{1/3} = C\ (\sin\alpha)^{0.71}\ Re^{0.66}\ (z/d)^{-0.66}$$

for average heat transfer

where C = degradation factor and depends on the area of integration.

Since $z/d = z'/d \sin\alpha$, these equations can be respectively reduced to :

$$Nu/Pr^{1/3} = 0.22\ Re^{0.81}\ (z'/d)^{-0.69}\ (\sin\alpha)^{0.15}$$

and

$$\overline{Nu}/Pr^{1/3} = C\ Re^{0.66}\ (z'/d)^{-0.66}\ (\sin\alpha)^{0.05}$$

These equations suggest that heat transfer is virtually independent of α provided that the nozzle-to-impingement surface separation is measured along the axis of the jet. Further analysis of the experimental data yields :

$$Nu/Pr^{1/3} = 0.21\ Re^{0.81}\ (z'/d)^{-0.69}$$

for stagnation point values.

and

$$\overline{Nu}/Pr^{1/3} = C\ Re^{0.66}\ (z'/d)^{-0.66}$$

for average heat transfer

(6) The present results for inclined jets are in reasonable agreement with the limited published data of Sparrow and Lovell (Ref. 23).

1.

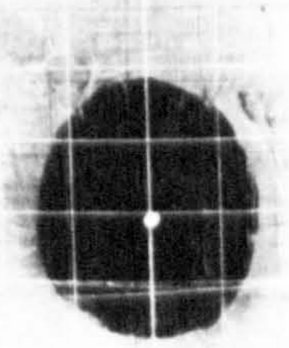

2.

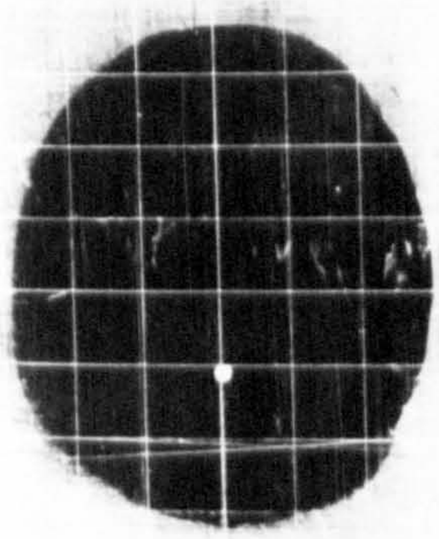

3.

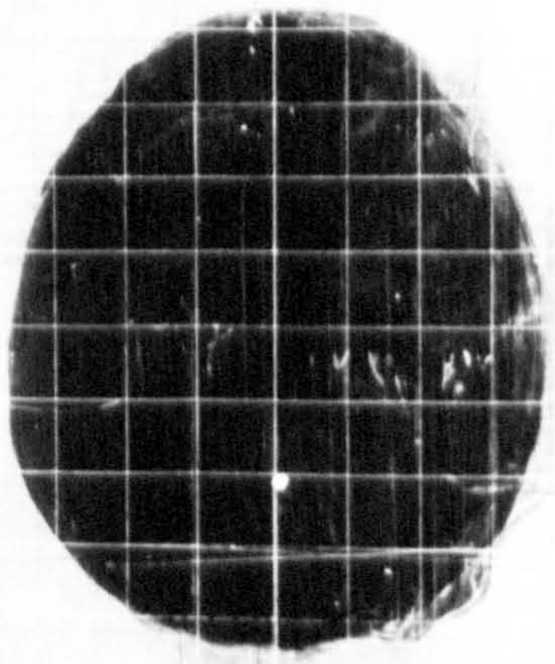

4.

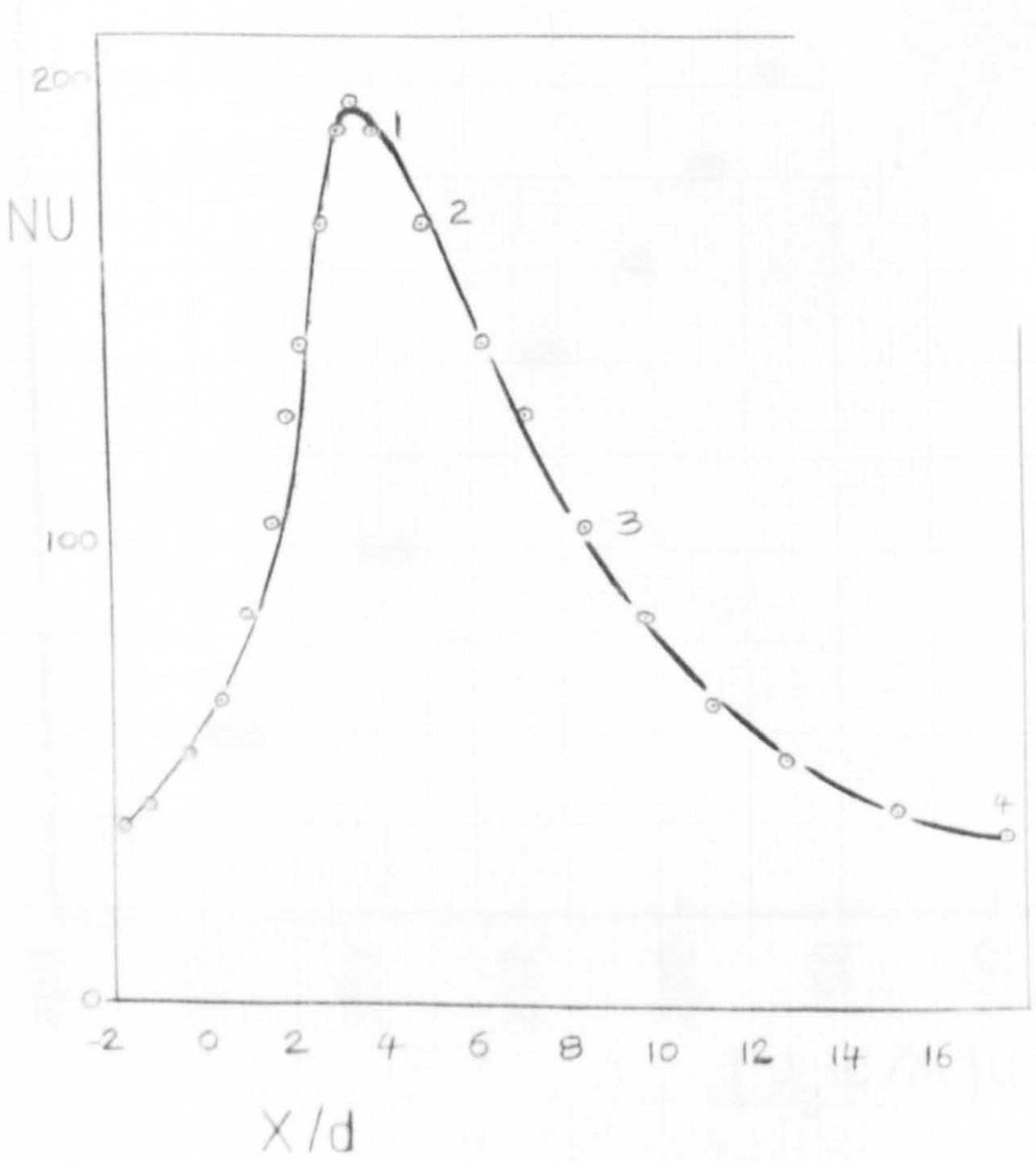

α = 60°

z/d = 6

Re = 32500

Stagnation Point.

PLATE 7.1.1 TYPICAL CLEARANCE PATTERNS OBTAINED FOR AN INCLINED IMPINGING JET.

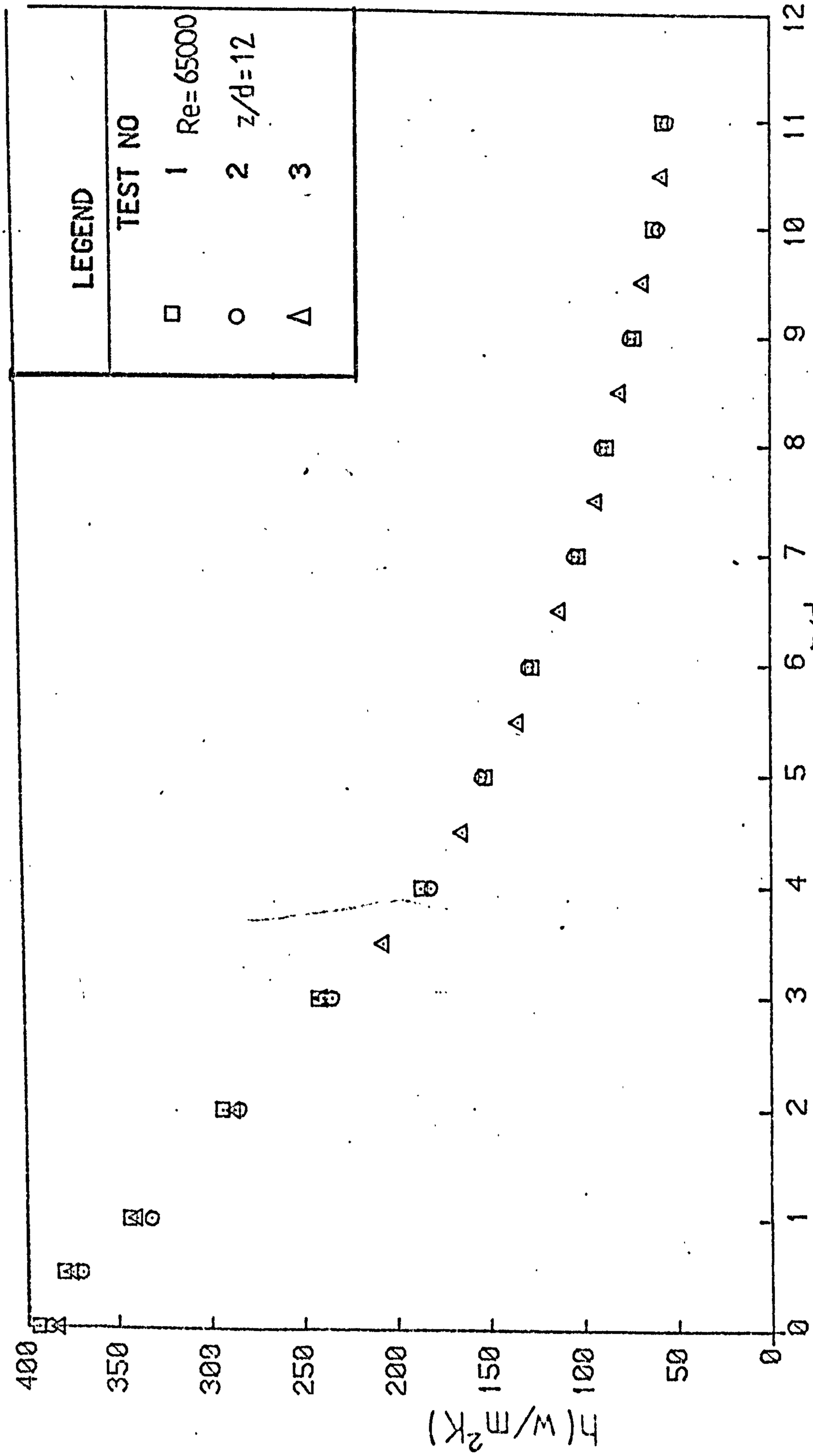

FIG. 7.2.1 REPEATABILITY OF HEAT TRANSFER TEST FOR A PARTICULAR GEOMETRY.

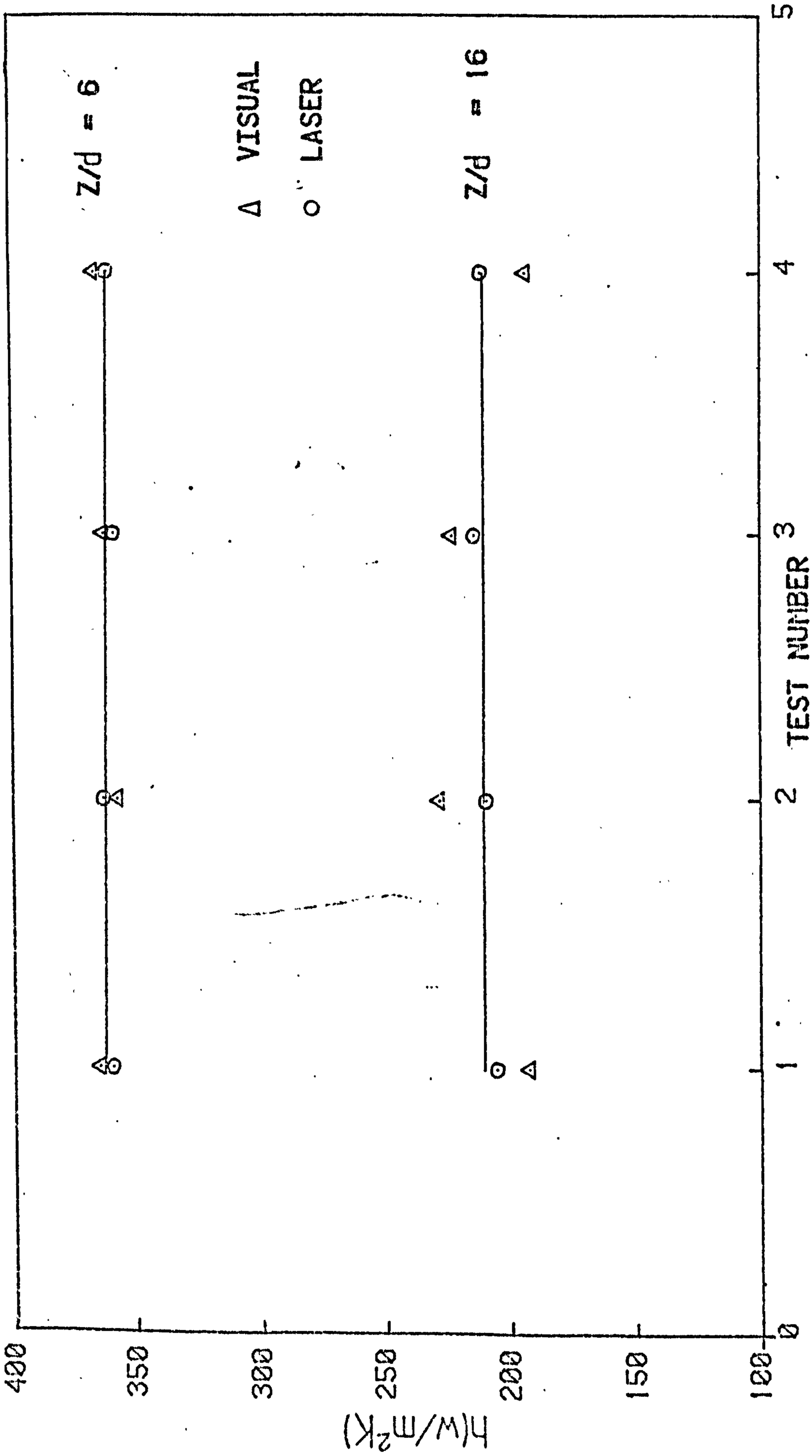

FIG. 7.2.2 COMPARISON OF STAGNATION POINT HEAT TRANSFER OBTAINED WITH TWO TECHNIQUES.

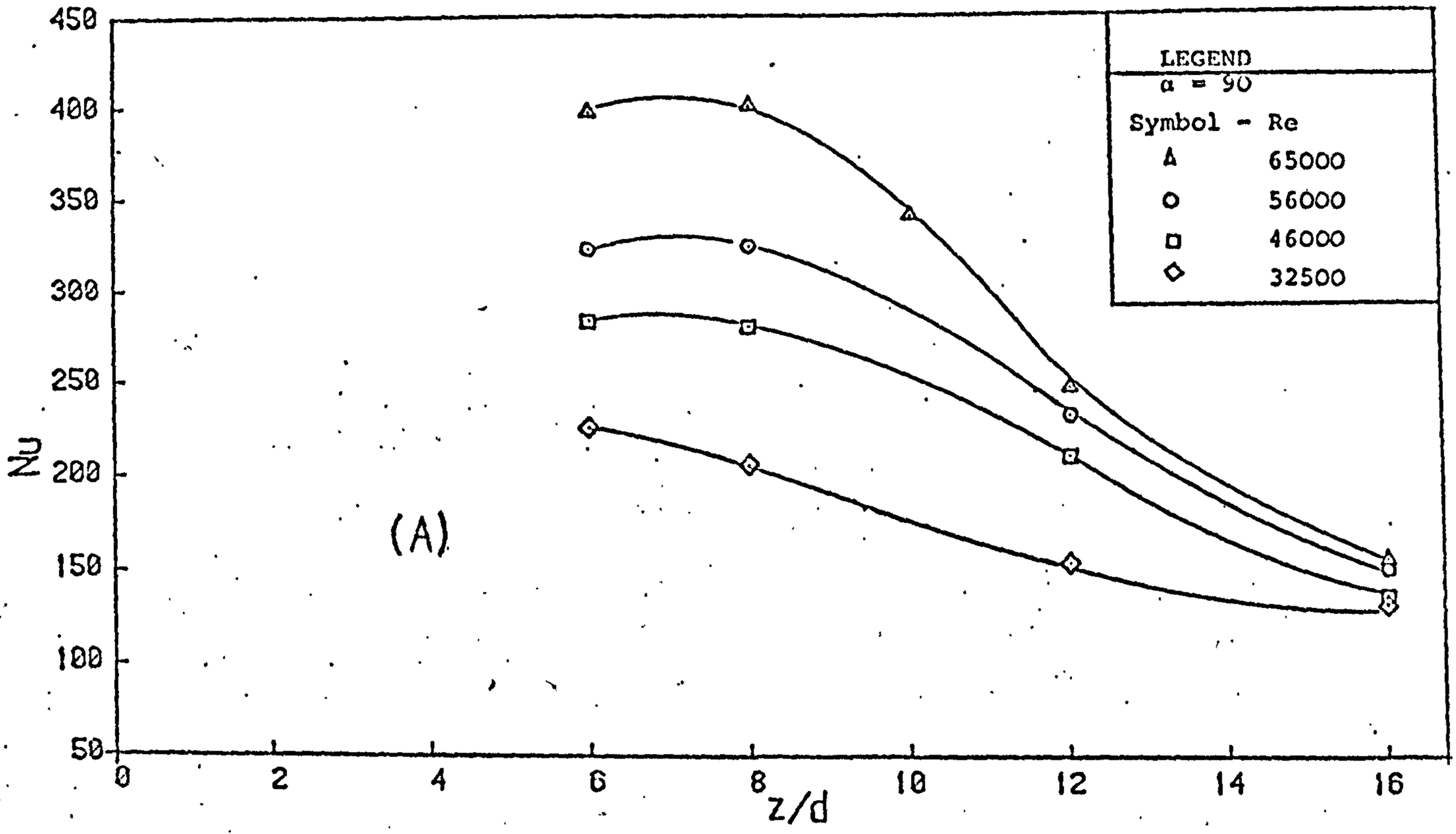

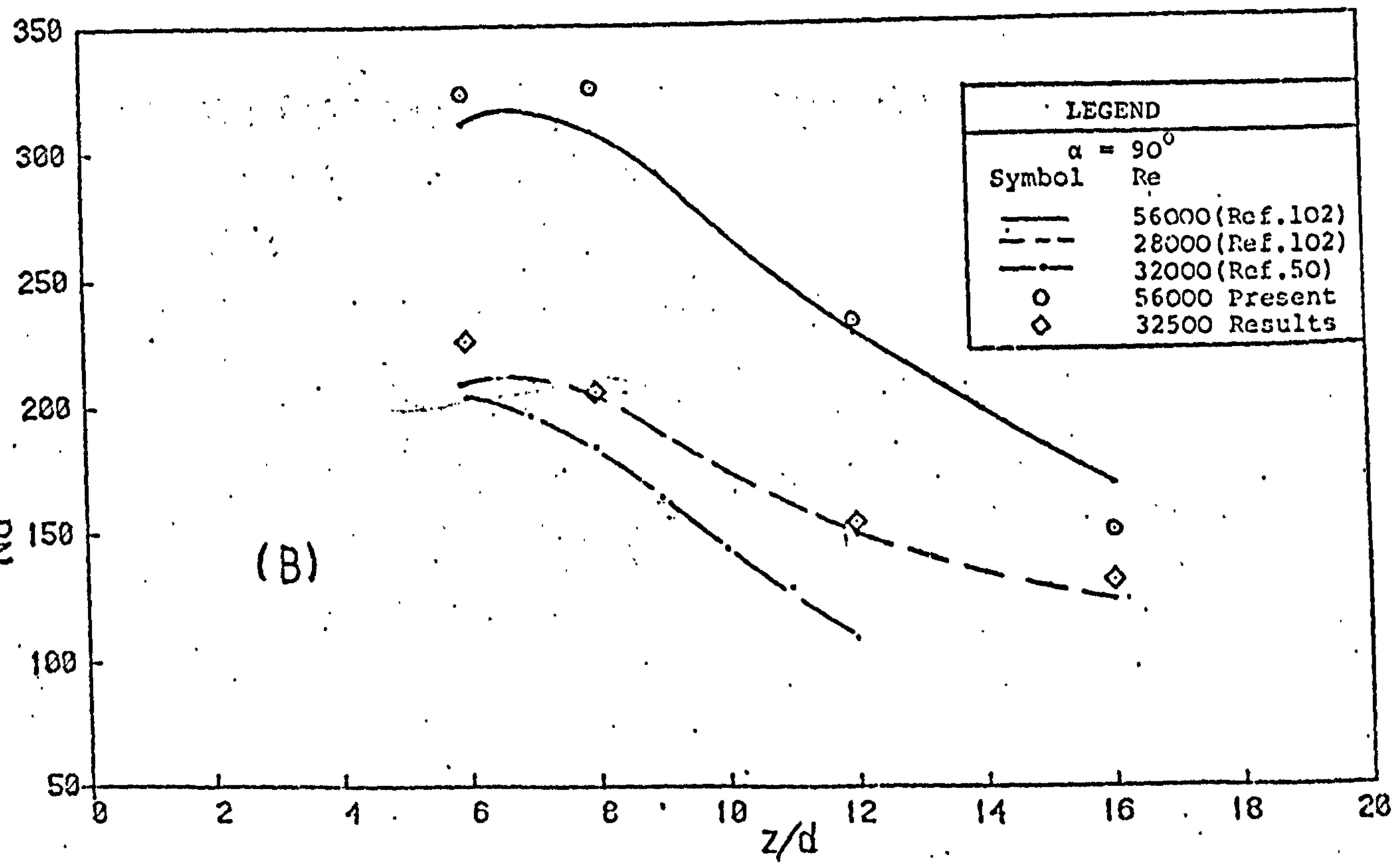

FIG. 7.3.1 EFFECT OF NOZZLE-TARGET SEPARATION ON STAGNATION POINT NUSSELT NUMBER.
(A) PRESENT RESULTS (B) COMPARISON WITH THOSE OF PREVIOUS STUDIES.

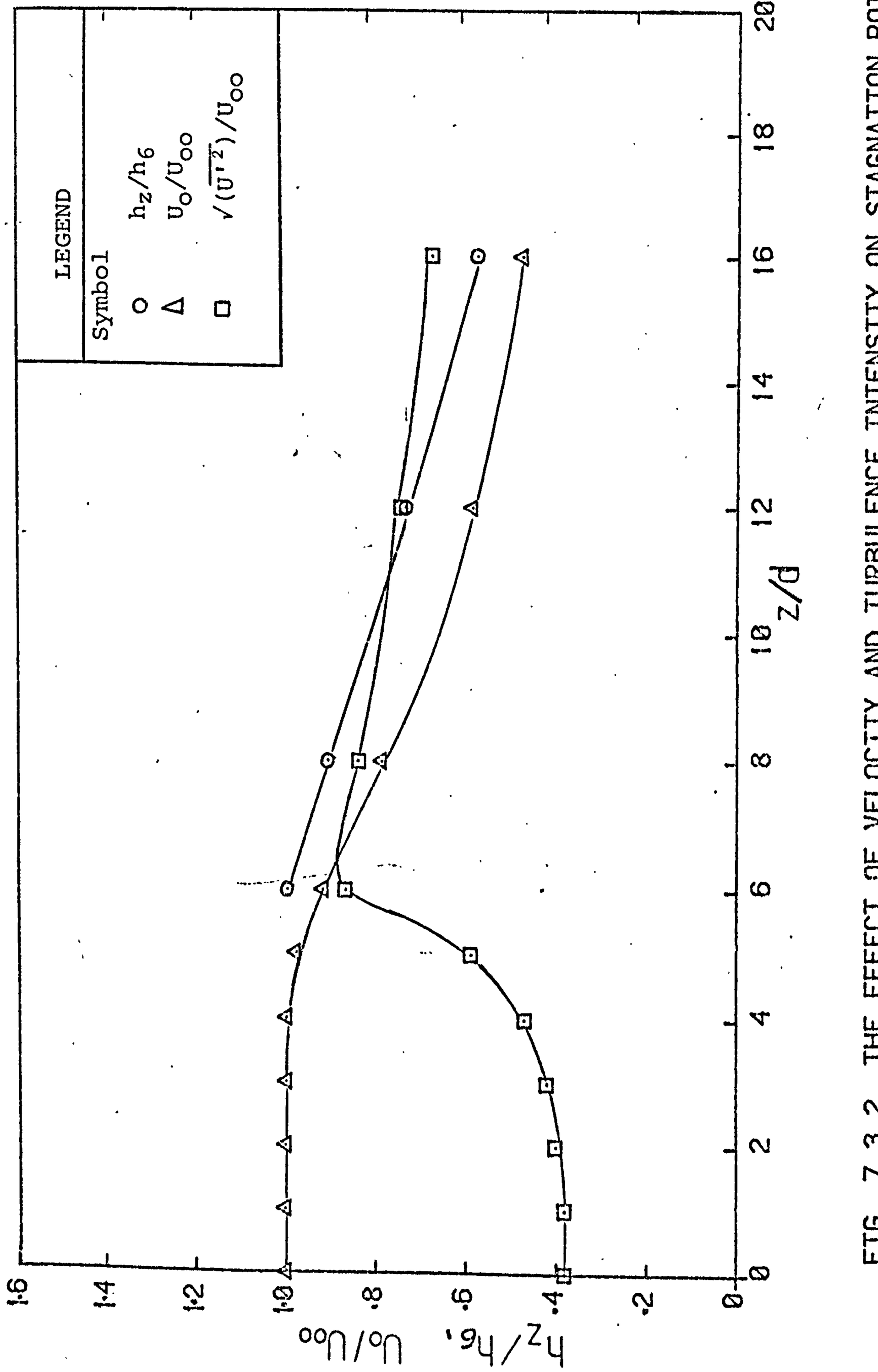

FIG. 7.3.2 THE EFFECT OF VELOCITY AND TURBULENCE INTENSITY ON HEAT TRANSFER RATE.

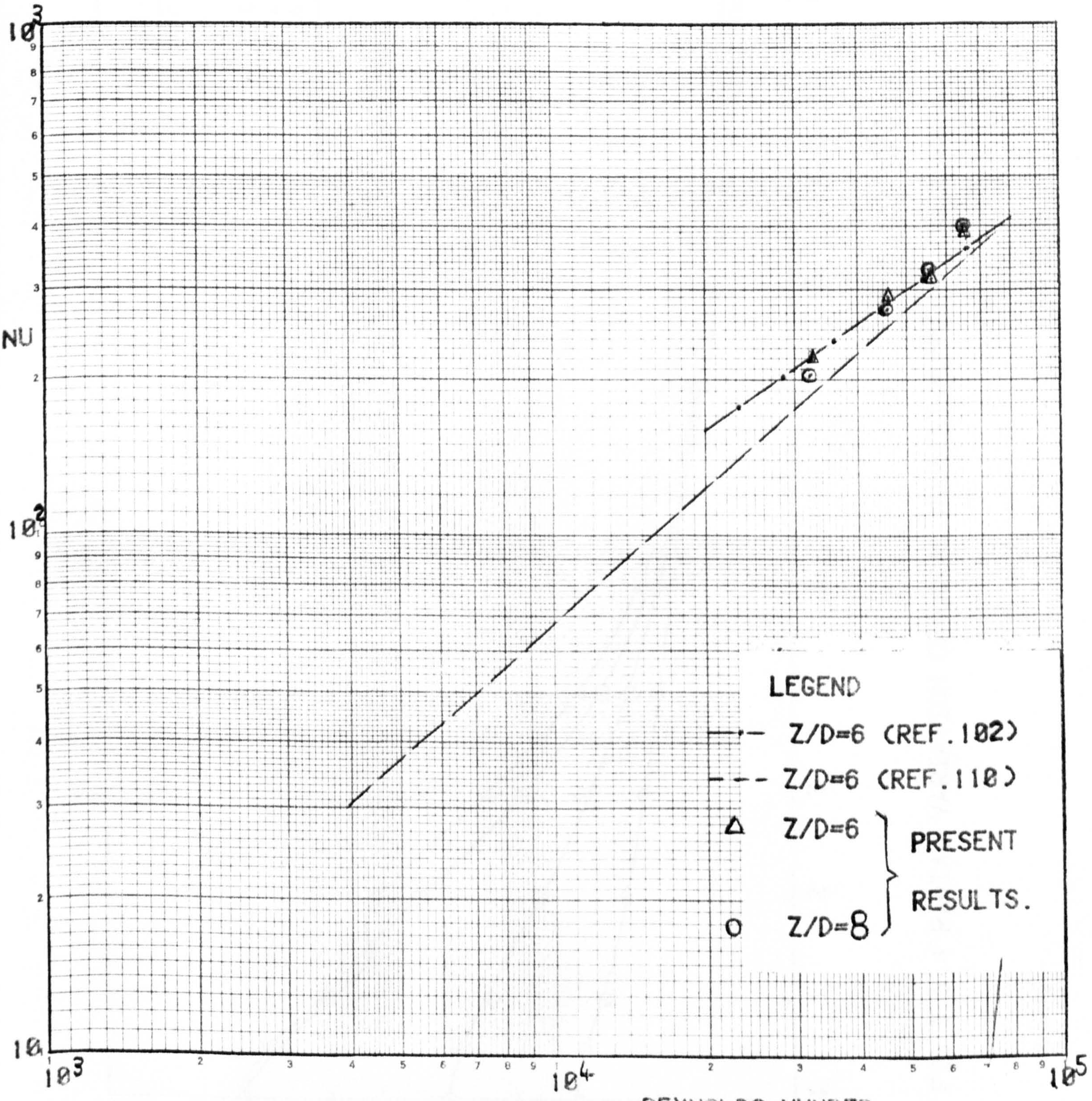

FIG. 7.3.3 COMPARISON OF STAGNATION POINT NUSSELT NUMBER WITH THOSE OF HEATED CYLINDER.

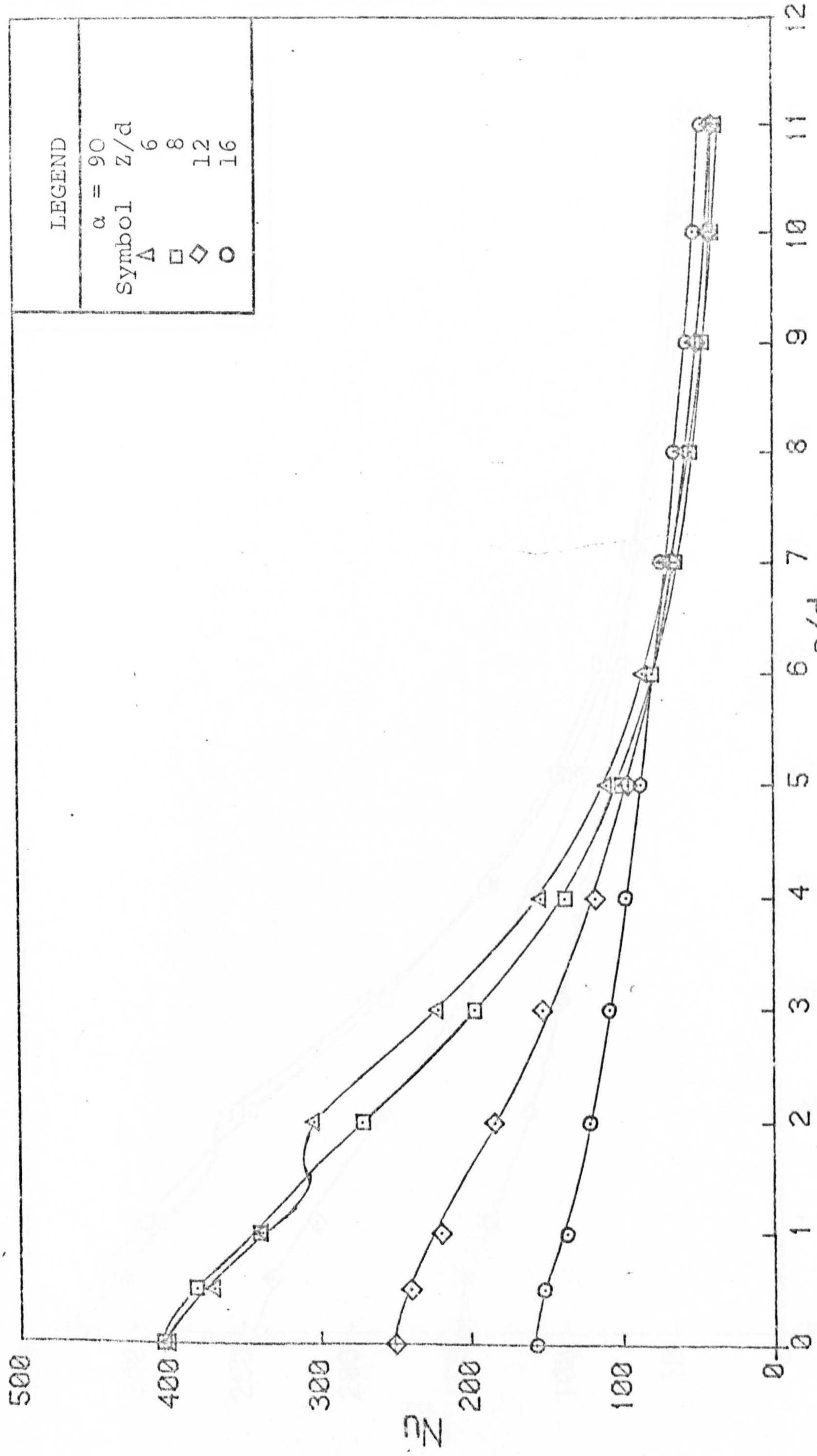

FIG.7.3.4 RADIAL VARIATION OF LOCAL NUSSELT NUMBERS. (Re = 65000)

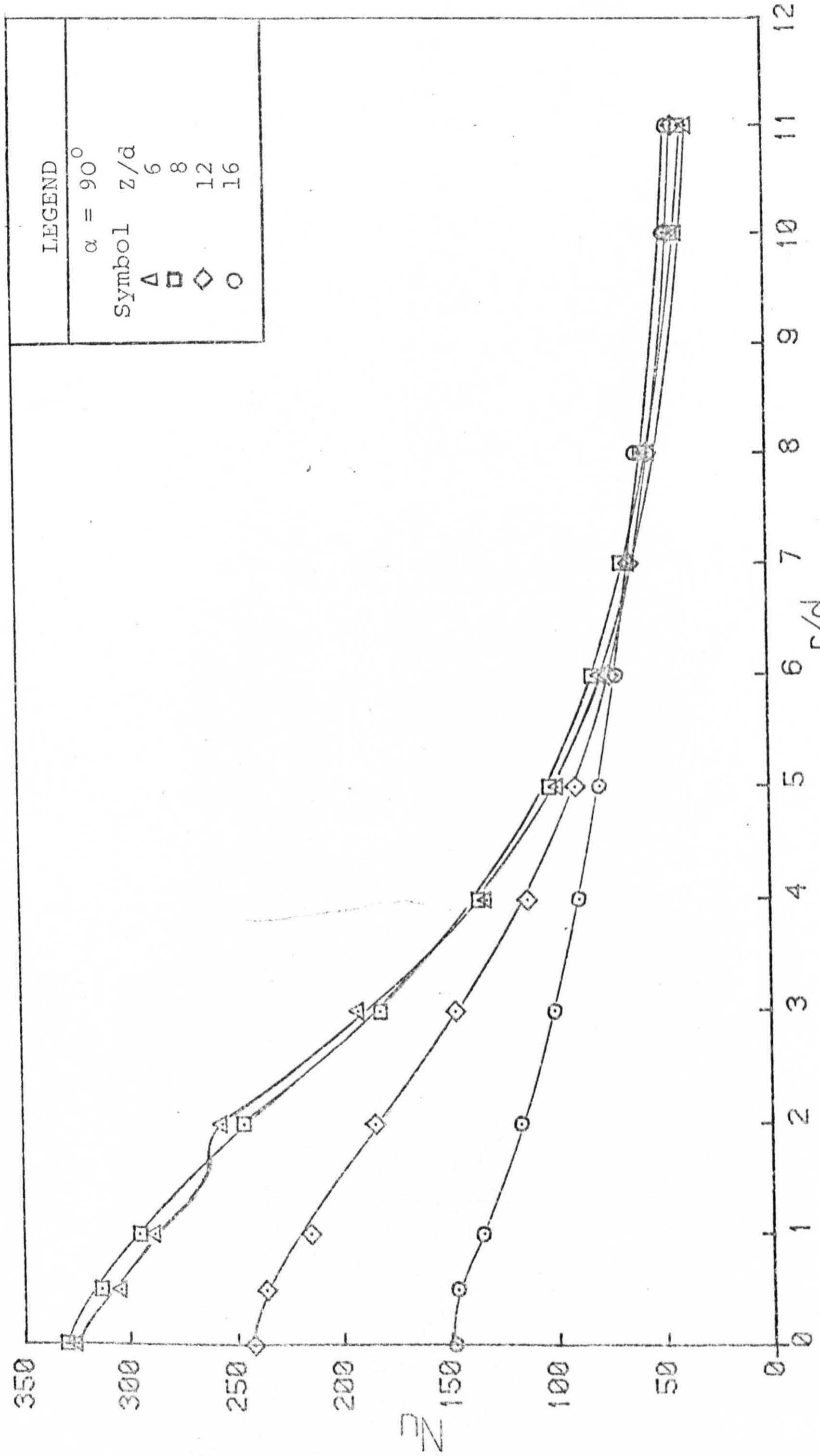

FIG.7.3.5 RADIAL VARIATION OF LOCAL NUSSELT NUMBERS. (Re = 56000)

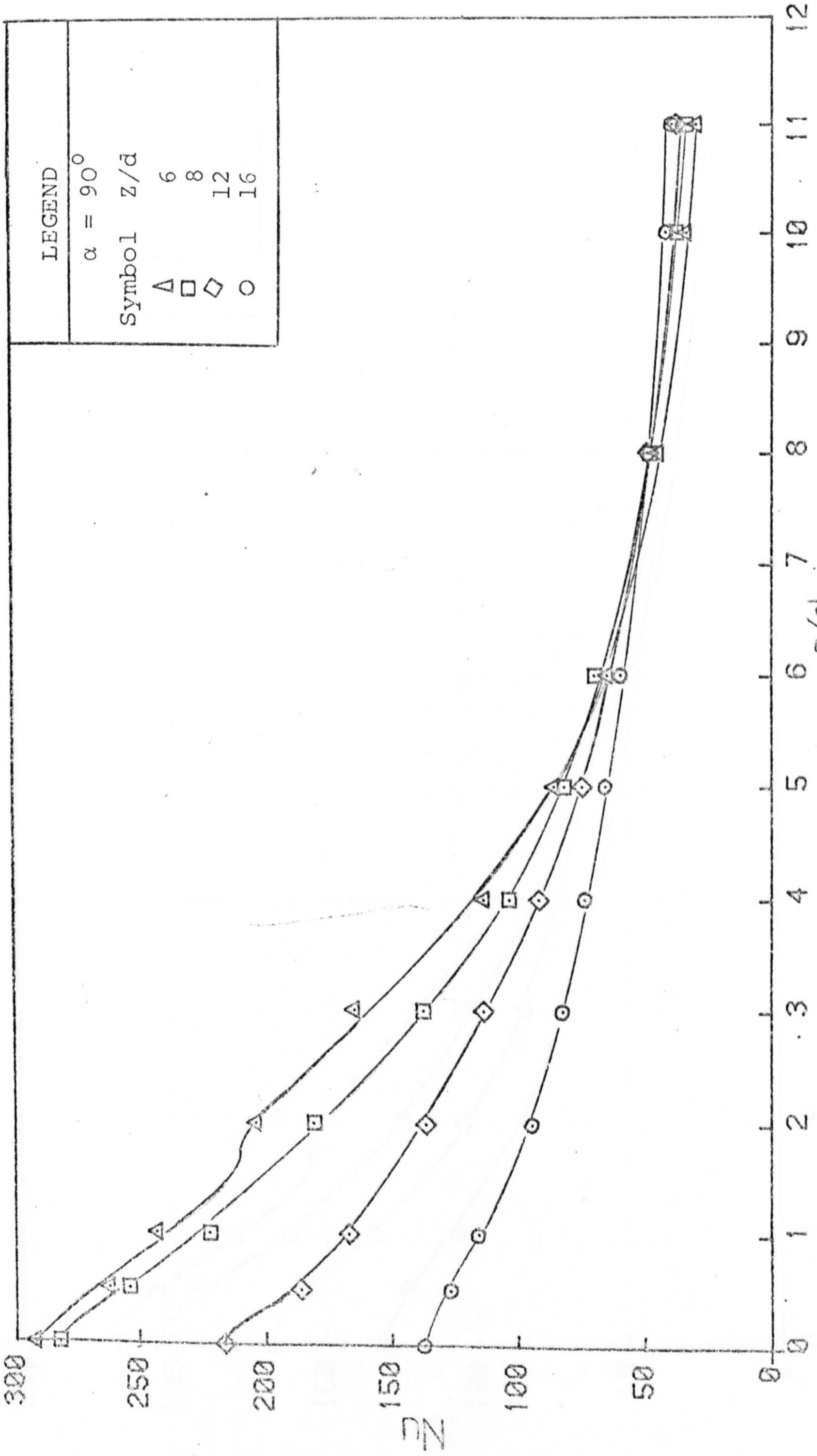
LEGEND
α = 90°
Symbol Z/d
6
8
12
16
NUSSELT NUMBERS. (Re = 46000)
RADIAL VARIATION OF
Nu
r/D
0
50
100
150
200
250
300
1
2
3
4
5
6
7
8
9
10
11
12

FIG. 7.3.6

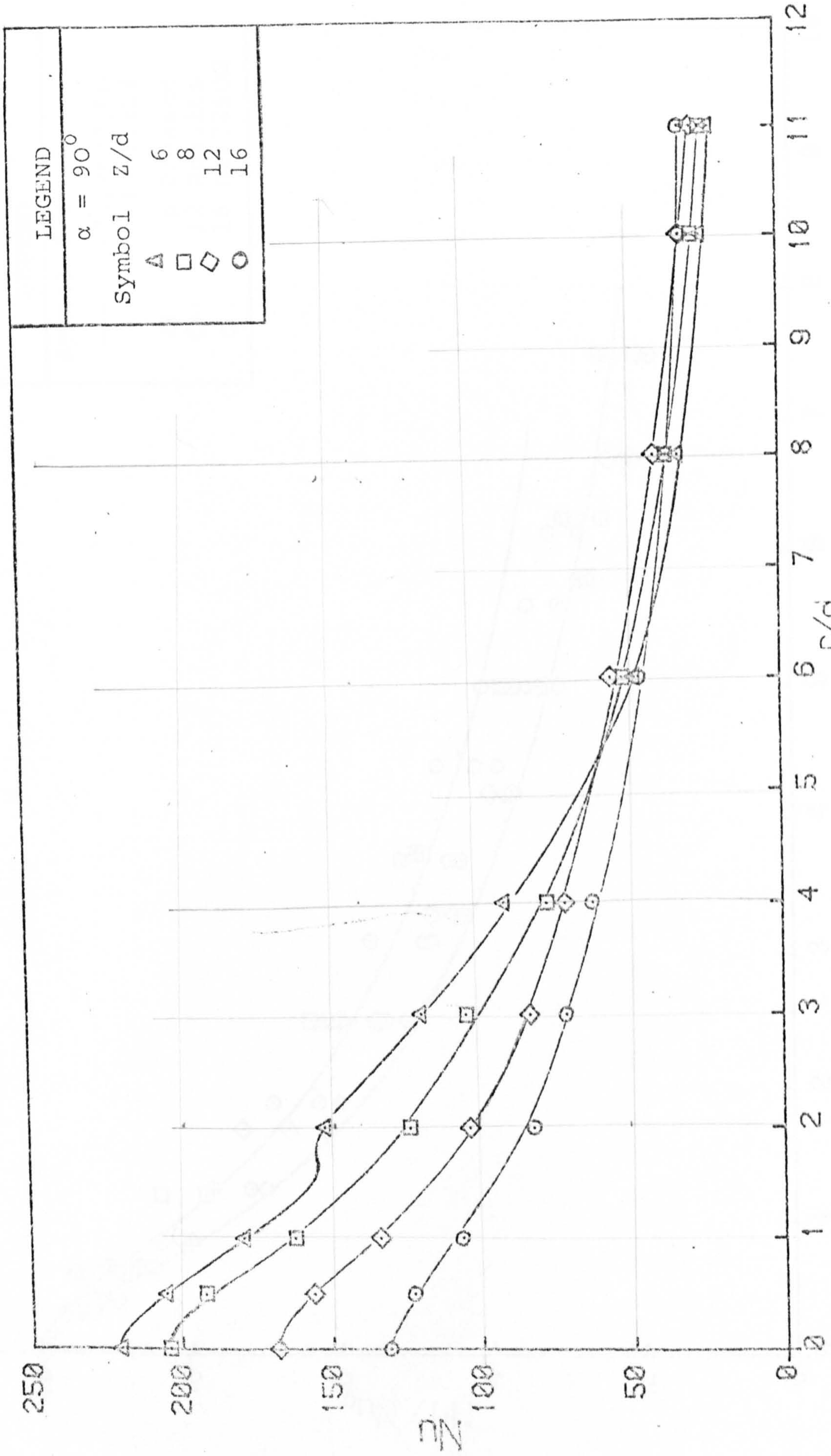

FIG. 7.3.7 RADIAL VARIATION OF LOCAL NUSSELT NUMBERS. (Re = 32500)

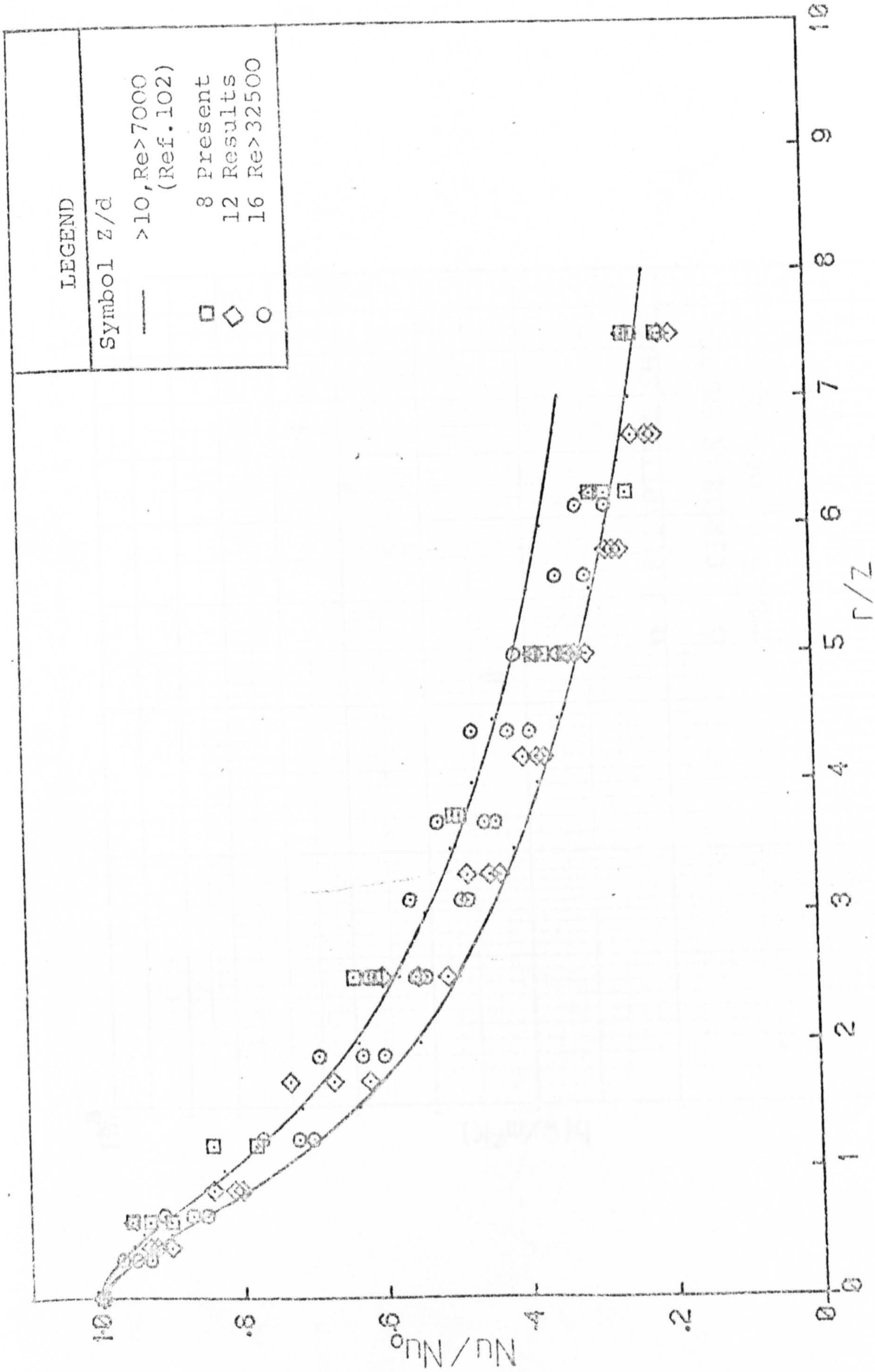

FIG. 7.3.8 RADIAL VARIATION OF NUSSELT NUMBER NORMALISED BY THE STAGNATION VALUE.

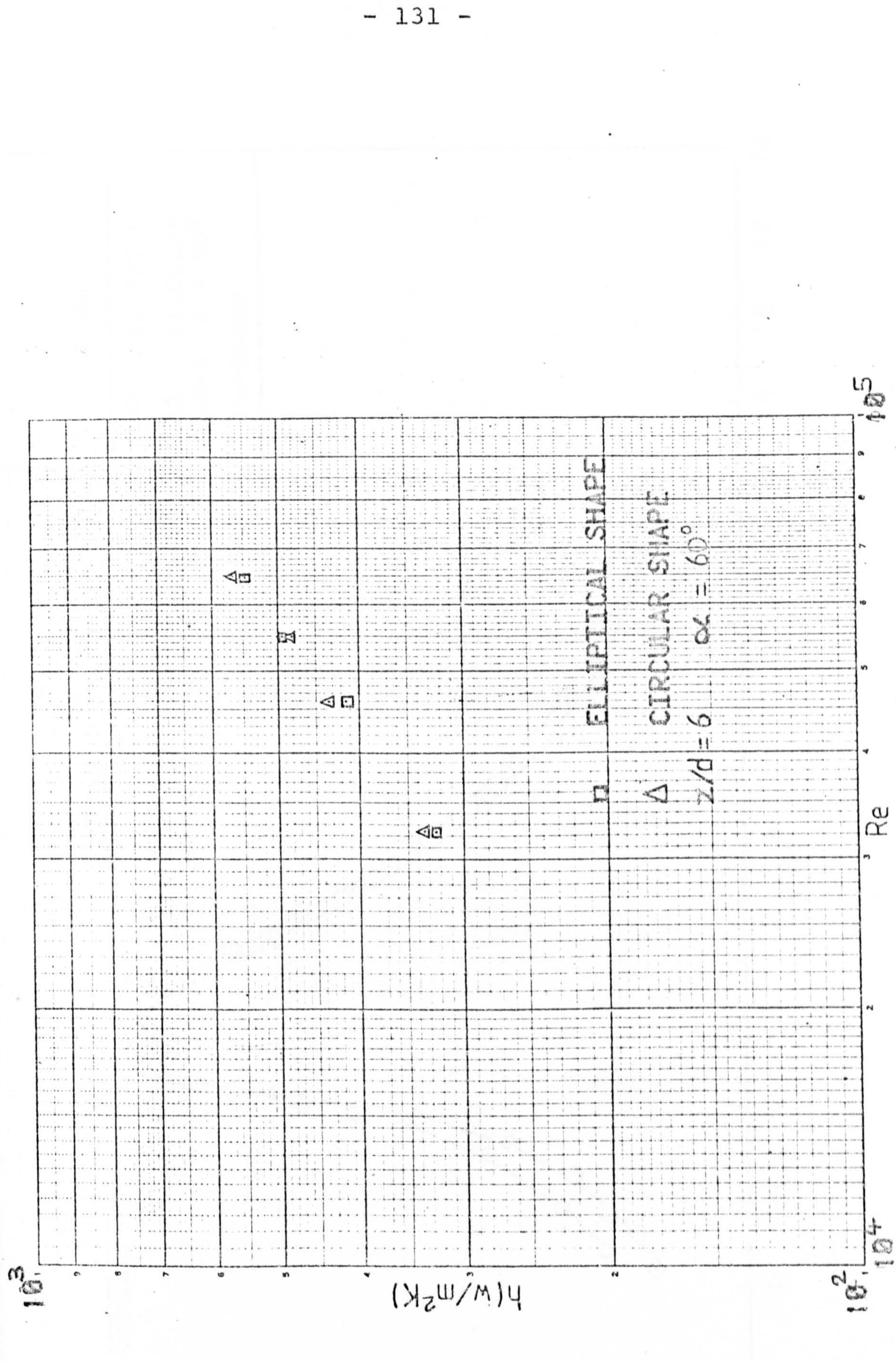

FIG. 7.4.1 VARIATION OF MAXIMUM HEAT TRANSFER COEFFICIENTS FOR DIFFERENT NOZZLE SHAPES.

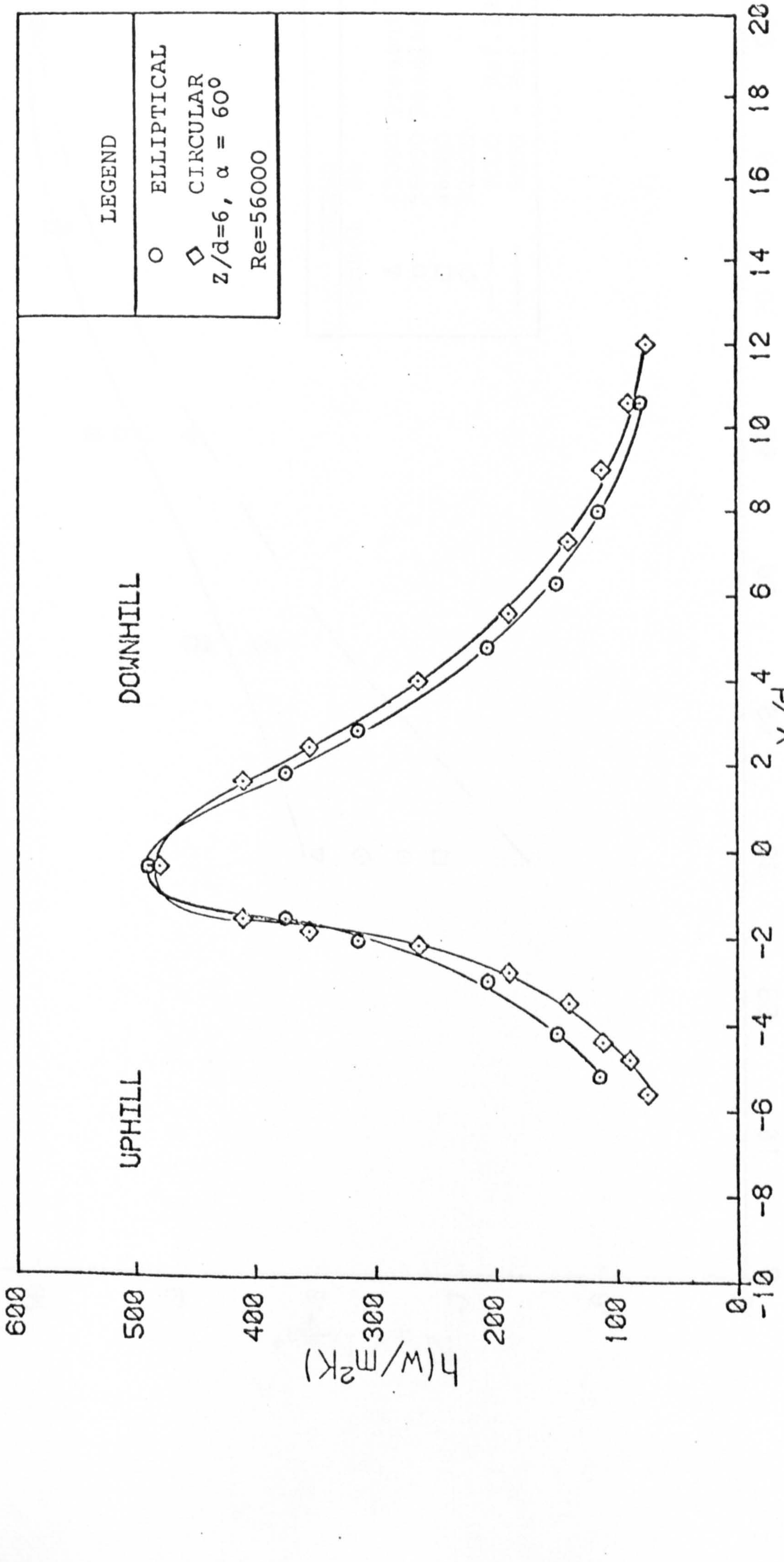

FIG. 7.4.2 VARIATION OF HEAT TRANSFER COEFFICIENTS ALONG THE LINE OF SYMMETRY.

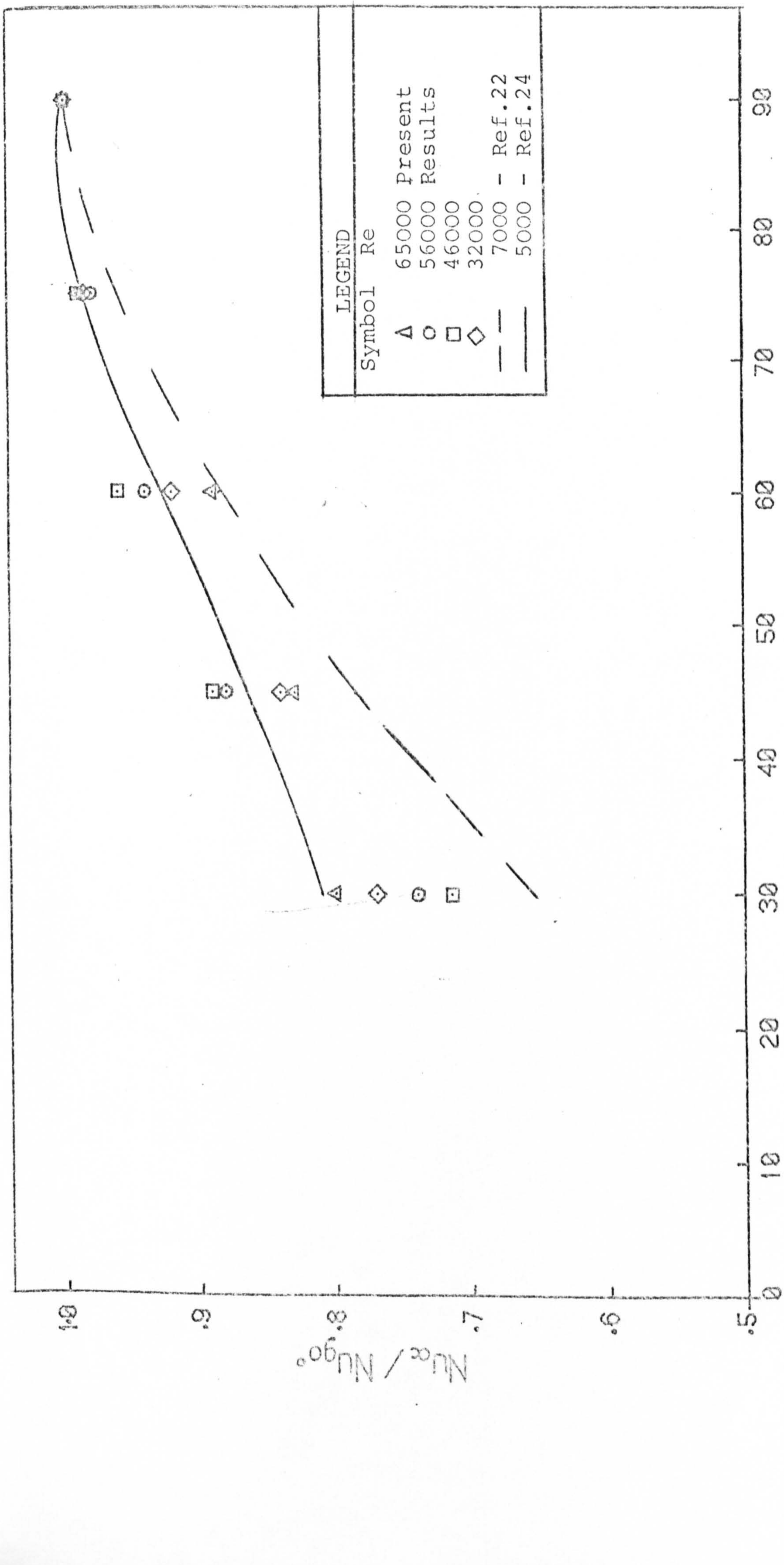

FIG. 7.4.3 EFFECT OF NOZZLE INCLINATION ON STAGNATION POINT NUSSELT NUMBER.

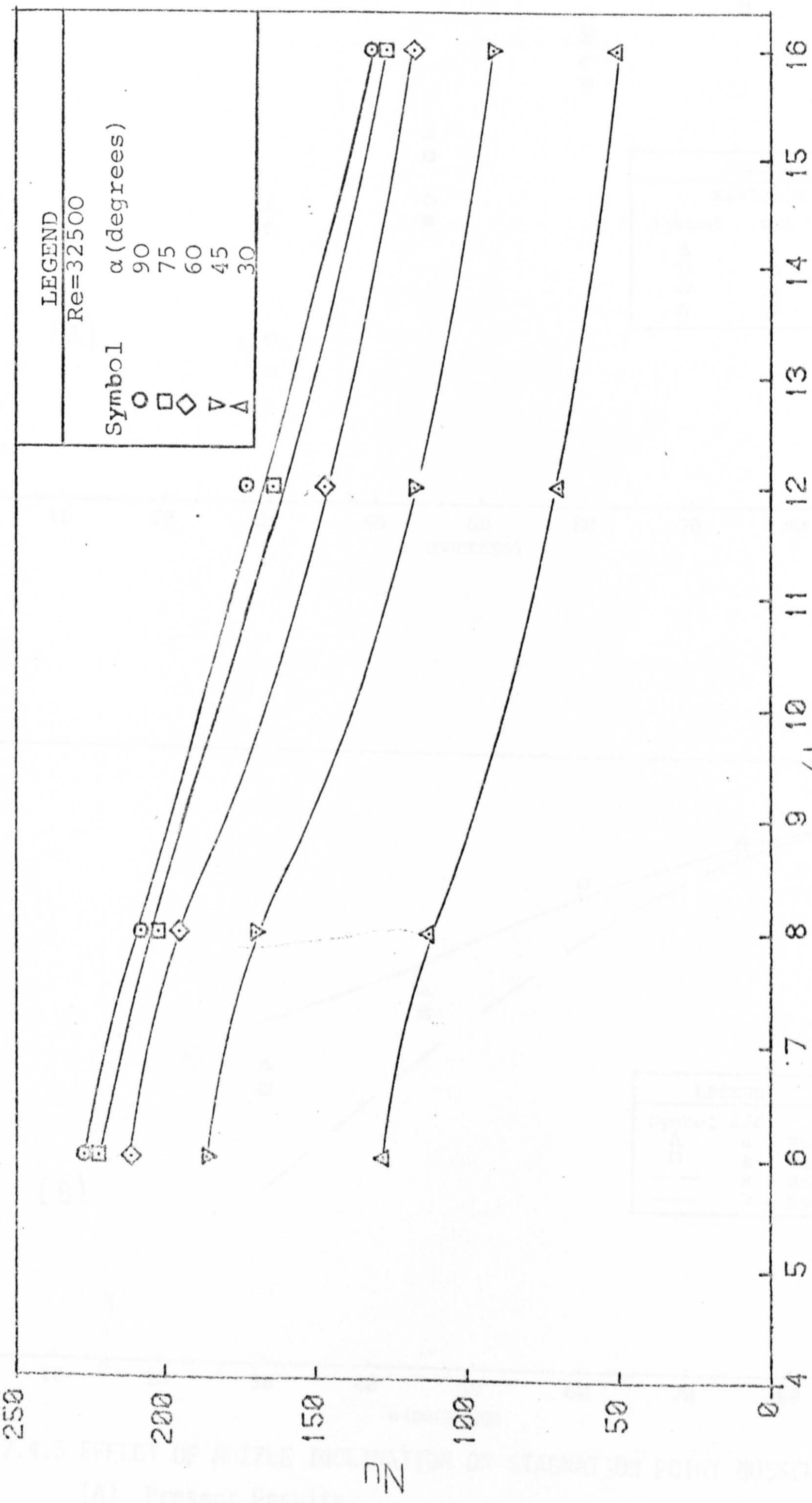

FIG. 7.4.4 EFFECT OF NOZZLE-TARGET SEPARATION ON STAGNATION POINT NUSSELT NUMBER.

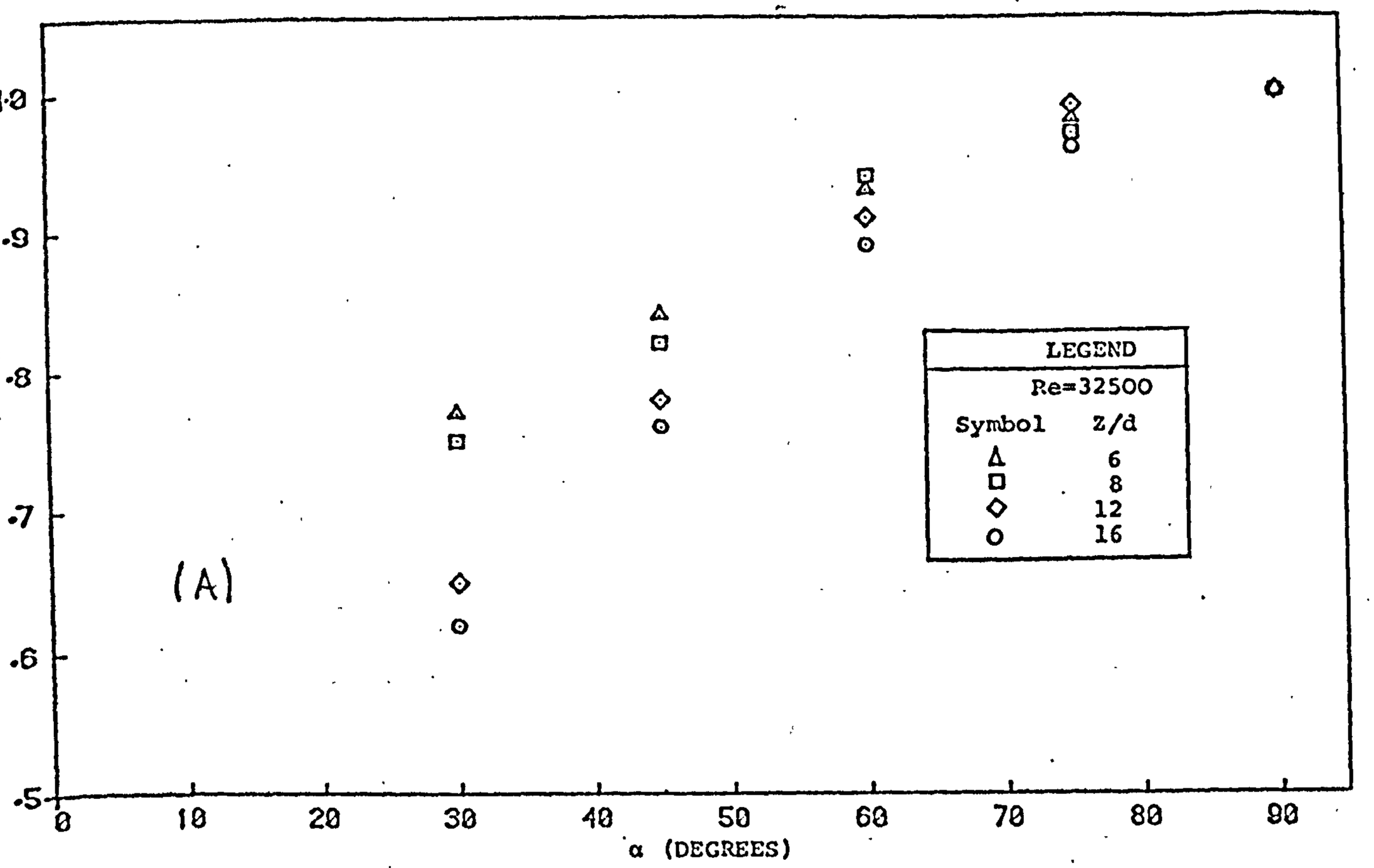

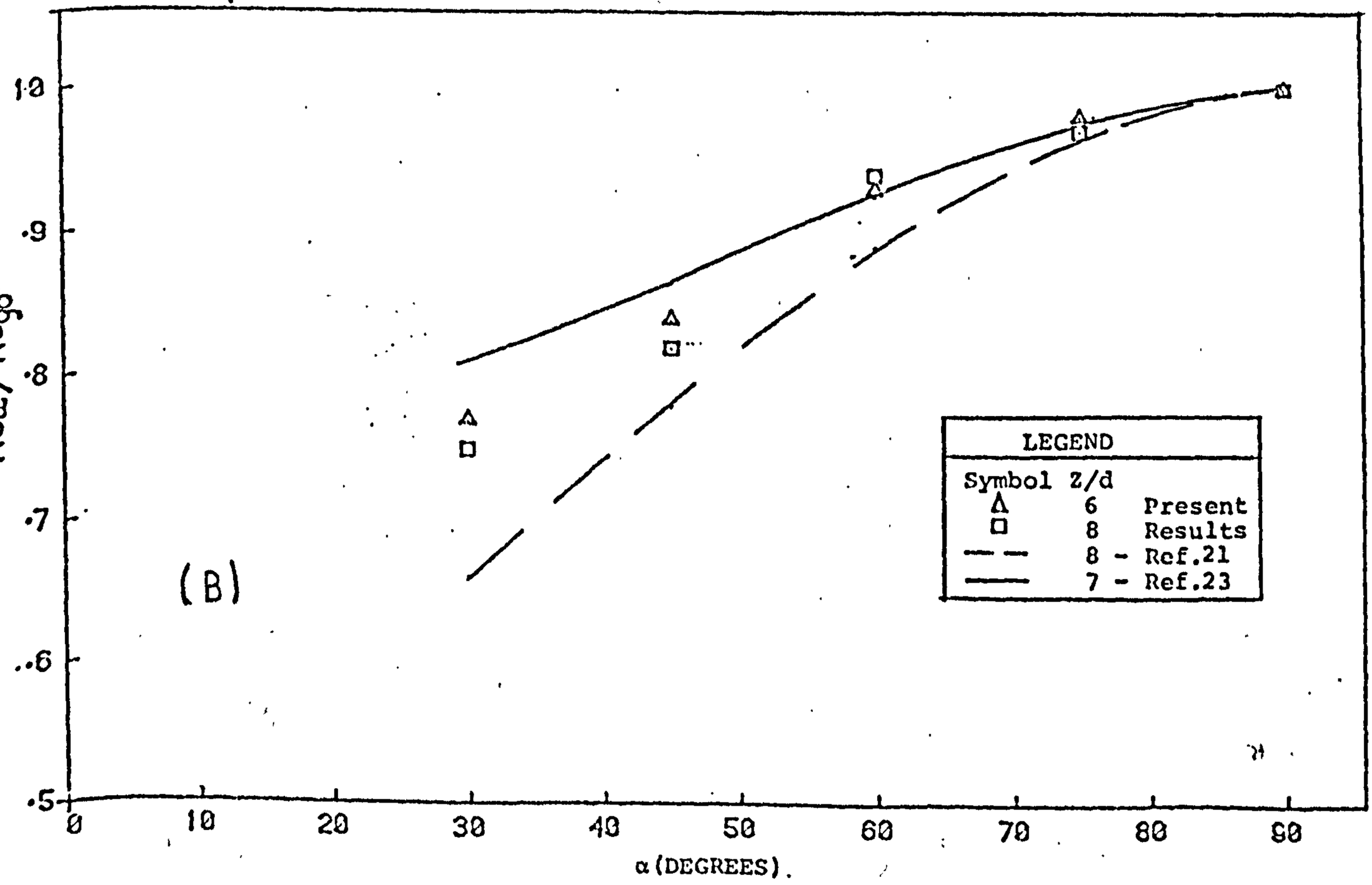

FIG 7.4.5 EFFECT OF NOZZLE INCLINATION ON STAGNATION POINT NUSSELT NUMBER.

(A) Present Results.

(B) Comparison with those of other workers.

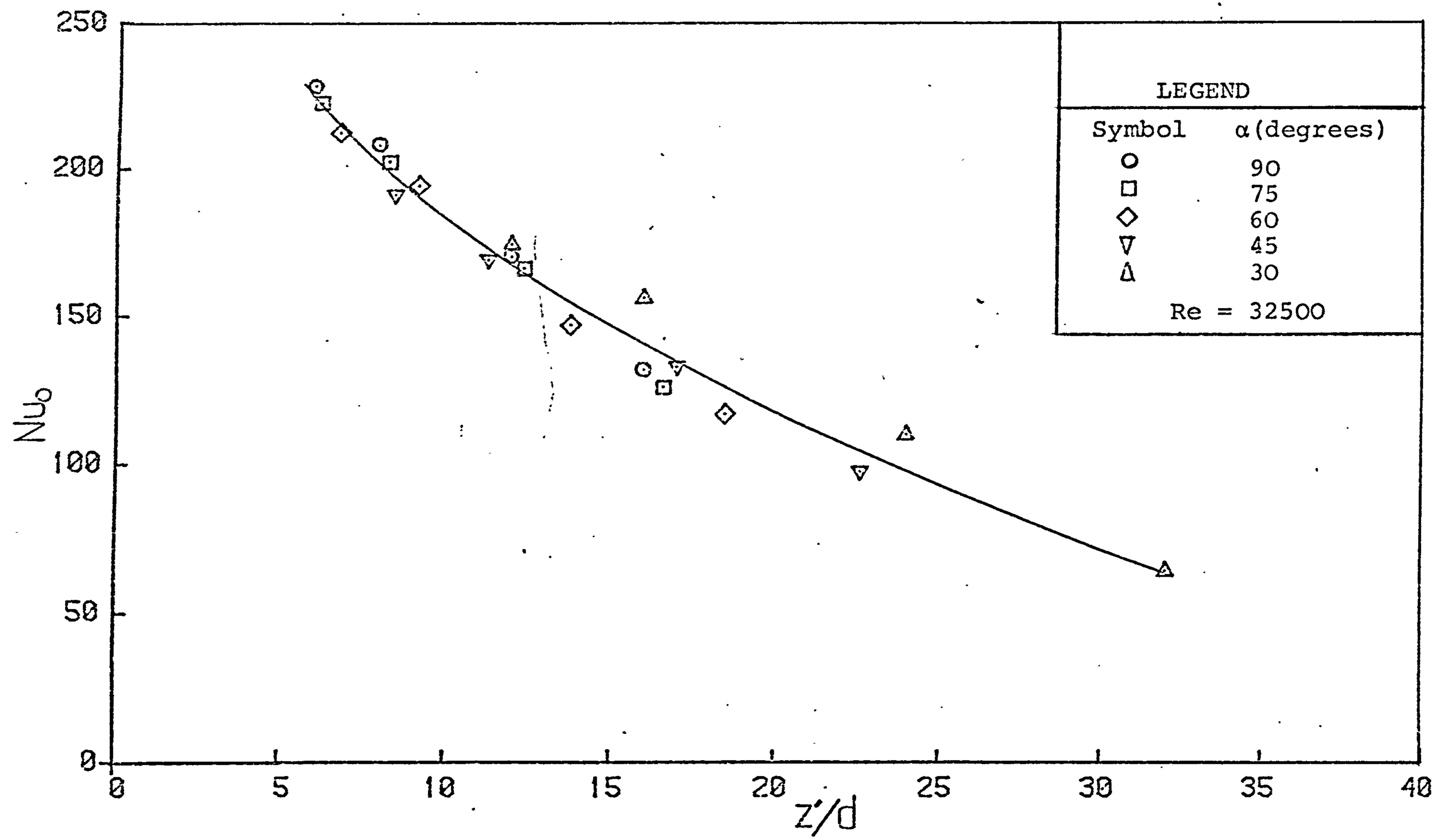

FIG. 7.4.6 EFFECT OF "APPARENT" NOZZLE-TO-TARGET SEPARATIONS ON MAXIMUM NUSSELT NUMBERS.

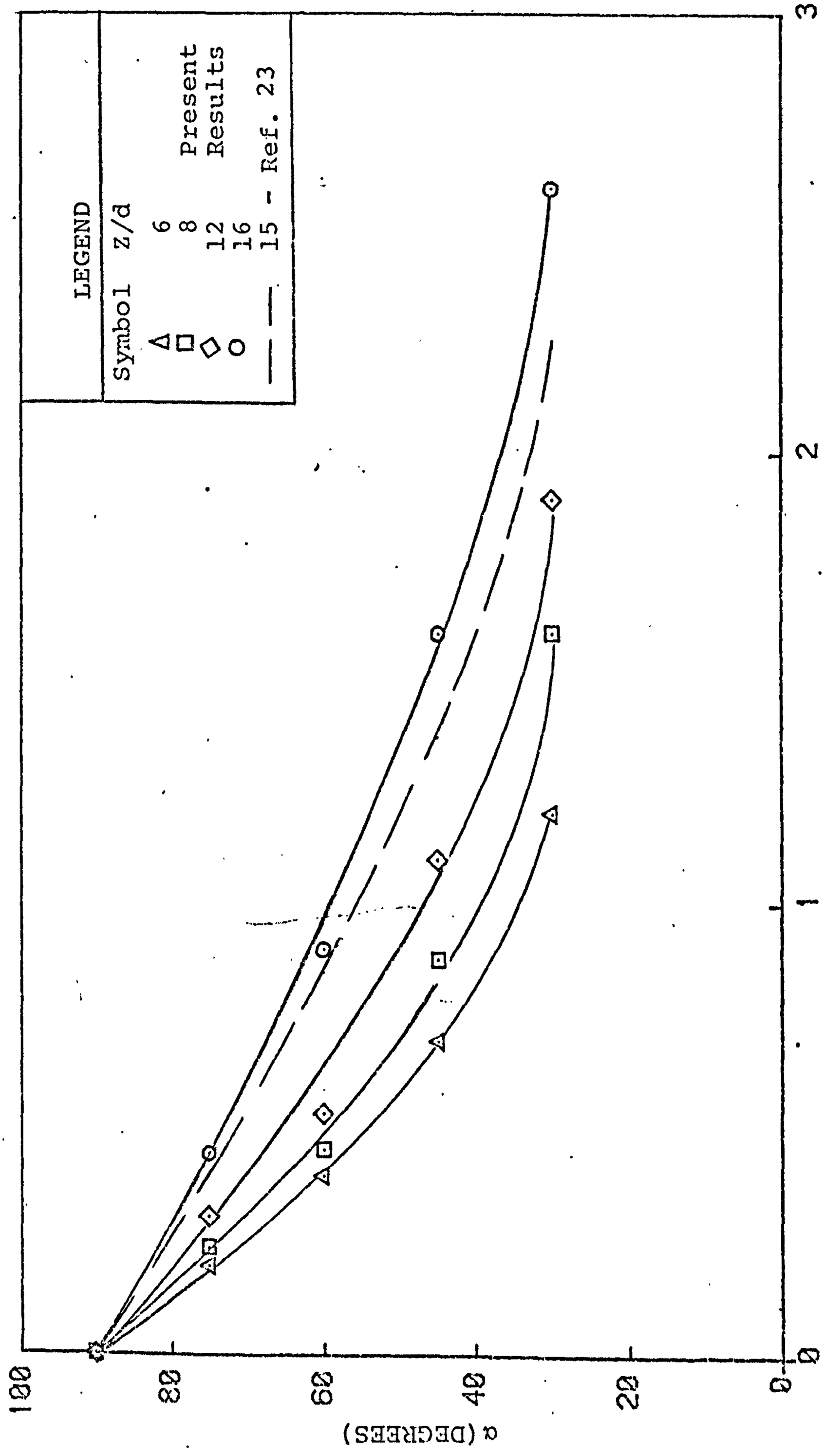

FIG. 7.4.7 EFFECT OF NOZZLE INCLINATION ON THE LOCATION OF STAGNATION POINT.

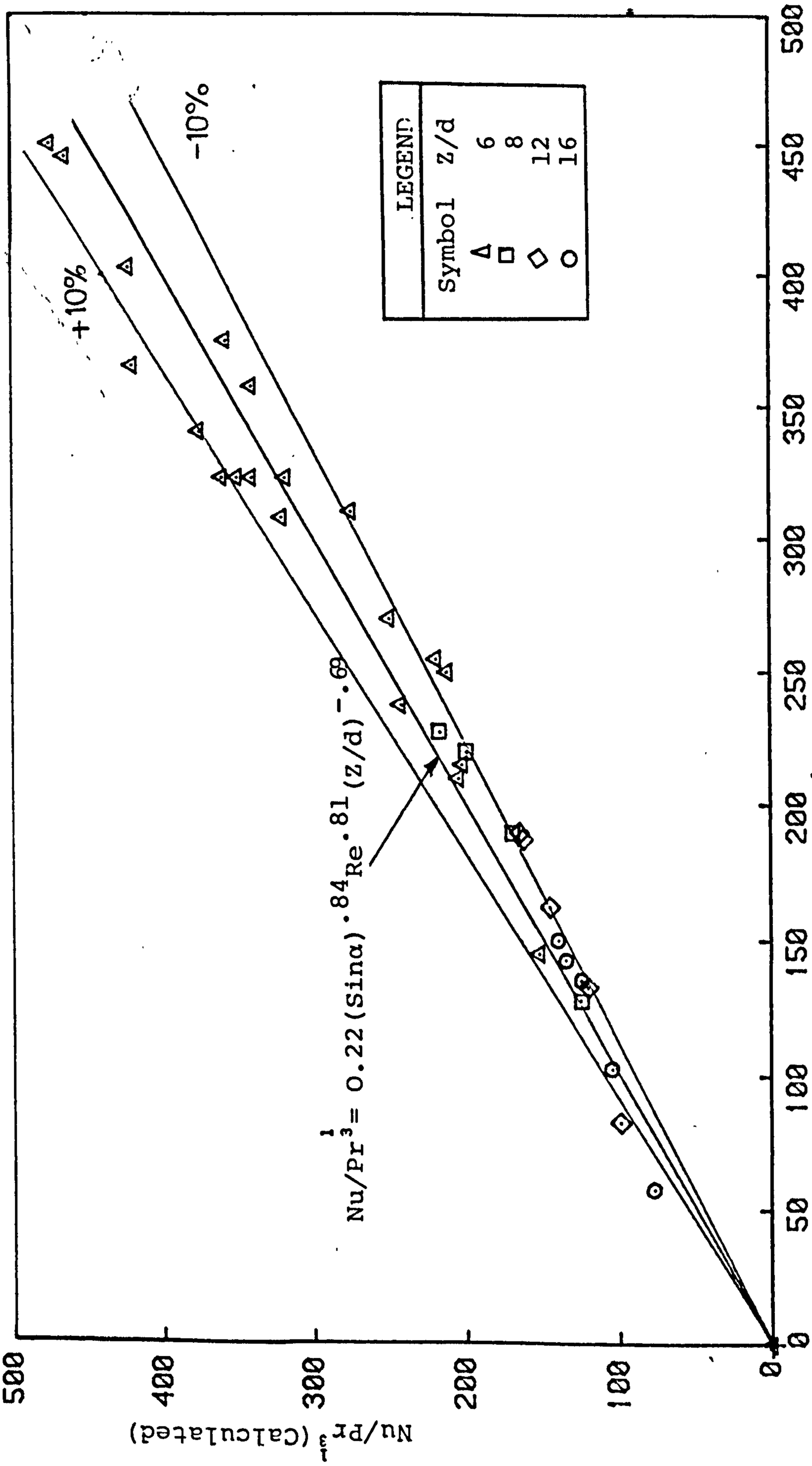

FIG. 7.4.8 CORRELATION OF NUSSELT NUMBER FOR THE STAGNATION POINT.

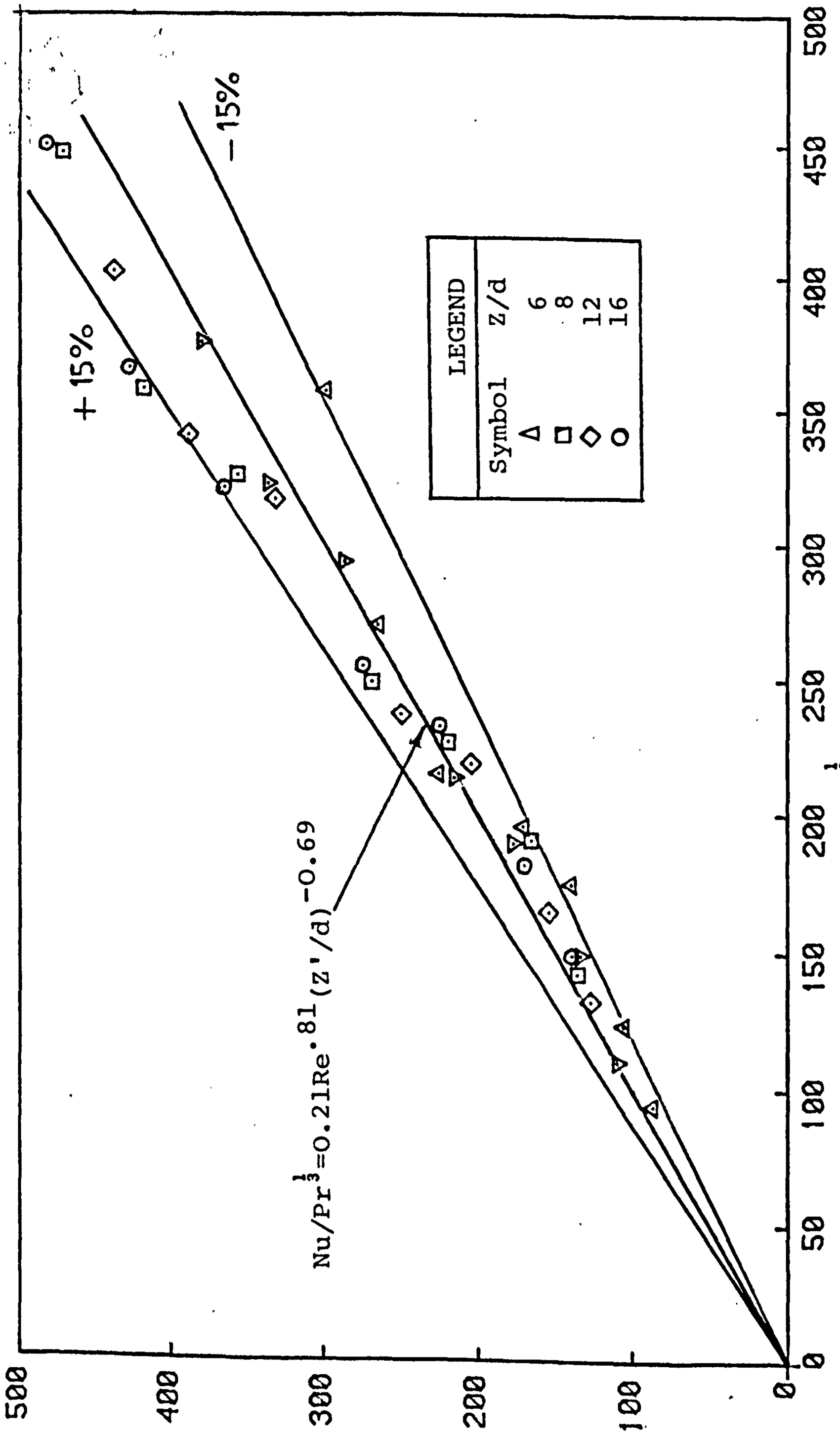

FIG. 7.4.9 CORRELATION OF NUSSELT NUMBER FOR THE STAGNATION POINT.

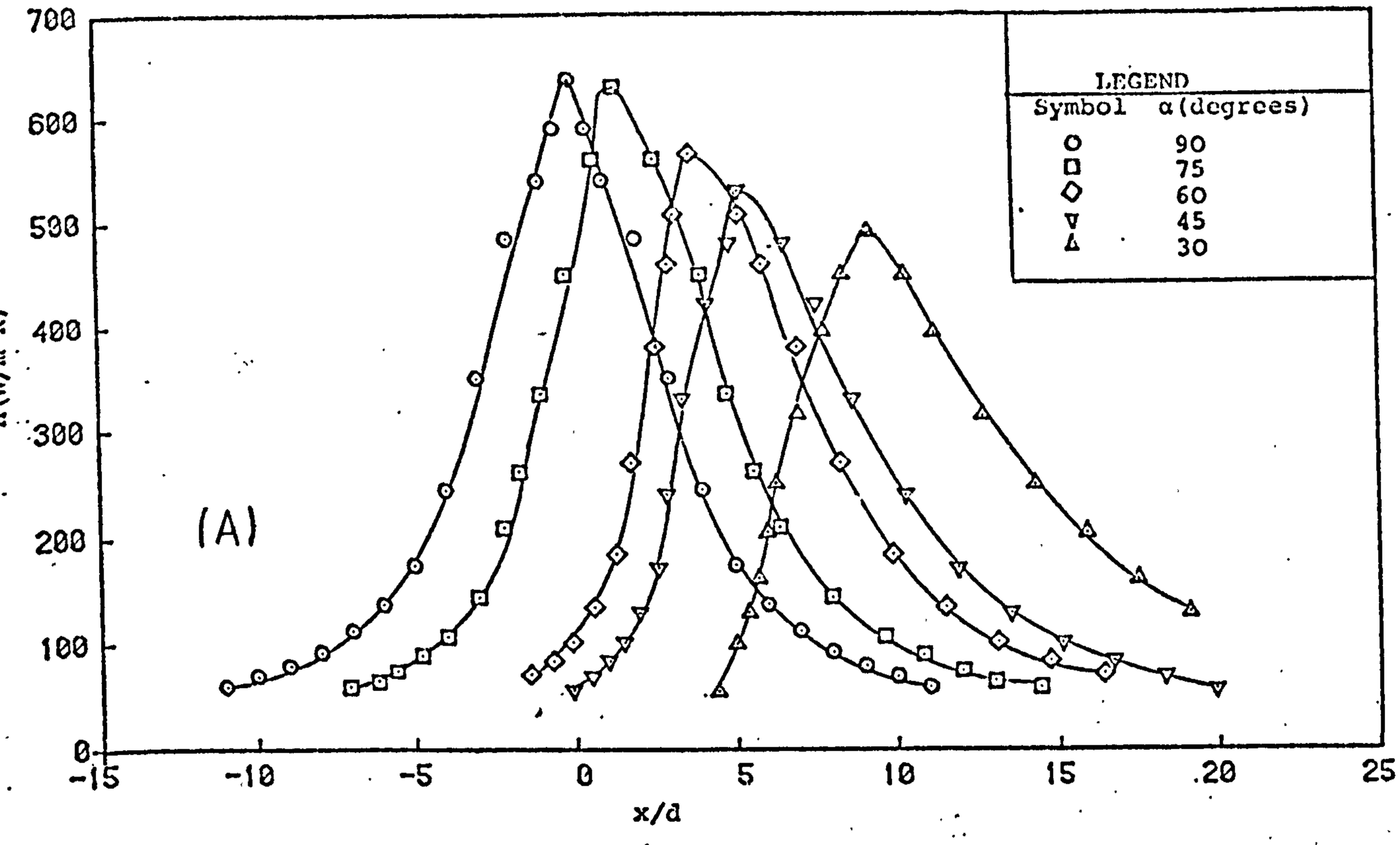

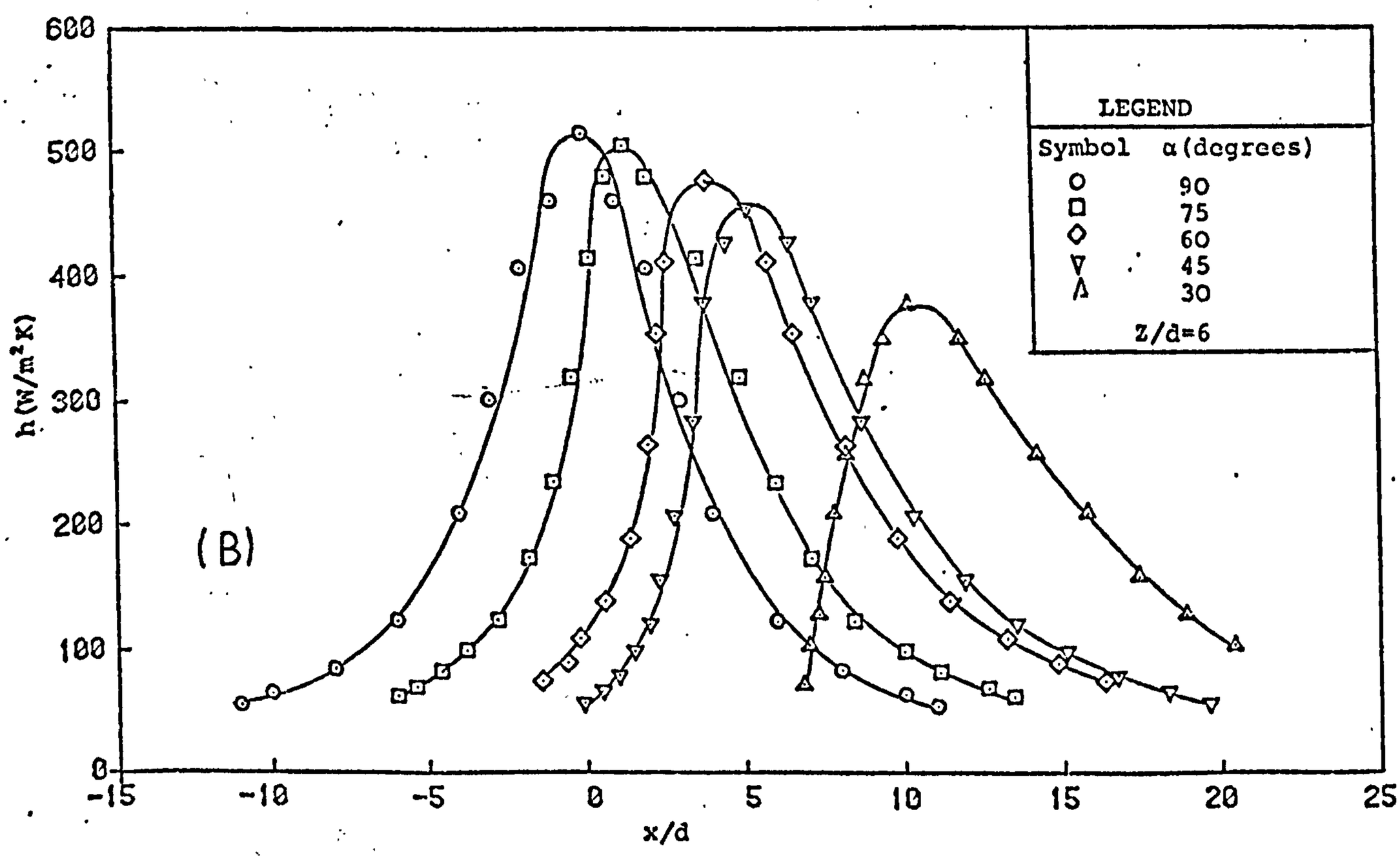

FIG. 7.4.10 HEAT TRANSFER COEFFICIENTS ALONG THE LINE OF SYMMETRY.

(A) Re = 65000 (B) Re = 56000

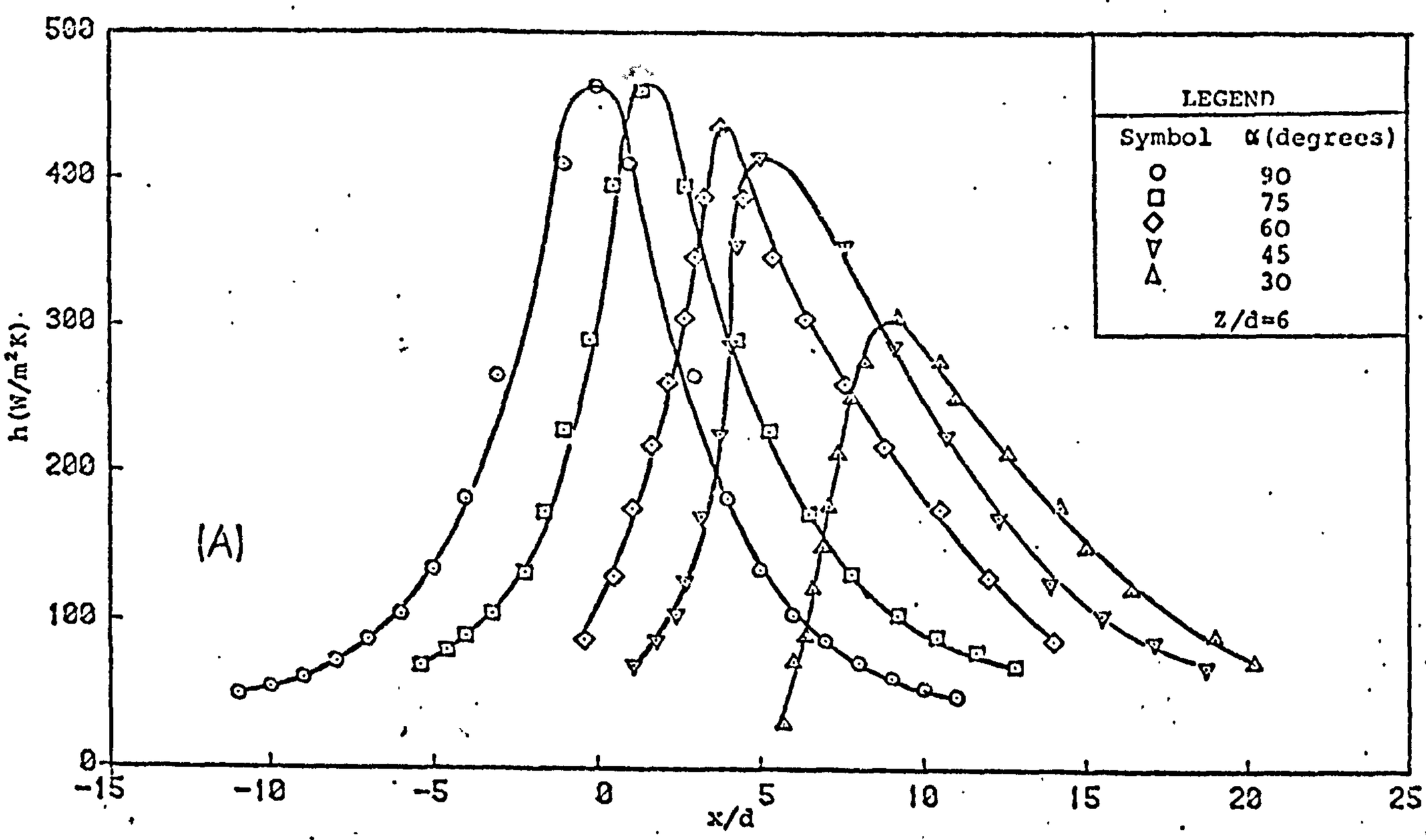

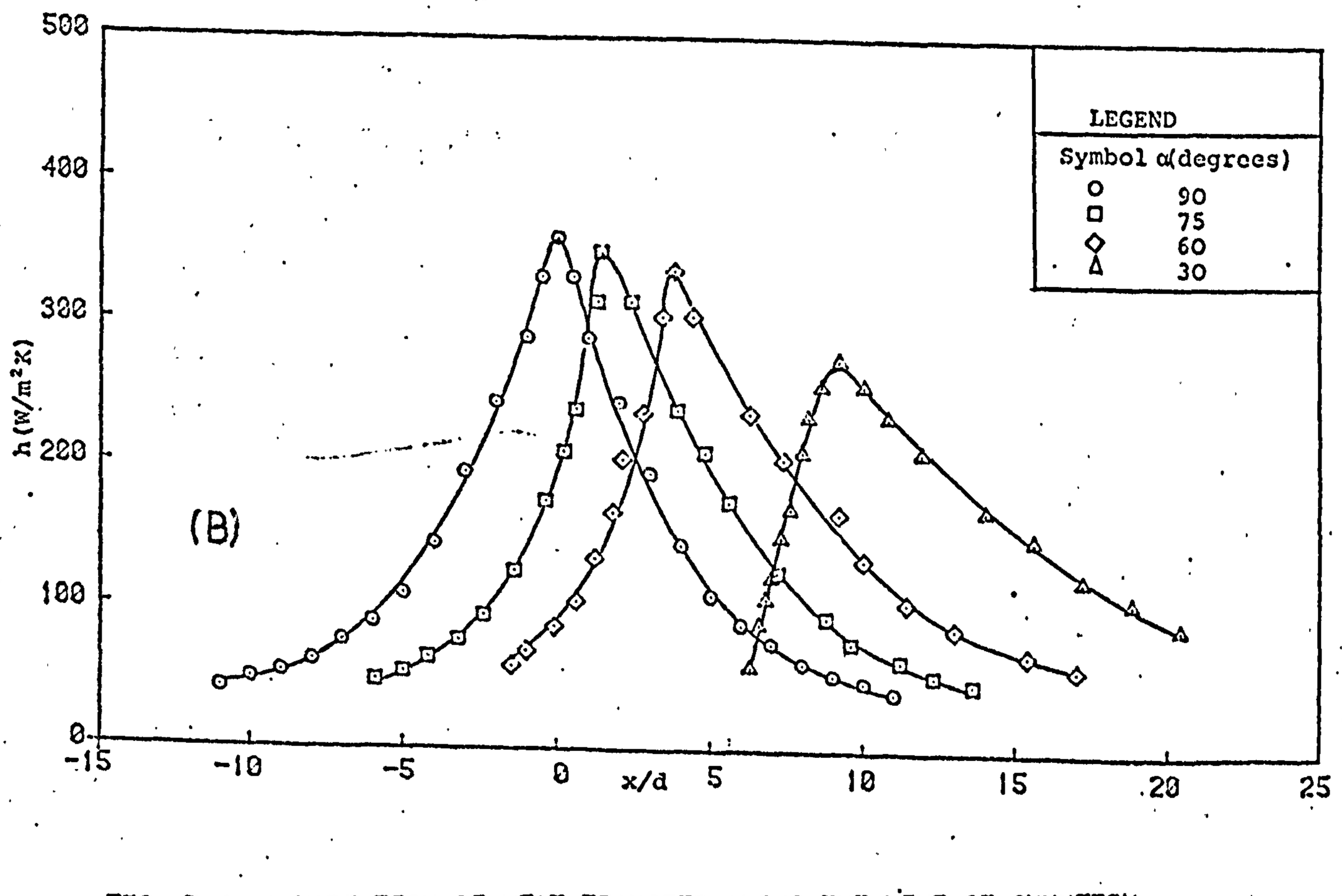

FIG. 7.4.11 VARIATION OF HEAT TRANSFER ALONG THE LINE OF SYMMETRY.

(A) Re = 46000 (B) Re = 32500

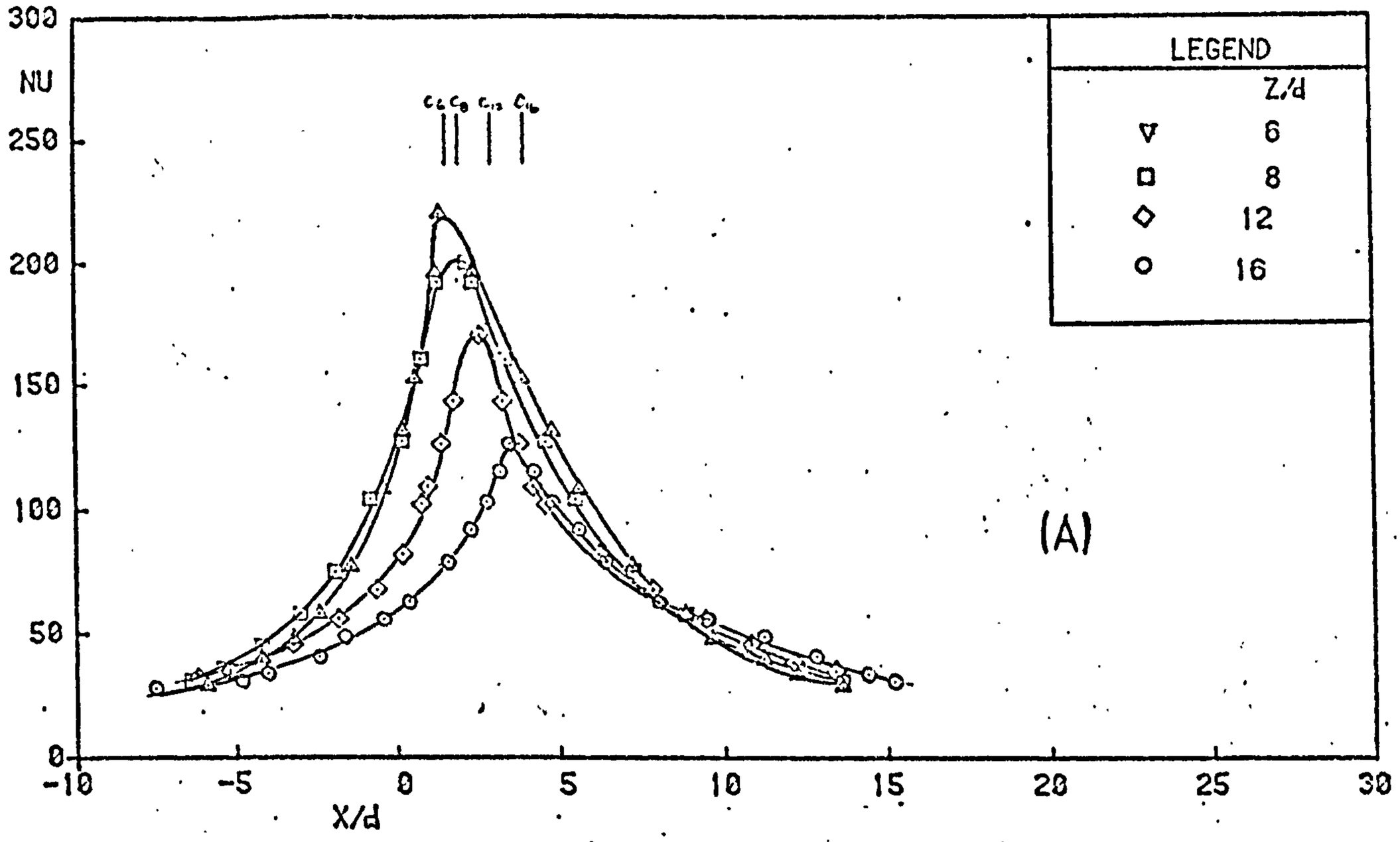

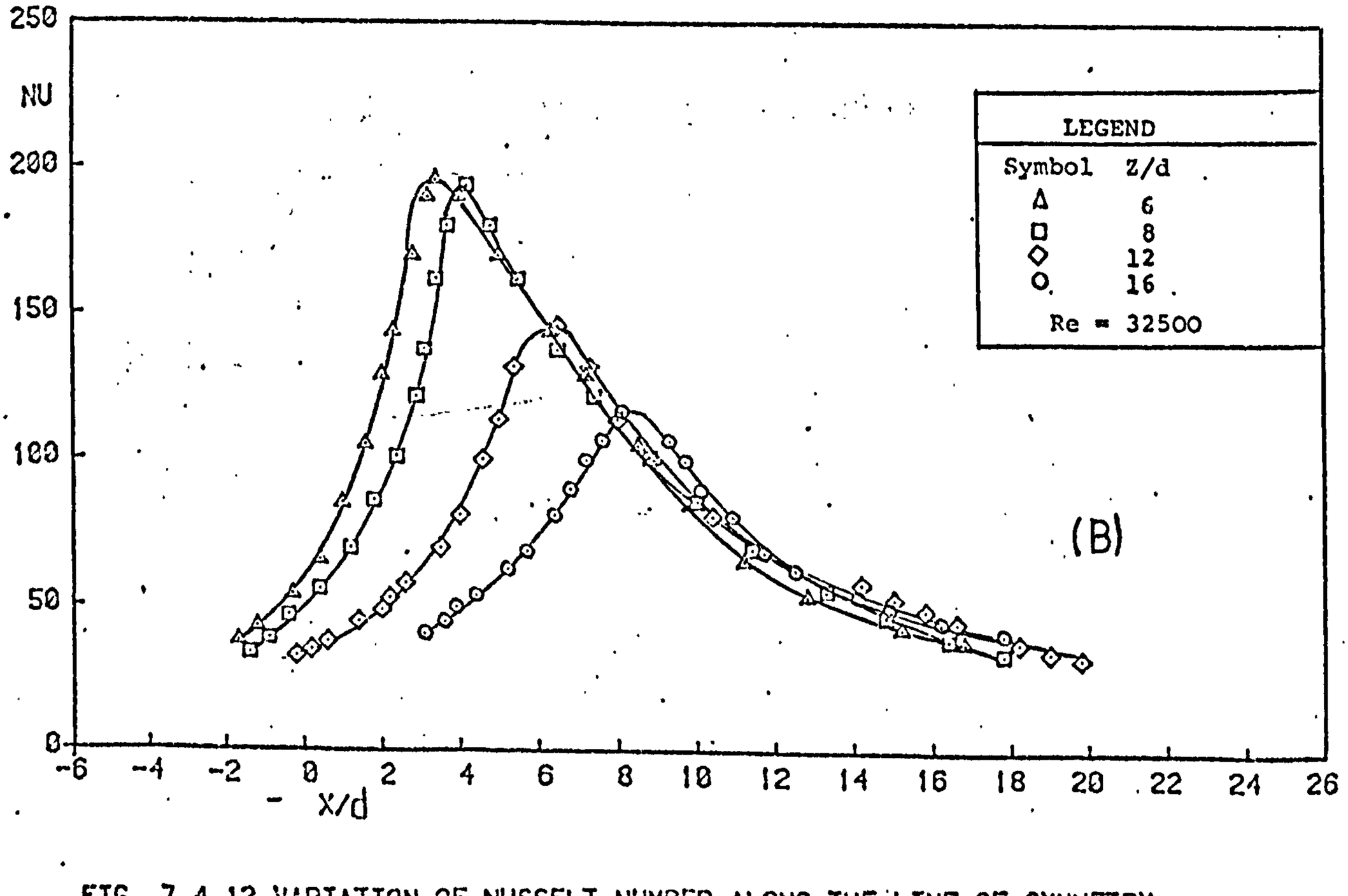

FIG. 7.4.12 VARIATION OF NUSSELT NUMBER ALONG THE LINE OF SYMMETRY.

(A) α = 75° (B) α = 60°

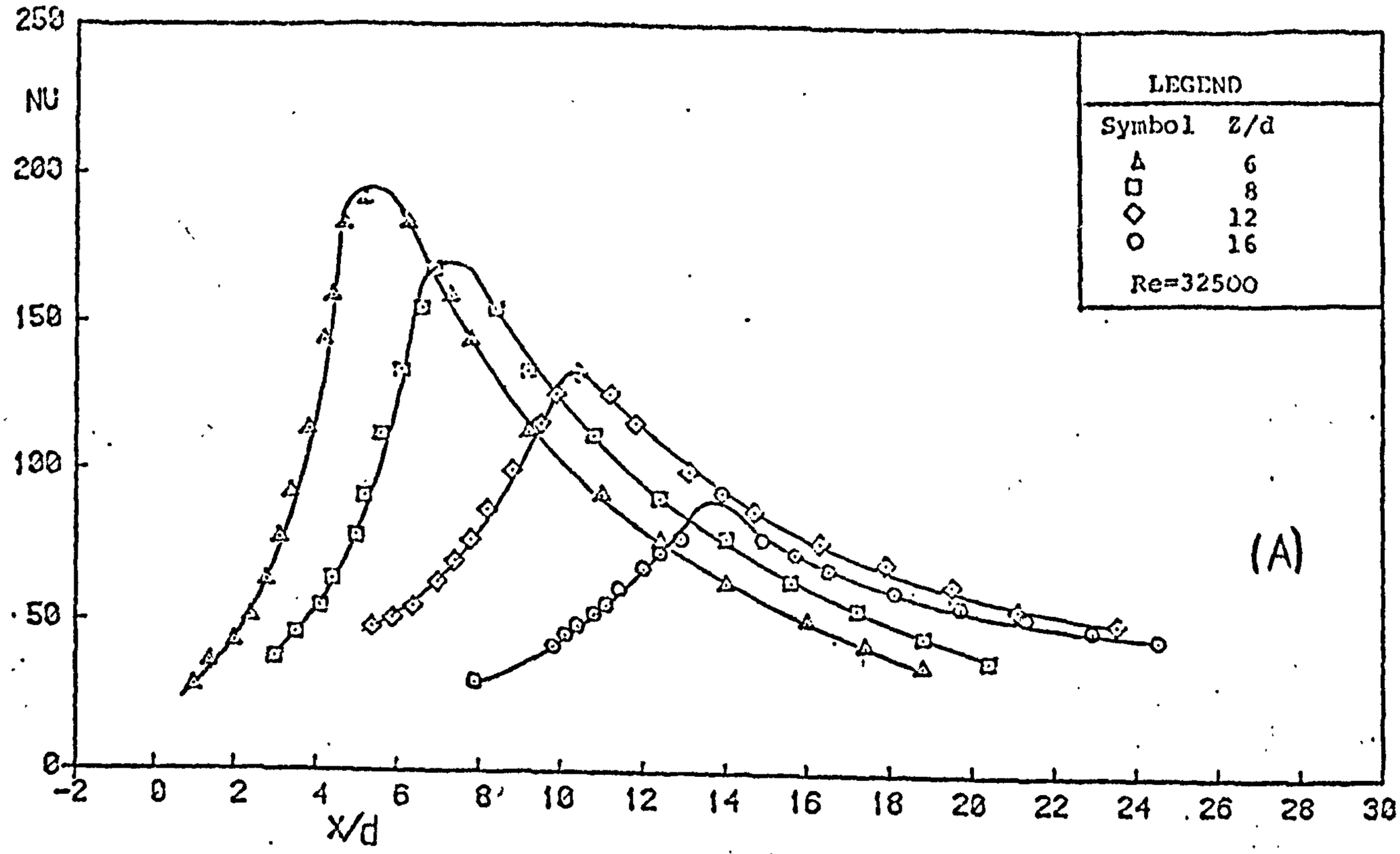

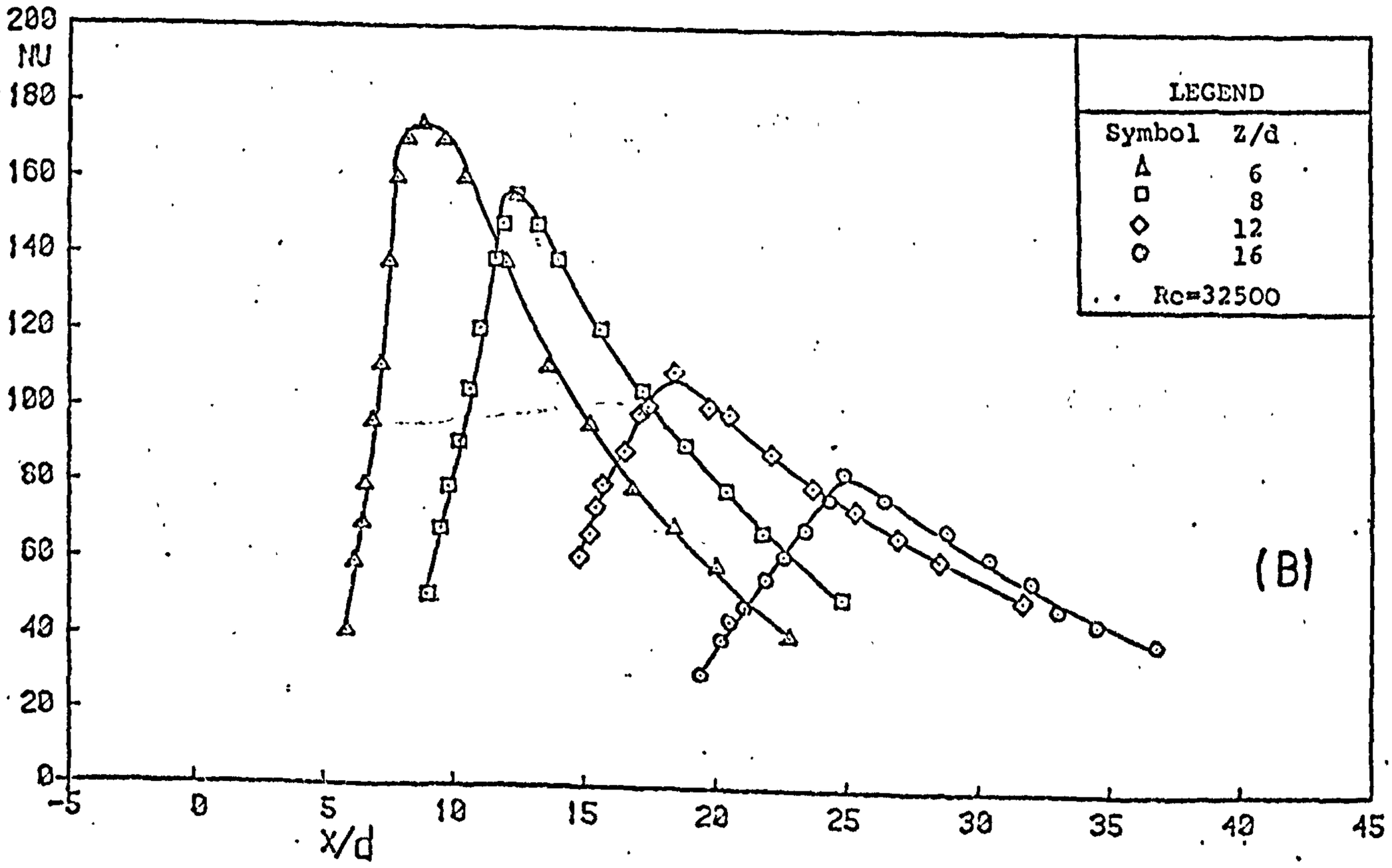

FIG. 7.4.13 VARIATION OF NUSSELT NUMBER ALONG THE LINE OF SYMMETRY.

(A) $\alpha = 45^{\circ}$ (B) $\alpha = 30^{\circ}$

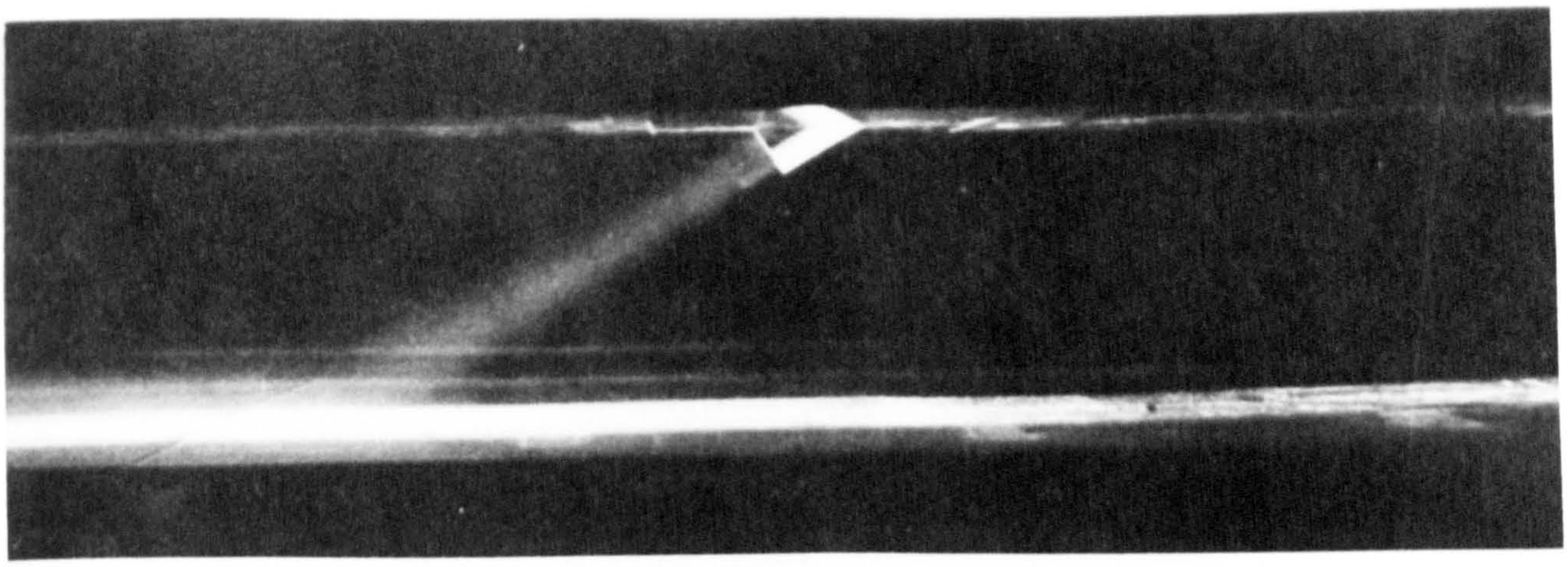

α = 30°

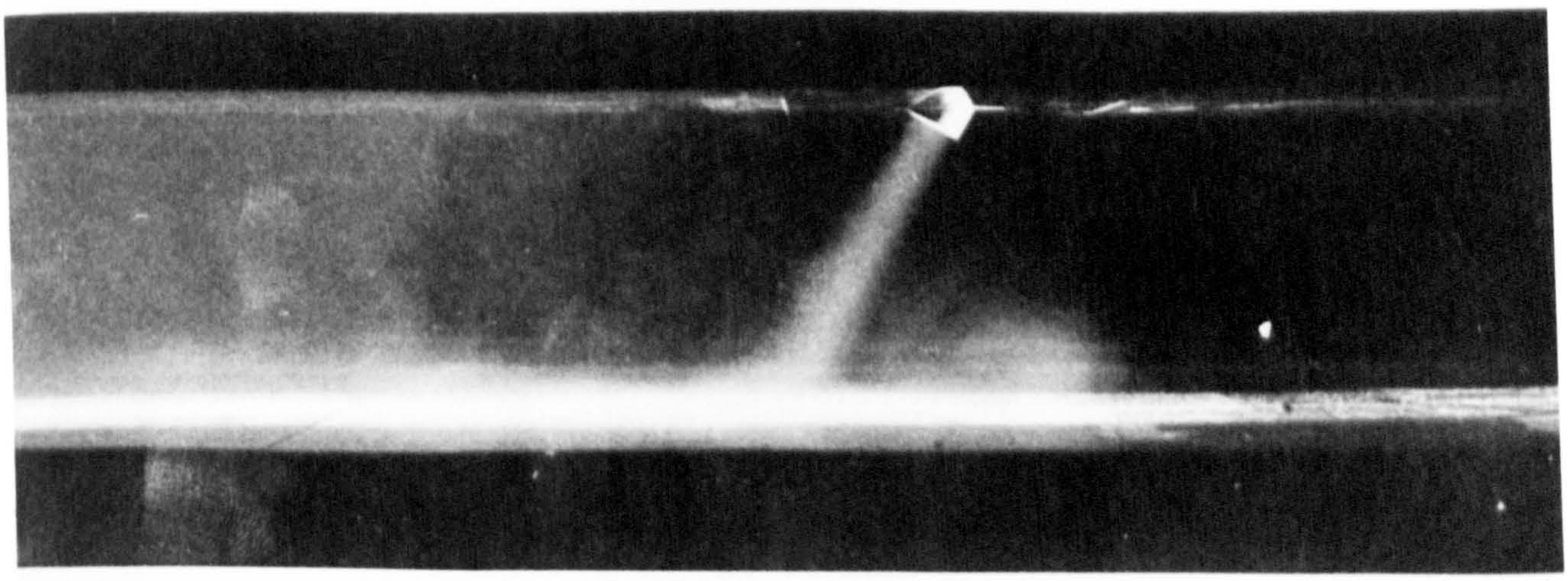

= 60°

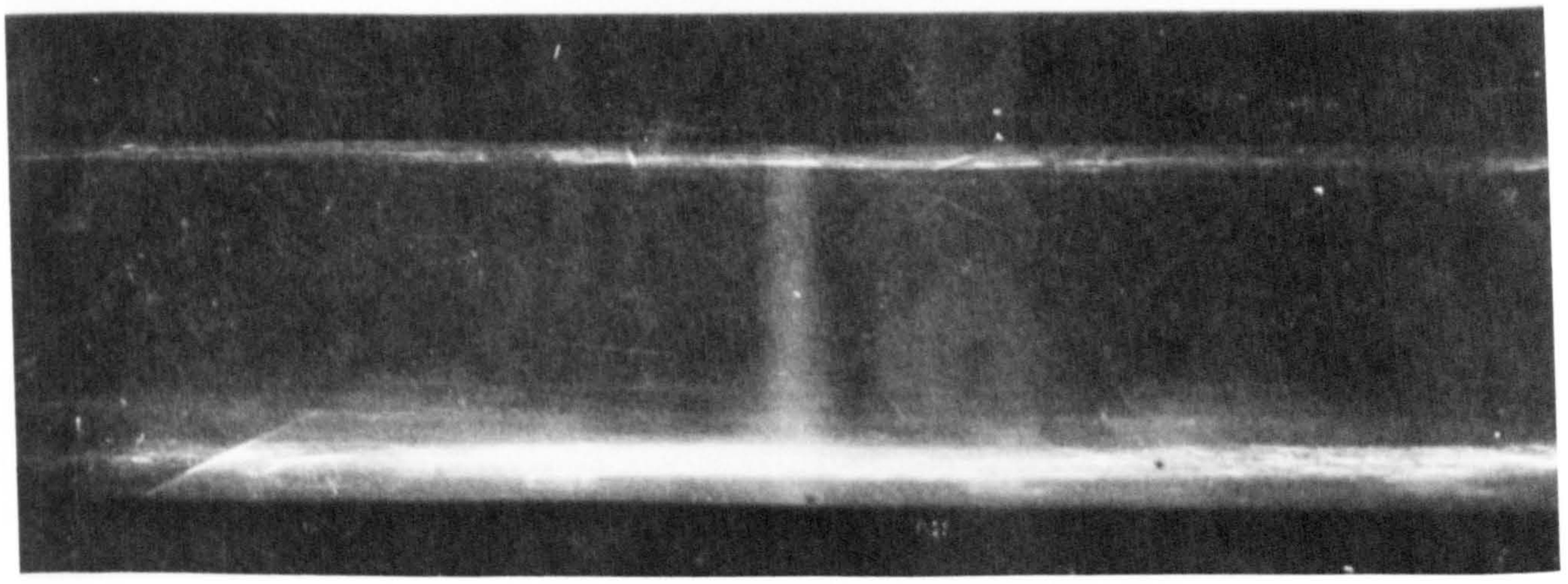

= 90°

PLATE 7.4-1 FLOW STRUCTURES OF INCLINED TURBULENT JETS.
Re = 32500, Z/d = 6.

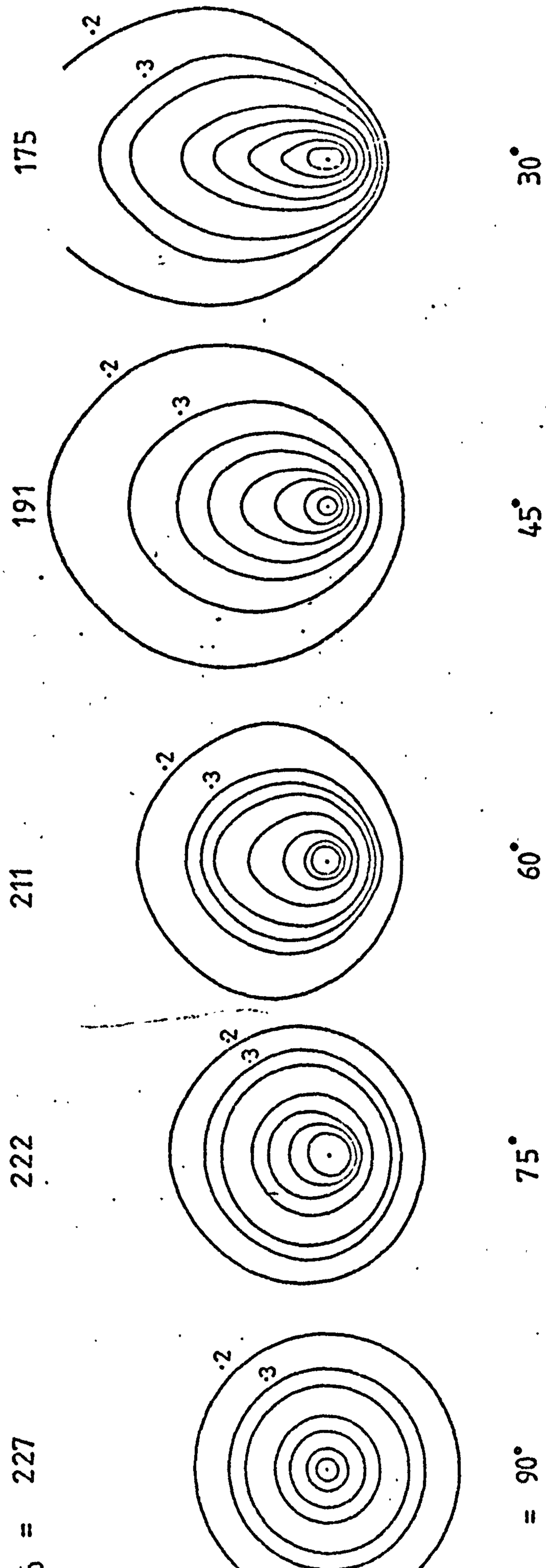
.2
.3
175
30°
191
45°
211
60°
222
75°
Nu_δ = 227
α = 90°
EFFECT OF NOZZLE INCLINATION ON HEAT TRANSFER
Z/d = 6, Re = 32500

FIG. 7·4·14

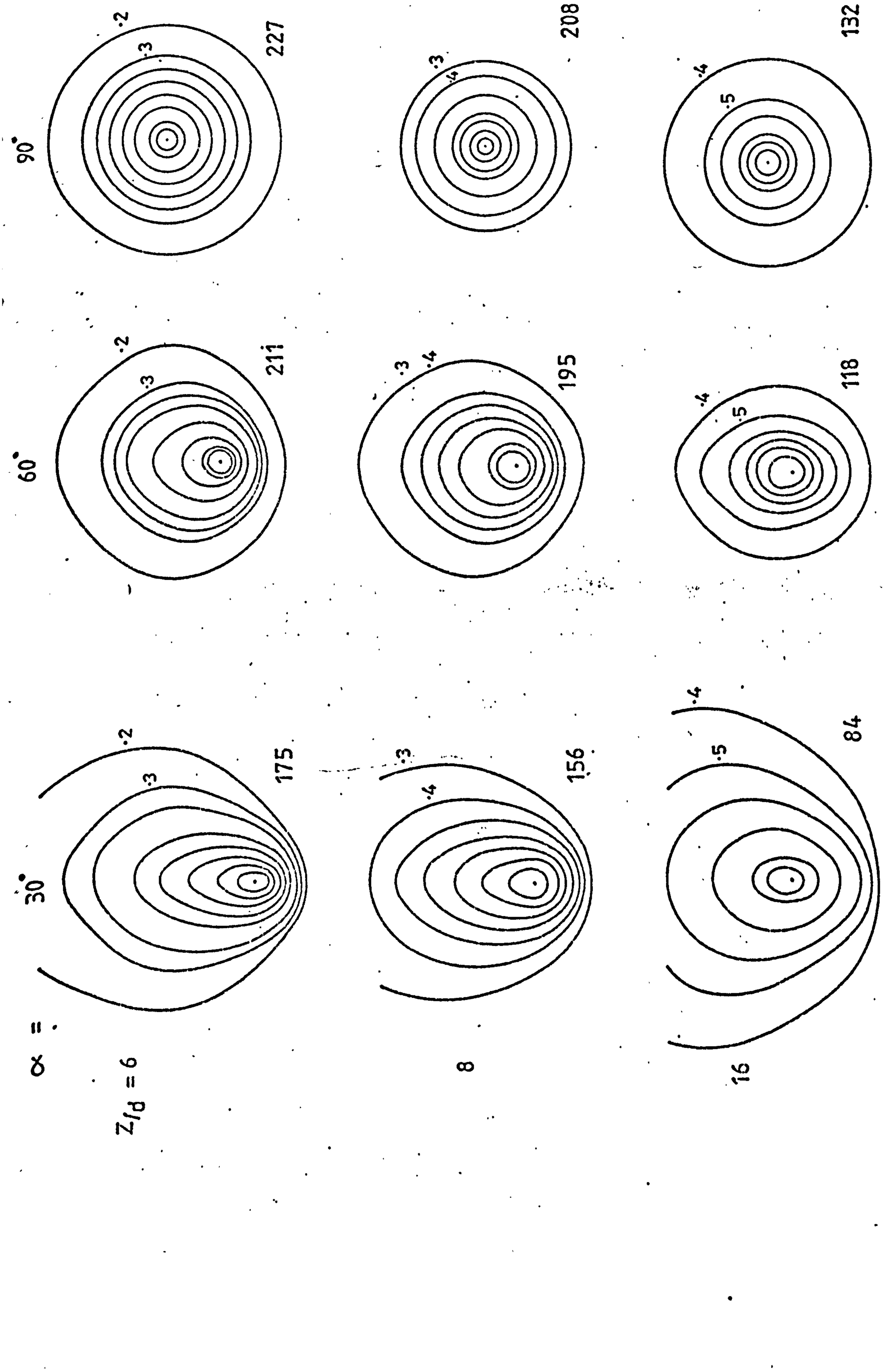
α
Z/d = 6
8
16
30°
60°
90°
.2
.3
.4
.5
175
156
84
211
195
118
227
208
132
EFFECT OF Z/d ON HEAT TRANSFER AT VARIOUS NOZZLE INCLINATIONS

FIG. 7.4.15

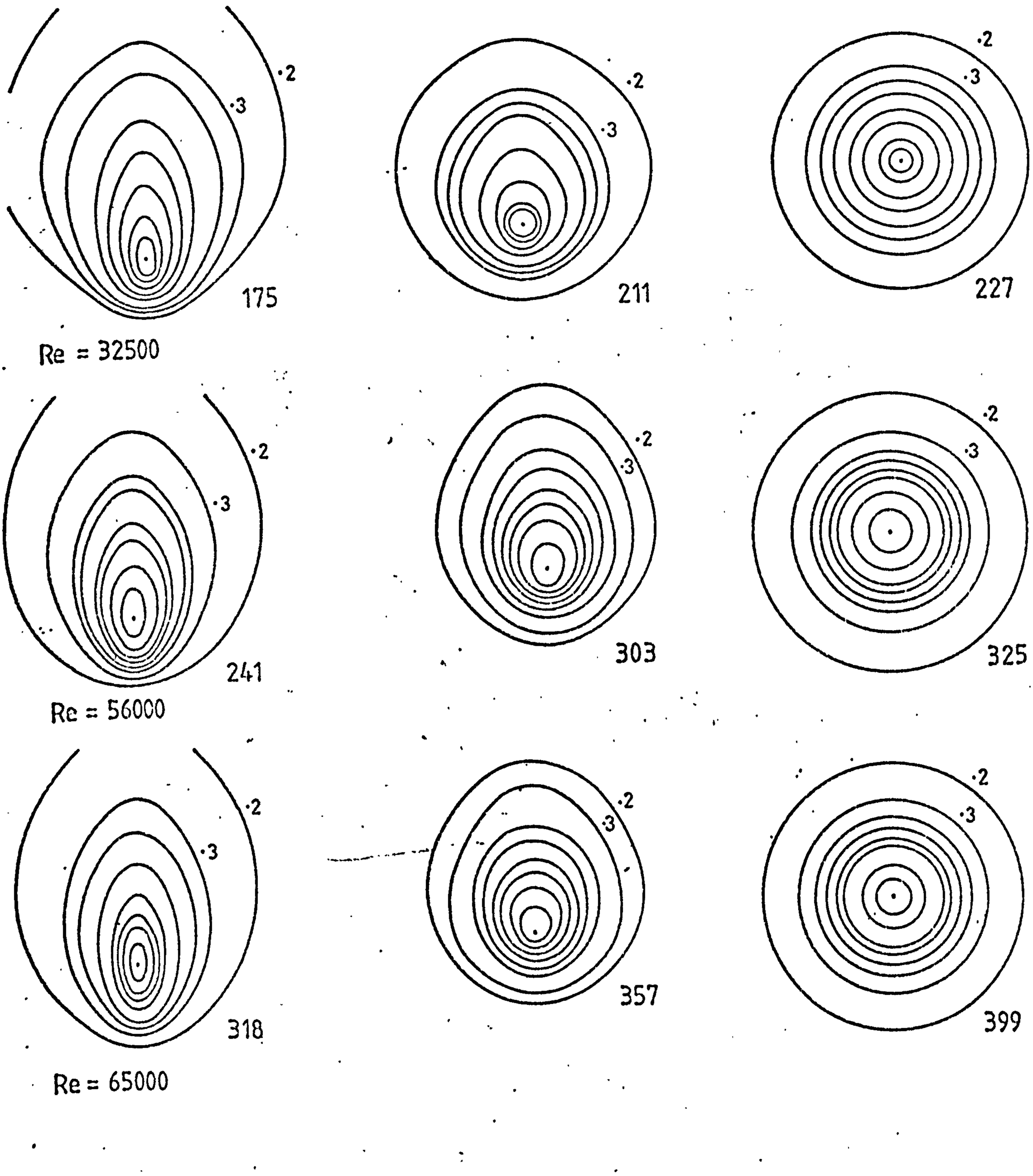

FIG. 7·4·16 EFFECT OF REYNOLDS NUMBER ON HEAT TRANSFER AT VARIOUS NOZZLE INCLINATIONS (Z/d = 6)

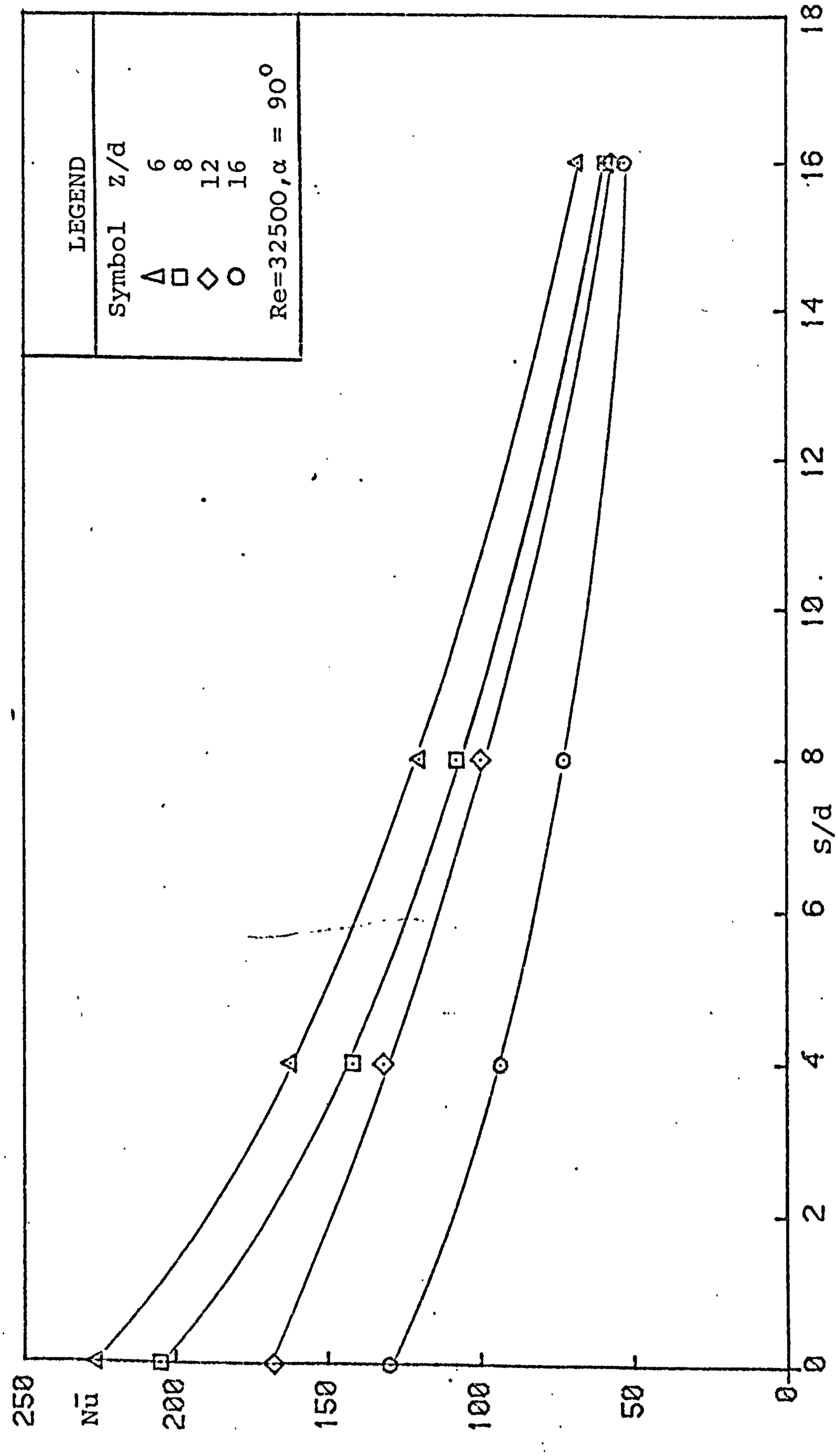

FIG.7.5.1 THE EFFECT OF INTEGRATION

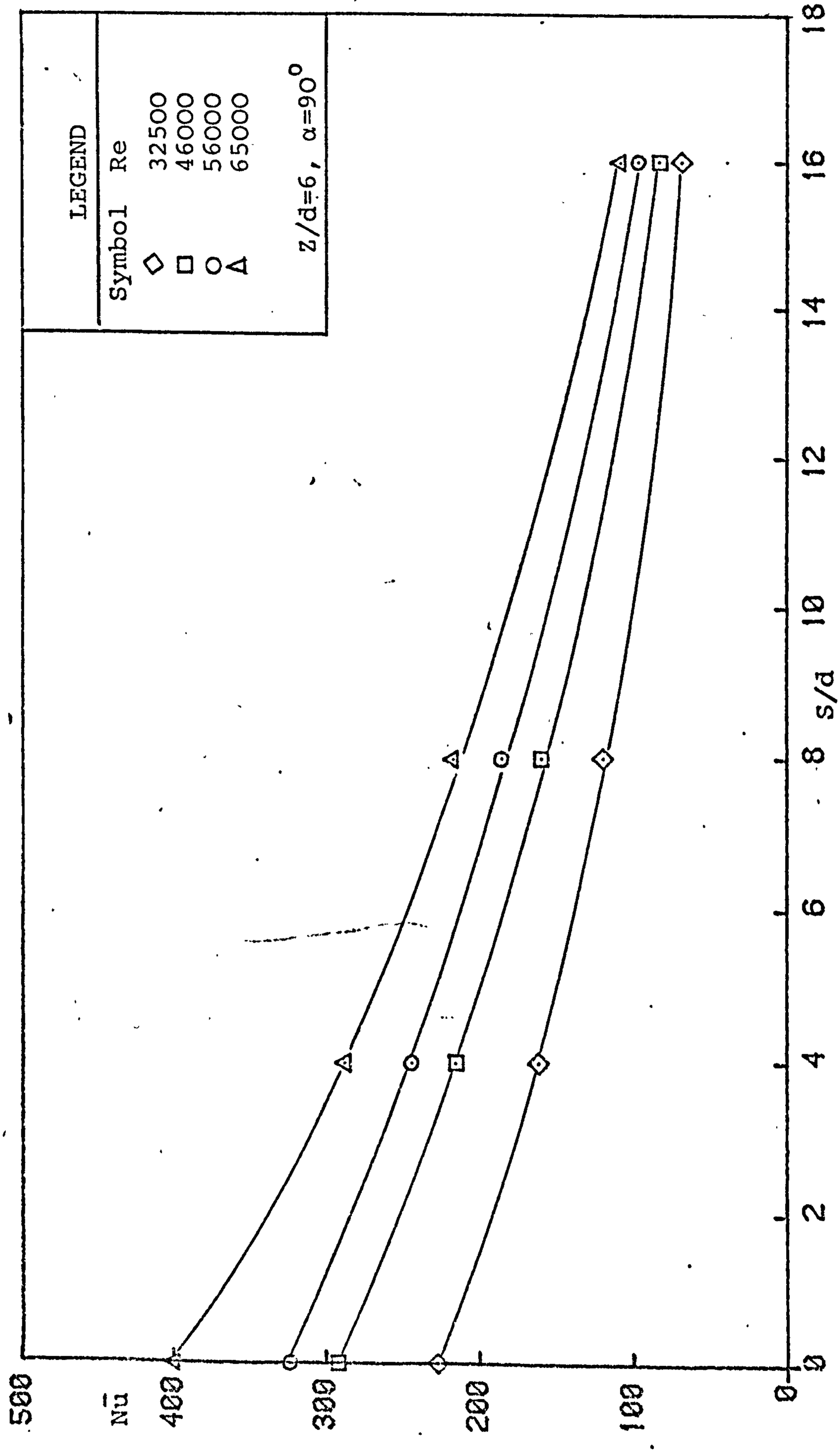

FIG.7.5.2 THE EFFECT OF INTEGRATION AREA ON AVERAGE NUSSELT NUMBER.

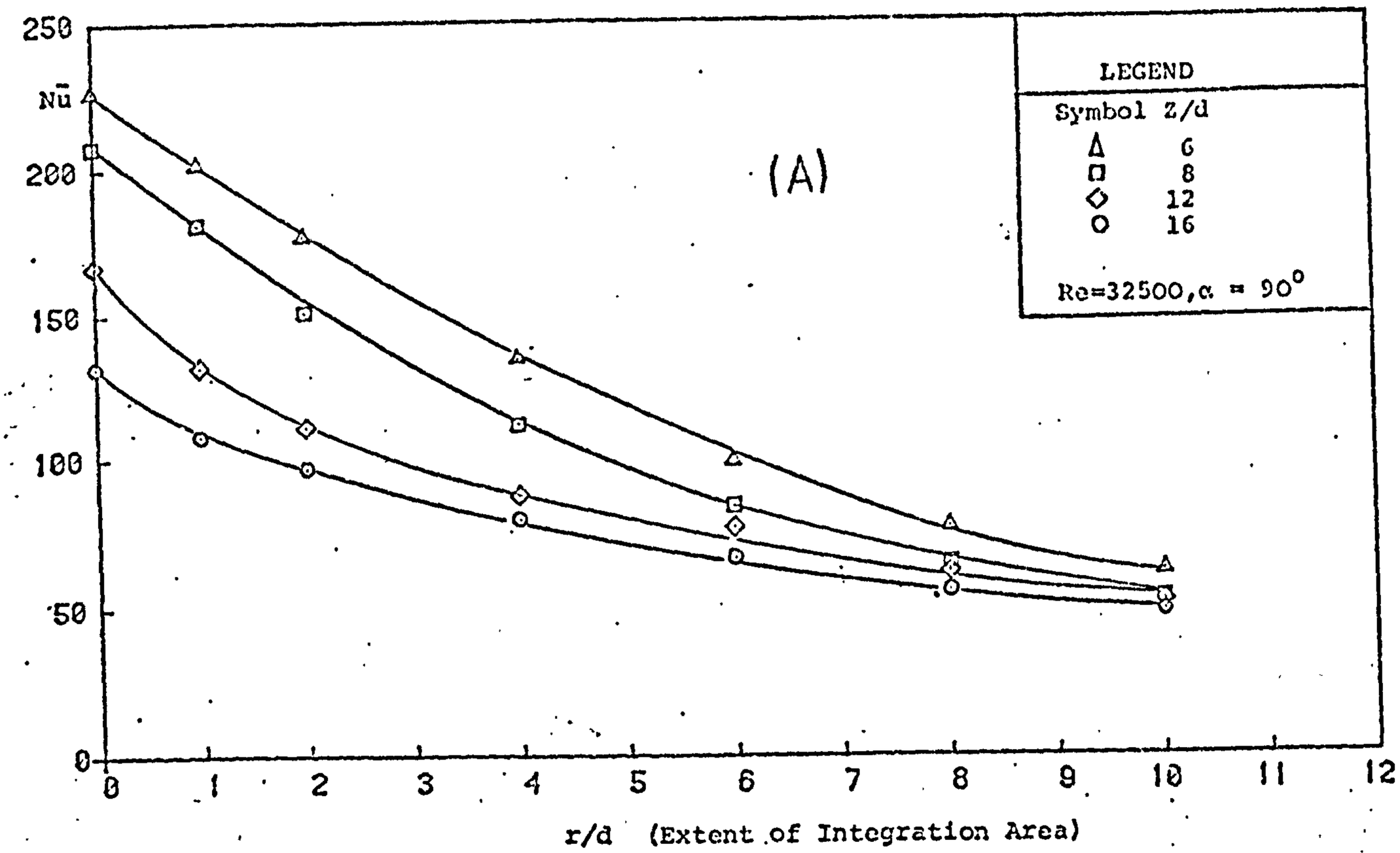

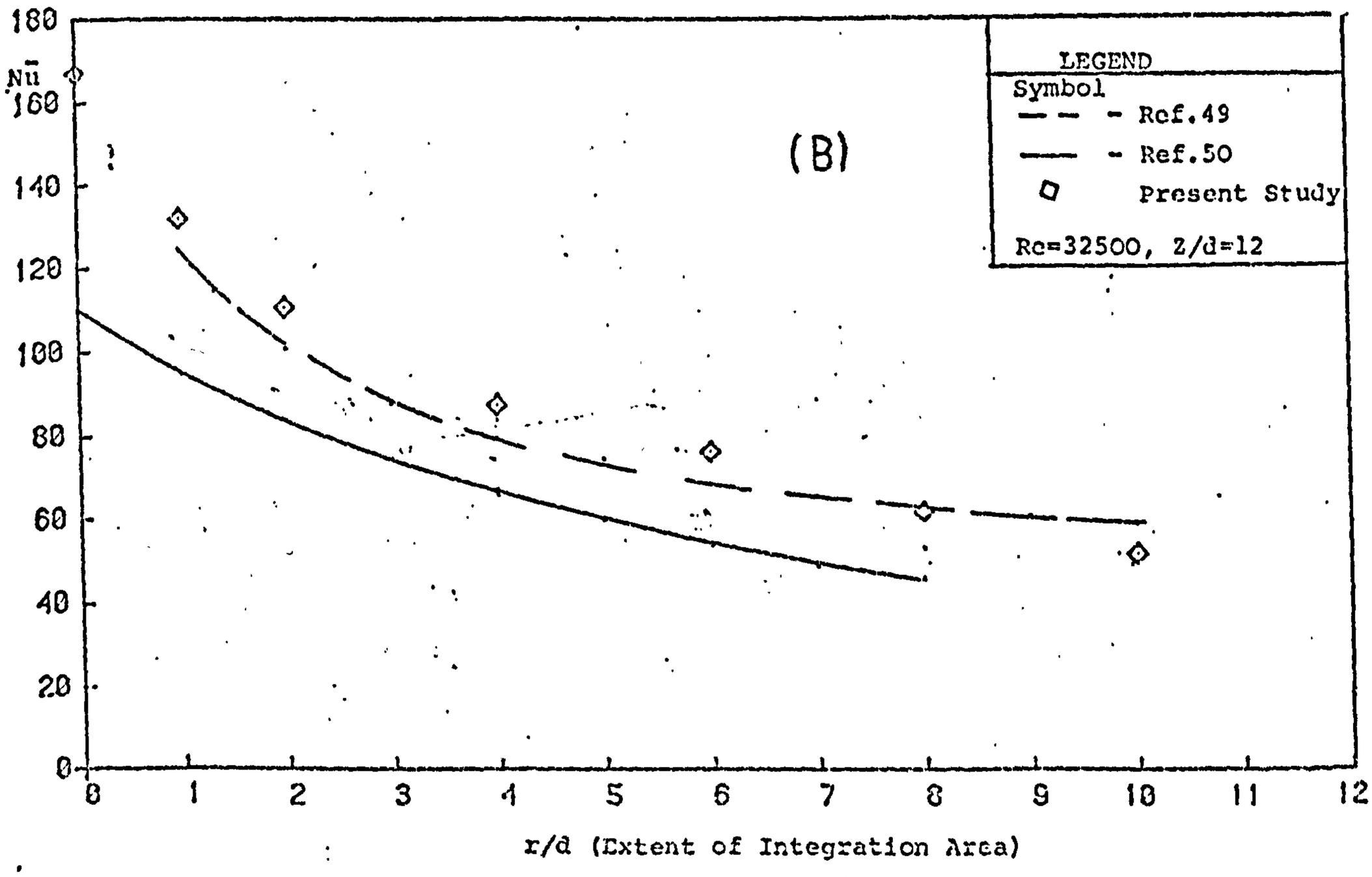

FIG. 7.5.3 RADIAL VARIATION OF AVERAGE NUSSELT NUMBER .
(A) PRESENT RESULTS (B) COMPARISON WITH THOSE OF PREVIOUS STUDIES.

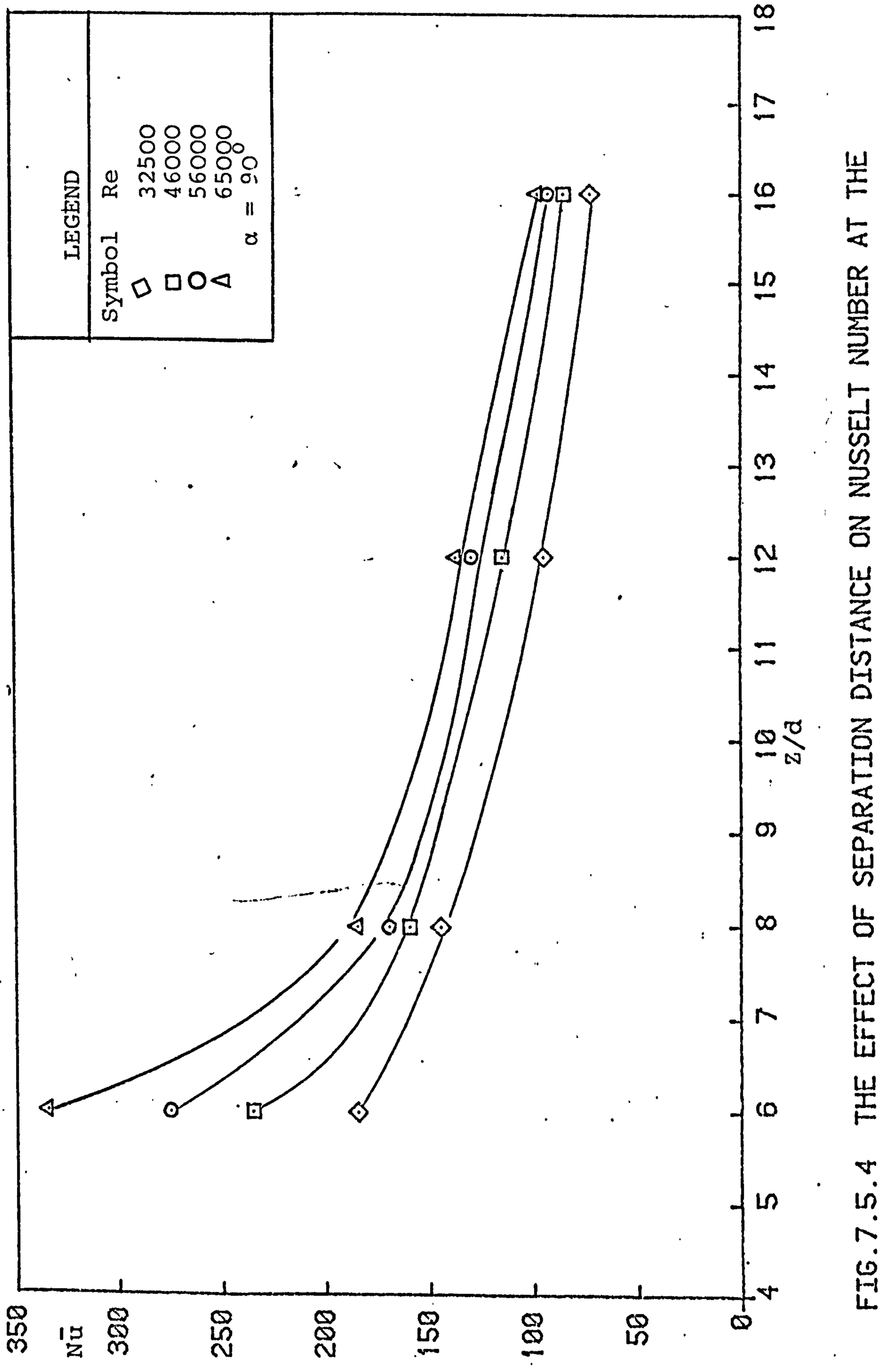
LEGEND
Symbol Re
32500
46000
56000
65000
α = 90°
$\bar{Nu}$
350
300
250
200
150
100
50
0
4
5
6
7
8
9
10
z/a
11
12
13
14
15
16
17
18
THE EFFECT OF SEPARATION DISTANCE ON NUSSELT NUMBER AT THE
IMPINGEMENT REGION.

FIG.7.5.4

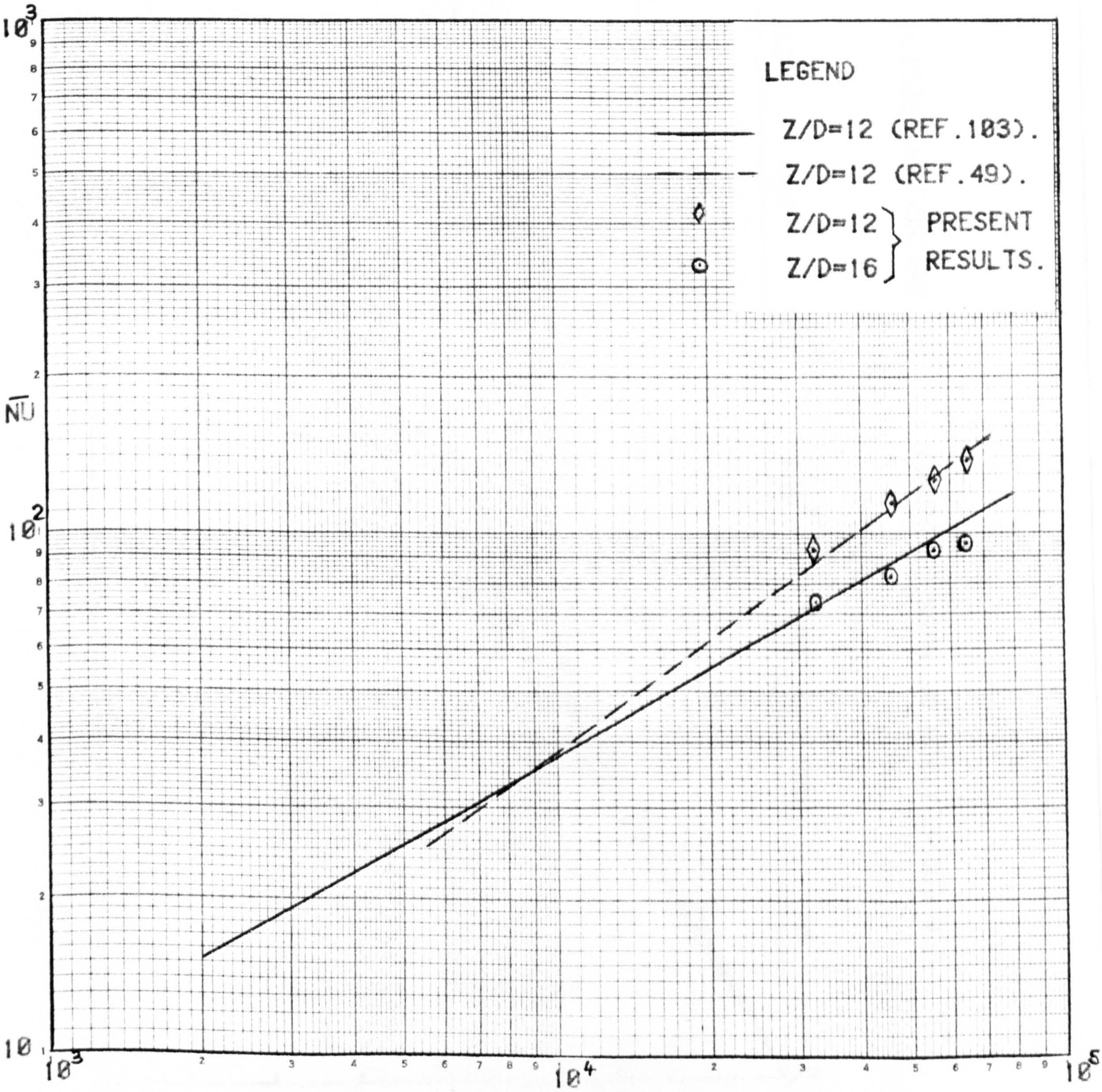

FIG.7.5.5 COMPARISON OF IMPINGEMENT REGION NUSSELT NUMBER WITH THOSE OF PREVIOUS STUDIES.

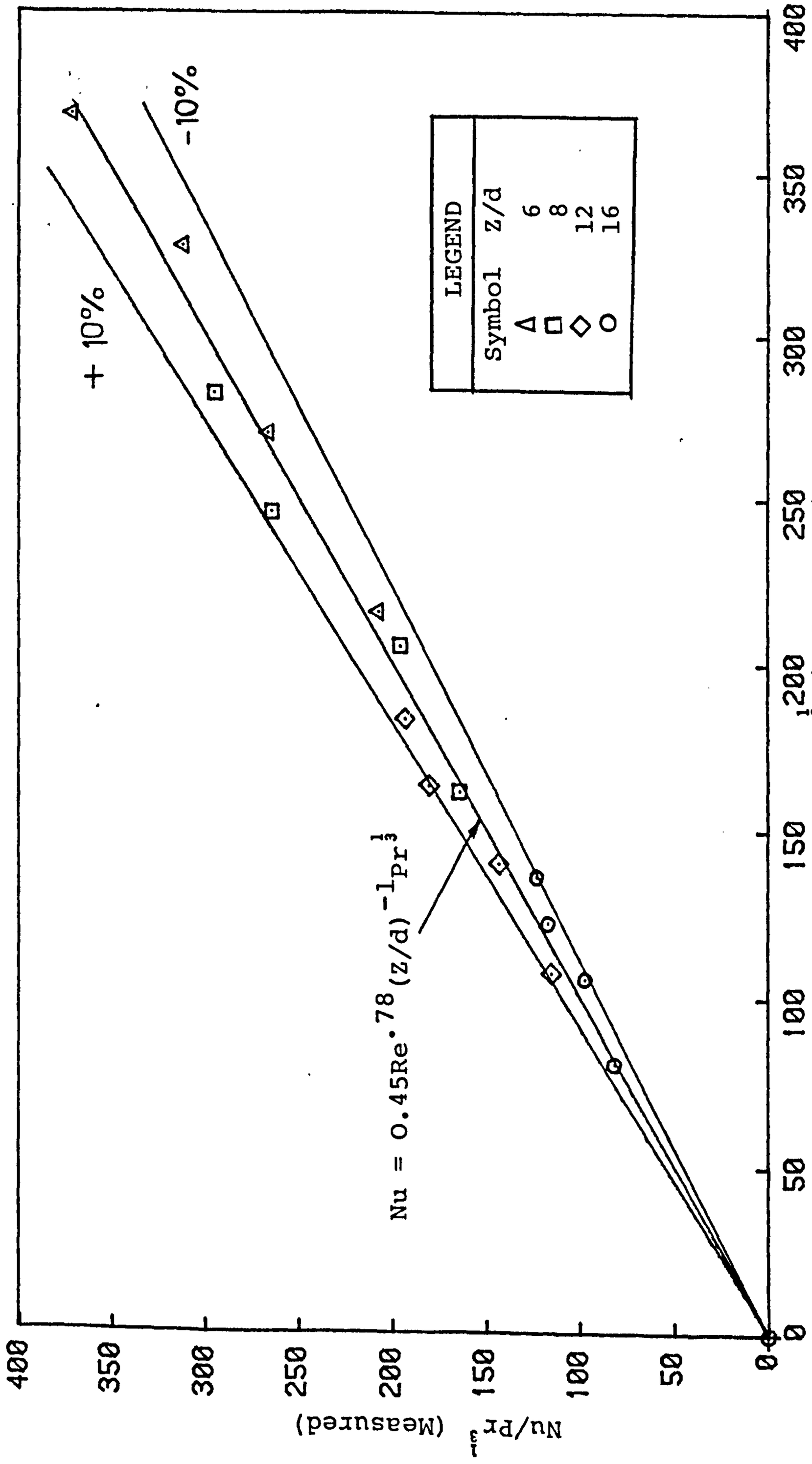

FIG.7.5.6 CORRELATION OF NUSSELT NUMBER FOR THE IMPINGEMENT REGION.

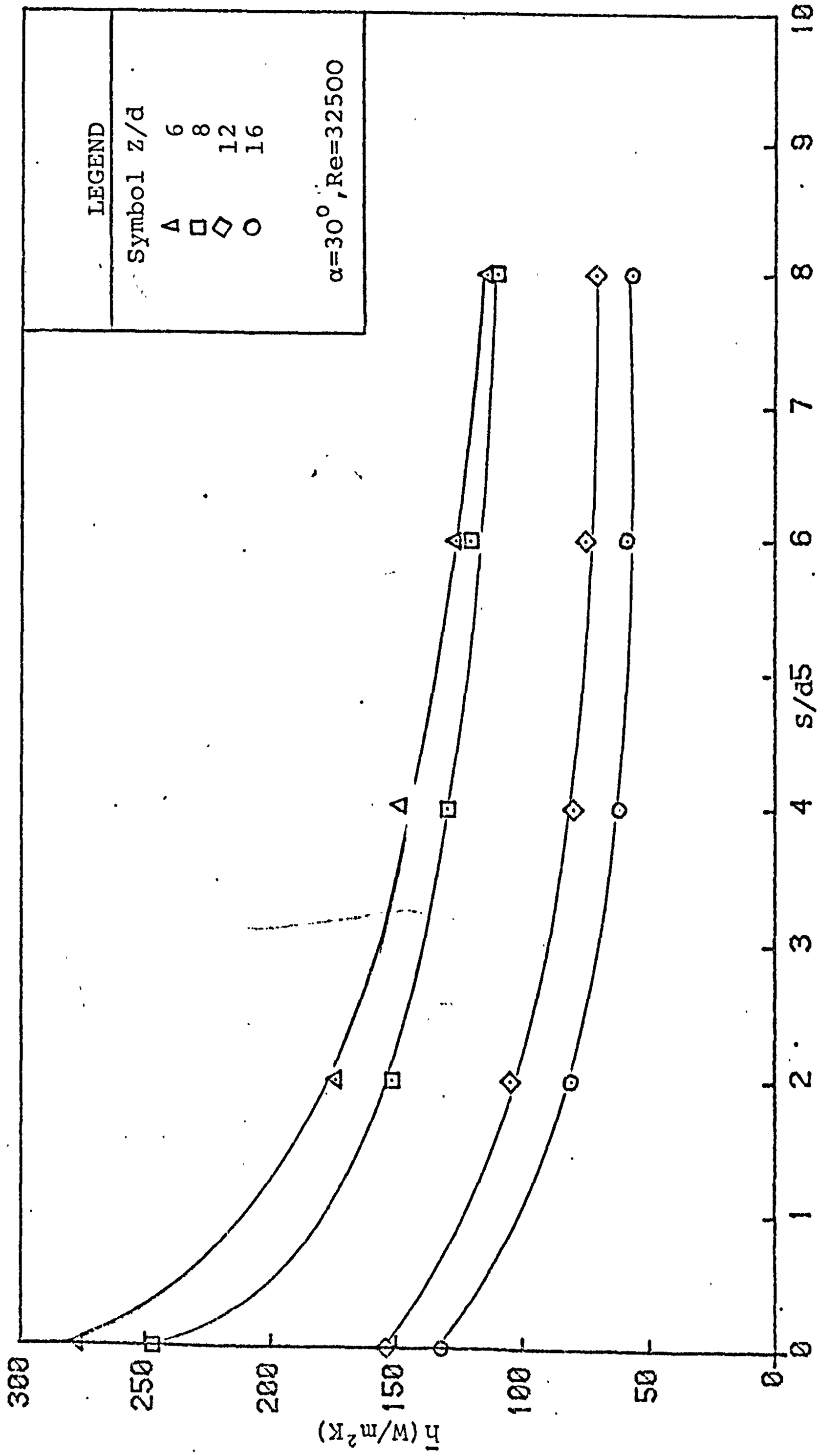

FIG. 7.5.7 EFFECT OF THE AREA OF INTEGRATION ON THE AVERAGE HEAT TRANSFER COEFFICIENT.

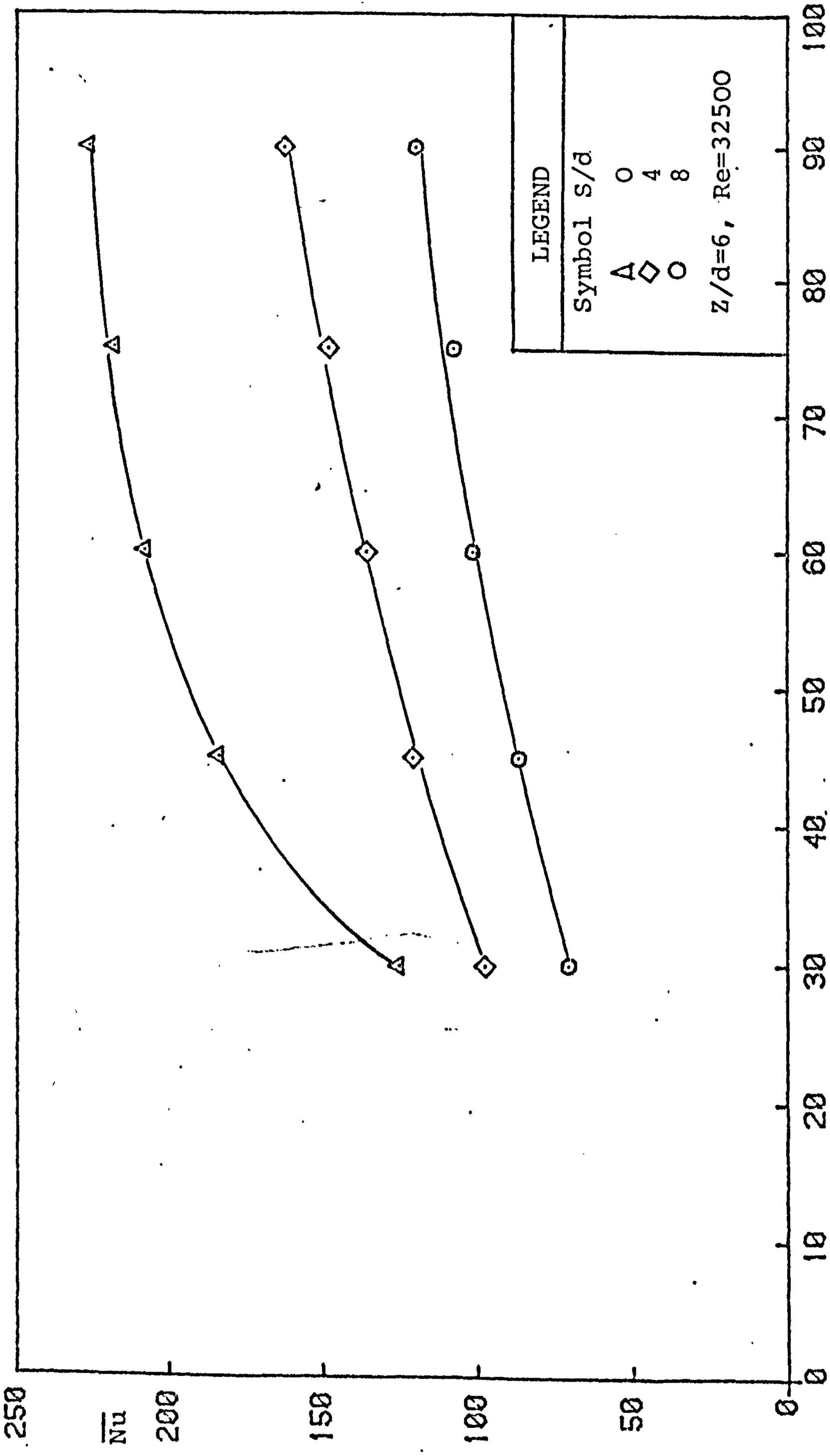

FIG.7.5.8 THE EFFECT OF NOZZLE INCLINATION ON THE AVERAGE NUSSELT NUMBER.

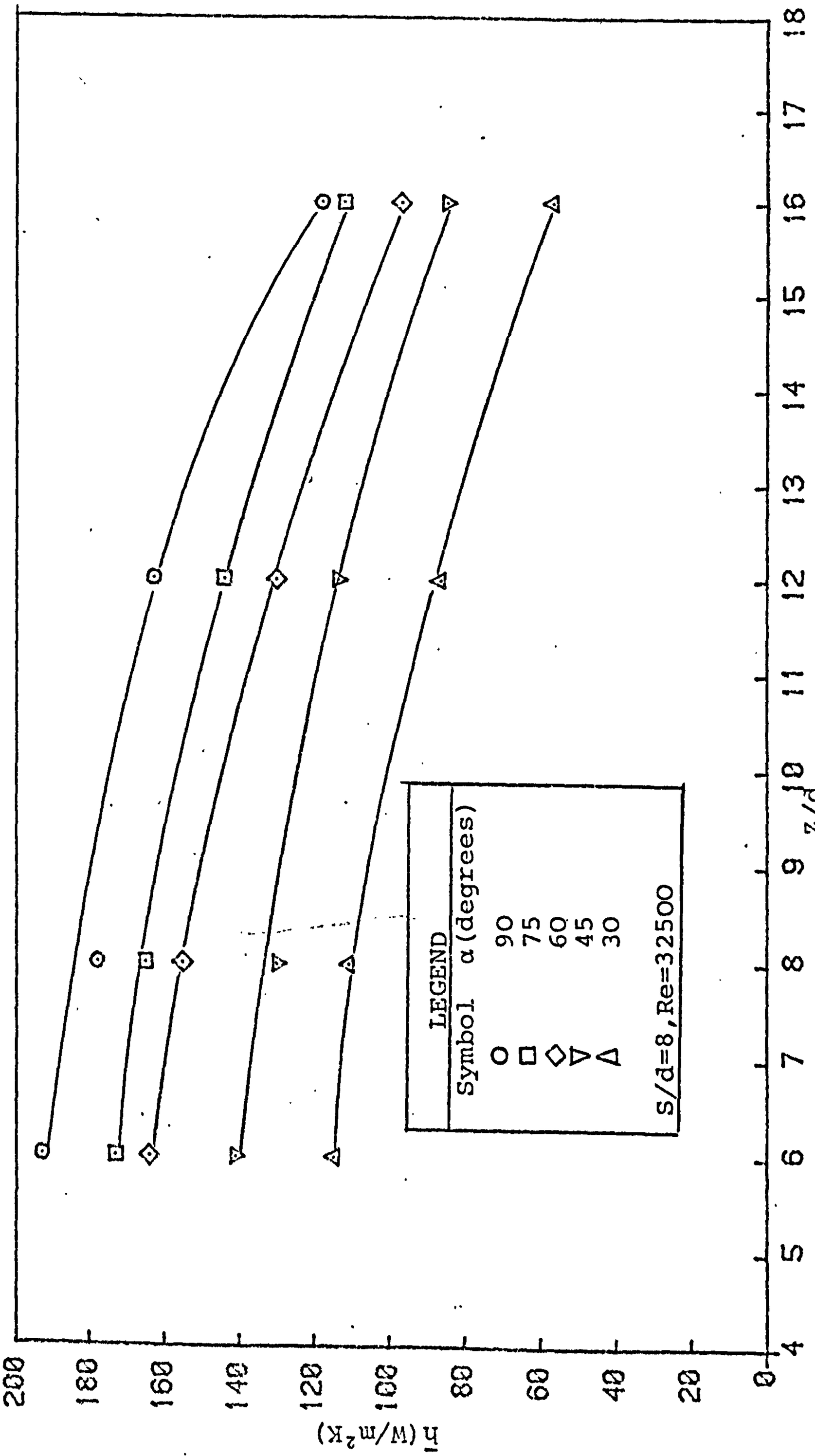

FIG.7.5.9 THE EFFECT OF SEPARATION

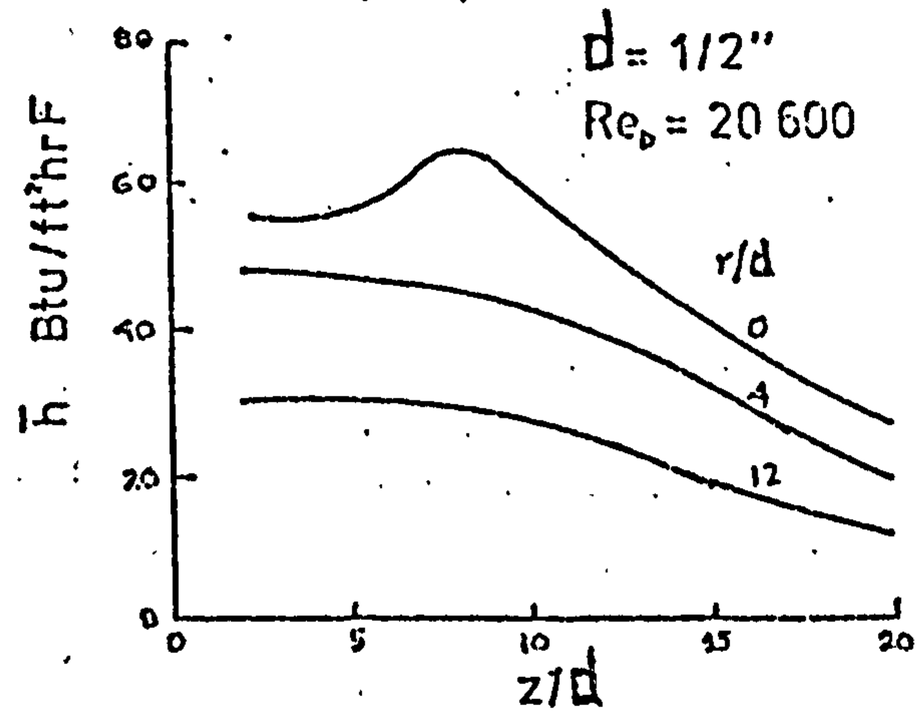

FIG.7.5.10 EFFECT OF Z/d ON AVERAGE HEAT TRANSFER (REF. 102).

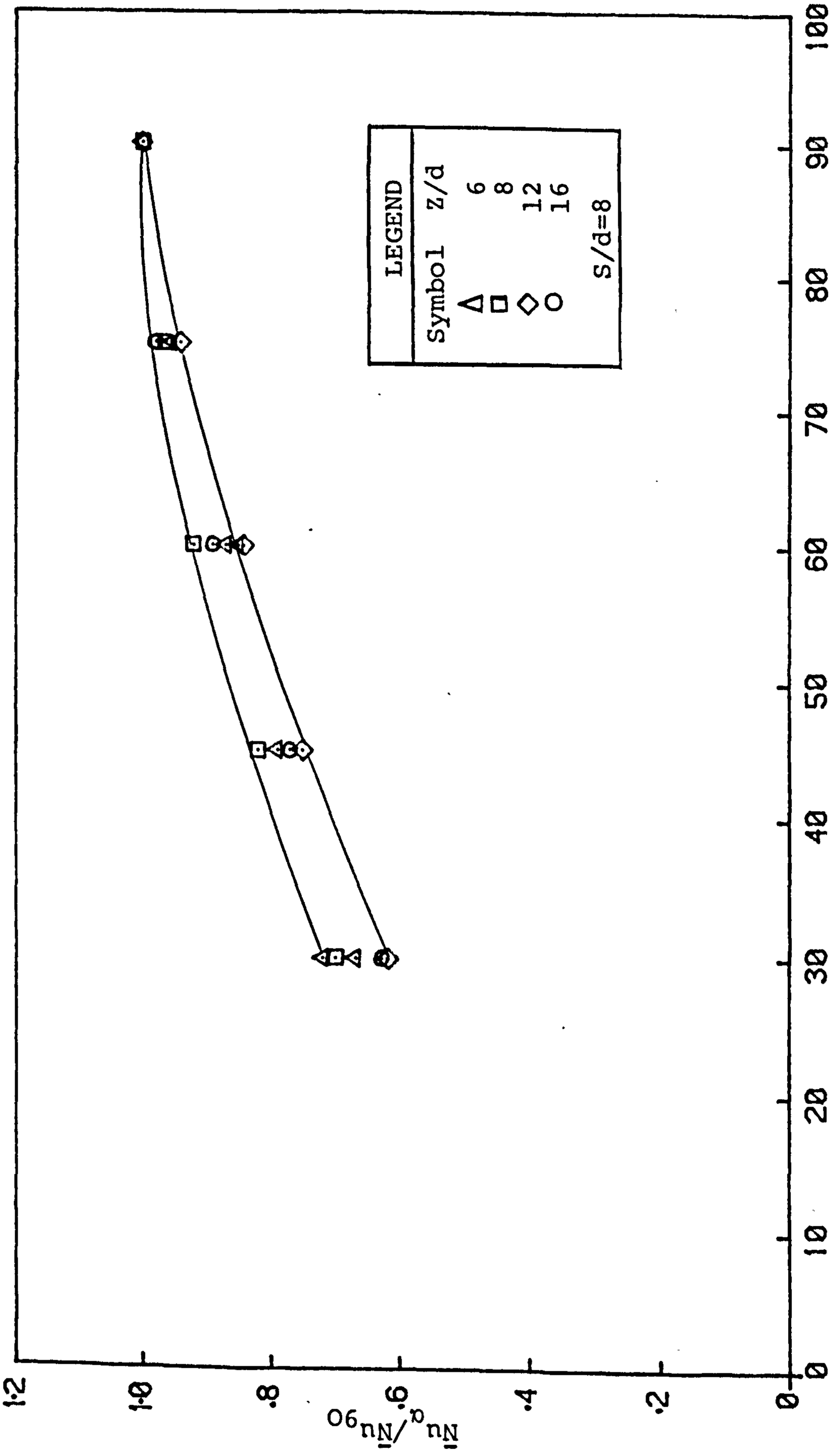

FIG.7.5.11 THE EFFECT OF NOZZLE INCLINATION ON NORMALISED NUSSELT NUMBER.

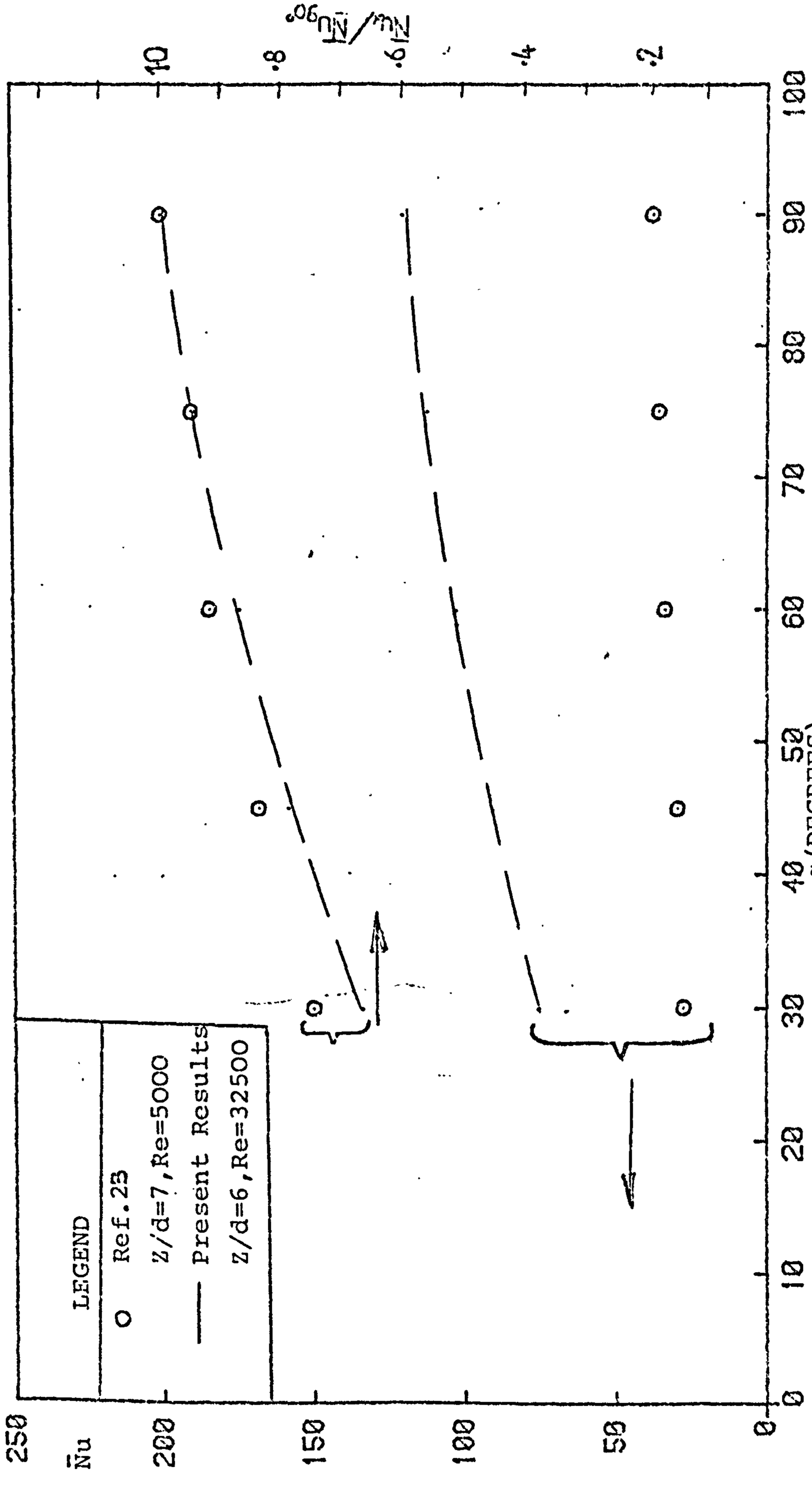

FIG.7.5.12 COMPARISON OF THE PRESENT AVERAGE HEAT TRANSFER RESULTS WITH THOSE OF SPARROW AND LOVELL (REF.23).

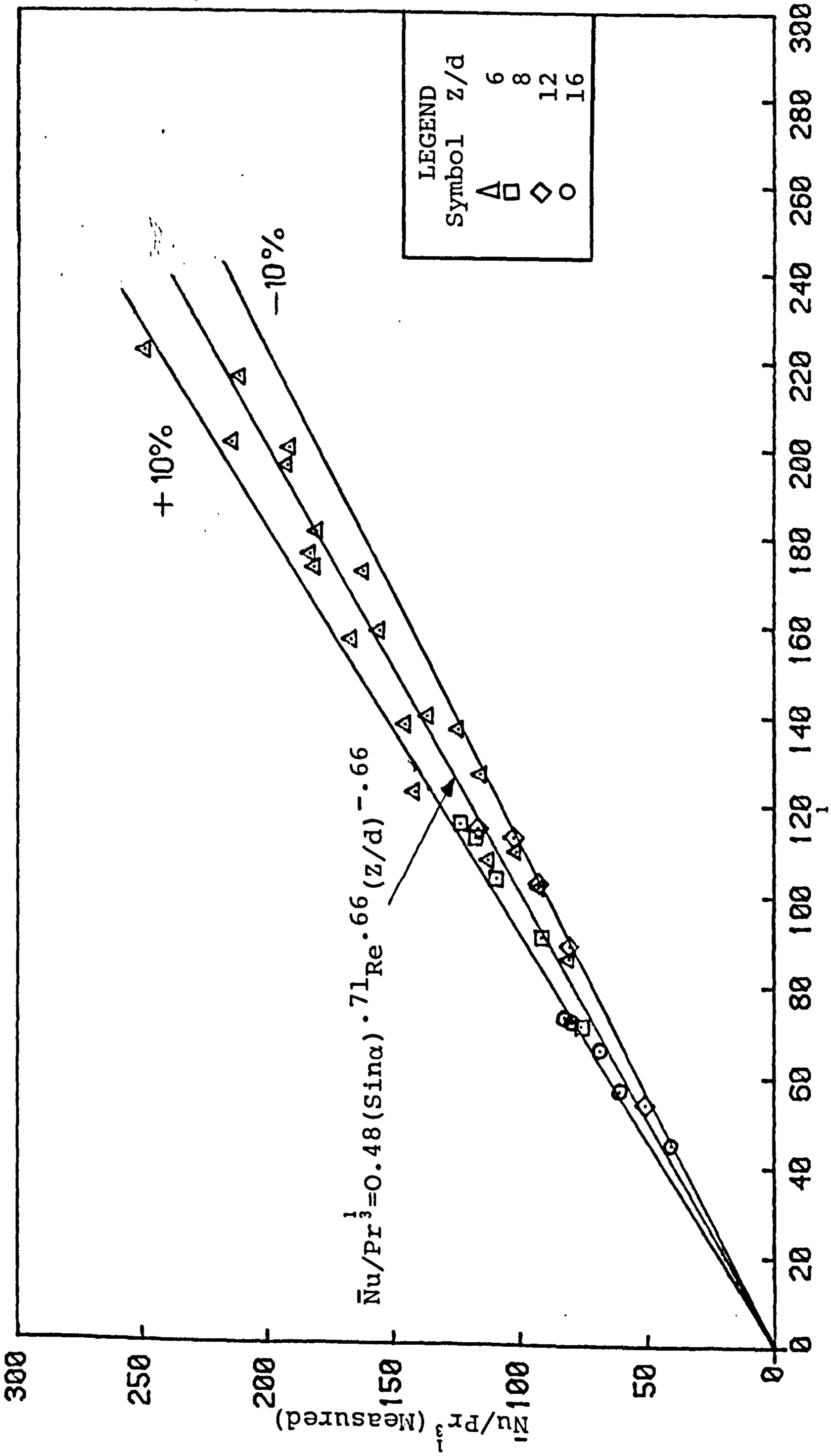

FIG.7.5.13 CORRELATION OF THE AVERAGE NUSSELT NUMBERS.

CHAPTER 8

by turbulent entrainment. This intensive mixing at the periphery of the jet reduces the momenta of the outermost edges so that the jet is readily deflected. The original circular jet is, thus, deformed into a characteristic kidney or horse-shoe shape, see Fig. 8.2.1 . In this first region of deflected flow, the potential core (analogous to that in a free jet) is unaffected by the turbulent activity (i.e. the pressure and velocity remain constant). However, the width of this core progressively decreases along the jet axis. This initial region extends from the nozzle exit to the end of the potential core.

Main Region

Beyond the potential core region, turbulent intermixing engulfs the whole structure of the jet so that the 'circular' jet is progressively deflected. The jet velocity also decays as the axial distance from the initial region increases. This zone is known as the main region. The kidney-shaped jet grows in size giving rise to the possibility of an additional circulatory motion in the jet itself, i.e. the development of vortex pairs, see Fig. 8.2.1.

The Surface Flow

The structure of the jet and the ensuring 'impingement' flow are largely dictated by the nozzle to target separation distance and the ratio of the jet velocity to the cross flow velocity. As the cross flowing stream approaches the boundaries of the jet, the streamlines decelerate as if blocked by a solid body. A region of high pressure is created upstream and depending on the strength of the cross flow, the jet is either swept downstream or alternatively, the cross stream divides and flows through the sides of the jet. At high cross flows ($U_j/U_c < 4$ or 5), it has been found (Ref. 122) that "jet impingement" does not occur on thetarget surface because the jet is blown away by the cross flow. At moderate velocity ratios ($5 < U_j/U_c < 20$), impingement occurs with the stagnation point displaced downstream of the nozzle centre line. At very low cross flows ($U_j/U_c > 20$), the stagnation point occurs almost directly on the nozzle centre line. Plate 8.2.1 is reproduced from Kabari (Ref. 36) and shows a surface flow pattern which can be associated with the latter two situations. The stagnation point is indicated by (a) whilst the so-called 'separation line' (which defines the maximum upstream and lateral penetration of the jet flow) is denoted by (b).

It can be seen in Fig. 8.2.1 that the orthogonal impinging jet is bounded by two streamlines. They are the free streamline (line OA) which separates the jet from the wake and the interfacial streamline (line BC) which separates the jet from the mainstream. This interface represents the maximum penetration

of the jet into the cross flowing stream and its extent is obviously dependent on jet-to-cross-flow velocity ratio. The line DE represents the axis of the jet and is also the locus of maximum velocity.

In the case of inclined jets in a cross flow, the fluid flow is qualitatively similar to that described above. However, the streamlines obviously penetrate farther upstream or downstream of the nozzle centre line depending on whether the nozzle is inclined into or with the cross flow.

8.3 REVIEW OF SELECTED PUBLICATIONS CONCERNED WITH THE FLUID DYNAMICS OF A JET IN A CONFINED CROSS FLOW

Although the current investigation is primarily concerned with heat transfer, a survey of published fluid dynamic studies is relevant since the fluid flow dictates the thermal transport. The papers in the ensuing survey were selected either because of their contribution to the understanding of the flow or alternatively because of significant improvements in the technique employed.

Probably, the first published work on a jet in cross flow was that of Callaghan and Rugeri (Ref. 29) who determined the penetration of an orthogonal air jet into a cross flowing stream. Four different orifice diameters ranging from 6.35 mm to 15.9 mm were used and the air jet was maintained at an exit temperature of approximately 205°C. The jet outer boundaries were arbitrarily defined by loci at which the temperature was only one degree above the initial bulk temperature. This assumption, though plausible, was made because of the problem of locating the exact jet boundaries. Measurements were made at four different downstream locations and an empirical equation was proposed for the free streamline, thus :

$$\left(\frac{z'}{d}\right)^{1.65} = 2.91 \frac{\rho_j}{\rho_c} \frac{U_j}{U_c} \left(\frac{x}{d}\right)^{0.5} \qquad 8.3.1$$

where

x = downstream distance from orifice centre line

ρ_j, ρ_c = density of jet and cross flow respectively.

z'/d = distance between the nozzle exit and the centre of the deflected jet at a particular location, x.

The pioneering work of Callaghan and Rugeri was so limited especially as the jet structure was not studied.

In 1956, Jordinson (Ref. 31) measured total pressure distributions to study the shape and path of an air jet injected normally into a main air stream. The tests were carried out with two nozzles of 12.7 mm and 25.4 mm diameter in a wind tunnel of size 1.5 m x 0.3 m and at various separation distances (z/d). The cross section of the jet was found to be horse-shoe shaped. It was concluded that the pressure difference across the jet caused the initial jet deflection and that entrainment became dominant only after a few nozzle diameters (approximately 3d) from the exit plane. The range of the velocity ratio, M (i.e. < 8) was however limited.

The understanding of a physical process can be greatly enhanced if the relevant flow pattern can be observed visually. Thus, Keffer and Baines (Ref. 30) carried out a flow visualization study in addition to dynamic measurements of normal penetration of a 9.5 mm initial diameter jet into a cross flowing stream. The tests were conducted in a 1.2 m x 2.4 m x 11 m long wind tunnel for velocity ratios of 4, 6 and 8. It was observed that the jet possessed distinct edges and that jet deflection depending (in the absence of a pressure gradient) on the momentum ratio, R ($\equiv \rho_j U_j^2/\rho_c U_c^2$) However, the measurements were carried out only at small distances downstream of the nozzle centre line and moreover the velocity ratio range was limited. They used a hot wire probe for the velocity measurements and this may have interferred with the flow.

Platten and Keffer (Ref. 123) investigated an axisymmetric jet that discharged at various angles into a uniform cross wind. The trajectories of a 6.4 mm diameter jet were determined in a 2.44 m wide x 1.22 m high wind tunnel for various inclinations ($45^\circ \leqslant \alpha \leqslant 135^\circ$) and velocity ratios ($4 \leqslant M \leqslant 8$). Their data were self consistent but differed quantitatively from the measurements of Keffer and Baines (Ref. 30) and Gordier (Ref. 124), see Fig. 8.3.1. The difference was attributed to the use of a long nozzle by Platten and Keffer in place ofthe shorter nozzles used in the other studies. It was found that a decrease in velocity ratio produced greater jet deflections.

In 1976, Rudinger and Moon (Ref. 125) used a laser-Doppler anemometer to investigate the flow field of a jet injected into a cross flow. Velocity distributions were obtained with a 5 mm diameter nitrogen gas jet in a cross flowing stream in a square duct of side 100 mm. The momentum flux ratio, R, was 16. The loci of the points of maximum velocity were correlated by :

$$z'/d = 3.38\ (x/d)^{0.38} \qquad 8.3.2$$

This penetration relationship was in reasonable agreement with the measurements of Kamotani and Greber (Ref. 32). Although only one momentum flux ratio was investigated by Rudinger and Moon, the use of a laser-Doppler anemometer implies that the flow field was not disturbed by the instrumentation.

Although many experimental investigations have been reported, the system has also been analytically modelled. For example, Stoy and Ben-Haim (Ref. 126) conducted an analytical and experimental study of the deflection and impingement of a turbulent axisymmetric jet in a cross flow. In their analysis, it was assumed that an average local velocity and cross sectional area were sufficient to characterise the jet (i.e. it is one dimensional in character). Hence, the mass and momentum equations were solved numerically to obtain jet trajectories and impingement points. Experiments were then undertaken under the following conditions: nozzle diameter = 12.7 mm, velocity ratio < 8 and a nozzle to target separation (Z/d) of 3. The experimental impingement positions, x, were correlated by :

$$x/d = 19.6\ (U_j/U_c)^{-1.82} \qquad 8.3.3$$

and this equation is valid for the range of their test conditions. Agreement between the analysis and the experimental values was good but the range of variables employed was very restricted.

Susec and Bowley (Ref. 35) used a semi-analytical method to calculate the trajectories of axisymmetric turbulent jets issuing at various angles (i.e. $45^o \leq \alpha \leq 135^o$) into a cross flowing stream. Whereas the jet-to-cross flow velocity ratios in previous studies were limited, Susec and Bowley covered a wide range (i.e. $2 < M < 18$). Their data were in good agreement with the experimental results of Platten and Keffer (Ref. 123) especially for $\alpha < 90^o$.

Sophisticated models using advanced numerical methods have also been used to study the problem. Recently, Patankar et al (Ref. 127) used an elliptic finite-difference procedure to solve the three-dimensional flow field that ensued when a round turbulent jet was injected orthogonally into a mainstream. The Reynolds stresses in the time-averaged momentum equations were calculated by a 'two-equation turbulence model' (see Ref. 128, 129, for details). Velocity profiles and the location of the jet centre line were obtained for an unconfined system with jet to cross flow velocity ratios of 2 to 10. The agreement between these calculated results and the experimental data of previous workers was judged to be satisfactory. Any slight differences were attributed to the scatter in the experimental data and the use of comparatively coarse grids (at stations away from the jet axis) in the numerical analysis.

To summarise the above review, the flow field associated with this system geometry is three-dimensional and complicated. Different experimental techniques have been used to determine jet trajectories and Figs. 8.3.2 and 8.3.3. respectively present the data of various workers for oblique and orthogonal jets in cross flow. It can be seen that the results exhibit

some considerable scatter (i.e. about 30 %). These can largely be attributed to variations in the experimental arrangements (see, for example Ref. 29 and 125). Although the velocity ratios covered in the experiments which have been reviewed were limited (usually M < 8) all the workers have made significant contributions to the general understanding of the behaviour of jets in cross flow situations. Lee (Ref. 130) published a review of research (up to 1966) on interaction of a jet with an external stream and Keffer (Ref. 131) also mentioned a large number of relevant papers. These authors may be referred to for more details on the subject.

It is appropriate now to mention that the locations of the impingement points obtained in the present investigation are compared with the data of Susec and Bowley (in Chapter 10) because of the similarity of the test conditions.

8.4 JET IMPINGEMENT HEAT TRANSFER IN THE PRESENCE OF A CROSS FLOW

8.4.1 Introduction

In multiple jet systems, the spent air or cross flow effect arises particularly when the exhaust fluid is removed from one end of the system. This usually produces complicated flow fields and, hence, complex heat transfer distributions. Owing to the flushing effect of the flows from the upstream jets on the downstream ones, the stagnation point heat transfer is decreased and the regions of high heat transfer are displaced in the direction of the cross flow. Consequently, local heat transfer coefficients upstream of the impingement region associated with each jet are generally decreased whilst downstream values are increased. This heat transfer variation can be explained by the fluid flow phenomena discussed in the preceeding section.

Most previous studies have concentrated in the main on axisymmetric jets so that these flows are the primary subject of this review. It is believed that no other comprehensive review of the heat transfer characteristics of a jet in a cross flow exists at present.

8.4.2 "Orthogonal" Impinging Jets in Cross Flows

Metzger and Korstad (Ref. 24) conducted one of the first studies into the effect of a controlled cross flowing stream on the heat transfer characteristics of a single row of impinging jets. The test surface was heated to approximately

$66^{o}C$ and then cooled by the jet and cross flows so that the heat transfer rate was determined under the following conditions : $2 \leqslant z/d \leqslant 6.7$, $2.5 \leqslant x/d \leqslant 5$, and cross flow to jet mass flow rate ratio, M*, i.e. $\rho_c a_c U_c / \rho_j a_j U_j$ ($\equiv$ 1, 2 and 3).

It was found that the upstream penetration of the jets was very limited, even at M* = 1 and this can be attributed to the high momentum of the cross flowing stream which prevented the jet from penetrating the main flow. Consequently, there was an upstream degradation and a simultaneous downstream enhancement in the mean heat transfer rates. These effects were found tobe a strong function of the nozzle pitch because the heat transfer rate diminished as the nozzle spacing was reduced. The average heat transfer rates obtained over a rectangular area of integration (symmetrical about the nozzle centre lines) were correlated by :

$$\overline{Nu}_d = 0.0822 M^{*-0.049} Re_d^{0.662} Pr \qquad 8.4.1$$

and is valid for

$$z/d = 2,\ 1 < M^* < 3,\ 2.5 < x/d < 5 \text{ and } s/d = 20$$

where

s = the length of the integration area

M* = mass flow rate ratio, i.e. $\rho_c a_c U_c / \rho_j a_j U_j$

a_c, a_j = area at the exit of cross flow and jet nozzle respectively.

Bouchez and Goldstein (Ref. 28) measured local heat transfer coefficients beneath a circular impinging jet in the presence of a superimposed cross flowing stream. The fluid jet which exited from a 12.7 mm diameter orifice impinged orthogonally (in the absence ofthe cross flow) onto the transfer surface. The velocity ratio was varied from 3.7 to 12.7 while the nozzle-target plate separation distance, Z/d was fixed at 6 or 12. The heat transfer coefficients along the central longitudinal axis of the jet were found to be maximum at the 'stagnation' point but then decreased rapidly, see Fig. 8.4.1. It is also apparent that the local heat transfer coefficients were strongly influenced by the value of the velocity ratio.

The range of z/d studied previously was limited so that Sparrow et al (Ref. 26) investigated the effect of this parameter on impingement heat transfer, for an axisymmetric jet in a cross flow. The variables studied were : $4 \leqslant M \leqslant 12$ and $3 \leqslant z/d \leqslant 12$. A direct heat transfer technique was used to obtain a streamwise variation of local heat transfer coefficients under a 12.7 mm diameter jet in a 152 mm x 203 mm x 1150 mm wind tunnel. It was observed that for $M \geqslant 8$, jet deflection

by the cross flowing stream was small. For these mass velocity ratios, maximum local heat transfer occurred at separation distances, z/d, of 5 to 6. For smaller M, the maximum local heat transfer was obtained at lower z/ds. The difference was attributed to the large deflections experienced by the jet at higher nozzle to plate separations.

Cross flows ensue in practice in multiple jet situations so that it is pertinent, at this stage, to review briefly the studies concerned with these geometries.

Hilgeroth (Ref. 132) employed a direct heat transfer technique to investigate the effect of 'exhaust or spent' air on the average heat transfer rates associated with circular fluid jets arranged in triangular arrays with equal traverse and longitudinal pitches. The parameters studied were the nozzle diameter, d(= 15 mm to 50 mm), nozzle pitch, x/d (= 3.5 to 10.5), nozzle-to-plate separation distance, Z/d, (= 1.6 to 5.5) and jet flow rates (i.e. Re_x = 4.0 x 10^4 to 3.0 x 10^5, where Re_x is the Reynolds number based on nozzle exit velocity and nozzle pitch). It was reported that there was a reduction in the average heat transfer coefficients due to the interference of the spent air with subsequent jets.

Kercher and Tabakof (Ref. 133) measured the average heat transfer coefficients under a square array of axisymmetric orthogonal impinging jets. The test section was enclosed on three sides and the spent air was constrained to exit from the fourth side. In this configuration, the exhaust air from the upstream row of jets imposed a cross flow of increasing magnitude on the succeeding downstream ones. A direct heat transfer method was utilised to evaluate the average heat transfer coefficients. The test conditions covered the range: $1 \leq z/d \leq 4.8$, $3.13 \leq x/d \leq 12.5$, 0.46 mm $\leq d \leq$ 2.03 mm and $300 \leq Re_d \leq 3 \times 10^4$. The following conclusions were drawn :

(1) in the absence of a cross flowing stream, the average heat transfer rates increased with z/d (for the range covered).

(2) in the presence of a cross flowing stream, the heat transfer rates decreasedwith increasing Z/d.

and

(3) an increase in the velocity ratio between the cross flow and the jet reduced the mean heat transfer rate.

An expression was proposed for the average heat transfer from an array of impinging jets, (taking into account the effect of spent air,) namely :

$$Nu_d = \phi_1\phi_2 \, Re_d^m \, (z/d)^{0.091} \, Pr^{1/3} \qquad 8.4.2$$

where

ϕ_1 is a degradation factor which accounts for the effect on spent air and varies between 0.5 and 1.0 (see Fig. 17 of Ref. 133). ϕ_2 and m are functions of x/d and Reynolds number and their values can be obtained from Figs. 14 and 16 of Ref. 133. For example, for 3×10^3 Red 3×10^4, m is 0.92 and 0.75 at x/d = 10 and 4 respectively with corresponding values of 0.01 and 0.085 for ϕ_2.

This equation is valid for their test conditions.

Recently (in 1981), Florschuetz et al (Ref. 134) similarly determined the characteristics of multiple arrays of circular impinging jets. The test conditions covered the range: $2.5 \times 10^3 \leq Re \leq 7 \times 10^4$, $1 \leq z/d \leq 3$, $4 \leq y/d \leq 8$ and $5 \leq x/d \leq 15$ (y/d and x/d are the spanwise and streamwise nozzle spacings respectively).

It was found that cross flows generally reduced the mean heat transfer coefficients and this is in agreement with previous studies. Furthermore, it was observed that the trend of the average heat transfer with z/d decreased for small values of x/d and y/d but increased for larger values. No transition ranges were, however, indicated.

The flow and heat transfer associated with jets in cross flows are complicated so that experimental data cannot be correlated in simple forms. The authors proposed the following expression :

$$Nu = A \quad 1 - C(x/d)^n \, (y/d)^m \, (z/d)^l \, (M_c^*/M_j^*)^k$$

where

$$A = 0.363 \, (x/d)^{-0.55} (y/d)^{-0.44} (z/d)^{0.068} \, Re^{0.73} \, Pr^{1/3}$$

C, n, m, l and k are constants and typical values are 0.596, -0.103, -0.380, 0.803 and 0.561 respectively.

M_c^*/M_j^* = cross flow - jet mass velocity ratio

It was indicated that 95% of the data points fall within 11% of the proposed equation.

8.4.3 Inclined Impinging Jets in Cross Flows

Kabari (Ref. 36) investigated the flow field and heat transfer associated with a 12.7 mm diameter circular impinging jet in a cross flow. From surface flow visualization studies, he observed that the 'separation line' (between the jet and the cross flow) had greater spread and penetration as the nozzle inclination into the cross flow increased. The heat transfer studies covered a range: $2 \leq z/d \leq 8$, $45^{o} \leq \alpha \leq 90^{o}$ and $M = 2$, 4 and 8, and he employed naphthalene sublimation together with a profilometric technique to obtain the mass/heat transfer rates. It was found that under cross flow situations, the stagnation point values generally decreased. Moreover, it was observed that local heat transfer rates upstream of impingement zones reduced whilst those on the downstream usually increased. These variations were attributed to deceleration of the cross flow on the upstream section and the subsequent flushing effect on the downstream. Although it was concluded that local heat transfer coefficients (at a constant M) were almost insensitive to nozzle inclination. This is inconsistent with his results (see for example Fig. 8.4.2). It can be noticed that the maximum heat transfer coefficient occurred at an incident angle of 60°. Moreover, the test conditions were poorly chosen so that the effects of individual variables (e.g. jet to cross flow velocity ratios) were not systematically investigated.

Jackson (Ref. 37) undertook flow and heat transfer measurements associated with inclined two-dimensional slot jets in confined cross flows. The thin-film napthathelene mass transfer technique (in conjunction with the Chilton-Colburn analogy) was used to infer the heat transfer coefficients. The variables investigated included : $6 \leq U_j/U_c \leq 14$, $2.5 \leq z/b \leq 10$ and the nozzle inclination (α) into the cross flow was varied from 45° to 90°. In this system geometry, the jet covers the width of the test section and is therefore, analogous to a row of very closely-spaced circular jets in a cross flow. In the latter case, cross flow effect becomes more severe as the nozzle pitch is reduced because the main stream cannot easily divide and flow between the jets.

Figure 8.4.3 shows a typical heat transfer result from Jackson's study. As can be seen, the local heat transfer coefficients increased with increasing nozzle inclination. This important effect of nozzle inclination was not, however, reported by Kabari. It is also significant to note that no optimal nozzle inclination was indicated by Jackson's work.

From the foregoing review, it is evident that the heat transfer characteristics of turbulent axisymmetric jets in cross flow have been fairly well established. However, the studies have in generally, been limited to either the mean heat transfer coefficient or the local values on the longitudinal axis of the jet. Even, the reported orthogonal impingement investigations only covered a narrow range of test conditions and information on the complete heat transfer field is unavailable.

It is also clear that there is very little published information on the effect of nozzle inclination on heat transfer for an impinging jet in the presence of a confined cross flowing stream. However, the limited studies carried out so far at Cranfield indicate that nozzle inclination is of great importance because the local heat transfer coefficients can be increased.

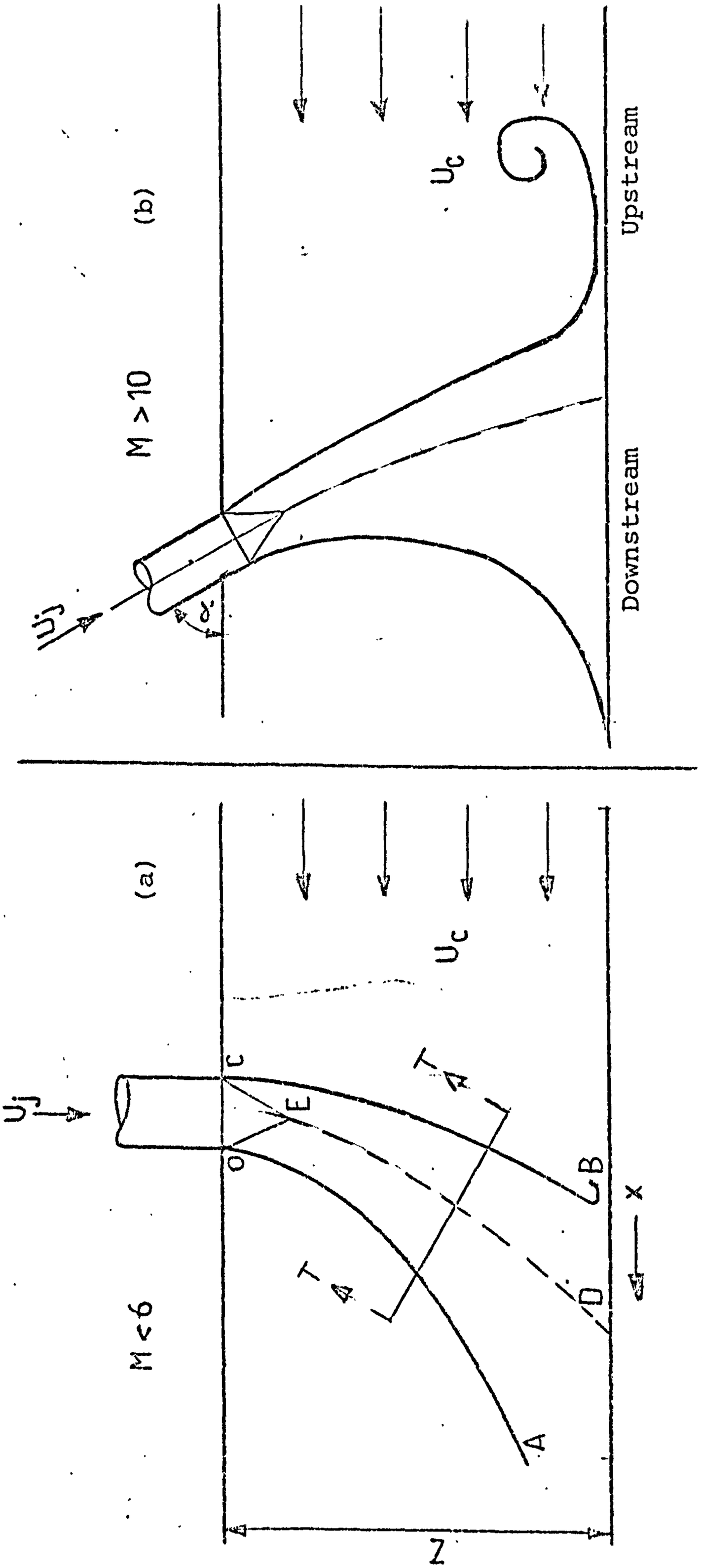

FIG.8.2.1. SCHEMATIC FLOW PATTERNS OF CIRCULAR JETS IN CROSS FLOWS (a) ORTHOGONAL CASE
(b) OBLIQUE CASE

DIRECTION OF CROSS FLOW →

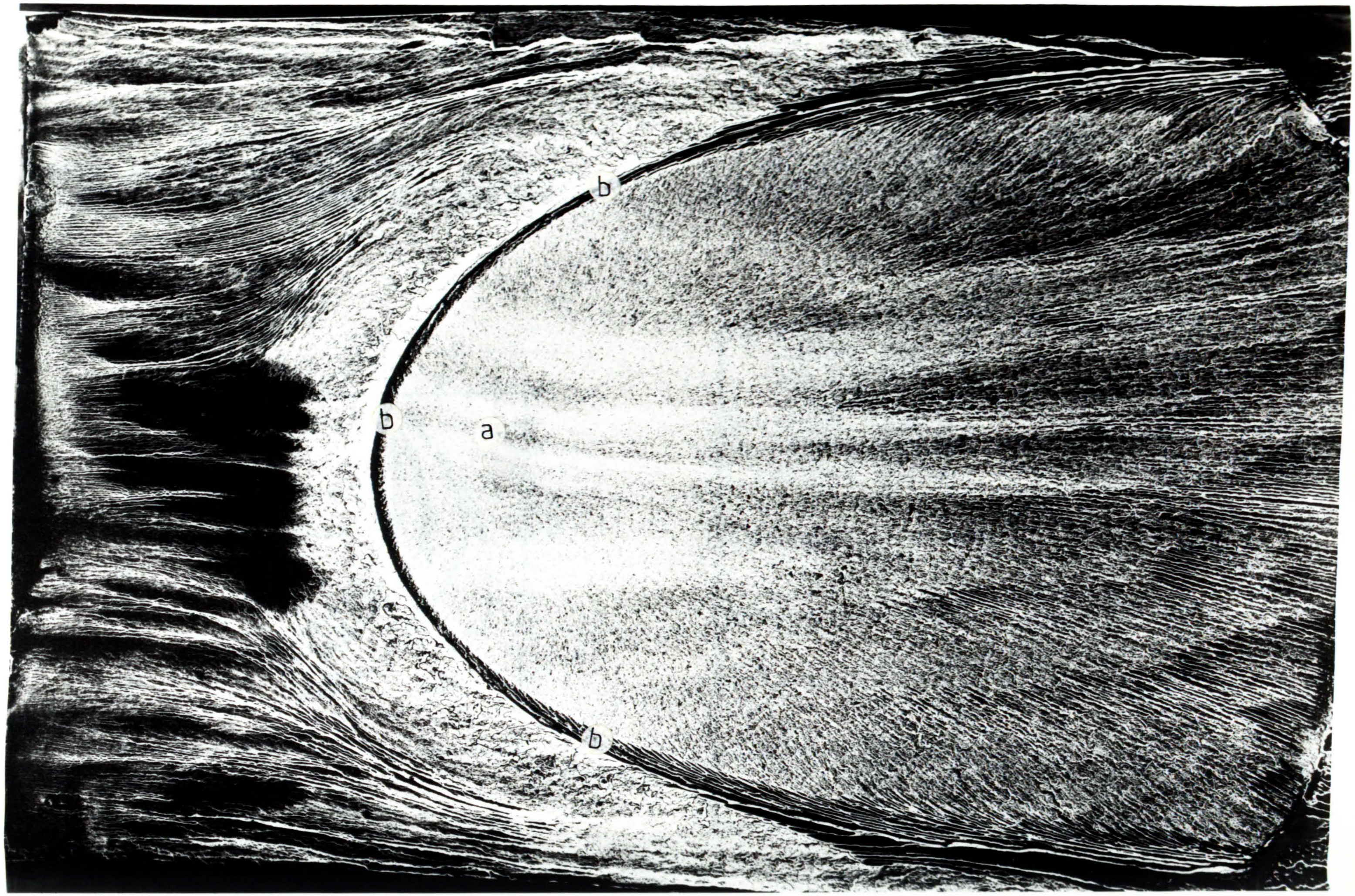

PLATE 8.2.1 SURFACE FLOW PATTERN ASSOCIATED WITH A CIRCULAR JET IN A CROSS FLOW (REF 36).

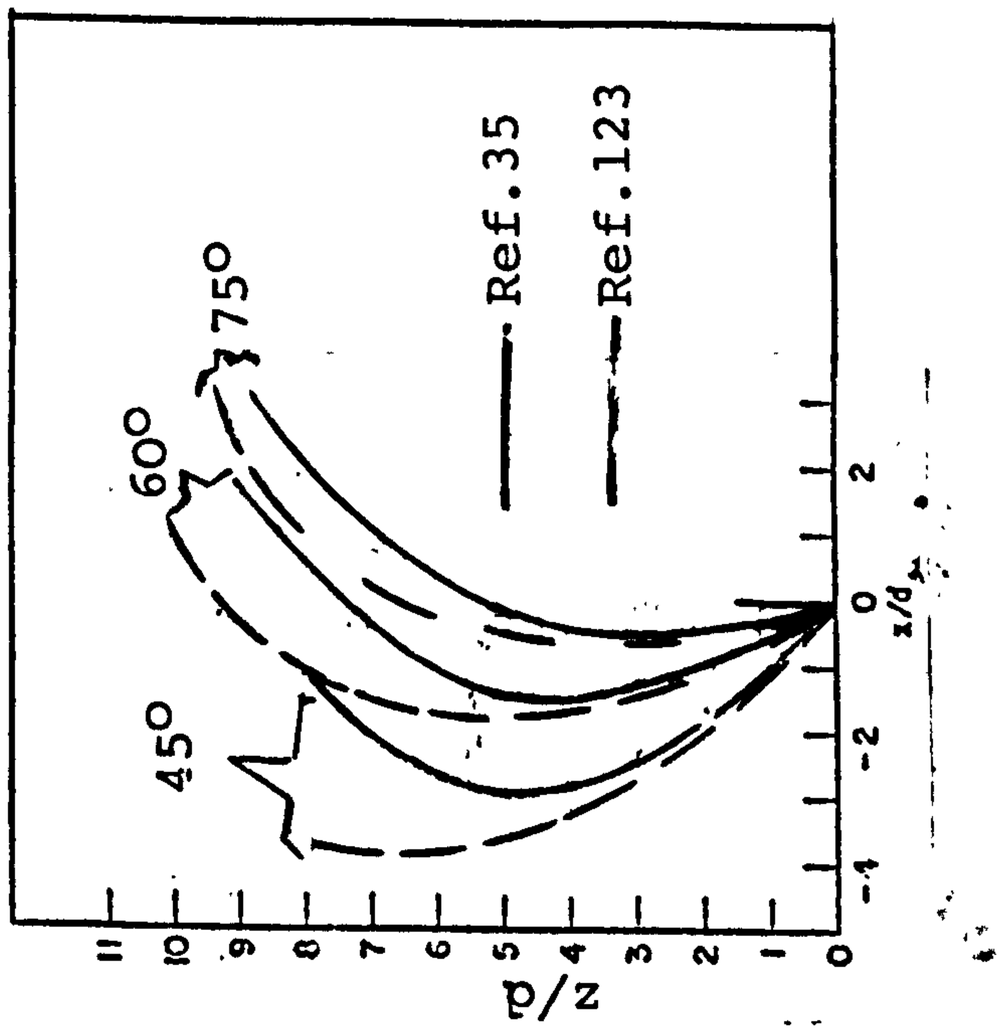

FIG.8.3.2. CENTRELINE TRAJECTORIES OF INCLINED JET FLOWS (REF.35).

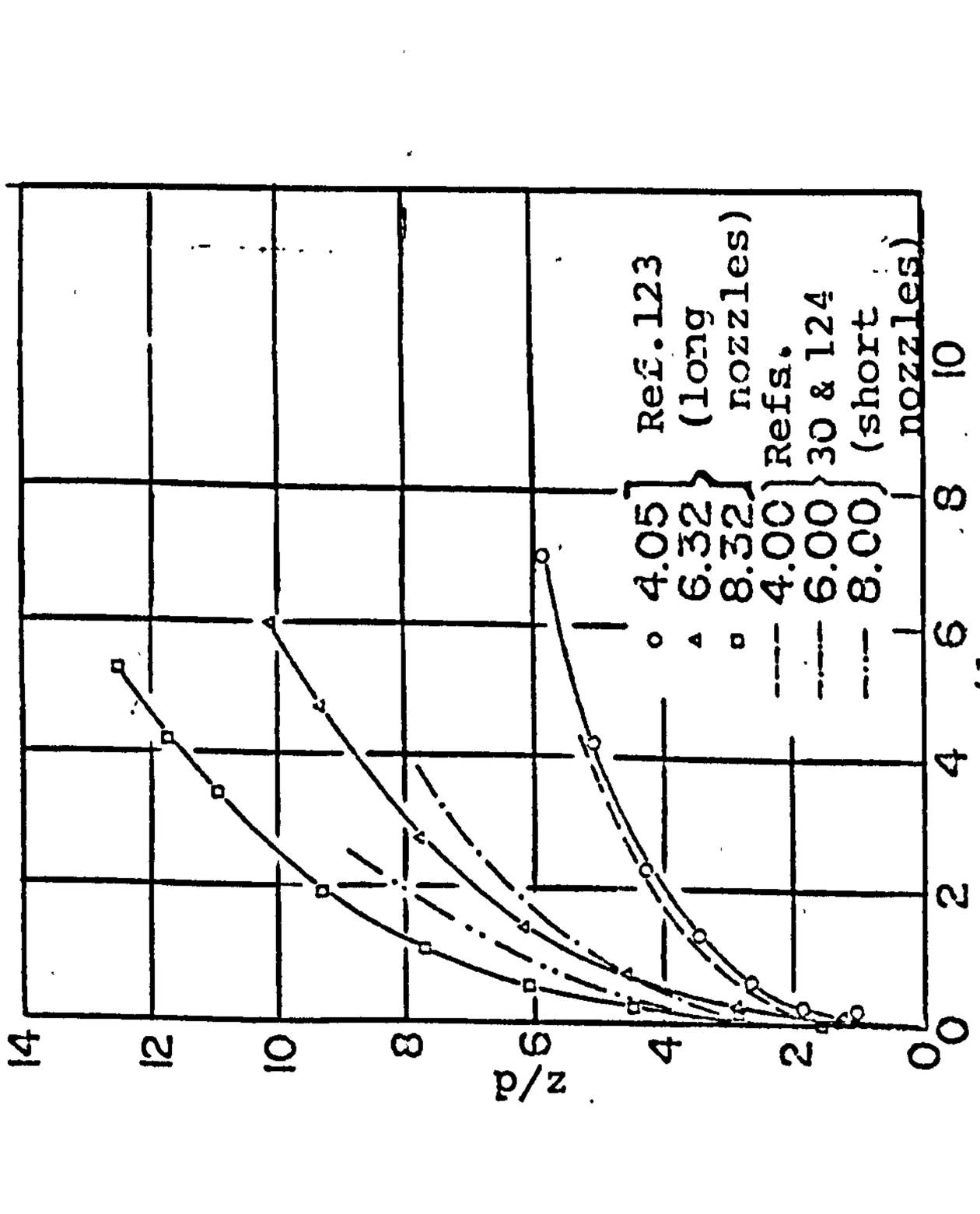

FIG.8.3.1. CENTRELINE TRAJECTORIES FOR SHORT AND LONG CIRCULAR NOZZLES (REF.123).

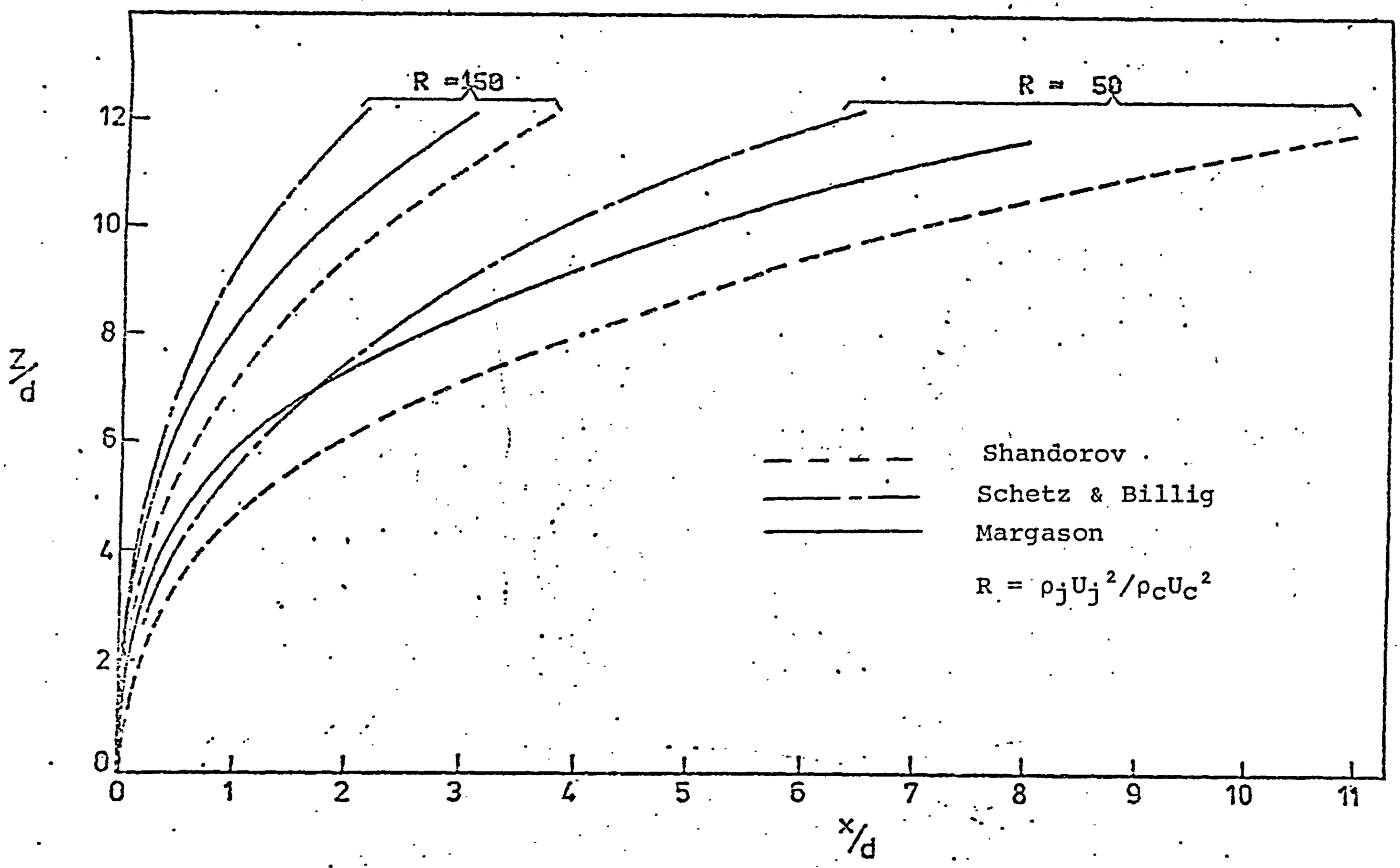

FIG.8.3.3 CENTRE LINE TRAJECTORIES OF ORTHOGONAL JETS IN CROSS FLOWS.

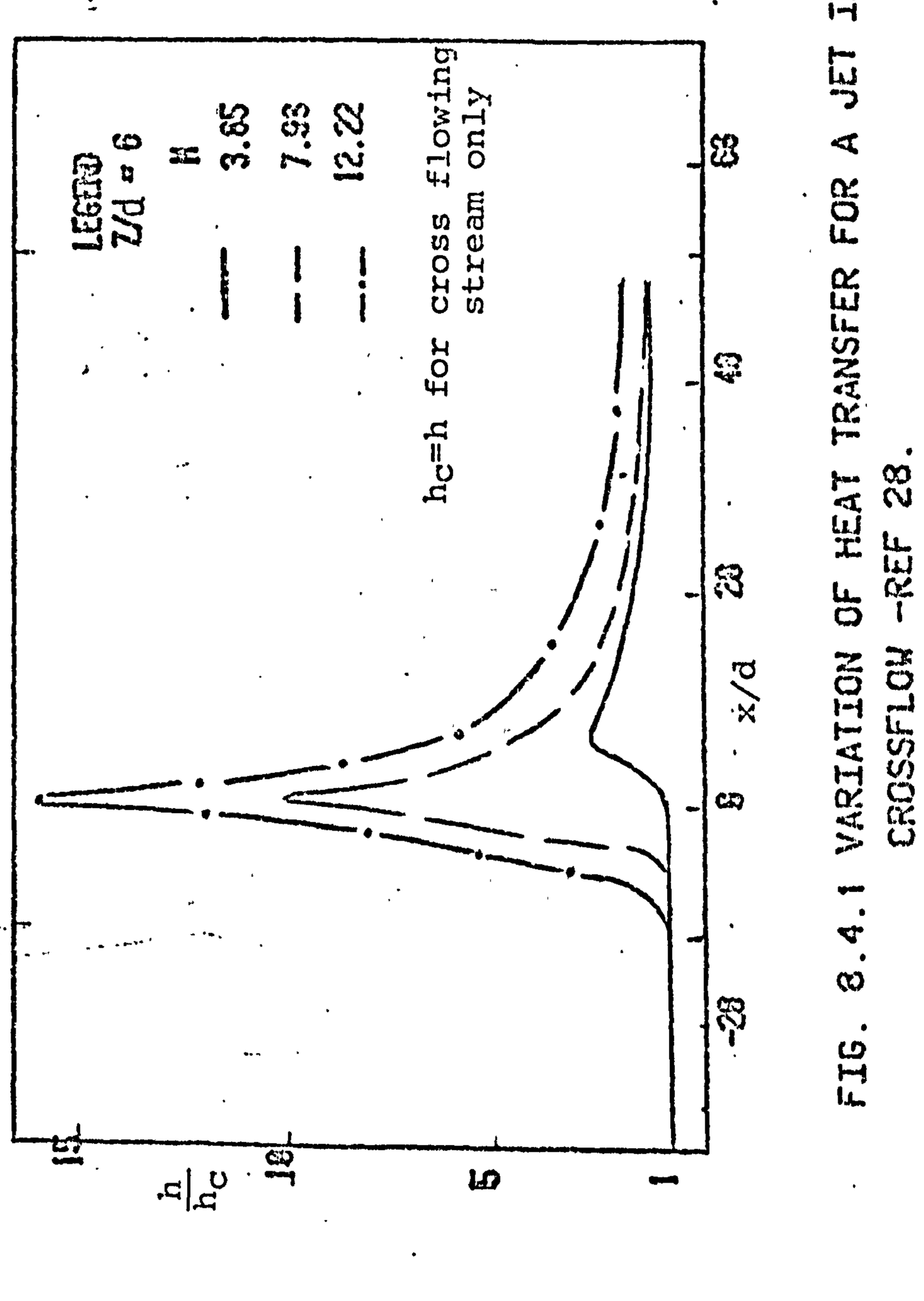

FIG. 8.4.1 VARIATION OF HEAT TRANSFER FOR A JET CROSSFLOW - REF 28.

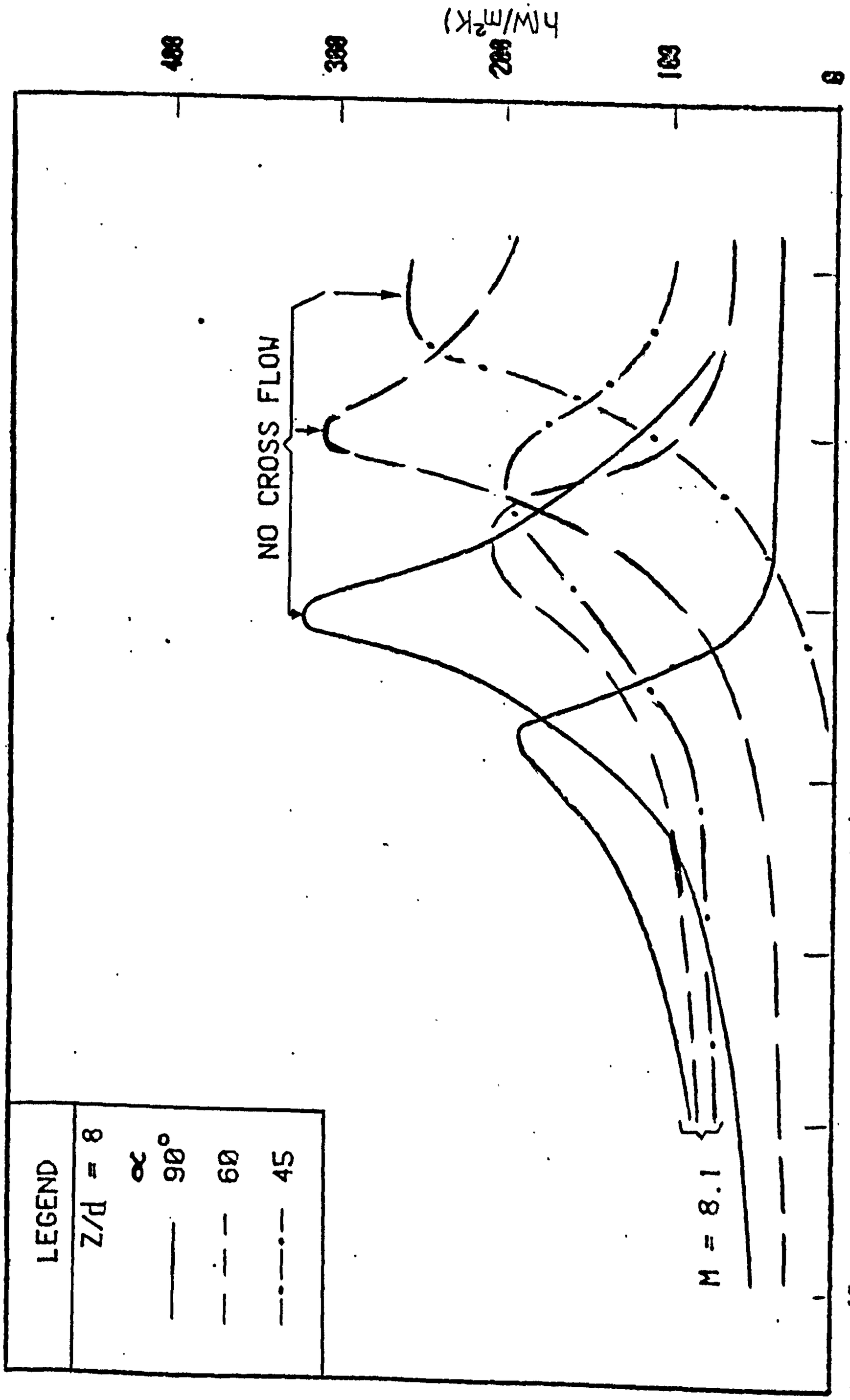

FIG. 8.4.2 VARIATION OF HEAT TRANSFER FOR INCLINED CIRCULAR JETS IN CROSS FLOWS (REF. 38).

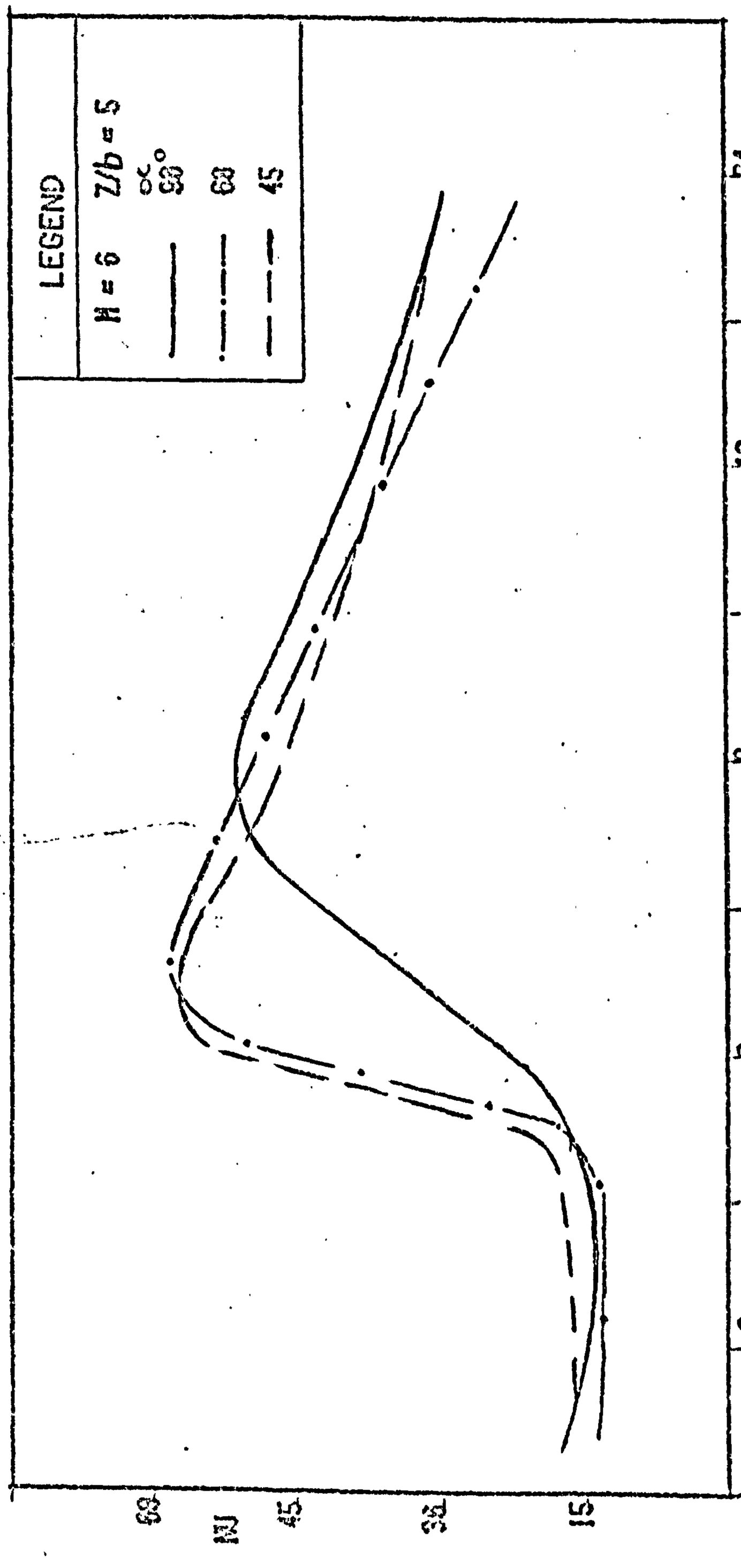

FIG. 2.4.3 HEAT TRANSFER UNDER AN INCLINED SLOT JET IN CROSS FLOW (REF. 37).

CHAPTER 9

9. CHARACTERISATION AND VISUALIZATION OF THE FLOW - EXPERIMENTAL TECHNIQUE AND RESULTS

9.1 INTRODUCTION

This Chapter describes details of the test rig used for both flow visualization and mass transfer studies of a turbulent circular jet injected into a cross flowing stream. The experimental fluid flow measurements and results are also presented and discussed. In all the tests, the jet velocity was maintained at 24 m/s.

9.2 THE TEST RIG

The test rig is depicted in Plate 9.2.1 and Fig. 9.2.1 and it primarily consists of the jet nozzle, the cross flow assembly and the test section. The nozzle assemblies were identical to those used for the unconfined jet studies. The cross flow air was supplied from a centrifugal blower (Secomark Model S3038) and the flow rate was monitored by using an orifice plate designed according to BS 1042 (Ref. 115), and mounted at the entry of the inlet duct. A regulating valve was used to control the flow rate. Fig. 9.2.1 shows a schematic layout of the test rig. The air was initially delivered to a plenum chamber via a cooling unit (a water-cooled cross flow type heat exchanger) which was mounted in the supply duct to maintain the air temperature at or very near the ambient value. Honeycomb screens were fitted in the plenum to straighten the flow which was then passed through a smooth reducing duct into the test section. This transition piece provided a gradual reduction in flow area to that of the test section.

The test section was 445 mm long and consisted of a rectangular duct the floor of which acted as the test plate for the mass transfer tests. The cross flow was introduced at one end and exhausted from the other into a large fume cupboard from where the air which was contaminated with naphthalene was ducted to outside the building. This technique ensured that the naphthalene vapour concentration in the ambient air was always insignificant. The side walls were constructed of 6.35 mm thick perspex because transparent walls were necessary during the flow visualisation studies and they also enabled the progress of the mass transfer tests to be observed.

The roof of the test section was manufactured of 445 mm x 820 x 15 mm thick perspex and incorporated a removable nozzle plate assembly. Six different nozzle carrier plates were manufactured and an inclined hole was drilled in each plate to correspond

to the nozzle inclinations investigated in the present study (i.e. $30^{o} \leq \alpha \leq 135^{o}$). The nozzle was fixed to the appropriate carrier plate with Araldite adhesive and the whole unit was then positioned in a slot on the top of the test chamber. Any mating surfaces were sealed by means of fibre gaskets to prevent air leakage.

The target plate (of size 445 x 413 x 6.35 mm) completed the test duct. This plate was designed to slide under the side spacers and rested on a metallic frame which was fixed to the base of the remainder of the rig. The test plate was inscribed with square grid system of lines of 16 mm pitch (i.e. a pitch equal to the nozzle diameter) to assist in mapping of the naphthalene clearance patterns. The grooves of these scribed lines were filled with black ink, which provided a suitable contrast against the white naphthalene background. This grid system of lines was also useful in determining jet penetration and trajectories during the smoke flow visualization tests.

9.3 VELOCITY AND TURBULENCE INTENSITY

As mentioned above, the jet nozzle in this "confined cross flow" study was previously used in the unconfined free jet studies so that the initial fluid dynamic characteristics of the jets have already been reported in Chapter 5.

It was considered necessary to determine the velocity profile of the cross flow before it entered into the test chamber since this can be helpful when comparing heat/mass transfer data from various studies. Furthermore, these data would also be used as boundary conditions in an "on-going" computational study of jets in cross flow.

The pitot tube and micromanometer described in Chapter 5 were used to obtain the velocity profiles of the cross flowing stream at exit from the smooth connecting duct. The tests were carried out with cross flow velocities in the range $1.2 \leq U_c \leq 4.9$ m/s.

Figure 9.3.1 presents typical velocity profiles across the section of the cross flowing stream. It can be observed that for the range of velocities investigated, the profiles were essentially flat indicating that the flow is fully developed.

9.4 FLOW VISUALISATION

9.4.1 Introduction

The variation of heat/mass transfer rates beneath turbulent

impinging jets can often be better understood if details of the associated fluid flow are available. Thus, flow visualization studies were undertaken to elucidate some of the general features of the flow.

Various methods have been developed for making the flow visible so that the general physical structure of the flow field can be obtained. The common techniques can be divided into surface flow (e.g. oil film) and flow structure (e.g. smoke tests) methods. The naphthalene thin-film mass transfer technique provides sufficient information on the surface flow pattern and thus further surface flow techniques were not employed. Kabari (Ref. 36) can, however, be consulted for details about these techniques.

"Flow structure" methods can further be classified into "optical" and "non-optical" techniques. In the former, local changes in density occur in the flow field and a suitable optical arrangement enables these gradients to be observed visually. The common methods in this group include Shadowgraph, Schlieren and Interferometric systems (e.g. Mach-Zender interferometry which can be used to obtain both qualitative and quantitative flow data), (Ref. 120). In the non-optical methods, tracers (e.g. smoke, discrete particles and dyes) are used. Injection of smoke was employed in the present study and it is, therefore appropriate to review briefly this technique.

9.4.2 Smoke Techniques

In principle, flow visualisation methods can be used to reveal qualitatively most of the significant features of fluid motion. However, mere visual observation is not sufficient for this purpose and supplementary photographic techniques are often employed. Smoke techniques have been used for widely different flow geometries (see, for example Ref. 121). In view of the large number of available publications, the ensuing brief review is restricted to "cross flows".

Keffer and Bains (Ref. 30) used an oil-vapour and nitrogen aerosol to generate a smoke which was employed in a qualitative study of the interaction of a round turbulent jet with a cross flowing stream. Purely visual observations were made and these investigators did not present any photographic records so that it is difficult to judge the quality of the visualization.

Ramsey and Goldstein (Ref. 135), Goldstein et al (Ref. 136) and Bouchez and Goldstein (Ref. 28) investigated the flow of circular jets in a cross flow by injecting a carbon-dioxide water fog (obtained by placing solid carbon dioxide in hot water) into the jet flow. The difference in the three studies was in the sophistication of the photographic techniques which were employed. Ramsey and Goldstein used shutter speeds of 0.125 and 10^{-3} secs. and more detail was observed with this

latter setting. It was observed that the jet boundary was irregularly shaped and the presence of large scale eddies was detected. Goldstein et al used high speed photography (3300 frames/sec) and observed formation of large scale eddies and vortices soon after the jet emerged from the nozzle. Bouchez and Goldstein used a stroboscopic light and a shutter speed of 8 μs. Three flow regimes were identified and these depended on the jet to cross flow mass velocity ratio. At high velocity ratios, a recirculation zone was formed upstream of the impingement area. This recirculation disappeared at moderate velocity ratios. However, at low velocity ratios, no impingement occurred on the test plate because the jet momentum was not sufficient to completely penetrate across the main stream. Quantitative values of the corresponding velocity ratios were not stated.

Kabari (Ref. 36), Chong (Ref. 27) and Jackson (Ref. 37) also employed a chemical smoke to investigate the flow structures of turbulent jets in a cross flow. In the last two studies, a so-called "recirculation bubble" was observed in the lee of slot jets in a confined cross flow.

The foregoing discussion suggests that smoke visualisation yields primarily qualitative information, albeit, on the overall structure of the flow field. Quantitative data (such as jet trajectories) can, however, be obtained from a succession of photographs although the procedure is lengthy and tedious and moreover is susceptible to inaccuracies.

9.4.3 Choice of a Smoke Generation Technique

Smoke methods can be employed for both laminar and turbulent flows, although they are particularly suitable for the former because the flow streamlines can then easily be distinguished. In both situations, however, care must be taken in choosing a suitable tracer smoke. The method of injection into the flow is also important. The simplicity of the smoke generation method must be considered and the injection velocity and position should be chosen so that the flowfield is not adversely disturbed. In order to obtain reliable flow visualisation data, it is essential for the smoke not to clog or condense (Ref. 120). Furthermore, the smoke should be non-toxic, and non-corrosive (especially when metallic test sections are involved).

Various techniques have been employed to produce smoke, for example, "combustion smoke" can be obtained by using filtered smoke from cigarettes or by burning rotten wood and these are suitable for some flow studies. Chemical smokes are however, usually more convenient, for example, when liquid titanium tetrachloride reacts with moist air, it forms dense white fumes of hydrochloric acid and titanium oxide which can be employed for smoke tests. However, the presence of suspended water vapour and chemicals much heavier than air sometimes inhibits

the use of this tracer in low velocity situations. Ammonium chloride (obtained by mixing ammonia and hydrochloric acid) can often be employed as an alternative chemical tracer. Other chemical smokes were described in the review.

Smoke produced by burning pellets of dichlorodiphenyl-trichlorcethane (supplied by P.H. Smoke Products Ltd.) was used in the present study. Generation of this smoke required only a simple and cheap experimental set up. The white colour of the smoke also provided a good contrast to a black background so that photographic records were easily obtained.

9.4.4 Experimental Arrangement and Procedure

The flow visualisation test rig is shown in Plate 9.2.1. The smoke generation system consisted mainly of a metal container (a smoke drum) with inlet and outlet pipes, 6.35 mm in diameter. The inlet pipe was connected to a low pressure (21 kN/m^2) compressed air which ensured a regular supply of smoke from the drum. The low pressure minimised disturbances (e.g. in the form of eddies) during injection into the neighbouring flow. The outlet pipe was connected to the jet flow line at a position 100 nozzle diameters upstream from the nozzle exit so that any slight local disturbance caused by smoke injection disappeared before the jet exited into the cross flowing stream.

As mentioned earlier, it was difficult to observe visually details of the flow phenomena and thus photographic information was necessary. A 35 mm Praktica model LTL3 camera was used. A narrow slice of the test section was illuminated by a 750-watt projector lamp which produced a light beam in a direction perpendicular to the location of the camera. In order to obtain sufficient contrast in the photographs, a black background was used.

The two centrifugal blowers supplying the jet and cross flow were switched on and the flow rates (corresponding to the required jet-to-cross flow velocity ratio) were set. The air outlet temperatures were measured and maintained at within $1^{o}C$ of each other by adjusting the cooling water flow rates.

A smoke pellet was ignited and placed in the drum which was immediately covered and pressurised so that smoke was slowly injected into the jet flow. Problems were encountered during the preliminary tests because the smoke filled the test section too quickly. Subsequently, only half a pellet was used in all the tests. The volume of smoke was thus reduced, but was nevertheless, adequate to permit still photographs (at least 4 per test) to be taken with a shutter speed varying from .03 to 10^{-3} secs. The smoke exhausted into the 'fume room' and was finally ducted outside the building.

9.5 RESULTS AND DISCUSSION

9.5.1 Introduction

The results of the flow visualisation study are presented and discussed in this section. Generally, the figures emphasize the importance of the interaction of the jet and cross flow on the resulting highly turbulent and complicated fluid motion. The various flow phenomena encountered in this section will subsequently be used in Chapter 10 to explain the heat/mass transfer measurements obtained with different system geometries.

9.5.2 Effect of the Velocity Ratio

Figure 9.5.1 depicts the flow structures for initially orthogonal jets at various jet-to-cross flow velocity ratios. The photographs were taken with an exposure time of 8×10^{-3}s and it can be seen that boundaries between the jet and the resulting flow are irregular. The interaction of the jet and cross flow creates a turbulent motion with the overall structure dominated by large eddies. Bouchez and Goldstein (Ref. 28) who, as mentioned in the previous section, employed a stroboscopic technique found that the flow fluctuations occurred at relatively short intervals thereby indicating a high degree of turbulence.

At M = 20.9, the jet impinges on the target plate and creates a region of low pressure denoted by 's' in Fig. 9.5.1. The upstream flow is rolled up to form a recirculation zone with strong vortices. This region can easily be identified in the photograph and it extends for about 8-9 nozzle diameters upstream of the centreline before it changes direction under the influence of the cross flowing stream. Fig. 9.5.2 is reproduced from Tyler and Williamson (Ref. 122) and shows an idealised representation of this recirculation and vortex formation. The cross flow exerts little pressure force on the jet and therefore divides and flows around it. Thus, the fluid immediately downstream of the impingement point appears not to be affected by the cross flowing stream but further downstream (i.e. > 16d), both flows are completely identical and a duct flow ensues.

At M = 10.9, the 'blocking effect' of the jet is reduced so that disturbances do not propagate so far upstream from the nozzle exit. Jet impingement on the target surface is, however, still evident and this is also accompanied by a recirculation zone which has a length of approximately 6 nozzle diameters. The height of the smoke immediately downstream of the impingement region indicates the blowing effect of the cross stream and this probably produces a slight displacement of the impingement point from the nozzle centreline.

At M = 6.6, the flow does not exhibit an upstream recirculation region because the cross stream effectively blows the flow

downstream from the nozzle exit and impingement only occurs at about 3 nozzle diameters downstream of the plane of injection. The potential core is also deflected by the cross flow. It can be seen that at M = 5.0, the jet appears to be 'lifted up' by the cross stream and is subsequently blown downstream because the jet is too weak to penetrate completely across the cross flowing stream. The deflection of the initial flow region is higher at this velocity ratio than in the previous situations. The photographs of Bouchez and Goldstein (Ref. 28), Goldstein et al (Ref. 136) indicate somewhat similar phenomena.

It is pertinent to mention that although vortex formation can be observed during smoke tests, the kidney shape characteristic of a circular jet in cross flow can only be observed by a surface flow visualization and discussion of this will, therefore, be deferred to Chapter 10. It is clear however that at a particular nozzle-to-plate separation, the velocity ratio (U_j/U_c) determines the flow structure.

9.5.3 Effect of Nozzle Inclination

1. Inclination Into the Bulk Cross Flow (i.e. $\alpha < 90^o$)

Figure 9.5.3 shows the flow structures at nozzle inclination (relative to the plate) α of 30^o, 45^o and 60^o (i.e. the jets were directed into the cross flow) and at various velocity ratios. As the inclination relative to the plate is decreased, greater penetration of the jet flow after impingement occurs. Interaction between the jet and the main flow is severe and reverses the flow (see for example $U_j/U_c > 6.6$).

At $\alpha = 60^o$ and M > 10.9, the impingement flow is qualitatively similar to that for the orthogonal geometry. At M = 6.6, the height of the upstream vortex is much reduced because the cross stream tends to sweep the jet flow rapidly downstream of the nozzle centreline; note, for example, the presence of fluid at point 'd'. At M = 5, the jet is further deflected and flushed downstream by the cross flow.

The jet and impingement flows for nozzles at 30^o and 45^o are qualitatively similar to those for 60^o. It can however be observed that for M < 6.6, the cross flow effect is less severe for the jets from the 60^o nozzle than for other nozzle inclinations. A comparison of the photographs (i.e. Fig. 9.5.1 and 9.5.3) reveals that the jet initial region is longer for $\alpha = 60^o$ and consequently its potential core appears to be better preserved. Since it has been found in previous studies (e.g. Ref. 24, 25) that cross flow usually reduces heat transfer, it may therefore be expected that at M < 6.6, the heat transfer for a jet at 60^o is likely to be higher than those for orthogonal jet impingement.

Figure 9.5.4 demonstrates "the impinging flow" at various jet to cross flow velocity ratios. The bottom row of photographs shows the flow as viewed from beneath the test section with the fluid jet entering towards the camera whilst the top row depicts the side view. At M = 20.9, the lateral spread of the flow is greater than at the other velocity ratios investigated. At the lower velocity ratios (M < 6.6), the strength of the cross flow restricts the lateral spread of the jet so that contact is not made with the side walls.

Rapid axial spreading of the jet (almost unimpeded by the cross flow) is evidenced by the length of the upstream flow in the right hand column of Fig. 9.5.4. It can be seen that this length reduces as the velocity ratio is reduced, for example at $\alpha = 60^{o}$, the penetration lengths are respectively 8d and 3d for M = 20.9 and 6.6. At M = 5, the impingement flow is restricted because the cross flow prevents upstream spreading of the jet which is hence flushed downstream.

2. Inclination in the Direction of the Cross Flow

Figure 9.5.5 presents the flow structures for nozzle inclinations α of 90^{o}, 120^{o} and 135^{o} at various jet to cross flow velocity ratios. At an inclination of 135^{o} and M > 10.9, the jet impinges on the target plate but the upstream 'wall jet' flow does not penetrate significantly and does not appear to be associated with recirculation and vortex formation. However, at $\alpha = 90^{o}$ and 120^{o}, it can be seen that the jet impinges on the test surface and obstructs the cross flow. This interaction produces a recirculation zone denoted by 'a' whose length decreases as the jet is inclined. At M < 6.6, it is noticeable that the jet deflection increases as α is increased.

Figure 9.5.6 shows the jet flows at the two extreme velocity ratios (i.e. M = 5 and 20.9) for nozzle inclinations α of 30^{o}, 60^{o}, 90^{o} and 120^{o}. In the bottom row, a reduction of both the length and height of the recirculation zone can be seen as α is increased. From the top row (i.e. $U_j/U_c = 5$), it can be observed that jet deflection by the cross flowing stream is least at a nozzle inclination of 60^{o}.

From the above, it is clear that at a fixed z/d, the type of flow associated with a circular jet in cross flow is dictated by both the jet to cross flow velocity ratio and nozzle inclination. These parameters can also be expected to affect the variation of heat transfer in this system.

1 JET

2 CROSS FLOW

3 SMOOTH REDUCING SECTION

4 PLENUM CHAMBER

5 TEST PLATE

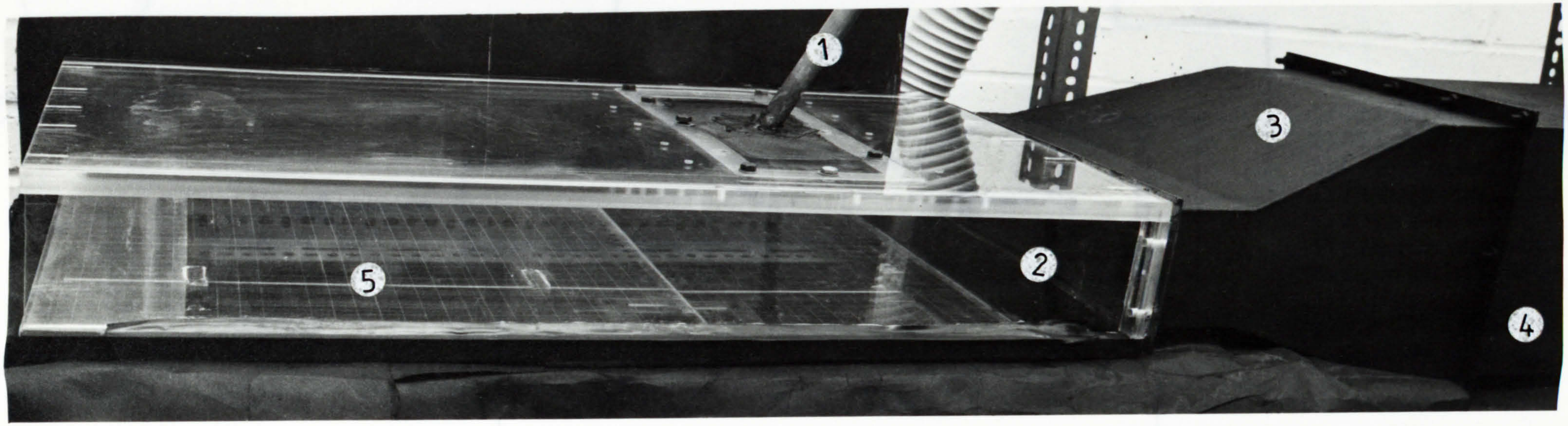

PLATE 9.2.1 THE TEST SECTION FOR CONFINED CROSSFLOW STUDIES.

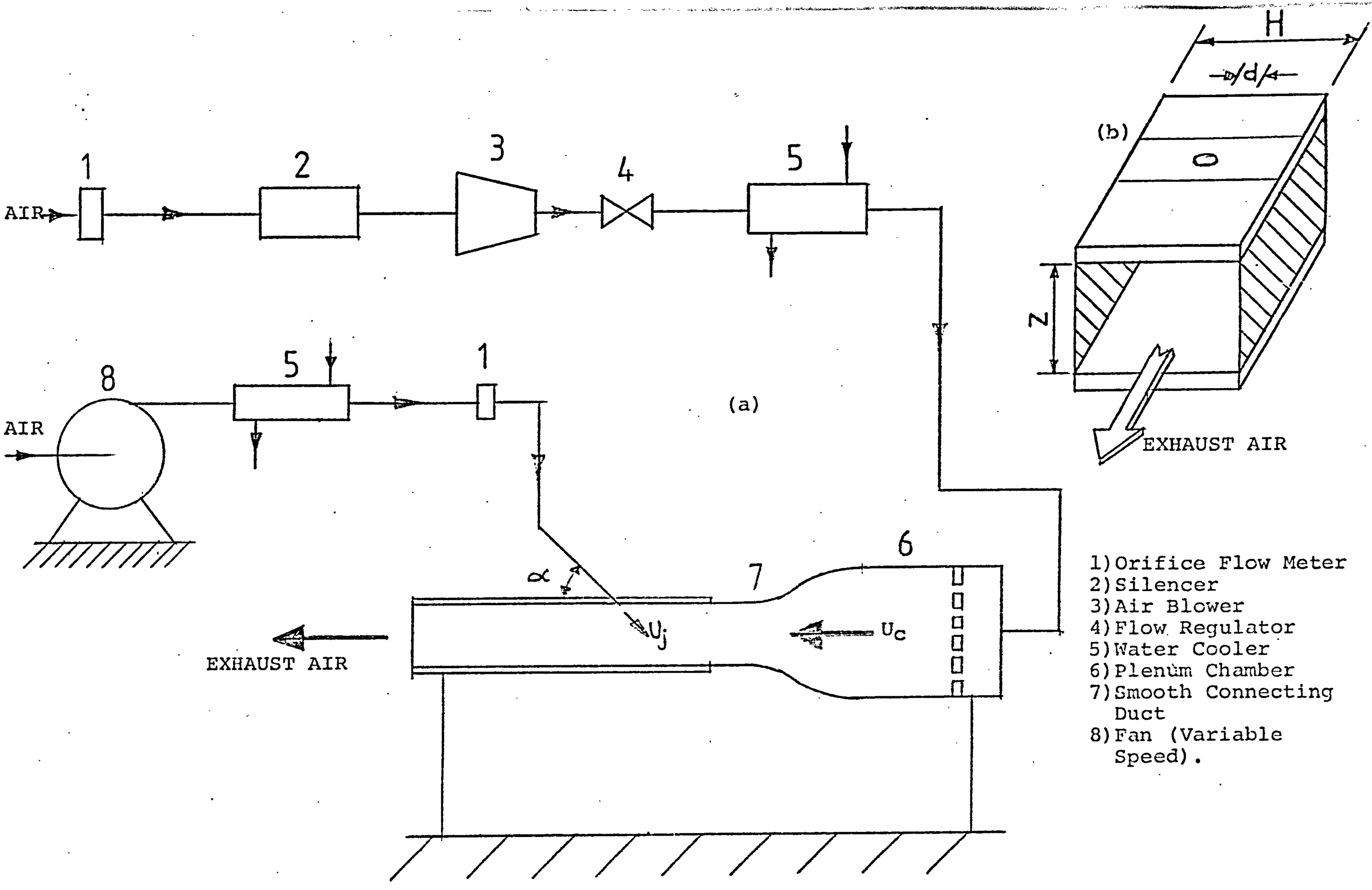

FIG.9.2.1. SCHEMATIC REPRESENTATION OF EXPERIMENTAL RIG (a) GENERAL LAYOUT
(b) THE TEST SECTION

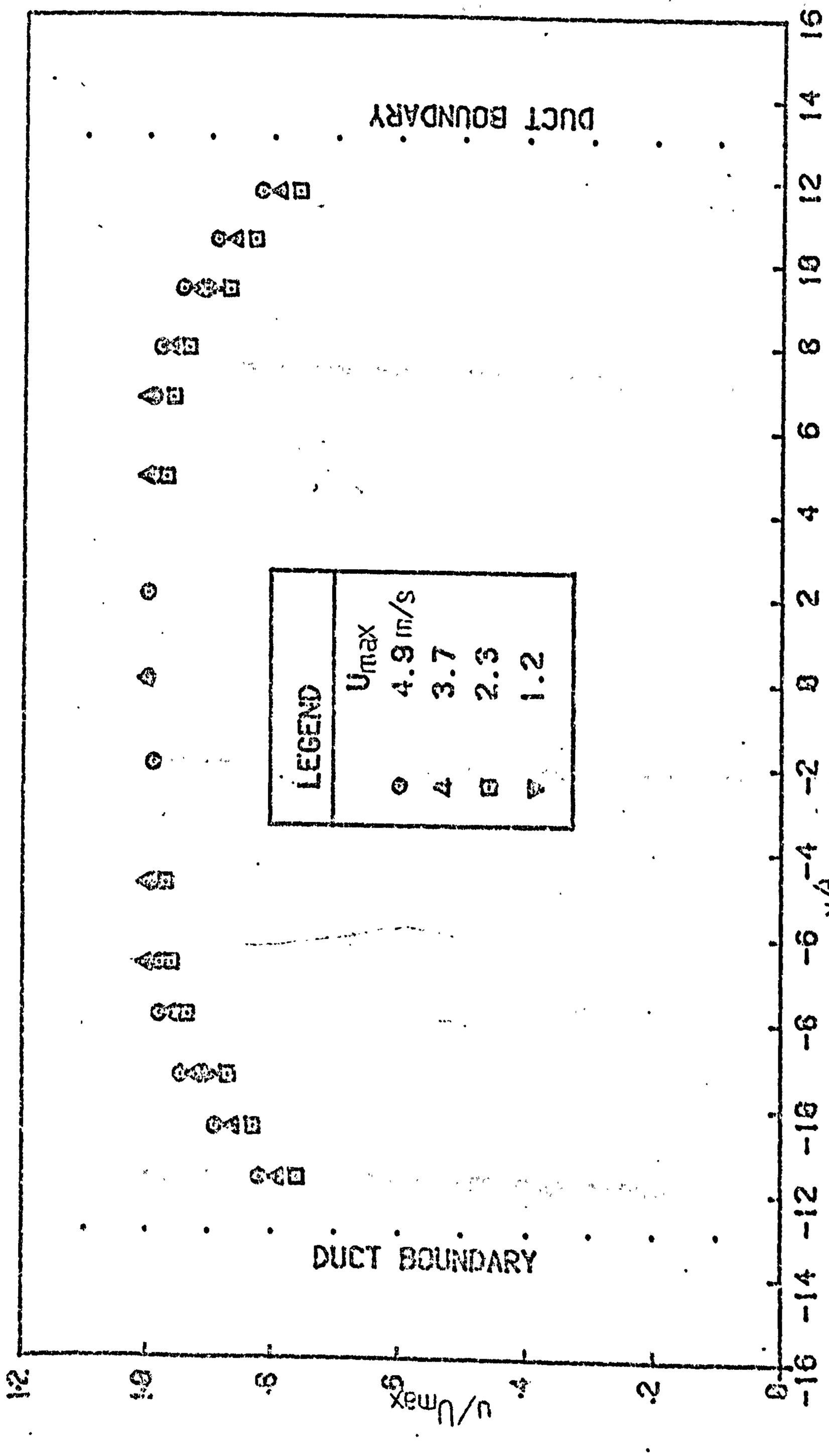

FIG.9.3.1 VELOCITY PROFILES ACROSS THE CROSS FLOWING STREAM.

M=

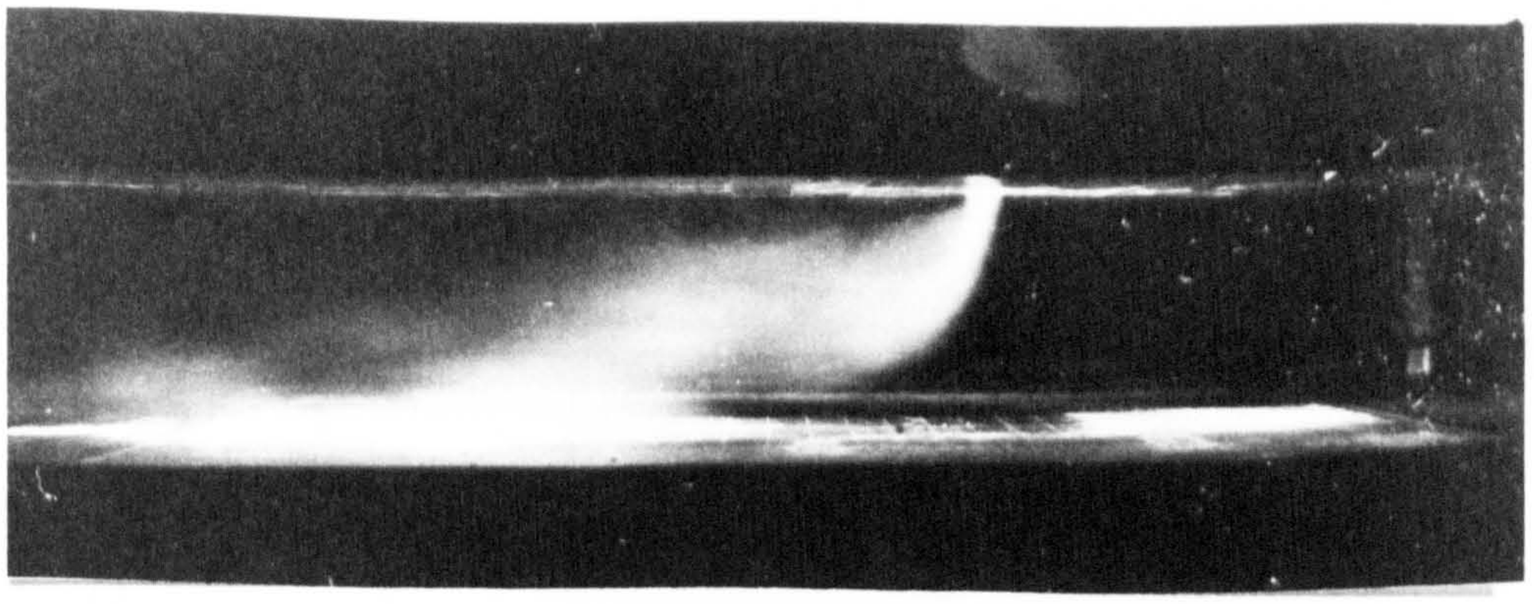

5.0

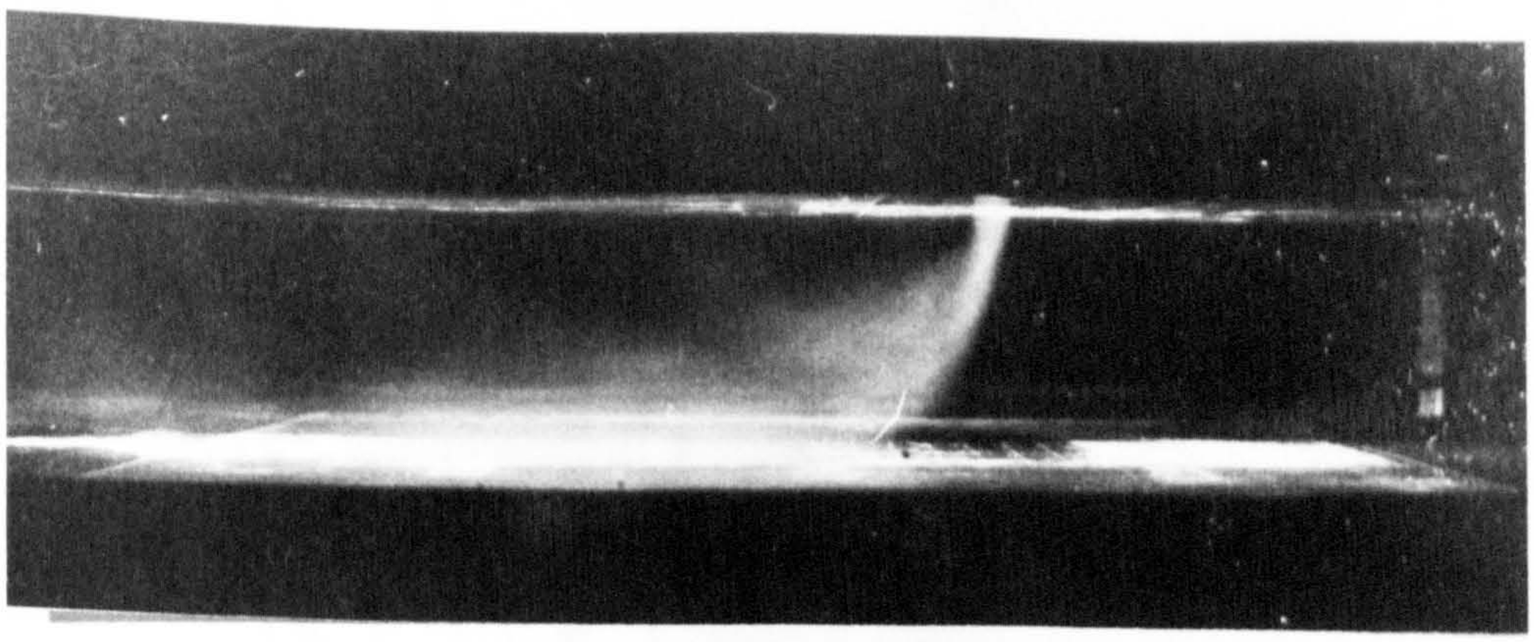

6.6

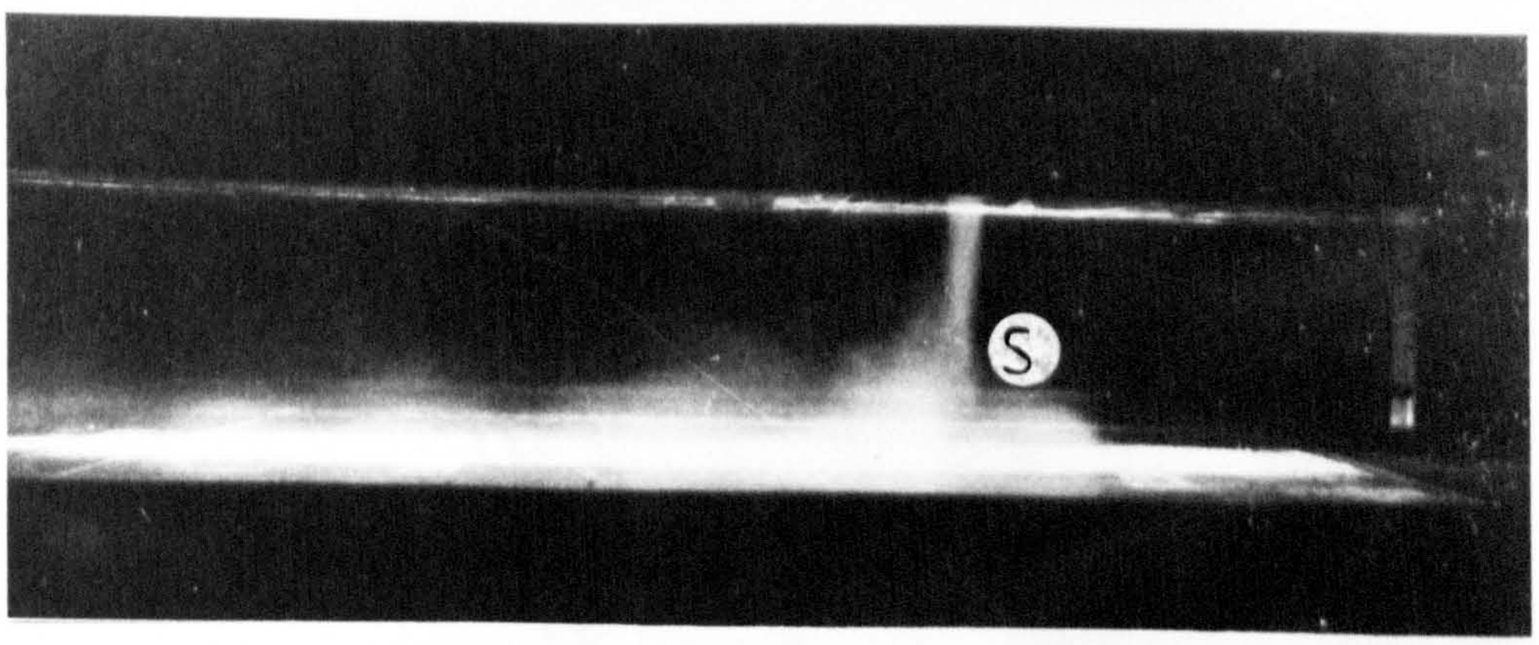

10.9

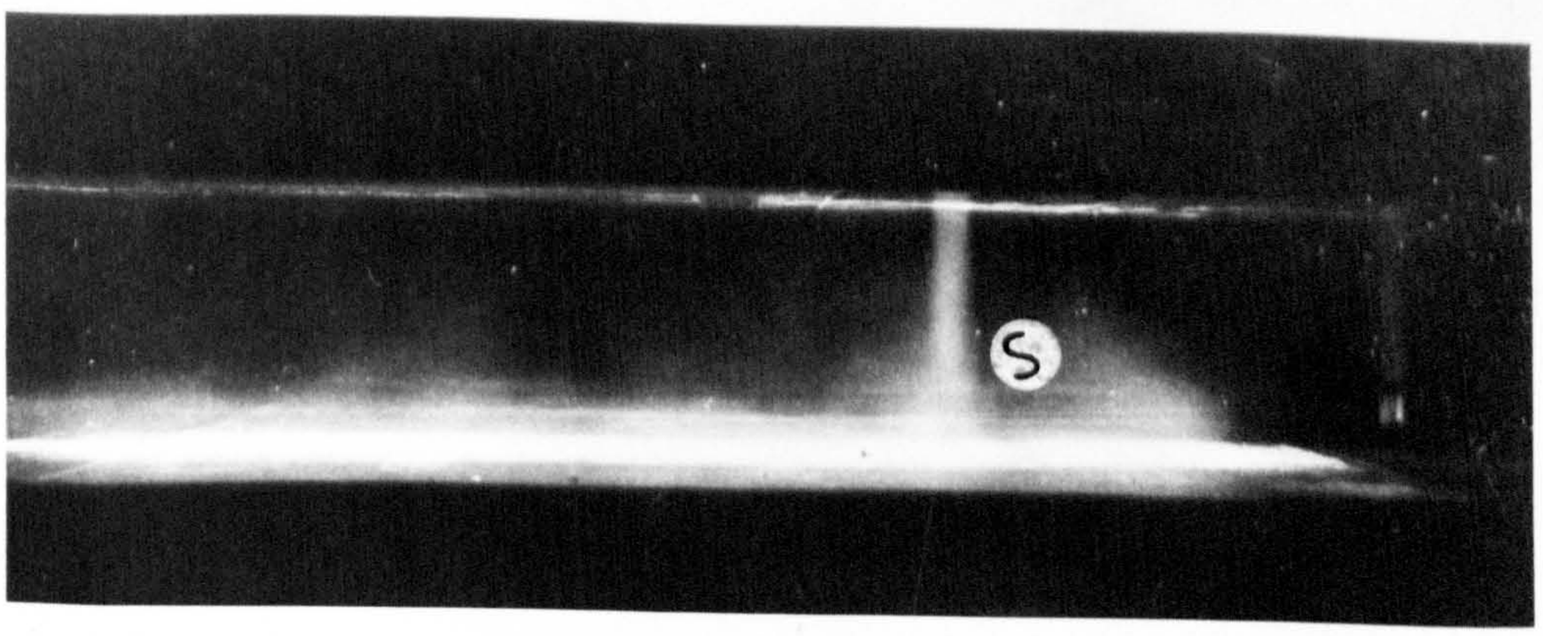

20.9

FIG.9.5.1 EFFECT OF JET-TO-CROSS FLOW VELOCITY RATIO ON THE STRUCTURE OF A CIRCULAR JET IN CROSS FLOWS.

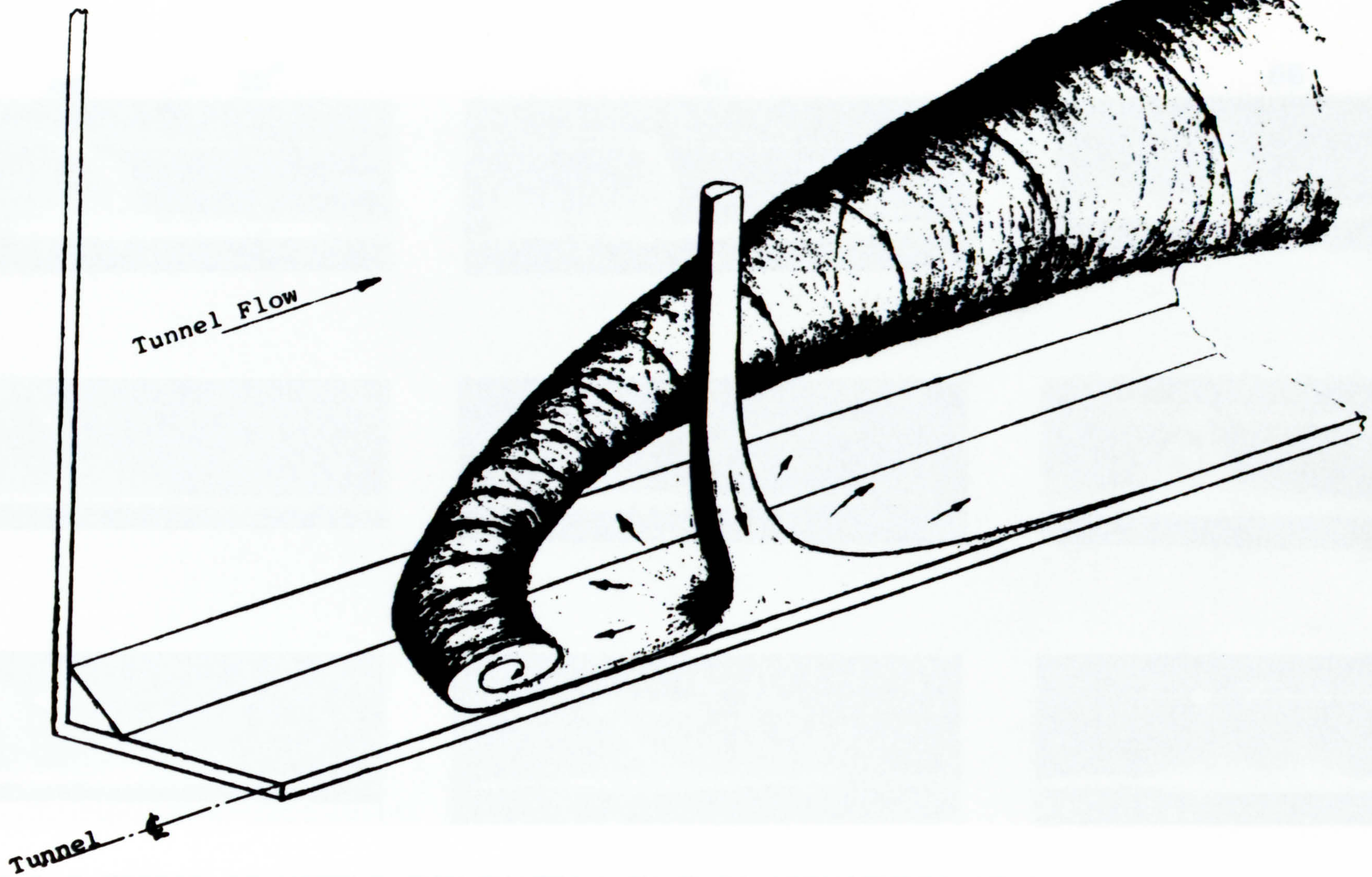

FIG. 9.5.2 SCHEMATIC REPRESENTATION OF A CIRCULAR JET IN A CROSS FLOWING STREAM - SITUATION WITH VORTEX FORMATION (REF 122).

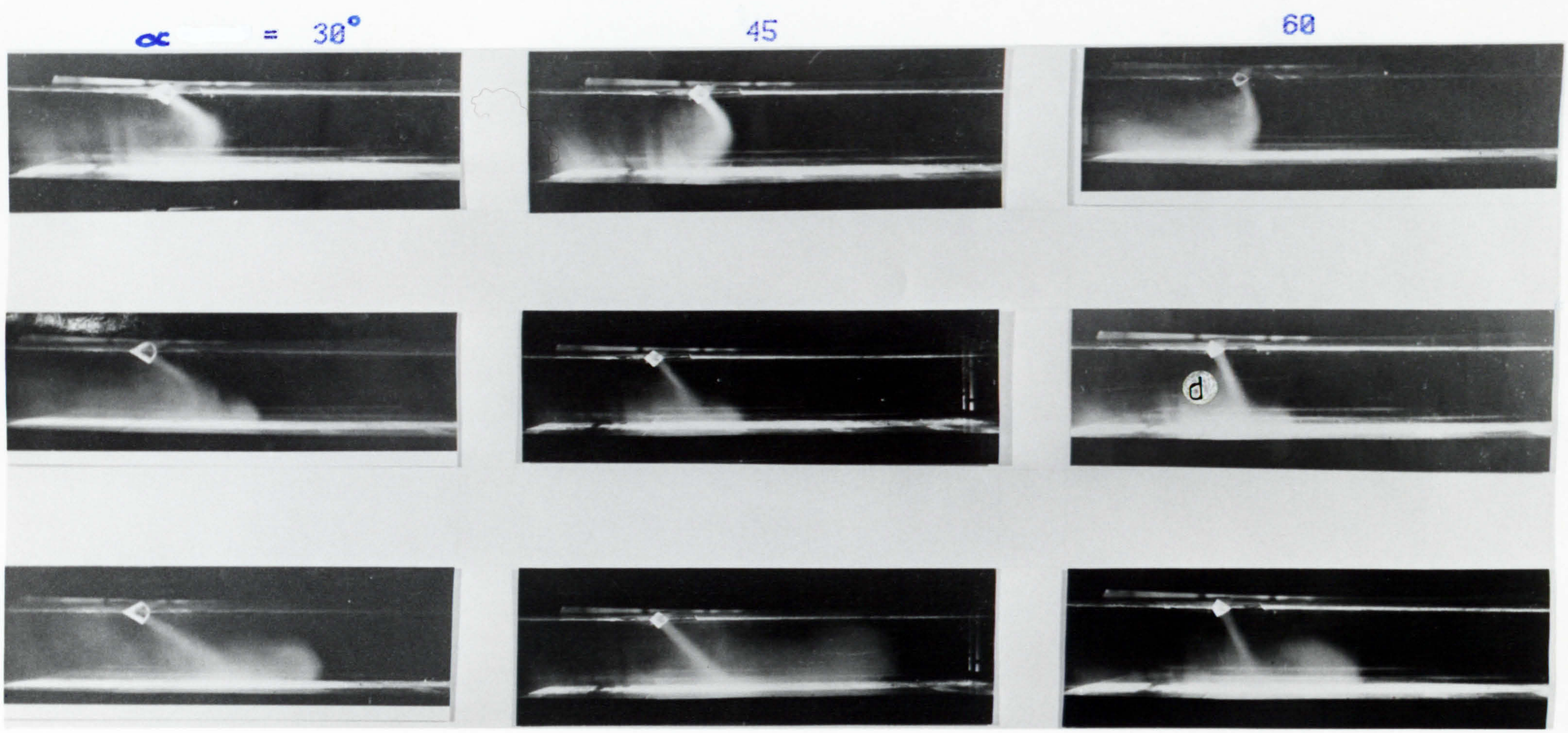

FIG 9.5.3 EFFECT OF NOZZLE INCLINATION ON FLOW STRUCTURES OF A CIRCULAR JET IN CROSSFLOWS

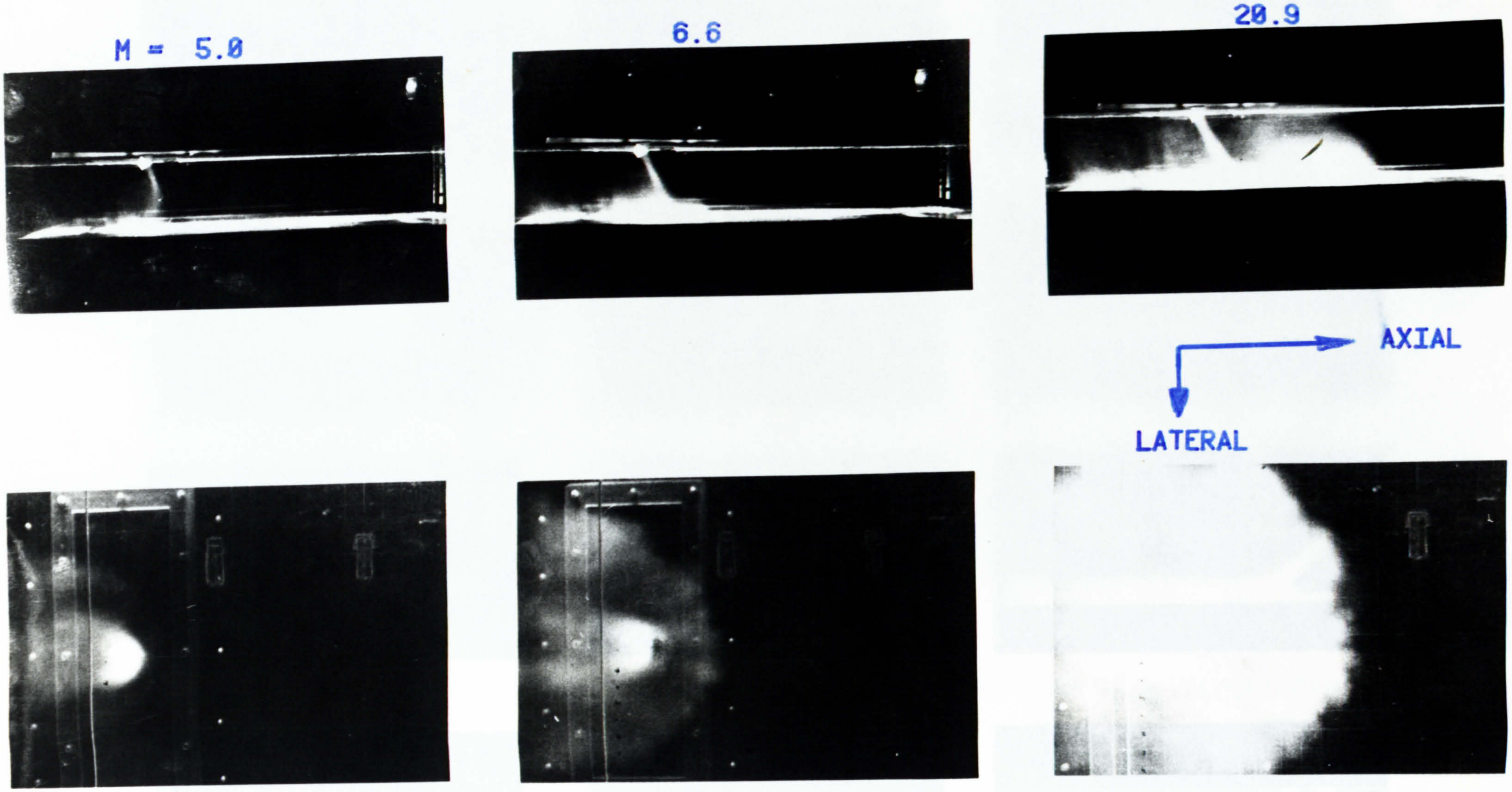

FIG. 9.5.4 THE EFFECT JET-CROSSFLOW VELOCITY RATIO ON THE FLOW OF AN INCLINED JET.

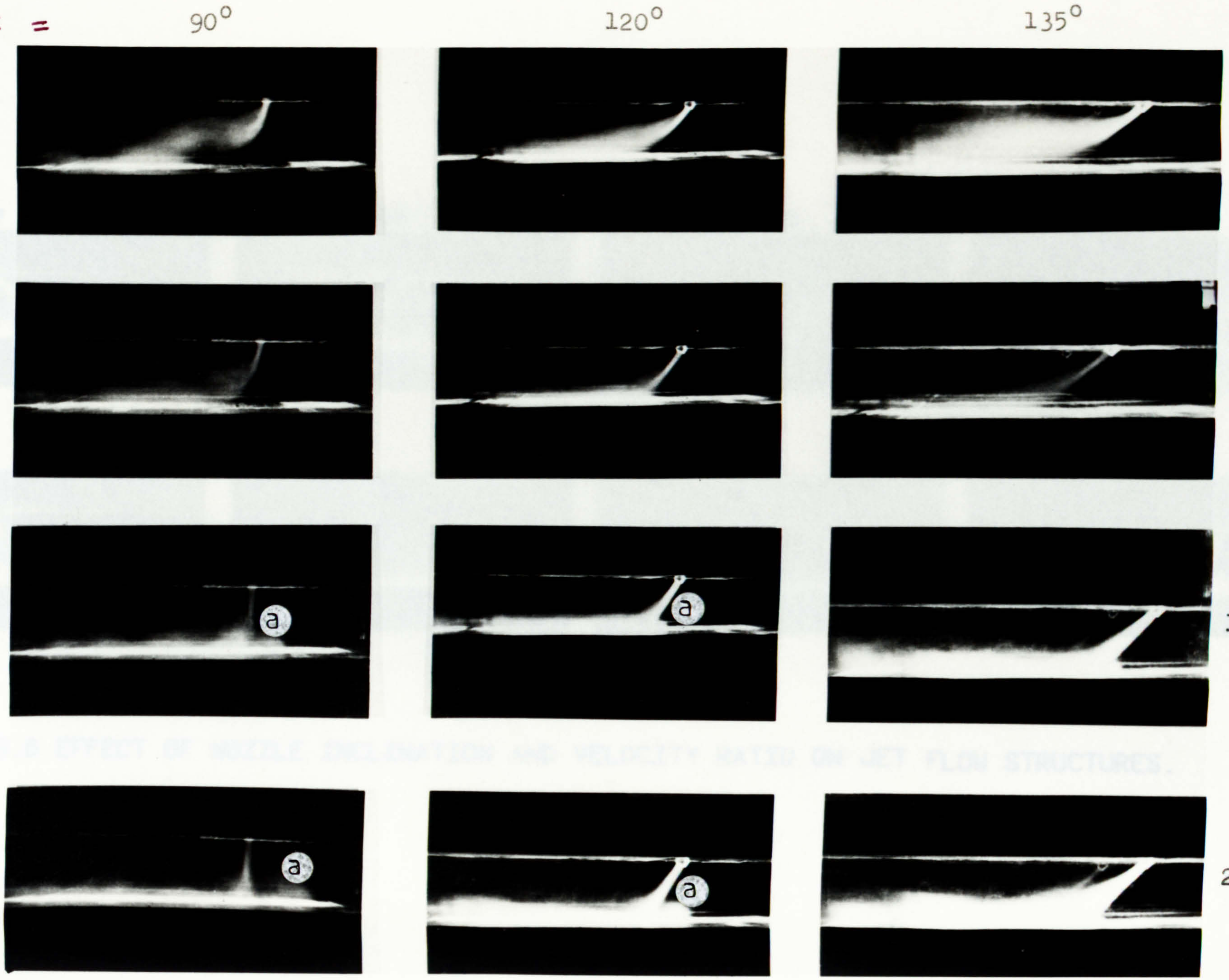

FIG.9.5.5 EFFECT OF NOZZLE INCLINATION ON JET FLOW STRUCTURES.

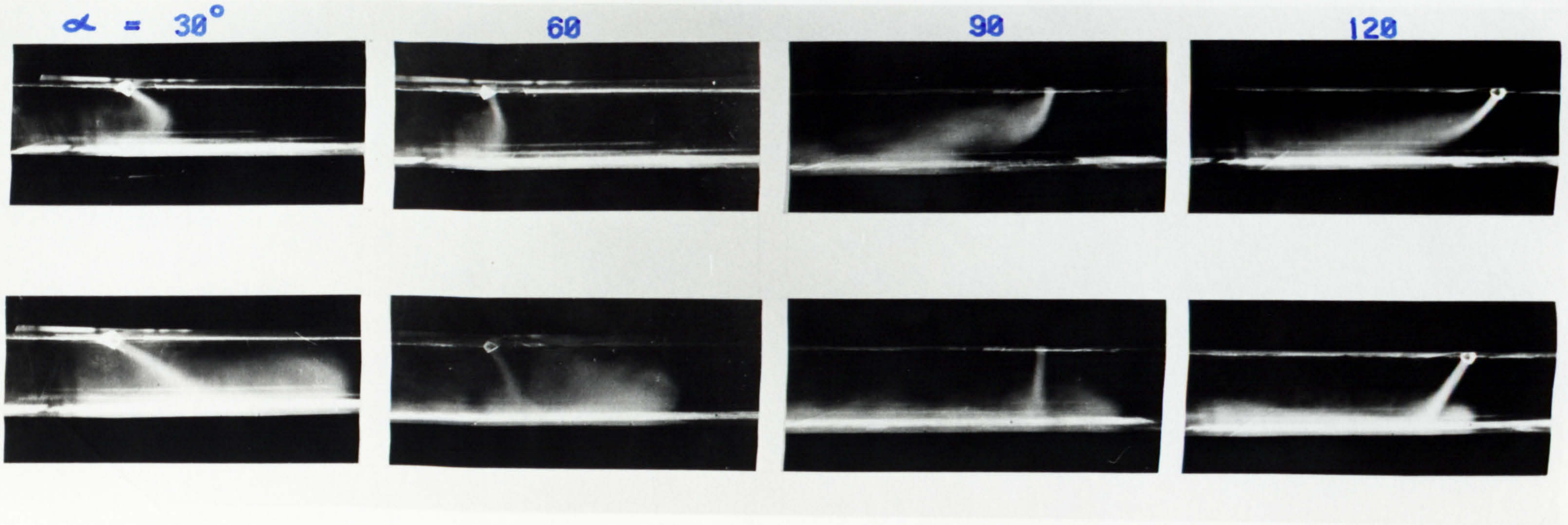

FIG. 9.5.6 EFFECT OF NOZZLE INCLINATION AND VELOCITY RATIO ON JET FLOW STRUCTURES.

CHAPTER 10

10. HEAT TRANSFER - MEASUREMENTS AND RESULTS

10.1 INTRODUCTION

The heat and mass transfer measurements obtained for turbulent jets issuing into cross flows are presented and discussed in this chapter. The parameters studied include the nozzle inclination (α), the jet-to-cross flow velocity ratio, $M(\equiv U_j/U_c)$ and the nozzle shape. In addition, the effect of "duct width" (H/d) was investigated for initially orthogonal jets. Thus, a total of 57 tests are reported and these were all carried out at a fixed Z/d of 6.

In these "cross flow" tests, the initial naphthalene clearance can be determined visually so that a laser system was not employed to determine the stagnation coefficients. The mass transfer test procedure is similar to that described for an unconfined jet in Chapter 6 and the details of the rig were presented in Chapter 9. Nevertheless, for completeness, the sequence of the experimental procedure in the cross flow tests is briefly described in the following section.

10.2 EXPERIMENTAL PROCEDURE

The nozzle was fixed to the appropriate carrier plate and the complete unit was mounted on the roof of the test chamber. The nozzle inclination was then checked with a combination set. The air flow rates were adjusted until the required velocity ratio was obtained and the air temperatures were maintained within 0.5^{o}C of each other and the ambient by means of the coolers. The test rig was then run for at least 45 minutes to obtain near steady state conditions.

The test plate was degreased, polished and sprayed with a thin film of naphthalene in a similar fashion to that described in Chapter 6. The coated calibration slides were weighed and the test plate was slid into position at the base of the duct before commencement of the mass transfer test. The exhaust air from the duct was discharged to outside the laboratory. Any build-up of naphthalene vapour in the ambient surrounding was thus prevented so that the bulk naphthalene vapour concentration was negligible in the test section.

The time and position of the initial naphthalene clearance were recorded and clearance patterns were mapped on the test plate at regular intervals. The complete duration of each test varied from 1½ to 3 hrs. During this period, the air temperature in the test duct was measured with a digital thermometer at intervals of 15 to 20 minutes. The mean of the corresponding vapour pressures was used in the

subsequent calculation of the mass transfer data. Corrections were made for free convective losses. These were converted to heat transfer rates by invoking the Chilton-Colburn analogy. A typical calculation procedure is presented in Appendix A.4.

10.3 HEAT TRANSFER RESULTS AND DISCUSSION

10.3.1. Effect of Duct Width (H/d)

The width of the test section was varied in these tests in order to obtain flows somewhat representative of those occurring with rows of jets of differing pitch. It is, however, pertinent to mention that in the current situation, the presence of the side walls imply that the velocity is zero at the position which corresponded to the mid-way point between adjacent jets in a row. This is obviously a different boundary condition to that in multiple jet systems.

Contour plots of heat transfer are presented initially because they cover the whole flow field and can thus assist in understanding the complicated flows. These contours are presented as h/h_{max} (where h and h_{max} are respectively the local and maximum heat transfer coefficients for a particular test). Fig.10.3.1. depicts the profiles of heat transfer (orthogonal impingement) at various duct widths and for jet to cross flow velocity ratios of 20.9, 10.9, 6.6 and 5.0. From the two columns on the left hand side, it may be observed that for $H/d<16$, the $h/h_{max} = 0.3$ does not form a closed profile. This may be attributed to interference of the flow with the bounding walls. From the results of a flow visualization study, Bouchez (Ref.25) found that the duct width should be at least 16 nozzle diameters in order that the wall effect may be negligible.

The horse-shoe or kidney-shaped contours typical of a circular jet in a cross flow are noticeable at all blockage ratios in the first two columns. As the jet emerges from the nozzle, turbulent mixing and entrainment develop around the edges of the jet and this creates a large velocity gradient across the jet. As the mainstream exerts pressure, the periphery of the jet is deflected and acquires a characteristic kidney shape. In the third column, the horse-shoe shape is however formed only at H/d of 8 and 12. A comparatively high heat transfer contour is also apparent upstream of the jet at these small duct widths. This contour may well be associated with the changes in the flow which occur as the strong cross flows try to by-pass the jet. It is also worth mentioning at this point that due to the retarding effect of the wide walls, the effective duct width is smaller than that implied solely by H/d. In the fourth column, complicated flows can be noticed at H/d of 8 and 12 but the kidney shape is only associated with the former duct width.

Figure 10.3.2. presents the effect of H/d on the maximum Nusselt numbers for an orthogonal circular jet in cross flow. As expected, higher maximum heat transfer is obtained for a jet without cross flow but the magnitude decreases as the duct width is reduced. Gardon and Akfirat (Ref.103) and Koopman and Sparrow (Ref.66) found small increases (<2%) in the maximum heat transfer as the nozzle spacing increased from 2 to 4 and 4.0 to 6.67 respectively. In both studies, however, the local variations in heat transfer significantly reduced as the nozzle spacing increased.

It can be seen that for M<10.9, the stagnation point heat transfer reduces as the duct width is increased in contrast to the situation for no cross flow and M=20.9. An examination of Figs.10.3.1 and 10.3.2 appears to indicate that with high cross flows (M<6.6) and high duct widths (H/d>16), the jet is diluted (by the entrainment of the cross flow) to such an extent that the vortex normally found in the lee of the jet disappears. A consequence of this dilution is that the maximum heat transfer is reduced over that for small duct widths where the cross flow is prohibited from diluting the jet and vortex.

It is noticeable in Fig.10.3.2. that the dependence of the maximum heat transfer on duct width is very slight when H/d>16. This supports the observation made in the contour plots and is also in agreement with Bouchez's observation.

Figure 10.3.3. illustrates the displacement of the stagnation point from the nozzle centreline at various duct widths. From Figs.10.3.2 and 10.3.3, it can be seen that for any particular velocity ratio, greater displacement is associated with lower heat transfer. It can be noticed in Fig.10.3.3 that at M=20.9, impingement almost occurs on the jet axis and this shows that at this low cross flow, the flow is comparable to that of a free jet. For M<6.6, the displacement reduces as the duct width is decreased. The displacement at M=10.9 does not however follow either of these trends and may therefore be regarded as a 'transition' velocity ratio. The present data are compared with those of Susec and Bowley (Ref.35) and the two are in generally good agreement.

Figure 10.3.4 shows the effect of jet-to-cross flow velocity ratios on Nusselt number and it can be seen that for a particular duct width, the heat transfer increases as the velocity ratio is increased i.e. as the jet flow becomes stronger. For M>10.9, the cross flow is too weak to significantly affect the jet flow and therefore impingement occurs close to the nozzle centreline with a high heat transfer rate.

There appears to be no previously published information on the effect of duct width on local heat transfer so that direct comparisons with the present data are not possible.

A somewhat relevant study is that of Metzger and Korstad (Ref.24) who investigated the effects of various nozzle spacings of circular jets in cross flow. It was found that as the spacing increased from 3 to 5, the average heat transfer in the upstream increased by approximately 25% and vice versa for the downstream. Their observation implies that as the nozzle spacing decreases, jet deflection is intensified with a corresponding reduction in the heat transfer rate. It must be mentioned, however, that in their tests, the cross flow to jet mass flow rate ratio ($\rho_c A_c U_c / \rho_j A_j U_j$) was employed in contrast to the velocity ratio (U_j/U_c) used in the present investigation.

Figures 10.3.5 to 10.3.8 depict the variation of Nusselt number along the line of symmetry (i.e. the centre line of the duct). It is noticeable that for all H/ds, upstream degradation of heat transfer increases as the velocity ratio is decreased. This may be attributed to the higher pressure forces exerted by the cross flow on the jet so that the jet flow is subsequently "pushed" downstream causing skewness in the local heat transfer distribution.

It can be observed that at M=5, the cross flow is more severe on the variation of heat transfer with H/d=26 than at H/d=8. See, for example, the fairly uniform variation of heat transfer with H/d=26 at M=5. At the greater duct width, the cross flowing stream 'blows' the jet downstream and the heat transfer rates on the impingement line approach a common value. However, at H/d=8, it seems that the cross flow is prevented from diluting the jet due to interference caused by the bounding walls.

To summarise the above discussion, the flow pattern appears to be significantly affected by varying the width of the test section and this is particularly pronounced at the lower duct widths (i.e.H/d<12). Accordingly, the variation of local heat transfer is strongly affected. It seems, therefore, that the velocity ratio as well as the duct width determine the characteristics of a circular jet in a cross flowing stream. The ensuing measurements were thus undertaken at a duct width (H/d) of 26 to ensure that wall interference did not affect the variation of convective transport coefficients.

10.3.2. Effect of Nozzle Shape

It was reported in Chapter 7 that the nozzle shape (e.g. elliptical and circular outlets) had a negligible effect on the convective transport coefficients for turbulent jets in nominally stagnant surroundings. A further investigation was carried out to determine the effect of the outlet geometry for jets in confined cross flows.

Figure 10.3.9 presents the effect of jet-to-cross flow velocity ratios on the maximum heat transfer coefficients for both circular and elliptical nozzles inclined at 60^{o}

and 120°. The results for an orthogonal jet are also included. It can be observed that at M=20.9, the heat transfer rates are in good agreement (see also Fig.10.3.10). At this velocity ratio, the cross flow is weak and thus the heat transfer rates at 60° and 120° are virtually the same. As the cross flow is increased, the heat transfer rates for the elliptical nozzles are lower than those associated with the circular jets. Moreover, the higher transfer rates occur when the jet is inclined into the cross flow.

Figures 10.3.11 and 10.3.12 depict the contours of local heat transfer coefficients, h/h_{max}. It can be seen that the jets issuing from the elliptical nozzles experience greater deflections downstream than the circular jets (compare the last two columns of Fig.10.3.11). The elliptical nozzles were machined flush to the carrier plate and the initial region of the jets are thus more easily deflected with corresponding reduced heat transfer. Furthermore, at all jet-to-cross flow velocity ratios, the characteristic horse-shoe shape can be noticed in the core of the profiles for the circular jets. The elliptical jets however exhibit this phenomenon only at $U_j/U_c>10.9$.

All other mass transfer tests in the present study were carried out with jets exiting from circular nozzles.

10.3.3 Effect of Nozzle Inclination

1. Variation of maximum heat transfer rates

Figure 10.3.13 presents the effect of nozzle inclination on the maximum heat transfer coefficient at various jet-to-cross flow velocity ratios. At all nozzle inclinations, the heat transfer rate decreases as the velocity ratio is reduced. This can be attributed to an increase in the pressure force of the cross flow which often inhibits penetration of the jet into the mainstream.

At M=20.9, interaction between the two flows is not severe so that the heat transfer variation is comparable to that for the corresponding oblique jets in stagnant surroundings. Thus, as α is reduced, the heat transfer decay is initially gradual (i.e. up to $\alpha=60^{\circ}$) but subsequently decreases rapidly. It can be seen that the variation of heat transfer for M=10.9 is qualitatively similar to that for M=20.9 although the heat transfer coefficients in the former case are obviously lower because of the increased kinetic energy of the cross flowing stream. The flow visualization data (see Fig.9.5.3) illustrate the greater jet penetrations at M=20.9 in comparison with those at M=10.9.

At M=6.6, the stagnation point heat transfer coefficient gradually increases from the orthogonal impingement value to a maximum at a nozzle inclination of 60° and then reduces subsequently. It may be deduced from the results of Kabari (Ref.36) that inclining the nozzle is beneficial and also

the data of Jackson (Ref.37) actually indicated that the maximum heat transfer rate increased as α was reduced. The present data indicate an optimal inclination, α, of 60^{o}. The phenomenon can only be explained by flow visualization study during which it was observed that interaction between the two flows produced more turbulence at 60^{o} than at other nozzle inclinations. An inspection of the jet structure in Figs.9.5.1 and 9.5.3 shows that at M=6.6, the cross flow distorts the streamlines of the orthogonal jet more than those in the corresponding jet from 60^{o} nozzle. Thus, in the former case, the impingement point is displaced further downstream of the jet centreline.

At M=5.0, a similar phenomenon is recorded. Quantitatively the heat transfer rate at 60^{o} reduced by 41% (when referred to the value without a cross flow) whilst the value for orthogonal impingement decreased by 67%. The severity of the cross flow effect can be seen in Fig.9.5.3. where the jet from the 60^{o} nozzle has been pushed much further downstream at M=5.0 than at M=6.6. However, the situation is even worse for the initially orthogonal jet since this has been partly lifted up from the target surface at the high cross flow. The stagnation point heat transfer rate at a nozzle inclination of 45^{o} decreases only moderately (i.e. <30%) when the velocity ratio is reduced to 5.0 but at 30^{o}, a decrease of about 57% is apparent. This can only be explained by a very complicated flow interaction.

In the main, therefore, it is clear that the nozzle inclination affects the heat transfer capabilities of turbulent jets in a main stream in addition to the jet-to-cross flow velocity ratio.

Figure 10.3.14 illustrates the velocity ratio at which inclination becomes beneficial. The actual value at which this happens depends on α, the nozzle inclination, e.g. at $\alpha=60^{o}$, inclination is beneficial for M<8, whereas, at $\alpha=45^{o}$, the corresponding M is <6.2.

Figure 10.3.15 shows the variation of maximum heat transfer coefficients at nozzle inclinations of 90^{o}, 120^{o} and 135^{o}. The latter two geometries imply that the jets are inclined with the cross flowing stream and it can be observed that at all velocity ratios, heat transfer generally decreases as the nozzle inclination is increased. It can be noticed that at M=20.9, a difference of 20% approximately exists between the data at $\alpha=90^{o}$ and 135^{o}. However, at M=5, the difference is about 12%. Probably this variation can be due to 'impingement' occuring at 90^{o} for M=20.9 and lesser impingement at $\alpha=135^{o}$. However, at M=5, no impingement occurs at any angle so that the results are more or less the same.

The centre line of an isothermal free jet has been defined by several authors (e.g.Ref.31) as the highest dynamic

pressure line, whilst for a heated jet Kamotani and Greber (Ref.11) used the locus of maximum temperatures to define it. In the current study it is convenient to define the loci of maximum jet velocity as passing through the position of initial maphthalene clearance during a mass transfer test (i.e. the location of maximum convective transport coefficient). Fig.10.3.16 shows the displacement of the maximum heat transfer from the geometrical impingement point. The displacements at M=20.9 are similar to those obtained for turbulent jets in a stagnant surrounding and this implies that the cross flow effect is insignificant at this value. A comparison of Figs.10.3.13 and 10.3.16 shows that for any particular jet-to-cross flow velocity ratio, the maximum heat transfer occurs at the nozzle inclination where the displacement of the impingement point from the jet centre-line is a minimum. It may be concluded, therefore, that at all nozzle inclinations, the quantitative value of the heat transfer rate depends completely on the deflection of the jet by the cross flowing stream.

Both the magnitude and location of maximum heat transfer can usually assist in eliminating local hot spots in a jet impingement furnace. Using the centre-line of the orthogonal nozzle as reference, Fig.10.3.17 presents the effect of nozzle inclination on the location of maximum heat transfer. It is apparent that for all velocity ratios, the stagnation point moves upstream as α is reduced. Similarly, for all nozzle inclinations, the stagnation point shifts downstream as the jet-to-cross flow velocity ratio is reduced.

2. Variation of local heat transfer rates

Figures 10.3.18 and 10.3.19 present the variation of local heat transfer along the line of symmetry for various nozzle inclinations. For the orthogonal jet geometry, both the nozzle centre-line and direction of cross flow are shown to illustrate the effect of the mainstream on the characteristics of the circular jet. For example, both the downstream displacement and reduction of heat transfer are immediately evident. An inspection of the results for orthogonal jets with and without cross flow indicates that local heat transfer coefficients are higher in the upstream direction for the latter geometry, although this is reversed in the downstream locations. This upstream degradation is particularly severe as the jet-to-cross flow velocity ratio is decreased.

Cross flows partly destroy the symmetry of the local heat transfer. This asymmetry only starts at some distance away from the impingement point. For example, at M=20.9, the heat transfer rate is fairly symmetrical within $x/d=\pm 1.5d$ (i.e. about the nozzle centre) and thereafter the downstream values are higher than those or corresponding

upstream locations. However, for all velocity ratios, the variation of local heat transfer is skewed towards the downstream direction. These trends can be attributed to deflection of the jet by the cross flow. This blowing effect is particularly evident at M=5.0 where the distribution of heat transfer coefficient approaches a relatively constant value, see Fig.10.3.18(a). It can be seen that for M<10.9, local heat transfer rapidly increases from the upstream direction to its maximum value and subsequently decreases monotonically as x/d increases.

The results for the jet from the 60^{o} nozzle show similar phenomena to those of orthogonal jets. However, downstream enhancement of heat transfer is more pronounced in the former geometry and also the skewness is reduced for M<6.6. Furthermore, the jet penetrates farther upstream as α is reduced. This observation is in agreement with the flow visualization data.

It may be observed from Figs.10.3.20 and 10.3.21 that variations of heat transfer along the line of symmetry for 120^{o} and 135^{o} nozzles are similar to those associated with orthogonal jets although the angled jet results are obviously more displaced in the downstream direction.

A comparison of Figs 10.3.18 to 10.3.21 indicates that at low cross flows, the "orthogonal" nozzle produces the highest jet impingement heat transfer rates. However, at high cross flows, nozzle inclination becomes especially beneficial because the heat transfer rates are generally higher than those in the corresponding initially orthogonal jet situations. See, for example, the distributions for 60^{o}, 90^{o} and 120^{o}. This observations corroborates the flow visualizations.

The contours of heat transfer are presented in Fig.10.3.22 and the effects of nozzle inclination are clearly evident. At all velocity ratios, penetration of the jet into the cross flow increases as α reduces (see, for example, the profiles for the jets at M=20.9). At M<6.6, the contours at all nozzle inclinations are more compact on the upstream region than those on the downstream side so that a larger area of the latter zone is subject to a high heat transfer. At these low velocity ratios, the cross flow is sufficiently strong to inhibit jet spread in the upstream direction.

It is important to notice that at all velocity ratios, the inner core of the profiles for jets inclined at 45^{o} and 60^{o} are deformed to the characteristic kidney shape associated with a circular jet in a cross flowing stream. Although, no heat transfer profiles have been published, the temperature profiles of Kamotani and Greber (Ref.11) and pressure profiles of Jordinson (Ref.31) for orthogonal jets in unconfined situations display similar behaviour.

Figure 10.3.23 presents the normalised heat transfer profiles for $\alpha>90^{o}$. It is noticeable that for 120^{o} and 135^{o}, the contours are more compact on the upstream side than those on the downstream and the area covered by the profiles increases (mainly downstream) as the velocity ratio is reduced. This behaviour may be attributed to the system geometry because nozzle inclination in the cross flow direction exposes the jet more to the effects of the cross flow (jet deflection is aided by nozzle inclination with the cross flow) and this is corroborated by the flow visualization study (see Fig.9.5.5). The characteristic kidney shape completely disappears in the contours for both the 120^{o} and 135^{o} jets because the jets are easily blown downstream without the formation of recirculation bubble and vortices (i.e.impingement does not occur).

SUMMARY

The discussion in this Chapter may be summarised as follows:

1. It was found that cross flows usually reduced the maximum heat transfer rates. As the cross flow increased, the rates of heat transfer on the upstream decreased whilst those on the downstream section increased. This can be attributed to the flushing effect of the cross flow.

2. The heat transfer rates associated with a circular jet in cross flows were significantly affected by the size of the duct. At high cross flows, the maximum heat transfer increased as the duct width was reduced and vice versa at low cross flows. These effects indicate that interference between the jet and the cross flow is very complicated. It is thus essential that any quoted heat transfer rates for jets in cross flows should indicate the defree of confinement.

3. The circular outlet geometry of the nozzle,(rather than elliptical) produced higher heat transfer rates especially at high cross flows. Thus, it is important to define the exit conditions of an inclined jet.

4. Without cross flow, nozzle inclination was found to reduce the heat transfer rate and this may be due to the longer distance travelled by the jet as α was reduced. However in the presence of a cross flow, jet penetration into the upstream increased as α was reduced. Thus, the combined effect of cross flow and α produced optimal heat transfer at a nozzle inclination, α of 60^{o} and for $M<6.6$.

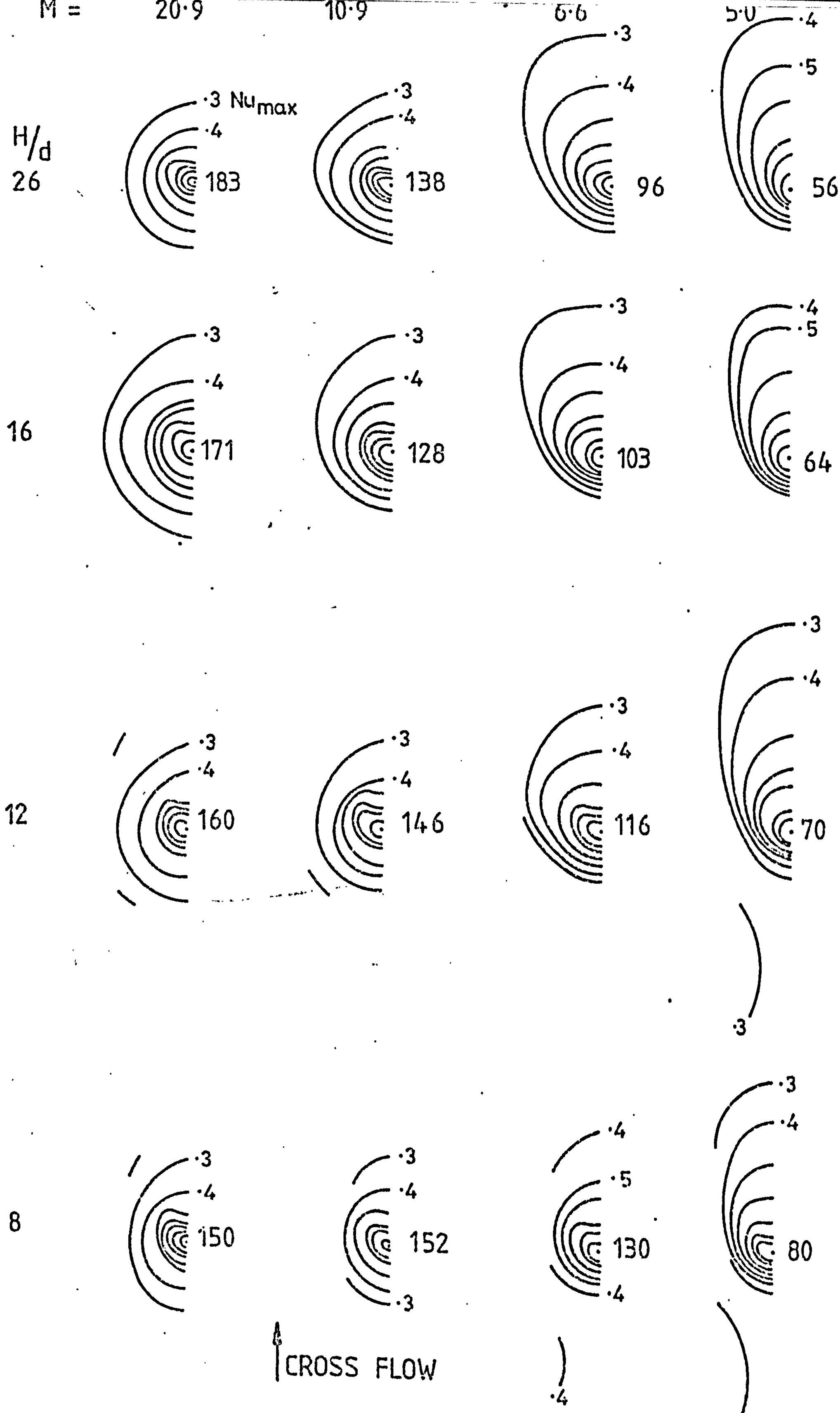

FIG. 10.3.1 EFFECT OF DUCT WIDTH ON HEAT TRANSFER

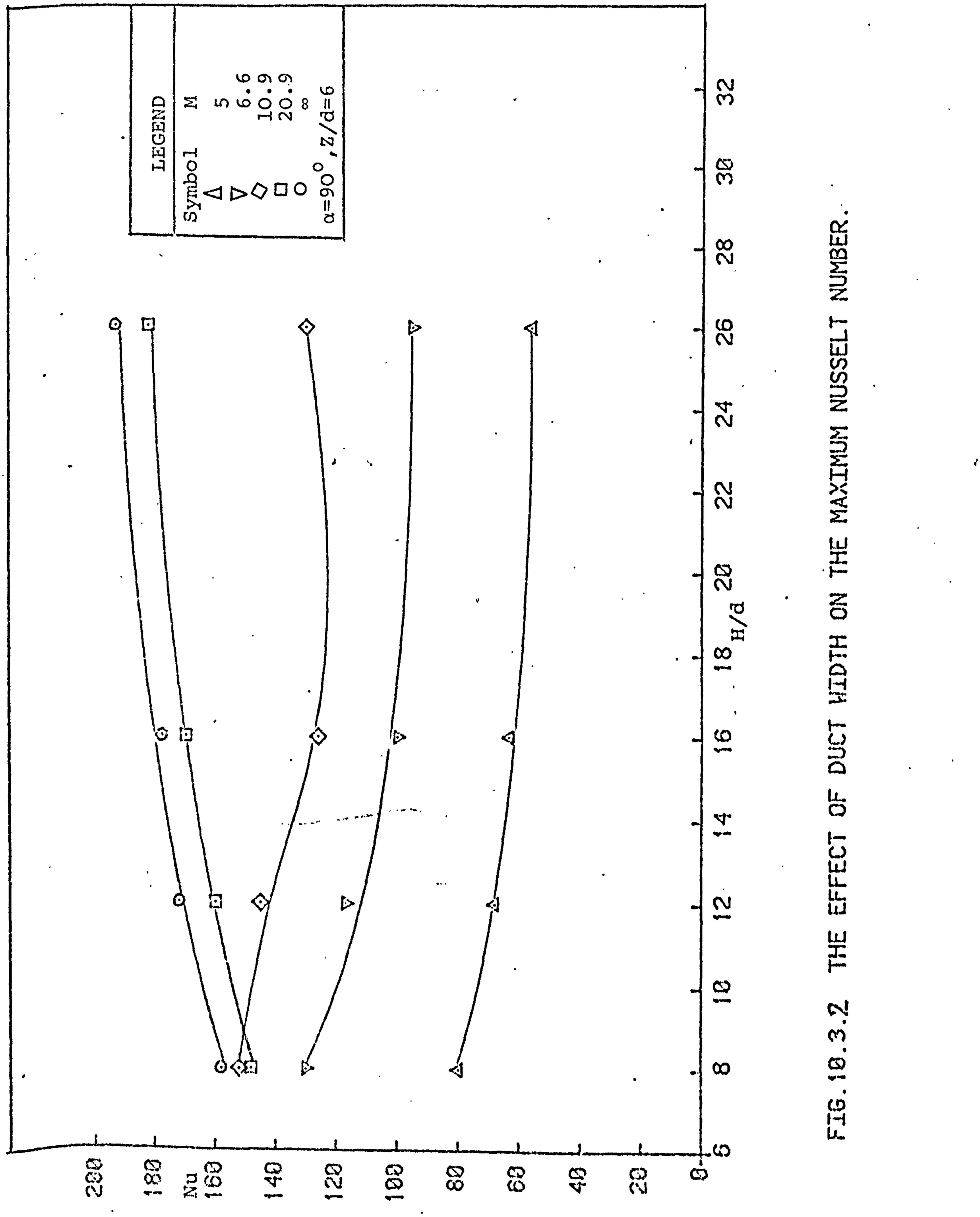

FIG. 10.3.2 THE EFFECT OF DUCT HEIGHT ON THE MAXIMUM NUSSELT NUMBER.

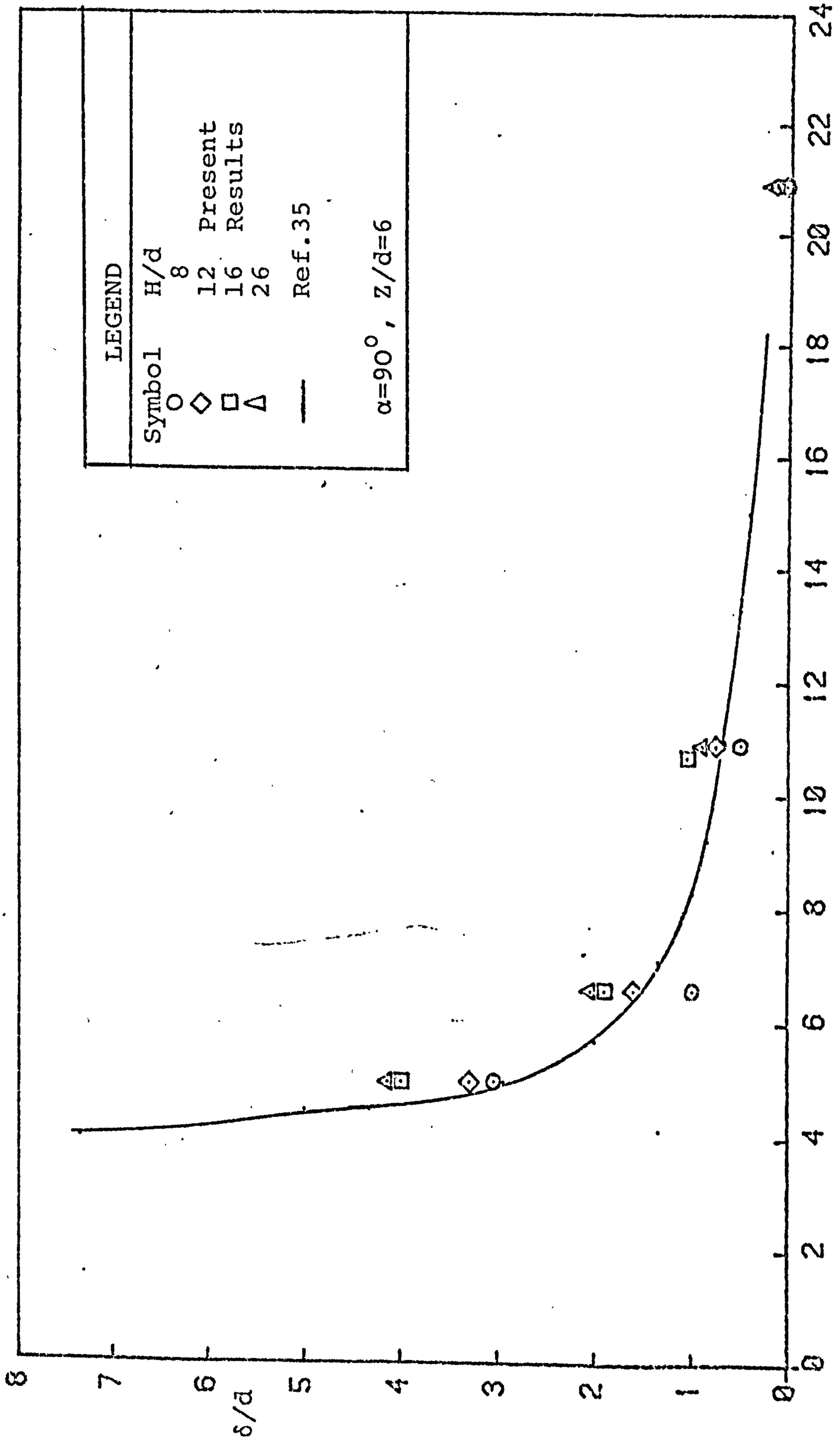

FIG.10.3 EFFECT OF JET-CROSSFLOW VELOCITY RATIO ON THE LOCATION OF MAXIMUM HEAT TRANSFER.

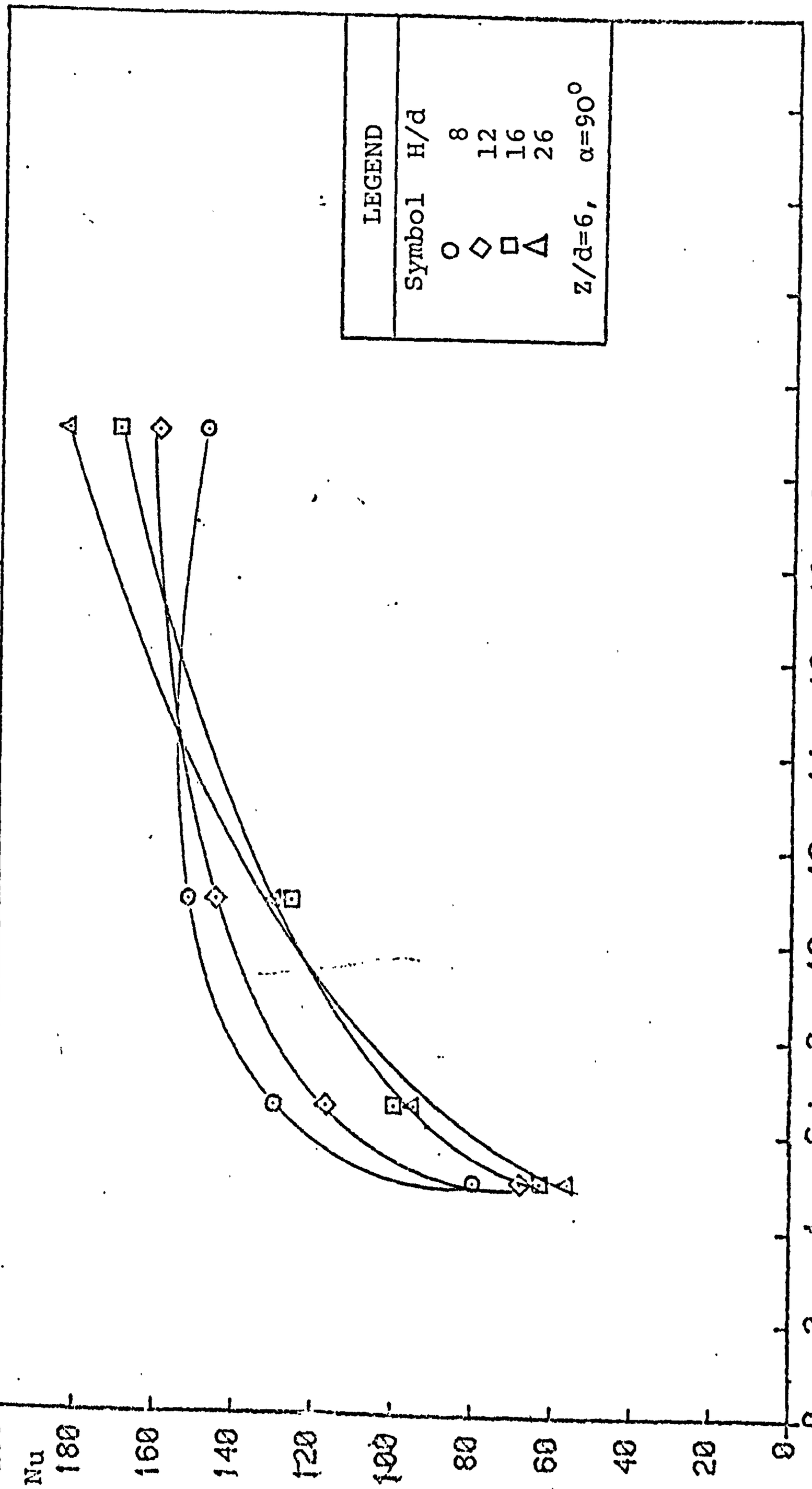
LEGEND
Symbol H/d
○ 8
◇ 12
□ 16
△ 26
z/d=6, α=90°
Nu
200
180
160
140
120
100
80
60
40
20
0
0
2
4
6
8
10
12
14
16
18
20
22
24
26
28
30
M
FIG.10.3.4 THE EFFECT OF JET-CROSS FLOW VELOCITY RATIO ON THE MAXIMUM NUSSELT NUMBER.

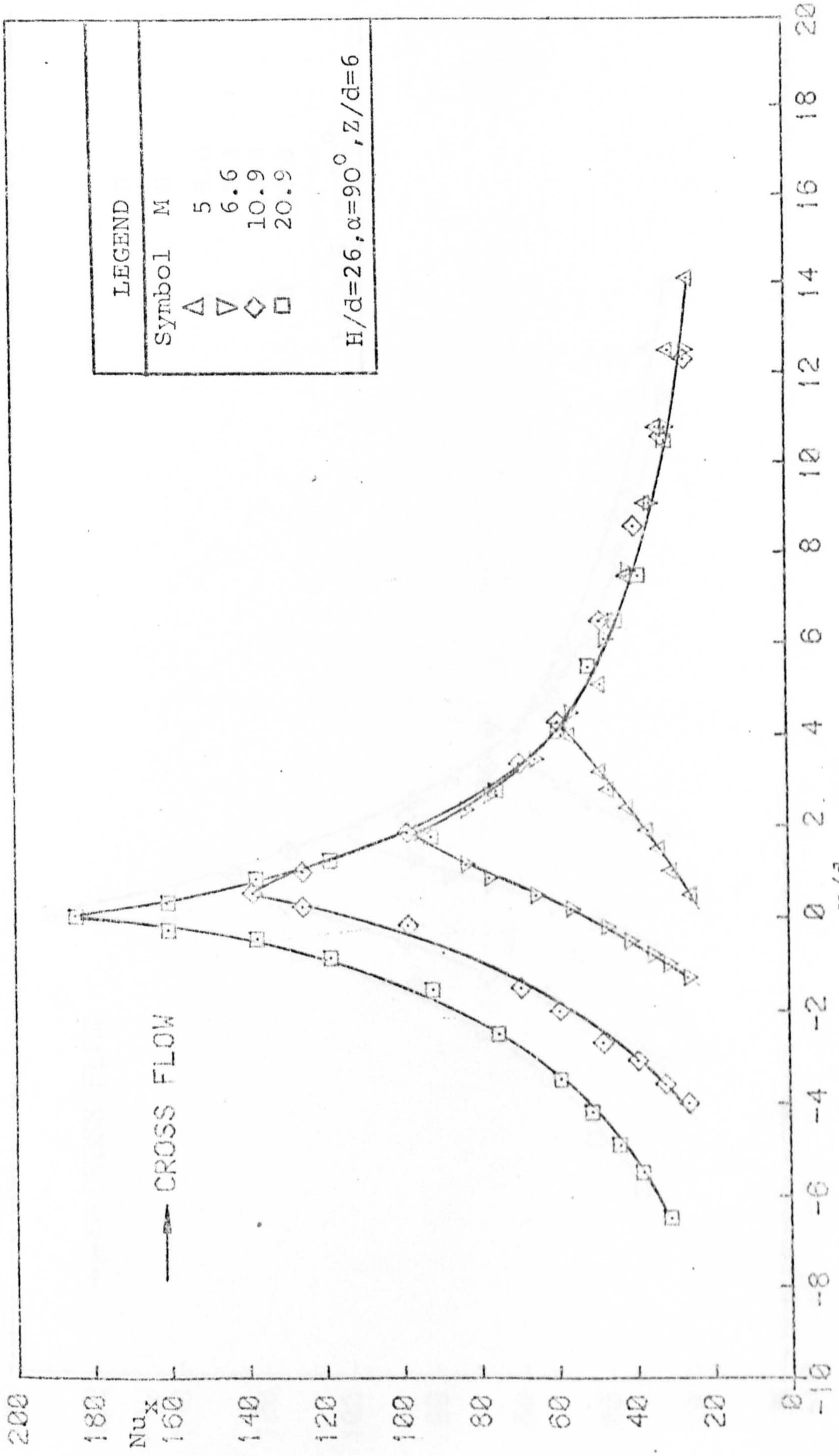

FIG. 10.3.5 VARIATION OF NUSSELT NUMBER ALONG THE LINE OF SYMMETRY (H/D=26).

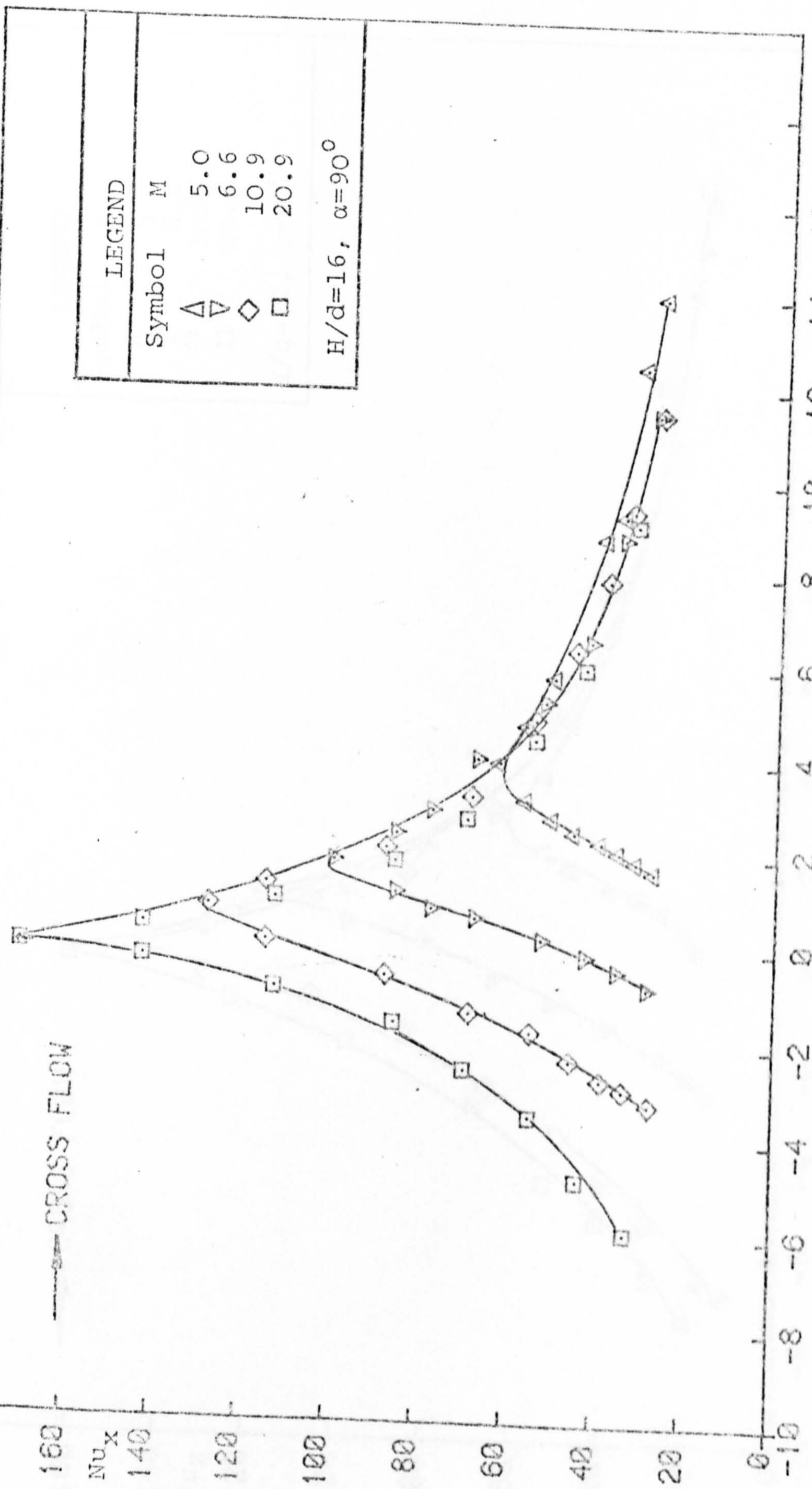

FIG. 10. 3.6 VARIATION OF NUSSELT NUMBER ALONG THE LINE OF SYMMETRY (H/D=16).

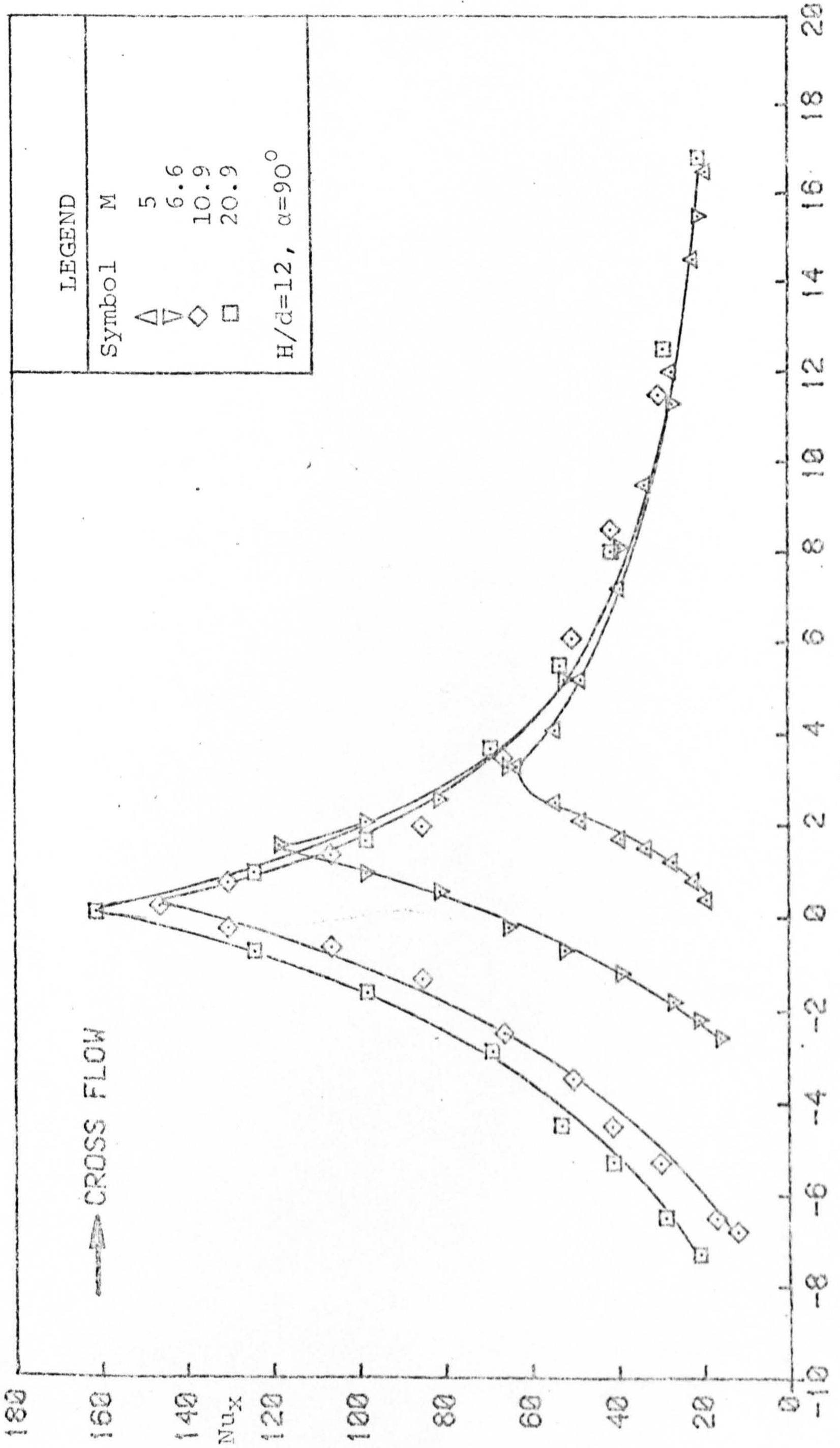

FIG.10.3.7 VARIATION OF NUSSELT NUMBER ALONG THE LINE OF SYMMETRY (H/d=12).

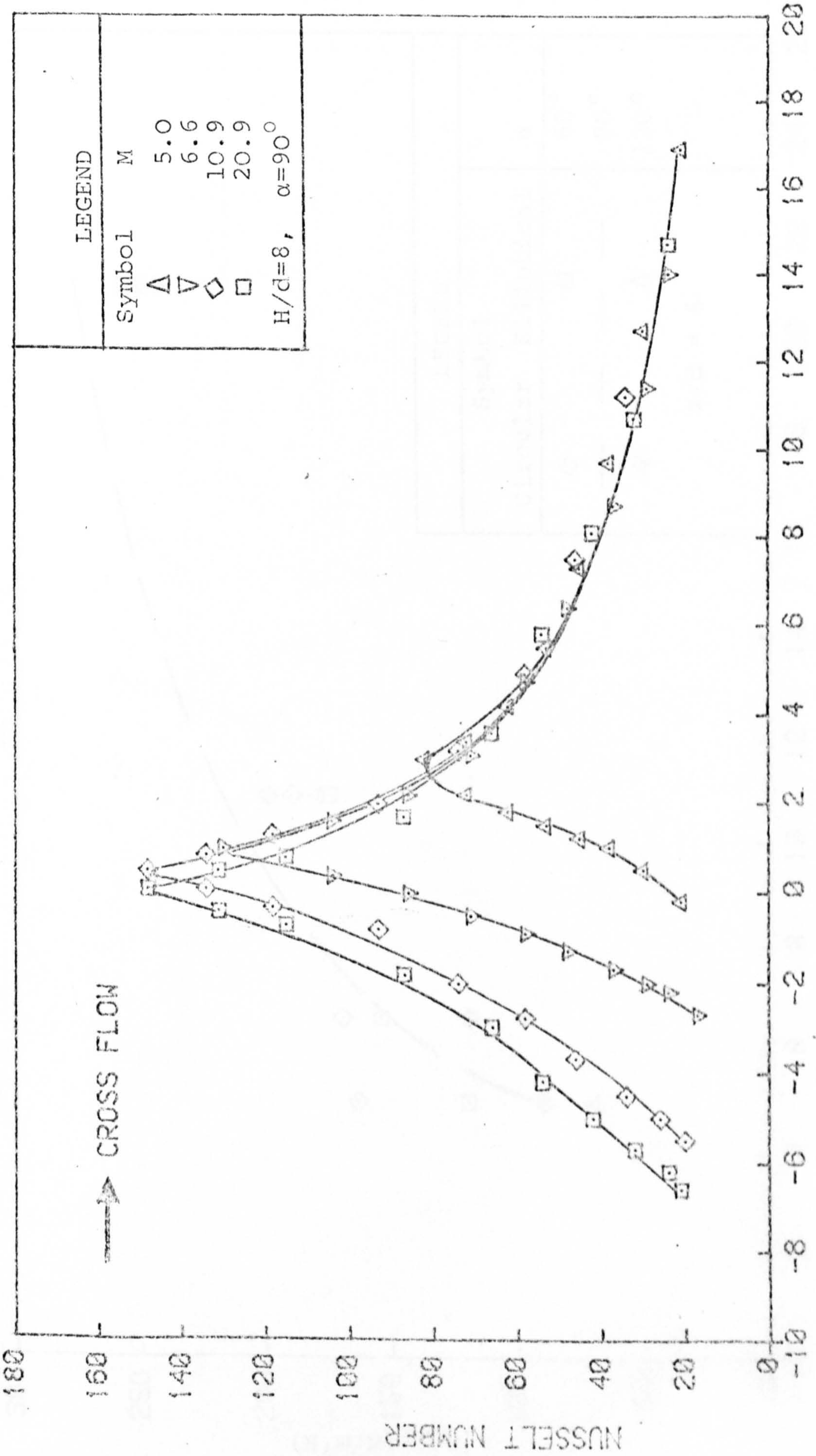

FIG. 10.3.8 VARIATION OF NUSSELT NUMBER ALONG THE LINE OF SYMMETRY

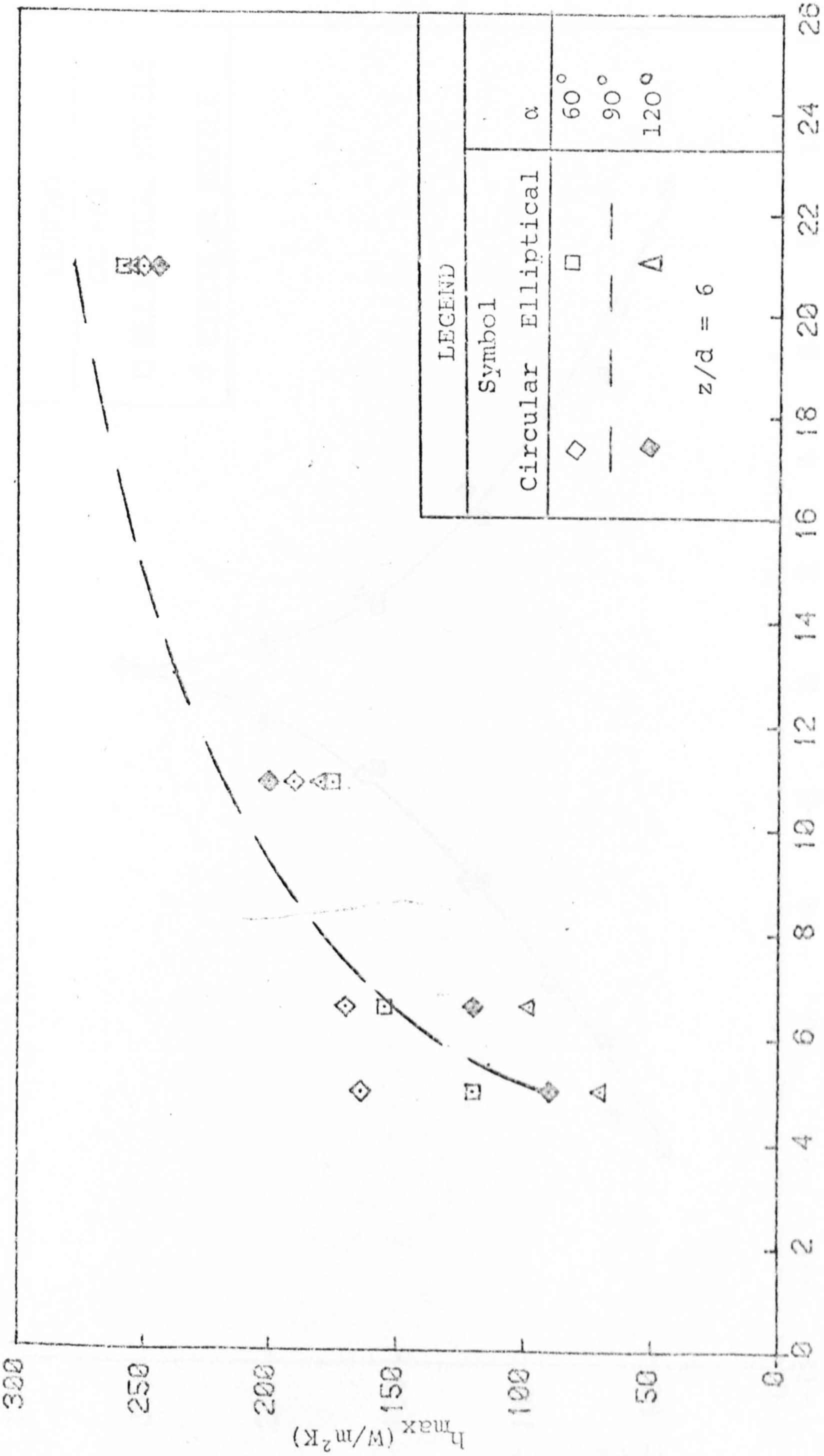

FIG. 10.3.9 EFFECT OF JET-CROSS FLOW VELOCITY RATIO ON MAXIMUM HEAT TRANSFER.

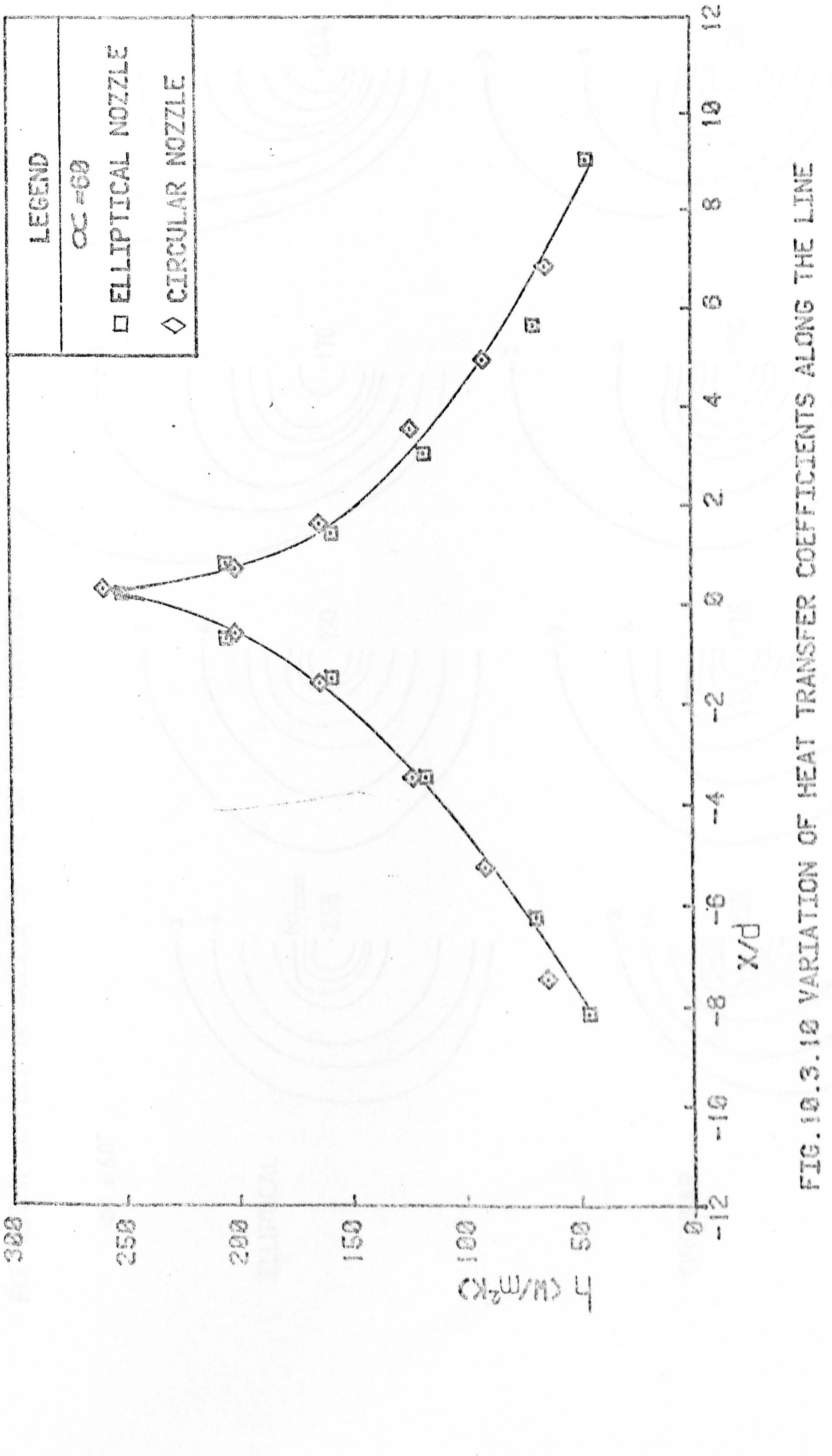
LEGEND
α =60
ELLIPTICAL NOZZLE
CIRCULAR NOZZLE
h (W/m²K)
X/D
FIG. 3.12 VARIATION OF HEAT TRANSFER COEFFICIENTS ALONG THE LINE OF SYMMETRY(M=20.9).

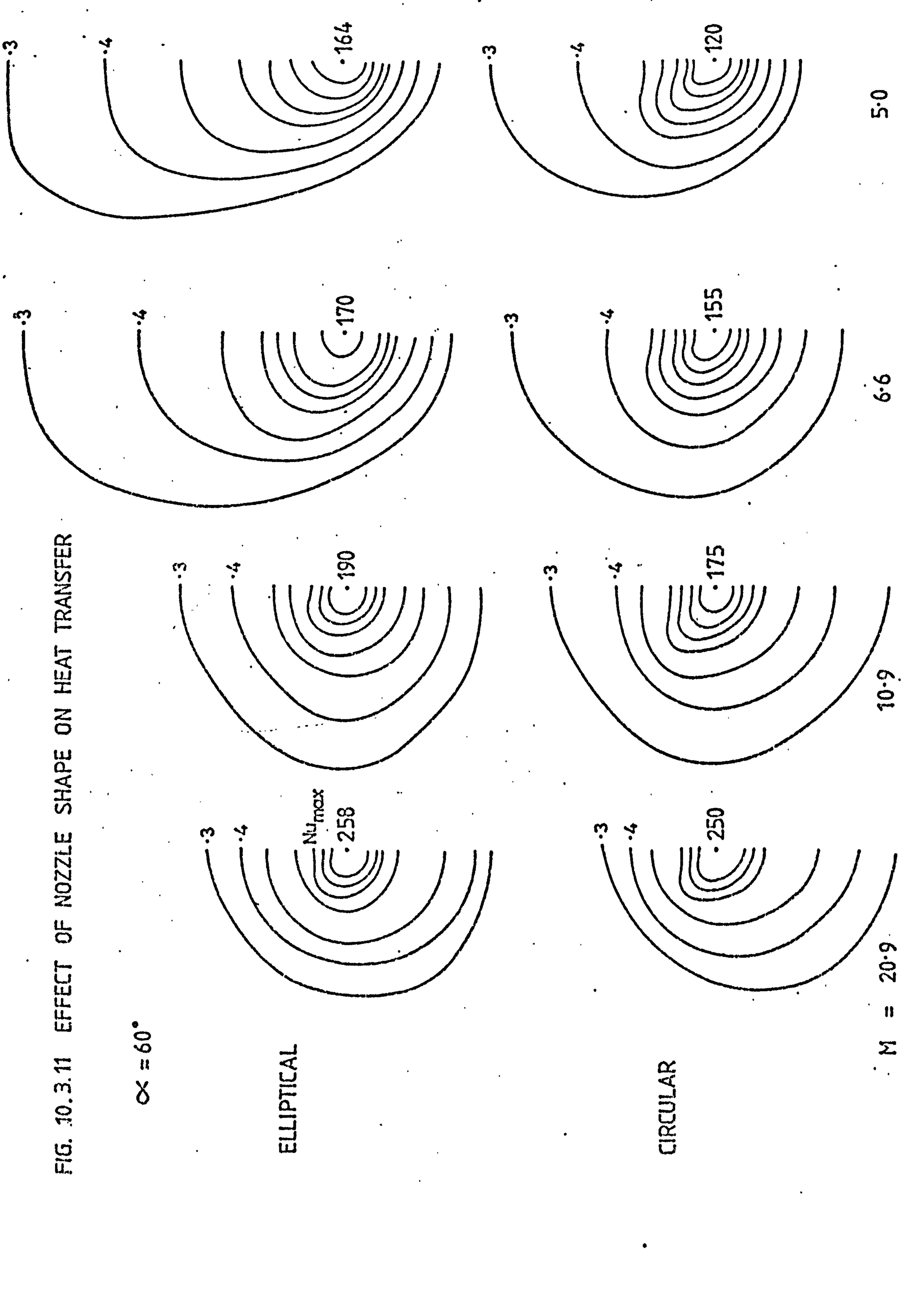

FIG. 10.3.11 EFFECT OF NOZZLE SHAPE ON HEAT TRANSFER

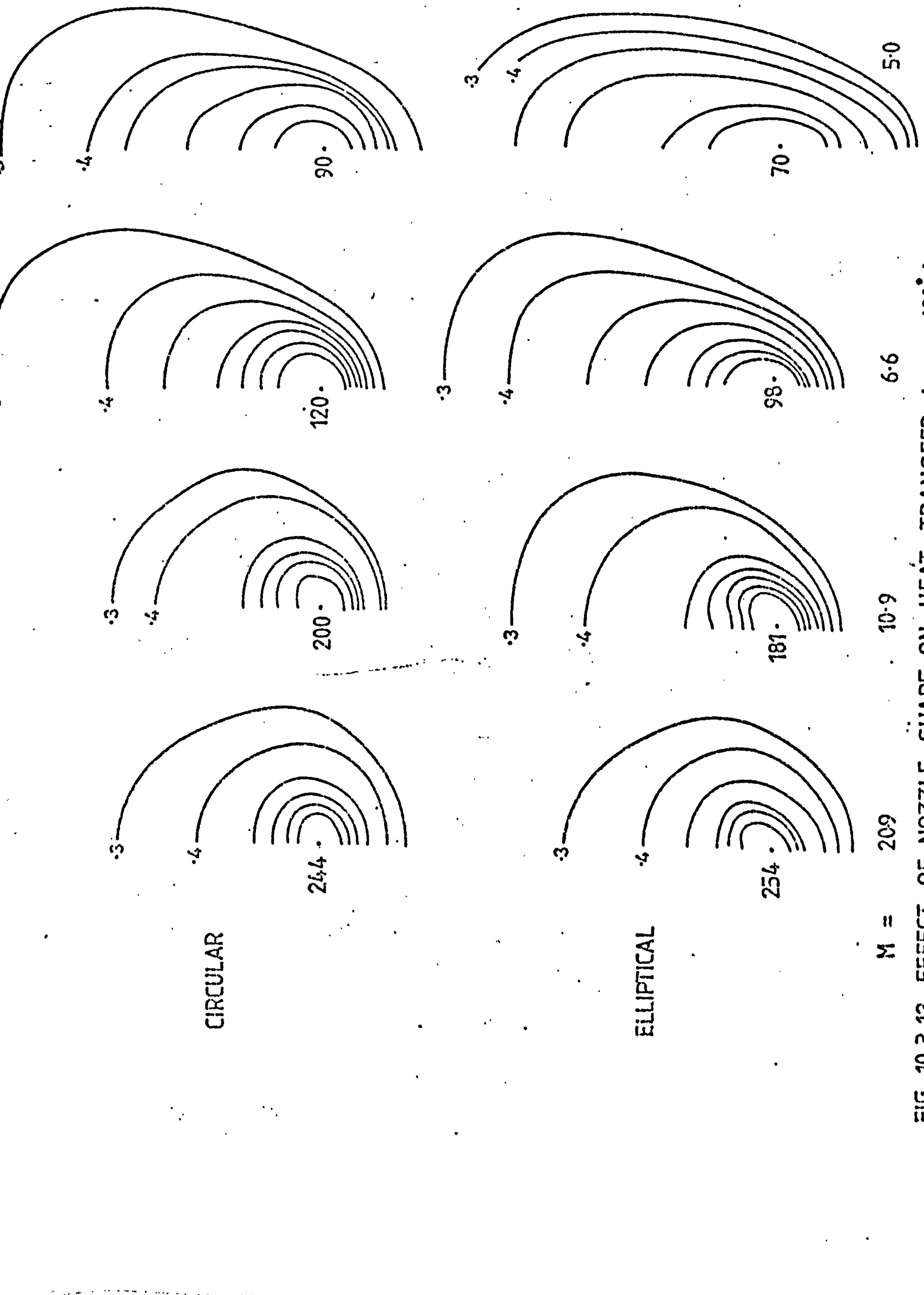

FIG. 10.3.12 EFFECT

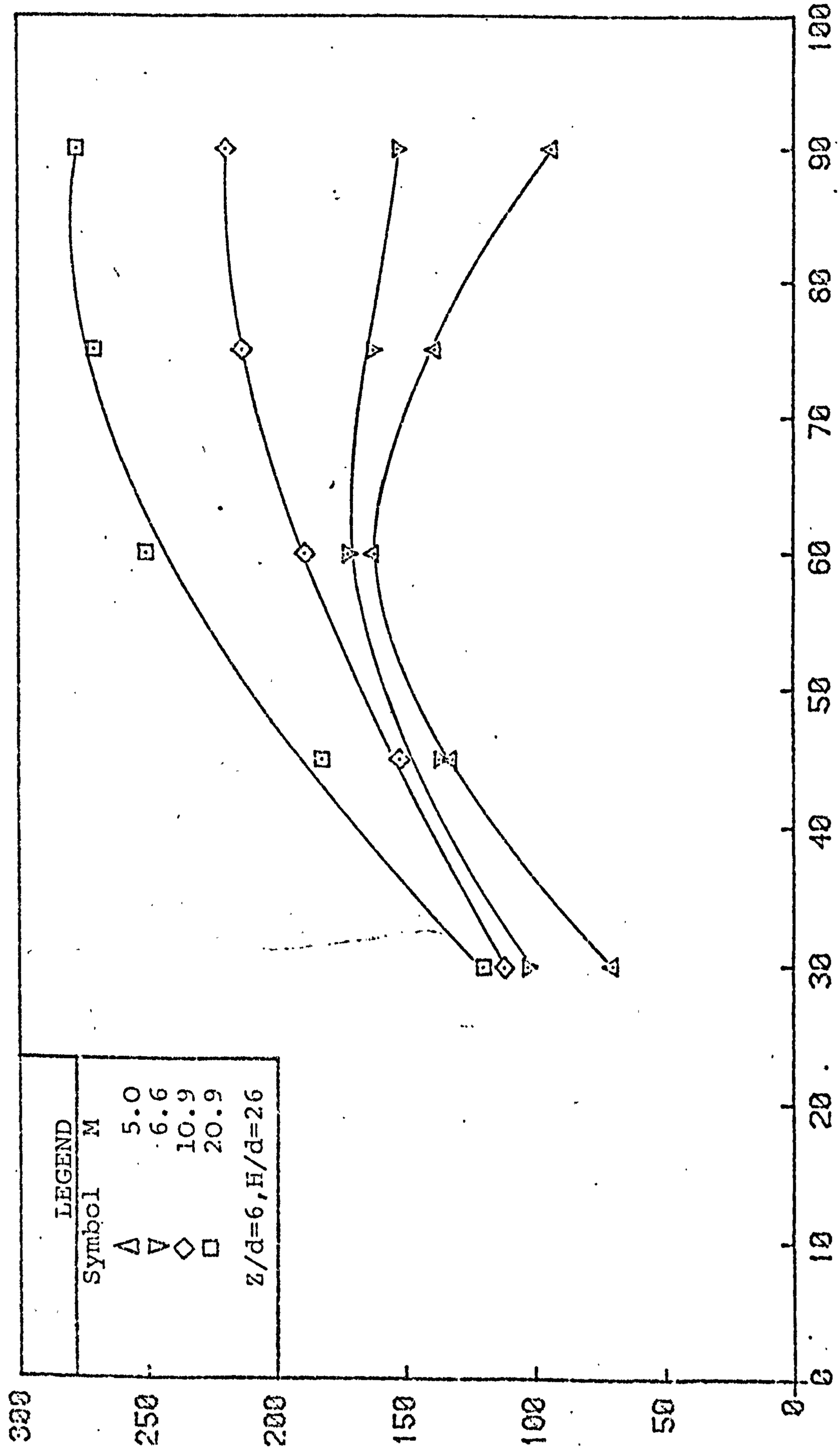

FIG. 10.3.13 THE EFFECT OF NOZZLE INCLINATION ON MAXIMUM HEAT TRANSFER

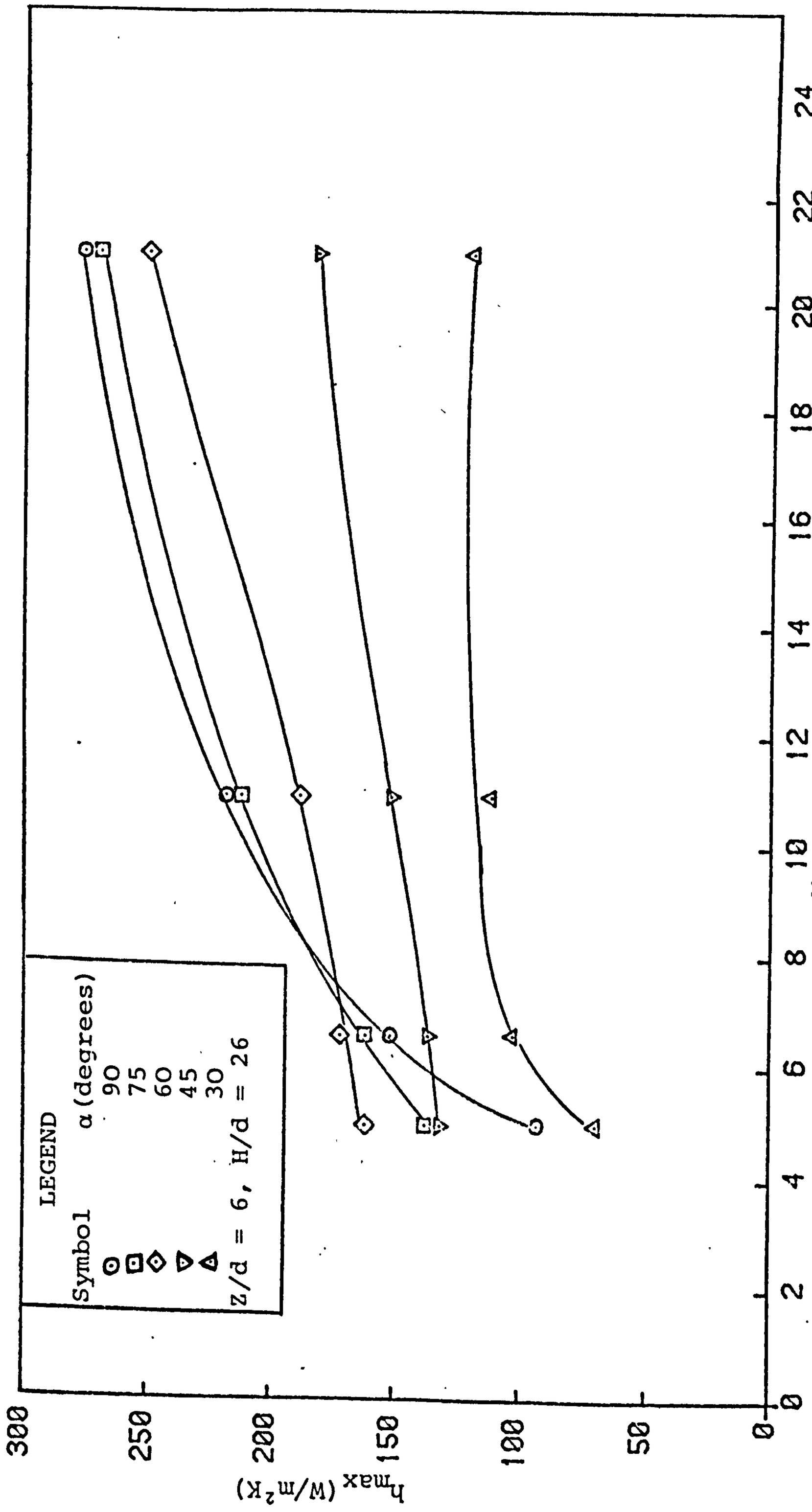

FIG.10.3.14 THE EFFECT OF JET-CROSS FLOW VELOCITY RATIO ON MAXIMUM HEAT TRANSFER COEFFICIENT.

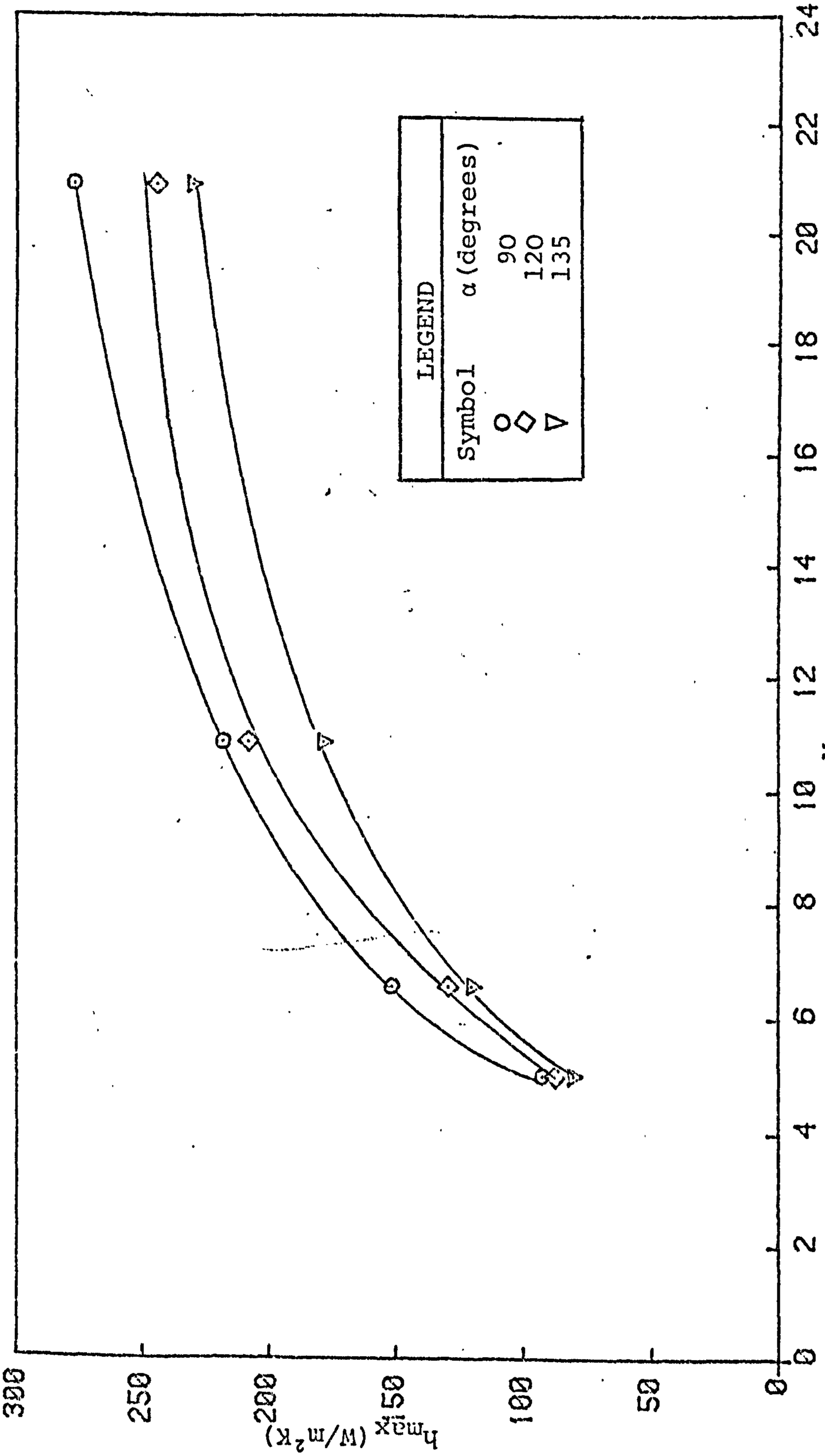

FIG. 10.3.15 EFFECT OF JET-CROSS FLOW VELOCITY RATIO ON HEAT TRANSFER.
($\alpha \leqslant 90°$)

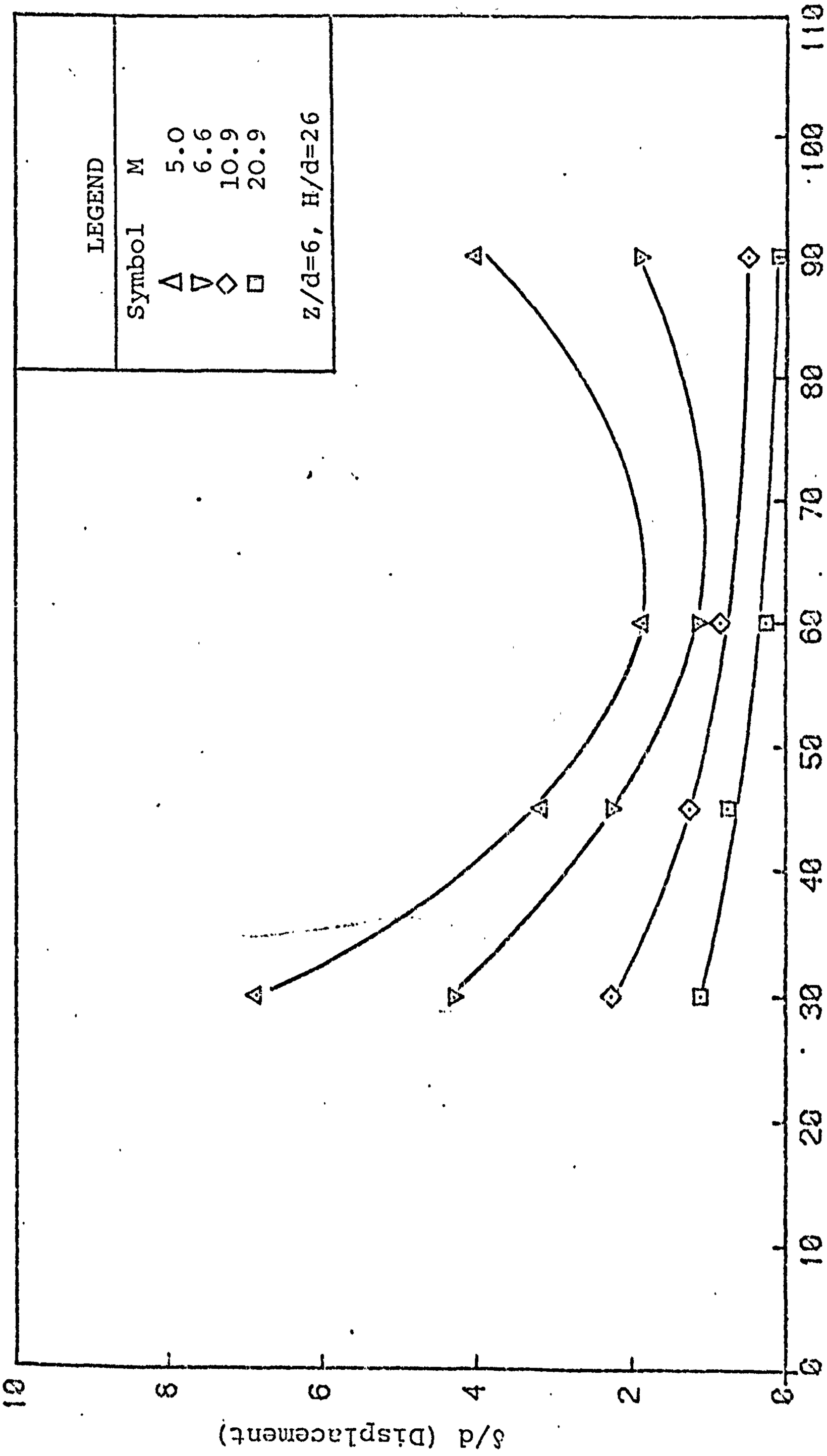

FIG.10.3.16 DISPLACEMENT OF MAXIMUM HEAT TRANSFER POINT FROM THE JET CENTRE-LINE.

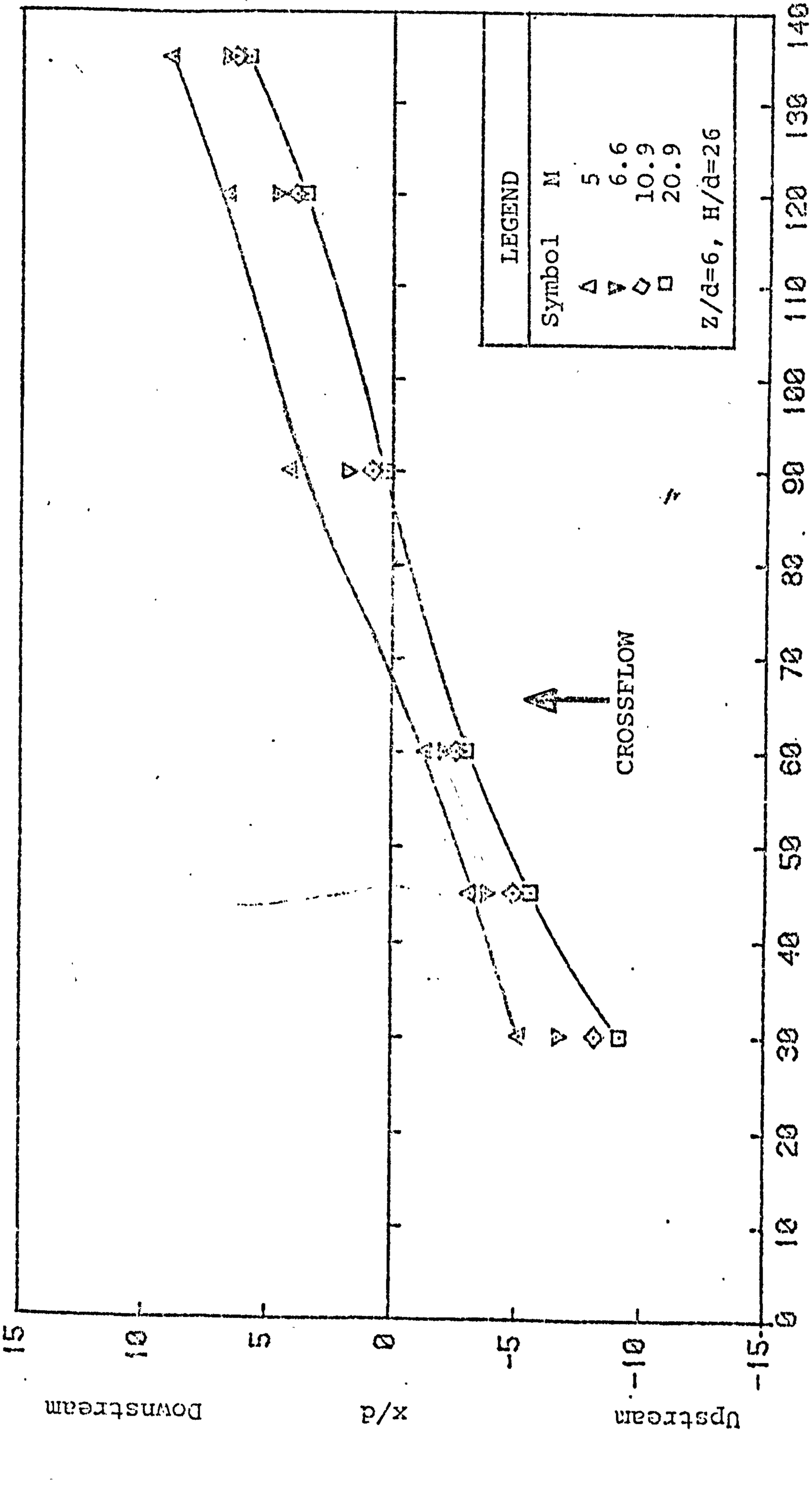

FIG. 10.3.17 EFFECT OF NOZZLE INCLINATION ON THE LOCATION OF MAXIMUM HEAT TRANSFER.

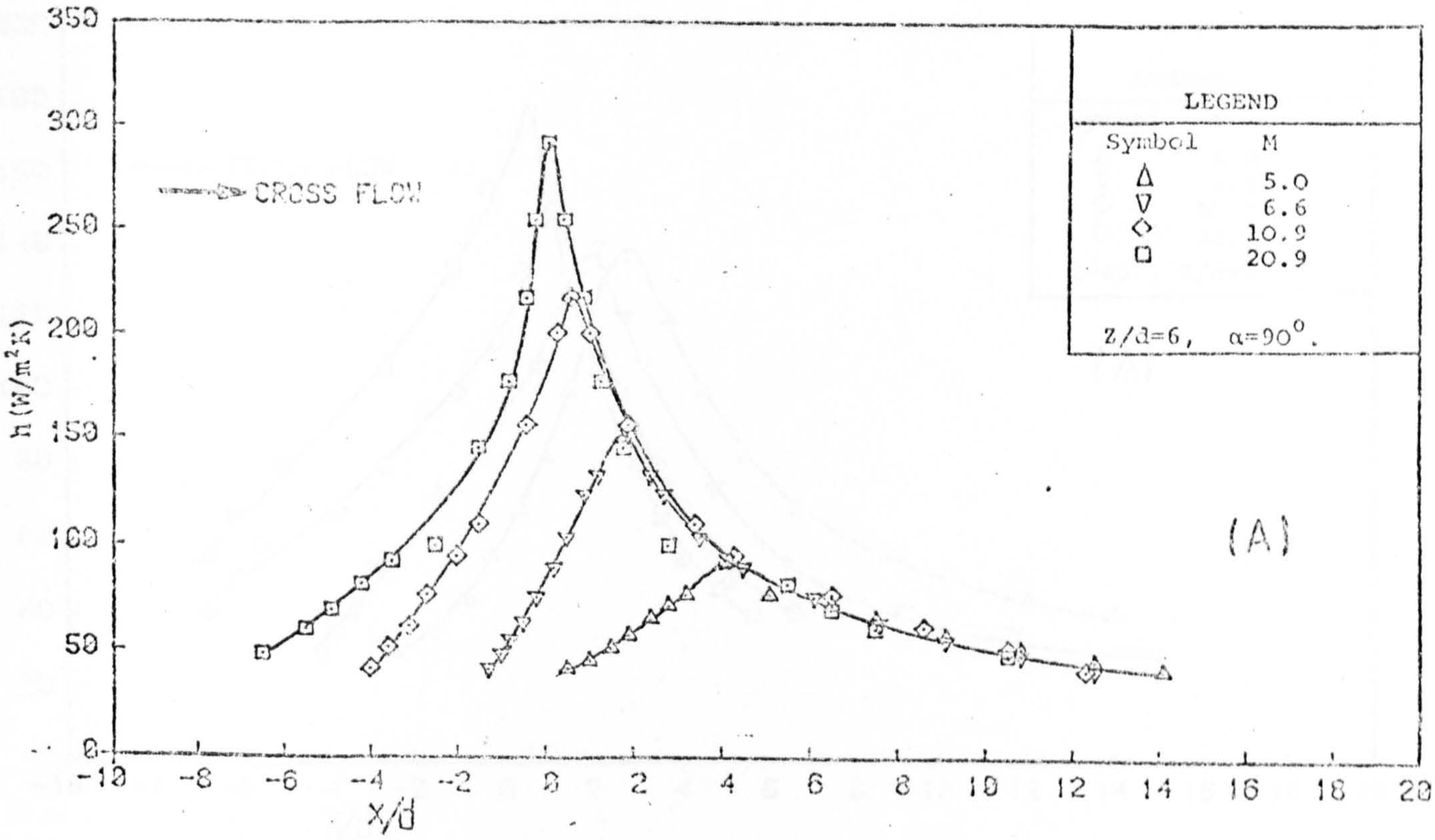

FIG.10.3.18 VARIATION OF LOCAL HEAT TRANSFER COEFFICIENT ALONG THE LINE OF SYMMETRY(α=90°).

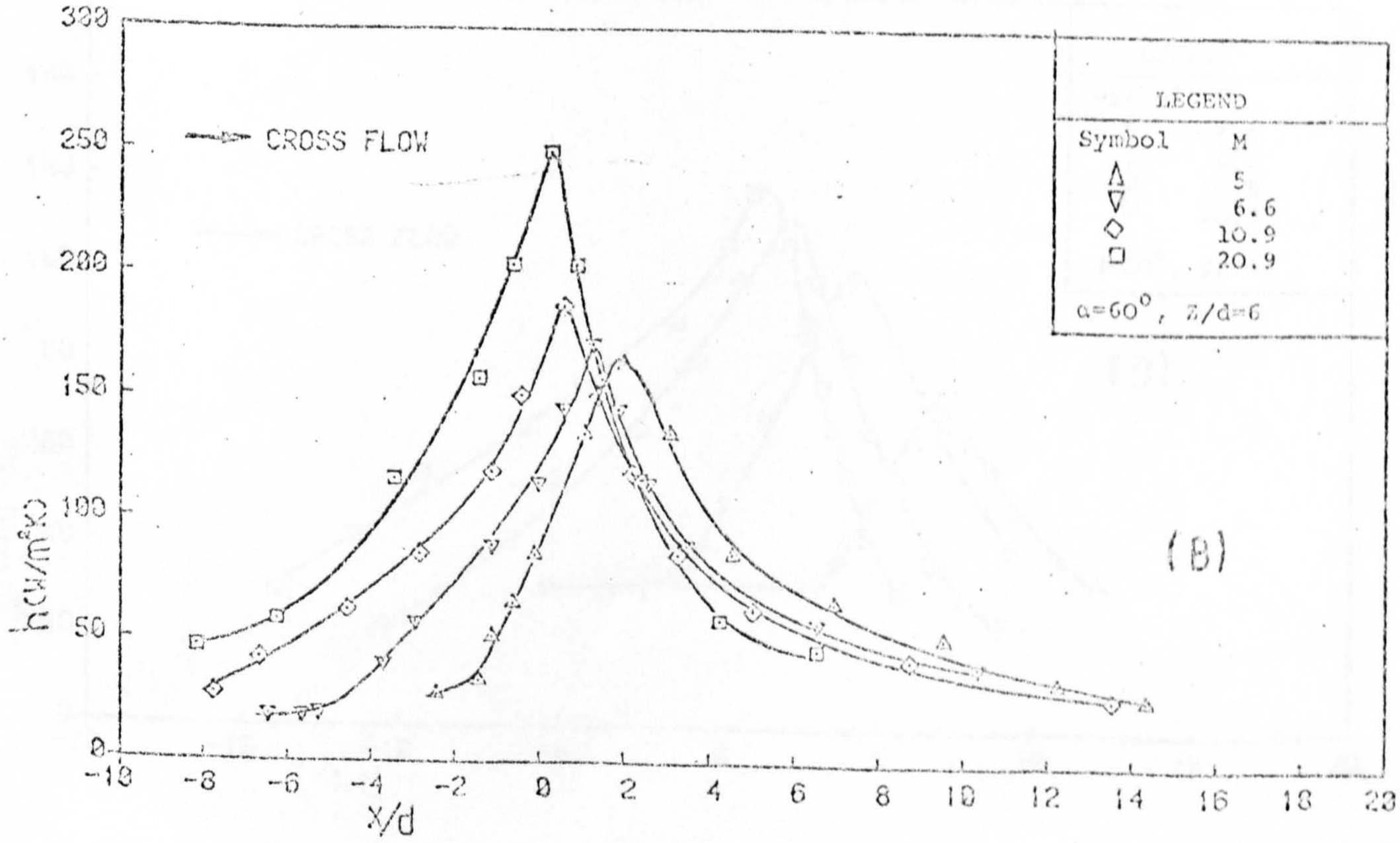

FIG.10.3.18 VARIATION OF HEAT TRANSFER ALONG THE LINE OF SYMMETRY(α=60°).

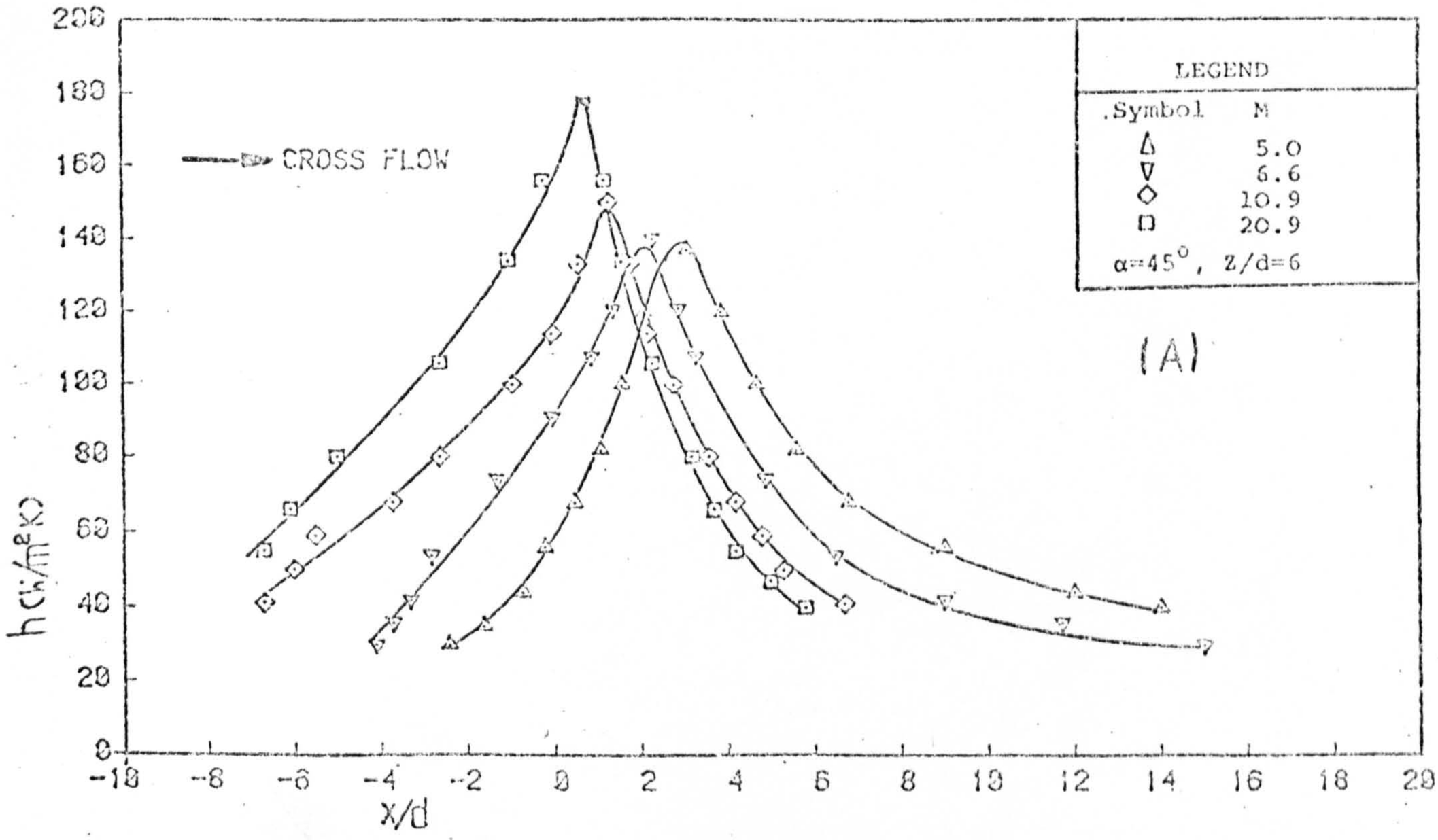

FIG.10.3.19 VARIATION OF HEAT TRANSFER ALONG THE LINE OF SYMMETRY (α=45°).

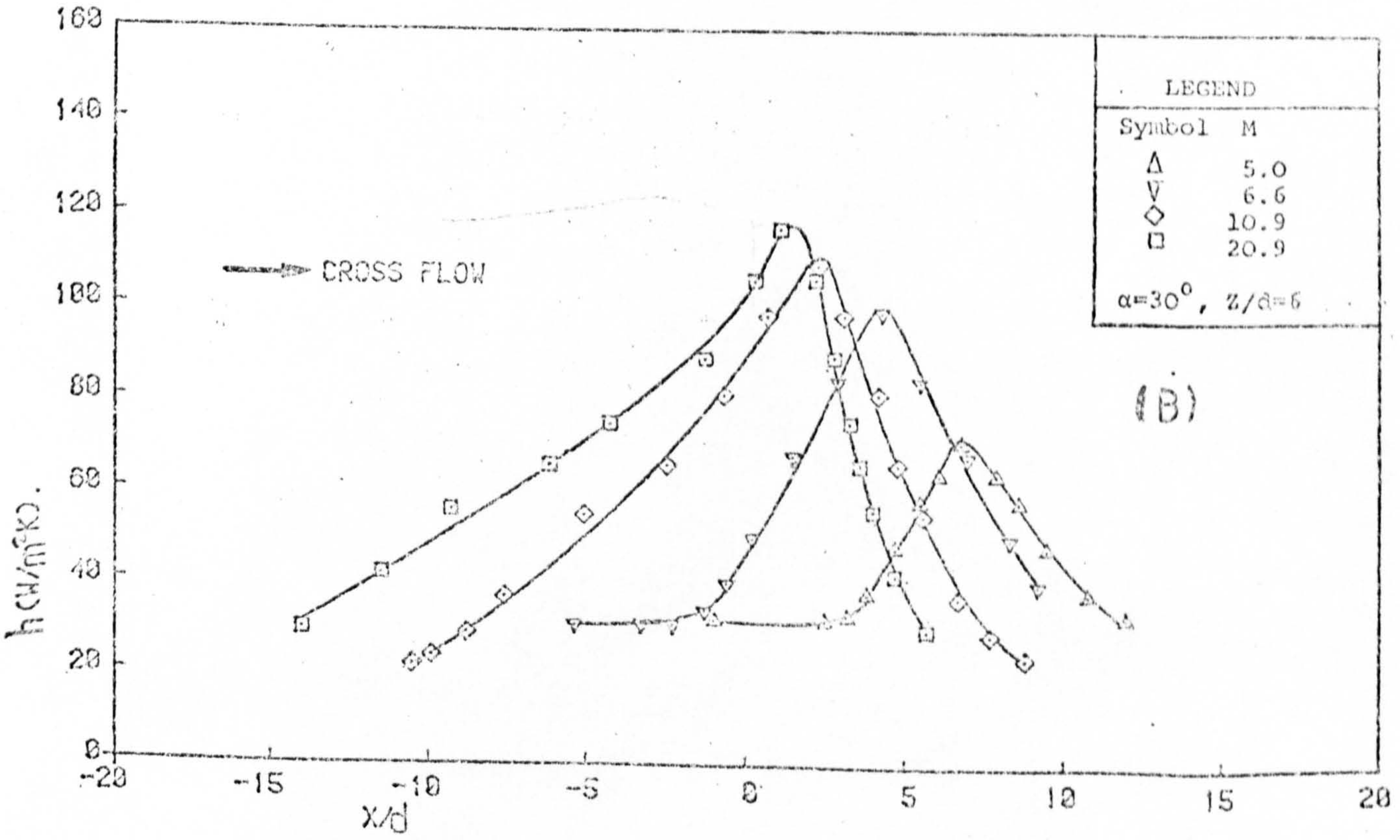

FIG.10.3.19 VARIATION OF HEAT TRANSFER ALONG THE LINE OF SYMMETRY (α=30°).

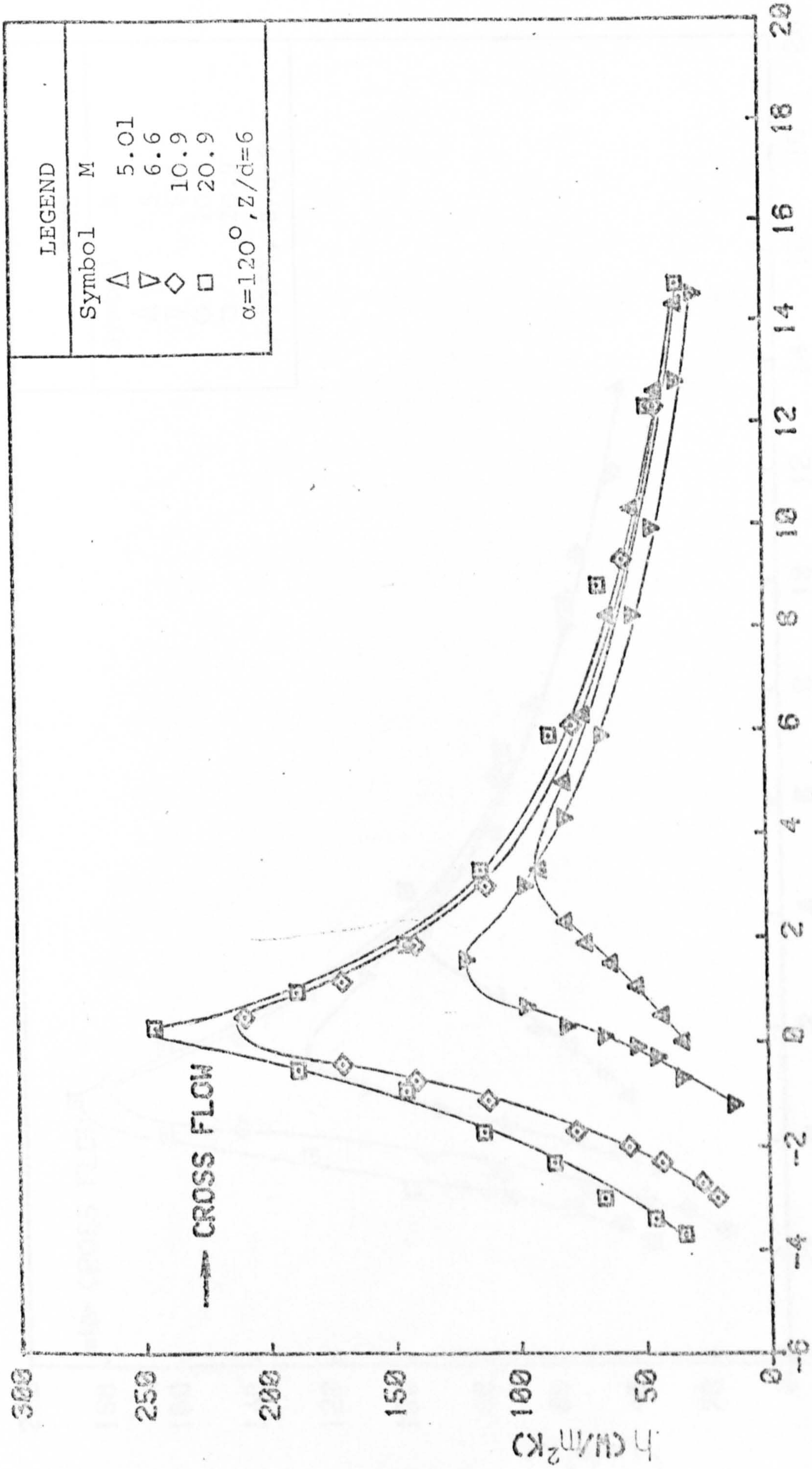

FIG. 19.3.28 VARIATION OF HEAT TRANSFER ALONG THE LINE OF SYMETRY (-120°).

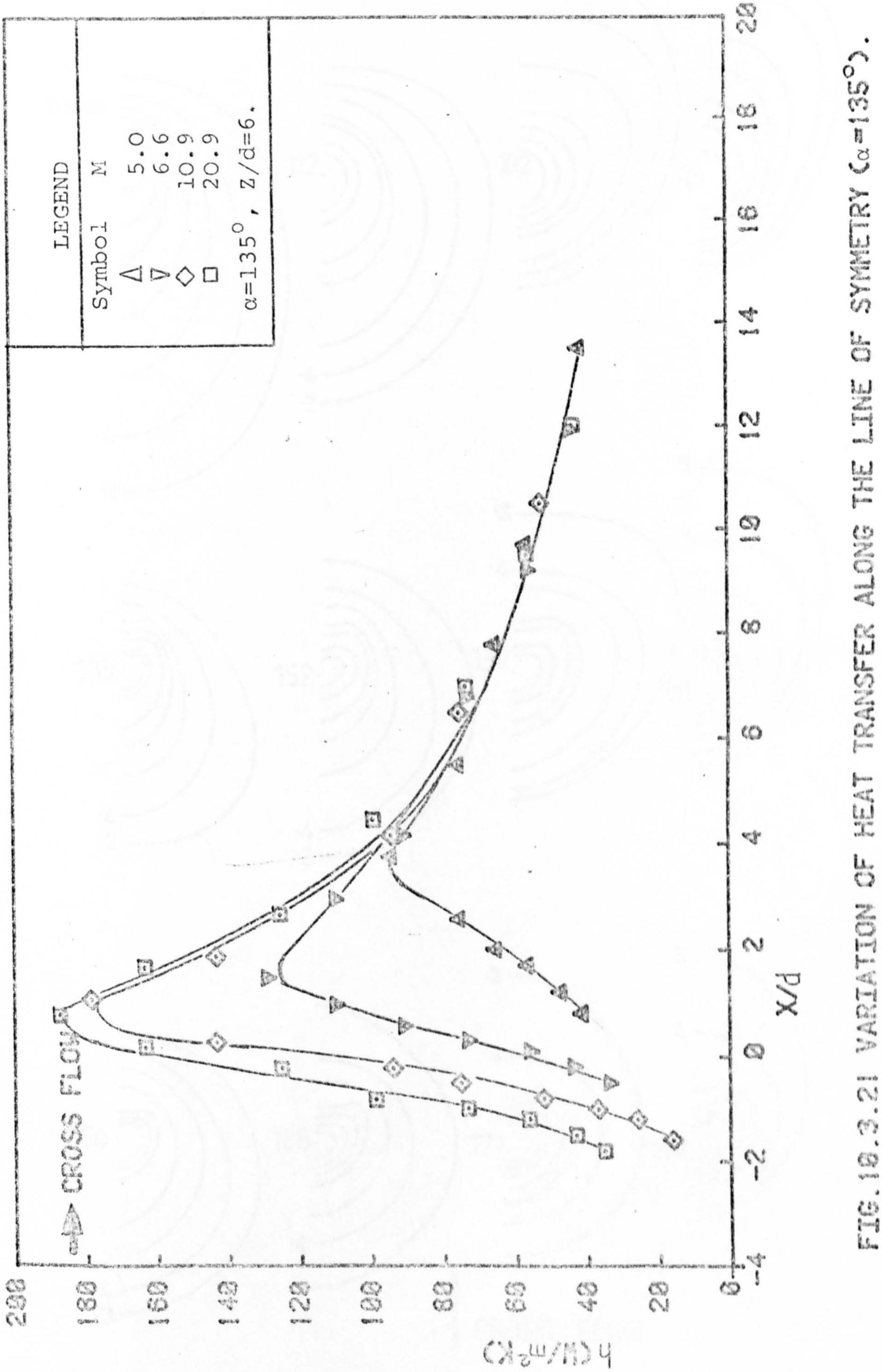

FIG. 19.3.21 VARIATION OF HEAT TRANSFER ALONG THE LINE OF SYMMETRY (α=135°.

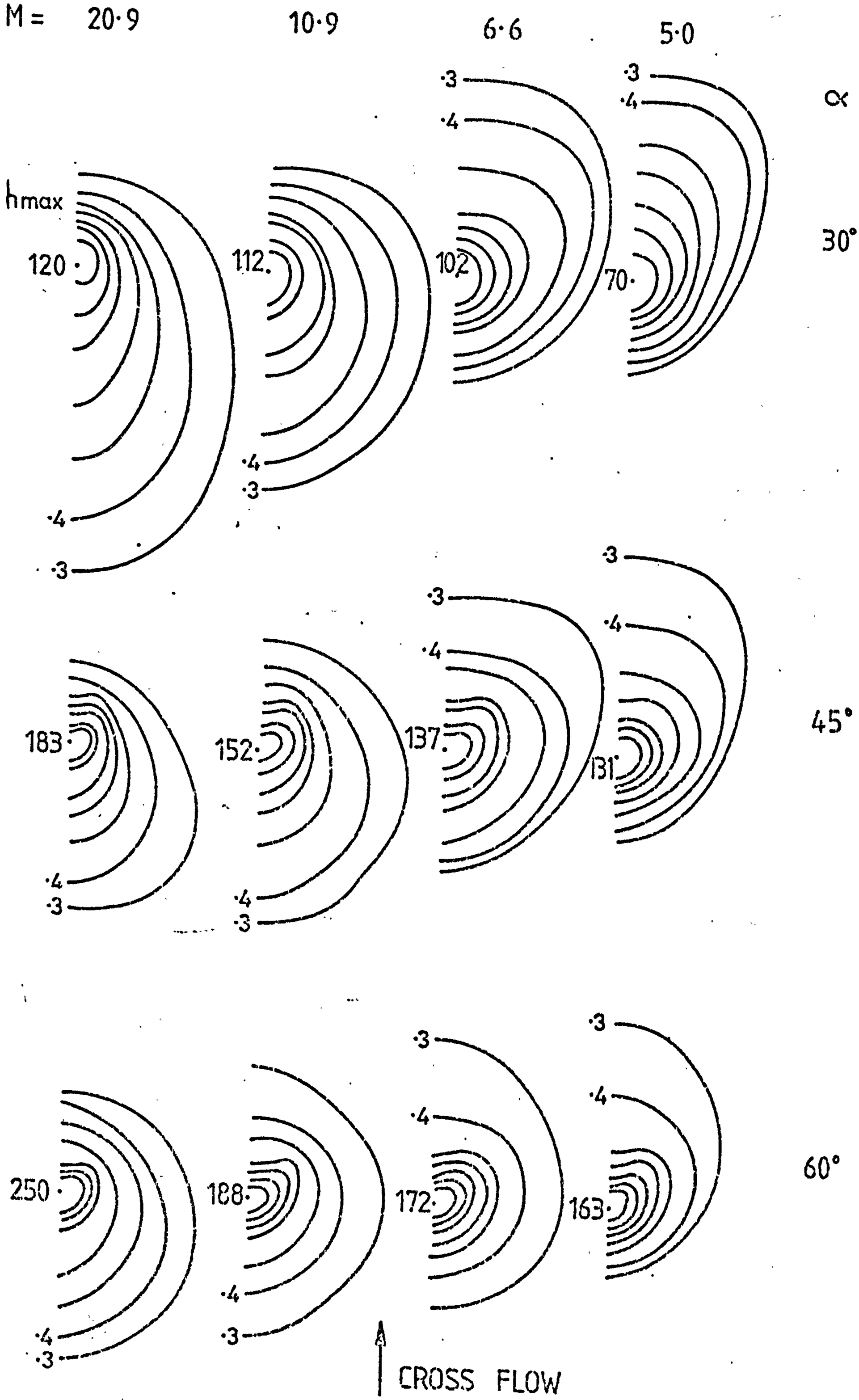

FIG. 10.3.22 EFFECT OF NOZZLE INCLINATION ON HEAT TRANSFER

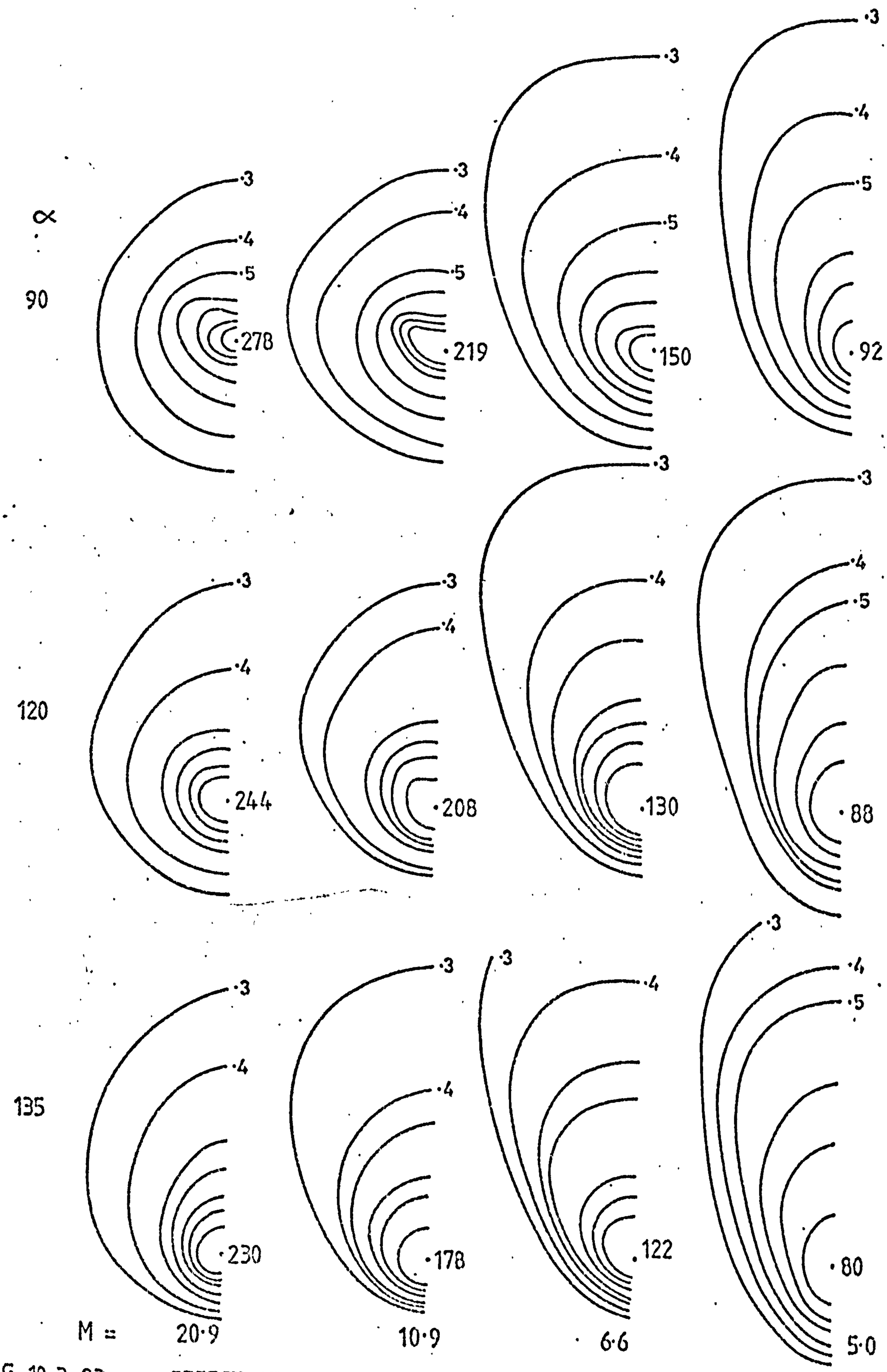

FIG. 10.3.23 EFFECT OF NOZZLE INCLINATION ON HEAT TRANSFER

CHAPTER 11

11. CLOSURE

11.1 CONCLUSIONS

The conclusions from this investigation can be summarised as follows:

General

1) The turbulent circular jets employed in the present study possessed similar velocity and turbulence characteristics to those obtained by earlier investigators of jet flows. Thus, the heat transfer results reported in this thesis would have reasonably general applications.

2) The 'thin-film' naphthalene sublimation technique together with the Chilton-Colburn analogy appears to be an accurate, cheap and convenient method of obtaining local heat transfer rates beneath turbulent impinging jets. The technique, however, is less suited to determining stagnation point values. Thus, an optical technique was employed to improve the repeatability and reliability of the results obtained at the stagnation point.

Oblique Jets Exiting into Initially Stagnant Surroundings

3) Inclination of the nozzle relative to the impingement surface produced an imbalance in the heating/cooling capabilities of the jets. This can be related to the non-symmetrical fluid flow over the surface. The heat transfer rates, however, were found to be relatively insensitive to the shape of the nozzle. Generally, the heat transfer rates decreased as the angle α decreased. The stagnation point, impingement region and average heat transfer coefficients were all correlated by means of simple power law dependence on Reynolds number, nozzle-target separation and the angle of inclination. For example, the stagnation point heat transfer rates can be correlated by:

$$Nu/Pr^{\frac{1}{3}} = 0.22(Sin\alpha)^{0.84}Re^{0.81}(z/d)^{-0.69} \qquad 11.1.1.$$

In this equation, the nozzle-target separation is measured normal to the impingement surface. However, if the separation is measured along the actual jet axis, then the effect of nozzle inclination becomes relatively small. For example, the stagnation point values can then be correlated by:

$$Nu/Pr^{\frac{1}{3}} = 0.22(Sin\alpha)^{0.15}Re^{0.81}(z'/d)^{-0.69} \qquad 11.1.2$$

and it is apparent that the 'angle effect' is only proportional to $(\text{Sin}\alpha)^{0.15}$. A similar effect was observed for the average heat transfer rates. The effect of inclination can, thus, be explained almost solely in terms of the increased actual nozzle-target surface separation.

Oblique Jets in Confined Cross Flows

4) For a particular nozzle inclination, increasing the magnitude of the cross flow which was superimposed onto the jet flow decreased the heat transfer rates. This decrease was particularly severe in the upstream region whereas in the downstream zone, there was an actual increase in heat transfer.

5) The degree of confinement (i.e. the width of the duct relative to the diameter of the nozzle) also affected the heat transfer rates. At low cross flows (i.e. $U_j/U_c > 20.9$), the heat transfer rates decreased as the duct width decreased. However, at higher cross flows the reverse effect occurred.

6) At low cross flows, inclination of the jet further reduced the heat transfer rates. However, at higher cross flows, as the jet was inclined an initial increase in heat transfer occurred. The maximum heat transfer was obtained at α of approximately 60° and thereafter the heat transfer rates subsequently decreased. This optimal angle of inclination at high cross flows seems to be brought about by a balance between two conflicting effects. In the absence of a cross flow jet inclination reduces heat transfer rates but with a superimposed cross flow, it increases the jet penetration upstream. The combined effect gives rise to the observed optimum in the heat transfer distribution.

11.2 RECOMMENDATIONS FOR FUTURE STUDY

1) The thin film naphthalene sublimation method yields large quantities of data. The possibility of introducing a more efficient data acquisition and processing system should be investigated.

2) The cross flow tests were carried out for a constant nozzle diameter, nozzle-target separation and jet Reynolds number. These parameters should be systematically varied in further studies. In particular, the nozzle-impingement surface separation should be examined since the optimal angle of inclination is likely to be particularly dependent upon this variable.

3) The results reported in this thesis are solely for single circular jets. Most practical installations, however, contain arrays of jets. It is, therefore, desirable that further studies should be carried out to investigate the effect of cross flows on a row of jets, at least.

4) Further velocity measurements and flow visualization studies should also be undertaken since this would assist in interpreting the heat transfer results. Turbulence measurements in such systems, although difficult to carry out, would also be useful. Numerical studies are being carried out at present for impinging jets in cross flows and any velocity and turbulence data would assist in validating these models.

REFERENCES

REFERENCES

1. WOLFSHTEIN, M. — Some Solutions of the Plane Turbulent Impinging Jet. Trans. ASME, J.Basic Eng., Vol. 92, No.4, pp.915, 1970.

2. RUSSELL, P.J. and HATTON, A.P. — Turbulent Flow Characteristics of an Impinging Jet. Proc. Inst. of Mech. Engrgs. Vol. 186, pp.635, 1972.

3. WINTER, E.F. — Jet Impingement - A Versatile Gas-Fired System for Process Heating of Metals. Shell International Gas Ltd., Report No. SIG 71/7, 1971

4. DUGGAN, A.P. ISAAC, J.G. and THOMAS, J.R. — Convective Heating Investigations and Recent Developments. Slab Reheating Conference, Iron and Steel Inst., Bournemouth, June 1972.

5. PERRY, J. WINTER, E.F. and WILCOCK, R. — Rapid Heating of Steel for Hot Working. Steel Times Vol.194, pp.761, 1964 Vol.195, pp.111, 1967 Vol.195, pp.170, 1970

6. LUCAS, D.M. MASTERS, J. and TOTH, H.E. — Predictions of the Performance of Rapid Heating Furnaces. J.Inst.Gas Eng., Vol.67, pp.397, 1969.

7. CHEETHAM, H.A. and LANARY, R.S. — Rapid Heating of Metals by Jet Impingement. Hamworthy Eng. Ltd., Poole, 1971.

8. FRANCIS, W.E. MOPPETT, B.E. and READ, G.P. — Studies of Flow Patterns and Convection in Rapid Heating Furnaces using Model Techniques. Gas Council Research Communication GC/32, 1966.

9. METZGER, D.E. YAMASHITA, T. and JENKINS, C.W. — Impingement Cooling of Concave Surfaces with Lines of Circular Air Jets. J. Eng. for Power, Vol.91, No.3, pp.149, July 1969.

10. CHUPP, R.E. HELMS, H.E. McFADDEN, P.W. and BROWN, T.R. — Evaluation of Internal Heat Transfer Coefficients for Impingement Cooled Turbine Air foils. J. of Aircraft, Vol.6, pp.203, 1969.

11. KAMOTANI, Y. and GREBER, I. — Experiments on a Turbulent Jet in Crossflow. AIAA Journal, Vol.10, No.11, 1972.

12. DAANE, R.A. and HAN, S.T. — An analysis of Air Impingement Drying. TAPPI, Vol.44, No.1, pp.73, 1961

13. ARGANBRIGHT, D.G. and RESCH, H. — A Review of Basic Aspects of Heat Transfer under Impinging Air Jets. Wood Science and Technology, Vol.5, pp.73, 1971.

14. CHANCE, J.L. — Experimental Investigation of Air Impingement. Heat Transfer Under an Array of Round Jets. TAPPI, Vol.57, pp.108, 1974.

15. SCHEUTER, K.R. and DOSDOGRU, G.A. — Investigation of Impinging Air Jet Driers with Respect to Possible Automation. Tech. Assoc. of Graphic Arts (TAGA) Proc. 224, 1971.

16. HARDISTY, H. — Industrial Drying using Impinging Air Jets - Part 1. Report No. 226 School of Mech. Eng. University of Bath, 1973.

17. HARDISTY, H. — Industrial Drying using Impinging Air Jets - Part II, Report No. 227 School of Mechanical Eng., University of Bath, 1973.

18. BLACK, J. and HARDISTY, H. — Heat and Mass Transfer in Ink Drying and Infra-Red Dryness Measurements. Journal of Mech. Eng. Sc., Vol.18, pp.99, 1976.

19. TAYLOR, J.F. GRIMMETT, H.L. and COMINGS, E.W. — Isothermal Free Jets of Air Mixing with Air. Chemical Engineering Progress, Vol.47, pp.175, 1951.

20. VICKERS, J.M.F. — Heat Transfer Coefficients between Fluid Jets and Normal Surfaces. Ind. Eng. Chem., Vol.51, No.8, pp.967, 1959.

21. PERRY, K.P. — Heat Transfer by Convection from a Hot Gas Jet to a Plane Surface. Proc. Inst. Mech. Engrs., London Vol.168, pp.775, 1954..

22. KORGER, M. and KRIZEK, F. — Verfahrenstechnik (Mainz). Vol.6, pp.223, 1972.

23. SPARROW, E.M. and LOVELL, B.J. — Heat Transfer Characteristics of an Obliquely Impinging Circular Jet. Trans. ASME Journal of Heat Transfer, Vol. 102, pp.202, May 1980.

24. METZGER, D.E. and KORSTAD, R.J. — Effects of Crossflow on Impingement Heat Transfer. Trans. ASME, J. of Eng. for Power, Vol.94, pp.35, 1972. .

25. BOUCHEZ, J.P. — Heat Transfer to an Impinging Circular Jet in a Crossflow. Ph.D. Thesis, University of Minnesota, 1973.

26. SPARROW, E.M. GOLDSTEIN, R.J. and ROUF, M.A. — Effect of Nozzle-Surface Separation Distance on Impingement Heat Transfer for a Jet in a Crossflow. Trans. ASME, J. Heat Transfer, Vol.97, pp.528, 1975.

27. CHONG, Y.K. — Two-Dimensional Slot Jet Impingement in a Confined Crossflow Stream. M.Sc. Thesis, Cranfield Inst. of Tech., 1979.

28. BOUCHEZ, J.P. and GOLDSTEIN, R.J.
Impingement Cooling From a Circular Jet in a Cross flow. International J. Heat and Mass Transfer, Vol.18, pp.719-730, 1975.

29. CALLAGHAN, E. and RUGGERI, R.-S.
Investigation of the Penetration of an Air Jet Directed Perpendicularly to an Air Stream. NACA Tech. Note 1615, 1948.

30. KEFFER, J.F. and BAINES, W.D.
The Round Turbulent Jet in a Cross-Wind. J.Fluid Mech., Vol.15, pp.481, 1963

31. JORDISON, R.
Flow in a Jet Directed Normal to the Wind. Aero Res. Council & R and M No. 3074, 1958.

32. KAMOTANI, Y. and GREBER, I.
Experiments on Confined Turbulent Jets in Cross Flow. NASA No. CR-2392, March 1974.

33. CAMPBELL, J.F. and SCHETZ, J.A.
Analysis of the Injection of a Heated Turbulent Jet into a Cross Flow. NASA TR R-413, Dec. 1973.

34. MARGASON, R.J.
The Path of a Jet Directed at Large Angles to a Subsonic Free Stream. NASA TN D-4919, 1968.

35. SUSEC, J. and BOWLEY, W.M.
Prediction of the Trajectory of a Turbulent Jet Injected into a Crossflowing Stream. J. Fluids Engrg., Vol.98, pp.667, Dec. 1976.

36. KABARI, L.
Flow and Heat Transfers Associated with Impinging Jets in Crossflows. Ph.D. Thesis, Cranfield Inst. of Technology, 1977.

37. JACKSON, T.W. — Two-Dimensional Inclined 'Jet-Impingement' Heat Transfer in Confined Cross flow. M.Sc. Thesis, Cranfield Institute of Technology, 1980.

38. ECKERT, E.R.G. and GOLDSTEIN, R.J. — Measurements in Heat Transfer Hemisphere Publishing Corp. Washington, 1976.

39. GARDON, R. — A Transducer for the Measurement of Heat Flow Rate. J. of Heat Transfer, Vol.82, pp.396-298, 1960.

40. OUDEN, C.D. and HOOGENDOORN, C.J. — Local Convective Heat Transfer Coefficients for Jets Impinging on a Plate; Experiments Using a Liquid-Crystal Technique. Proceddings of the 5th Inter. Heat Transfer Conf., Vol.V, pp.293-297, A.J.Ch.E., New York 1974.

41. RHINES, J. — Private Communication. British Gas, Midland Research Station, West Midlands. April 1981

42. GOLDSTEIN, S. — Modern Developments in Fluid Dynamics. Vol.II, Dover Publications, Inc., New York, 1965.

43. PRANDTL, L. — Eine Beziehung Zwischen Warmeaustaush und Stromungswiderstand der Flussigkeiten. (A Relationship Between Heat Transfer and Friction in the Fluids). Physik Z., Vol.11, pp.1072, 1910.

44. TAYLOR, G.I. — Conditions at the Surface of a Hot Body Exposed to the Wind. British Adv. Comm. Aeron. Rep. and Mem. 272, Vol.31, pp.423, 1961.

45. REYNOLDS, A.J. — Turbulent Flows in Engineering. Wiley & Sons, London, 1974.

46. COLBURN, A.P.
A Method of Correlating Forced Convection Heat Transfer Data and a Comparison with Fluid Friction.
Trans. A.I. Chem. Eng., Vol.29, pp.174-210, 1933.

47. CHILTON, T.H. and COLBURN, A.P.
Mass Tranfer (Absorption) Coefficients.
Ind. Eng. Chem., Vol.26, pp.1183, 1934.

48. WARD, J.
IDERIAH, F.J.K.
PROBERT, S.D. and DUGGAN, A.
Mass Transfer Technique for Investigation of Heat Transfer by Jet Impingement Systems.
J. Inst. of Mech. Eng., Vol.14, No.6, pp.389-392, 1972.

49. VALLIS, E.A.
PATRICK, M.A. and WRAGG, A.A.
Radial Distribution of Convective Heat Transfer Coefficient between an Axisymmetric Turbulent Jet and a Flat Plate Held Normal to the Flow.
Paper FC(b)-21, 6th Int. Heat Transfer Conference, Toronto, Canada, Aug. 1978.

50. MAHMOOD, M.
Heat Transfer from Swirling Impinging Jets.
Ph.D. Thesis, Cranfield Institute of Technology, April 1980.

51. LEWIS, J.S.
A Heat-Mass Transfer Analogy Applied to Fully Developed Turbulent Flow in Annulus.
J. Mech. Eng. Science, Vol.13, No.4, pp.286-292, 1971.

52. JAYATILLEKE, C.V.L.
The Influence of Prandtl Number and Surface Roughness on the Resistance of the Laminar Sub-Layer to Momentum and Heat Transfer.
Progress In Heat and Mass Transfer, Vol.1, pp.193-329, Pergamon Press, 1969.

53. BLOOM, J.
Experimental Determination of the Turbulent Prandtl Number in a Developing Temperature Boundary Layer
Paper FC2.2, 4th Int. Heat Transfer Conf., Paris-Versailles, 1970.

54. KNUDSEN, J.G. and KATZ, D.L.
Fluid Dynamics and Heat Transfer
McGraw Hill, New York, 1958.

55. SIMPSON, R.L. and FIELD, R.L.
A Note on the Turbulent Schmidt and Lewis Numbers in a Boundary Layer.
Int. J. Heat and Mass Transfer, Vol.15, pp.177, 1972.

56. ECKERT, E.R. and DRAKE, R.M.
Heat and Mass Transfer
McGraw Hill, New York, 1959.

57. LUCAS, D.M. DAVIS, W.A. and GAY. B.
Evaluation of Local and Average Convective Heat Transfer Coefficients in a Furnace Using an Electrolytic Mass Transfer Model.
J. of the Institute of Fuel, Vol.48, pp.31-37, 1975.

58. JEWAD, M.A.
Thermal Design of a Compact Recuperative Heat Exchanger for a Stirling Engine.
Ph.D. Thesis, Cranfield Institute of Technology, 1977.

59. WARD, J. and JEWAD, M.A.
Heat Transfers and Hydraulic Resistances Associated with Small Diameter, Closely Spaced Tube Arrangements.
Report for K.B. United Stirling.
School of Mechanical Engineering, Cranfield Institute of Technology, 1977.

60. McADAMS, W.H.
Heat Transmission.
3rd Edition, McGraw Hill, New York, 1954.

61. MIZUSHINA, T.
The Electrochemical Method in Transport Phenomena.
Advances in Heat Transfer, Vol.7, pp.87, Academic Press, London 1971

62. KLEIN, V.
Dissertation, Tech. Hochsch, Hanover, 1933.

63. WINDING, G.C. and CHENEY, A.J.
Mass and Heat Transfer in Tube Banks.
Ind. Eng. Chem., Vol.40, p.1087, 1948.

64. CHRISTIAN, W.J. and KEZIOS, S.D.
Experimental Investigation of Mass Transfer by Sublimation from Sharp Edged Cylinders in Axisymmetric Flow with Laminar Boundary Layer.
Heat Transfer and Fluid Mech. Inst., held at California Inst. of Tech., California, pp.359, 1957.

65. HOUSTON, R.M.
Nozzle Heat Transfer Predictions from Sublimation Measurements on a Model of a Solid Fuel Rocket.
M.Sc. Thesis, Cranfield Institute of Technology, Cranfield, 1960.

66. KOOPMAN, R.N. and SPARROW, E.M.
Local and Average Transfer Coefficients due to an Impinging Row of Jets.
Int. Journal of Heat Mass Transfer, Vol.19, pp.673, 1976.

67. MAC, S.S.
Space-Average Heat Transfer in Rapid Heating.
M.Sc. Thesis, Cranfield Institute of Technology, 1974.

68. AL-MOBAREK, A.M.B.
Heat Transfer in a Billet Reheating Furnace.
M.Sc. Thesis, Cranfield Institute of Technology, 1977.

69. OLADIRAN, M.T.
Local Heat Transfers in a Billet Reheating Furnace.
M.Sc. Thesis, Cranfield Institute of Technology, 1977.

70. DUNN, A.R.
Heat Transfer from an Array of Swirling Jets.
M.Sc. Thesis, Cranfield Institute of Technology, 1978.

71. OLADOSU, J.O.
Heat Transfer Under an Array of Counter-Rotating, Swirling Impinging Jets.
M.Sc. Thesis, Cranfield Institute of Technology, 1980.

72. TODD, R.B.
The Profilometric Determination of Mass Transfer Rates using Swelling and Shrinking Polymer Films.
Ph.D. Thesis, University of Edinburgh, 1965.

73. MACLEOD, N. and TODD, R.B.
The Experimental Determination of Wall-Fluid Mass Transfer Coefficients using Plasticised Polymer Surface Coatings.
Int. J. Heat Mass Transfer, Vol.16, pp.485-504, 1973.

74. MACLEOD, N. COX, M.D. and TODD, R.B.
A Profilometric Technique for Determining Local Mass-Transfer Rates.
Chem. Eng. Science, Vol.17, pp.596, 1966.

75. WILKIE, D. and WHITE, L.
Fuel Element Heat Transfer Near Dimple Braces.
Nucl. Eng., Vol.11, pp.596, 1966.

76. NEAL, S.B.H.C., NORTHOVER, E.W. and HITCHCOCK, J.A.
The Development of a Technique for Applying Naphthalene to Surfaces for Mass Transfer Analogue Investigations.
J. Physics E. Scientific Instrum., Vol.3, pp.636, 1970.

77. NEAL, S.B.H.C.
The Development of the Thin-Film Naphthalene Mass Transfer Analogue Technique for the Direct Measurement of Heat Transfer Coefficients.
Int. J. Heat Mass Transfer, Vol.18, pp.559, 1975.

78. BANKSTON, C.A. and McELIGOT, D.M.
Turbulent and Laminar Heat Transfer to Gases with Varying Properties in the Entrance Region of Circular Ducts.
Int. J. Heat Mass Transfer, Vol.13, pp.319-344, 1970.

79. SHERWOOD, T.K. and TRASS, O. — Sublimation Mass Transfer through Compressible Boundary Layers on a Falt Plate. Trans. ASME, J. of Heat Transfer, Vol.82, pp.313, 1960.

80. WONG, P.W. — Mass and Heat Transfer from Circular Finned Cylinders. J.I.H.V.E., Vol.34, pp.1, 1966.

81. SHERWOOD, T.K. and BRYANT, H.S. — Mass Transfer Through Compressible Boundary Layers. Canadian Int. of Chem. Eng., Vol.35, pp.51, 1957.

82. — Handbook of Chemistry and Physics. 46th edition. Chemical Rubber Co., Cleveland, Ohio, 1965.

83. — Int. Critical Tables. McGraw Hill Book Co., New York, Vol.3, pp.208, 1926.

84. STEPHENSON, P.L. MASSEY, T.H. and OLIVER, A.J. — Developing Turbulent Flow and Heat Transfer in a Circular Tube - A Finite Difference Solution using the Mixing Length Hypothesis. CERL, Report No. RD/L/N8/74, Jan. 1974.

85. KAYS, W.M. and CRAWFORD, M.E. — Convective Heat and Mass Transfer. McGraw Hill, 2nd Ed., New York, 1980.

86. SATO, H. and SAKAO, F. — An Experimental Investigation of the Instability of a Two-dimensional Jet at Low Reynolds Numbers. Jnl. Fluid Mechanics, Vol.20, pt.2, pp.337, 1964.

87. GAUNTNER, J.W. LIVINGOOD, J.N.B., and HRYCAK, P. — Survey of Literature on Flow Characteristics of a Single Turbulent Jet Impinging on a Flat Surface. Report No. NASA TND-5652, 1970.

88. RAJARATNAM, N. — Turbulent Jets. Elsevier Scientific Publishing Company, Amsterdam, 1976.

89. BEER, J.M. and CHIGIER, N.A. — Combustion Aerodynamics. Applied Science Publishers. London, 1972.

90. ABRAMOVICH, G.N. — Theory of Turbulent Jets. MIT Press, Cambridge, Massachusetts, 1963.

91. SCHAUER, J.J. — The Flow Development and Heat Transfer Characteristics of Plane Turbulent Impinging Jets. Ph.D. Thesis, Stanford University, 1964.

92. DAWSON, D.A. and TRASS, O. — Mass Transfer in Turbulent Radial Wall Jet. Canadian Journal Chem. Eng., Vol.44, pp.121, 1966.

93. SCHRADER, H. — Drying of Moist Surfaces by Means of Hot Air Jets. Flow Characteristics and Mass Transfer (In German) Forschungsh, Ver. Deutsch. Ing. 484, 1961.

94. BAKKE, P. — An Experimental Investigation of a Wall Jet. J. Fluid Mech., Vol.2, Pt.5, pp.467, 1957.

95. BELTAOS, S. — Oblique Impingement of Circular Turbulent Jets. J. of Hydraulic Research, Vol.14, pp.17, 1976.

96. CORRSIN, S. — Investigation of Flow in an Axially Symmetrical Heated Jet of Air. NASA Wartime Report W-94, 1943.

97. BOGUSLAWSKI, L. and POPIEL, Cz.O.
Flow Structure of the Free Round Turbulent Jet in the Initial Region.
J. Fluid Mech., Vol.90, Pt.3, pp.531, 1979.

98. DONALDSON, C.du.P. SNEDELLER, R.S. and MARGOLIS, D.P.
A Study of Free Jet Impingement. Part II: Free Jet Turbulent Structure and Impingement Heat Transfer.
J. of Fluid Mech., Vol.45, pp.477, 1971.

99. RODI, W.
A New Method of Analysing Hot-Wire Signals in Highly Turbulent Flow and its Evaluation in a Round Jet.
DISA Information No.17, Feb.1975.

100. BECKO, Y.
Impingement Cooling - A Review von Karman Institute for Fluid Dynamics.
Lecture Series 83, Jan. 1976.

101. MARTIN, H.
Heat and Mass Transfer Between Impinging Gas Jets and Solid Surfaces.
Advances in Heat Transfer, Vol.13, pp.1. Academic Press, London, 1977

102. GARDON, R. and COBONPUE, J.
Heat Transfer Between a Flat Plate and Jets of Air Impinging on it.
Int. Develop. in Heat Transfer, pp.454, ASME, New York, 1962.

103. GARDON, R. and AKFIRAT, J.C.
Heat Transfer Characteristics of Impinging Two-Dimensional Air Jets.
Trans. ASME J. of Heat Transfer, Vol.88, pp.101, 1966.

104. GLAUERT, M.B.
The Wall Jet.
J. Fluid Mech., Vol.1, pp.625, 1956.

105. RAO, V.V. and TRASS, O.
Mass Transfer from a Flat Surface to an Impinging Turbulent Jet.
The Canadian J. Chem. Engrg., Vol.42, pp.95, 1964.

106. GARDON, R. and AKFIRAT, J.C. — The Role of Turbulence in Determining the Heat Transfer Characteristics of Impinging Jets. Int. J. Heat Mass Transfer, Vol. 8, pp.1261, 1965.

107. HOOGENDOORN, C.J. — The Effect of Turbulence on Heat Transfer at a Stagnation Point. Int. J. Heat Mass Transfer, Vol. 20, pp.1333, 1977.

108. KATAOKA, K. and MIZUSHINA, T. — Local Enhancement of the Rate of Heat Transfer in an Impinging Round Jet by Free Stream Turbulence. 5th Int. Heat Transfer Conf., Tokyo, Japan. Vol.2, pp.305, 1974.

109. METZGER, D.E. — Spot Cooling and Heating of Surfaces with High Velocity Impinging Air Jet. Tech. Report No.52, Dept. of Mech. Engrg., Stanford University, April 1962.

110. HUANG, G.C. — Investigations of Heat Transfer Coefficients for Air Flow Through Round Jets Impinging Normal to a Heat Transfer Surface. J. Heat Transfer, Vol.85, pp.237, 1963.

111. THURLOW, G.G. — Communication on Ref. 21. Proc. Inst. Mech. Engrg., Vol.168, pp.781, 1954.

112. SMIRNOV, V.A. VEREVOCHKIN, G.E. and BRDLICK, P.M. — Heat Transfer Between a Jet and a Plate Held Normal to Flow. J. Heat Mass Transfer, Vol.2, pp.1, 1961.

113. KILIK, E. — The Influence of Swirler Design Parameter on the Aerodynamics of the Downstream Recirculation Region. Ph.D. Thesis, Cranfield Institute of Technology, 1976.

114. MAKSOUD, T.M.A. — A General Method for Investigating Blade to Blade Distribution of Flow Field Quantities Inside a Turbomachinery. M.Sc. Thesis, Cranfield Institute of Technology, 1978.

115. — Methods of Measurement of Fluid Flow in Pipes. Part I: Orifice Plates, Nozzles, and Venturi Tubes. British Standards Institute, London, 1964.

116. BRADSHAW, P. — An Introduction to Turbulence and its Measurements. Pergamon Press, Oxford, 1971.

117. KING, L.V. — On the Convection of Heat from Small Cylinders in a Stream of Fluid. Phil. Trans. Royal Society, 214A, pp.373, 1914.

118. SIDALL, R.G. and DAVIES, T.W. — An Improved Response Equation for Hot-Wire Anemometry. Int. Journal Heat and Mass Transfer, Vol.15, pp.367, 1972.

119. DISA — Instruction and Service Manual for Type 55D01 Anemometer Unit.

120. MERZKIRCH, W. — Flow Visualisation. Academic Press, 1974.

121. TRITTON, D.J. — Physical Fluid Dynamics. van Nostrand Reinhold Co., Workingham, England, 1977.

122. TYLER, R.A. and WILLIAMSON, R.G. — Tunnel Flow Breakdown from Inclined Jets. Nat. Res. Council of Canada, Aero Report LR-545, March 1971.

123. PLATTEN, J.L. and KEFFER, J.F. — Deflected Turbulent Jet Flows. Jnl. Applied Mech., Vol.38, pp.756, 1971.

124. GORDIER, R.L.
Studies of Fluid Jets Discharging Normally into Moving Liquid.
St. Anthony Falls Hydraulic Lab., Tech. Paper No.28, Series B, Minnesota, 1959.

125. RUDINGER, G. and MOON, L.F.
Laser Doppler Measurements in a Subsonic Jet Injected into a Subsonic Crossflow.
J. of Fluid Eng., Vol.98, pp.516, 1976.

126. STOY, R.L. and BEN-HAIM, Y.
Turbulent Jets in Confined Crossflow.
Trans. ASME, J. of Fluids Eng., Vol.95, pp.551, 1973.

127. PATANKAR, S.V. BASU, D.K. and ALPAY, S.A.
Prediction of the Three-Dimensional Velocity Field or a Deflected Turbulent Jet.
Trans. ASME, J. of Fluids Eng., Vol.99, pp.758, 1977.

128. LAUNDER, B.E. and SPALDING, D.B.
Mathematical Models of Turbulence.
Academic Press, New York, 1972.

129. PANTAKAR, S.V.
Numerical Heat Transfer and Fluid Flow.
McGraw Hill Book Co., New York, 1980.

130. LEE, C.C.
A Review of Research on the Interaction of a Jet with an External Stream.
Brown Eng. Co. Inc., Huntsville, Alabama Research Labs. Report No. IN-R-184, 1966.

131. KEFFER, J.F.
The Physical Nature of the Subsonic Jets in a Crosswind.
NASA Symposium on Analysis of a Jet in a Subsonic Crosswind, NASA SP-298, 1969.

132. HILGEROTH, E.
Heat Transfer in a Jet Stream Normal to the Transfer Surface.
Chemic-Ingenieur-Technik, Vol.37, No.12, pp.1264, 1965.

133. KERCHER, D.M. and TABAKOFF, W.
Heat Transfer by a Square Array of Round Air Jets Impinging Perpendicular to a Flat Surface Including the Effect of Spent Air.
Trans. ASME, J. of Engrg. for Power, Vol.92, pp.73, 1970.

134. FLORSCHUETZ, L.W. TRUMAN, C.R. and METZGER, D.E.
Streamwise Flow and Heat Transfer Distributions for Jet Array Impingement with Crossflow.
Trans. ASME, J. of Heat Transfer, Vol.103, pp.337, 1981.

135. RAMSEY, J.W. and GOLDSTEIN, R.J.
Interaction of a Heated Jet with a Deflecting Stream.
Trans. ASME, J. of Heat Transfer, Vol.83, pp.365, 1971.

136. GOLDSTEIN, R.J. ERIKSEN, V.L. and RAMSEY, J.W.
Flow and Temperature Fields Following Injection of a Jet Normal to a Cross Stream.
Proceedings of the 6th Int. Heat Transfer Conference, Toronto, Canada, Vol.5, pp.255, 1978.

137. BDH CHEMICALS LTD., POOLE, ENGLAND
Private communication, May, 1980.

138. BESTOBELL CHEMICAL PRODUCTS LTD., SURREY, ENGLAND
Private communication, April, 1980.

139. KLINE, S.J. and McCLINTOCK, F.A.
Describing Uncertainties in Single-Sample Experiments
Mech.Engrg.Pg.3.Jan.1953.

140 HOLMAN, J.P.
Experimental Methods for Engineers.
McGraw-Hill, 2nd Edition, New York, 1971.

APPENDICES

A.1 PROPERTIES OF THE CHEMICALS USED IN THIS MASS TRANSFER STUDY

A.1.1 Characteristics of Naphthalene (Ref. 137)

General Description: White crystalline solid with aromatic odour.

Chemical Formula: $C_{10}H_8$

Physical Properties

Molecular Weight:	128.16
Melting Point:	80°C
Boiling Point:	218°C
Flash Point:	80°C
Specific Gravity:	1.145
Lower & Upper Explosive Limits in Air:	0.9% and 5.9% by volume
Gas Constant, R_v:	64.7 J/kgK

Hazard Analysis

In the event of:	Effect	Treatment
Inhalation	Moderate	Remove from exposure, rest and keep warm; in severe cases, obtain medical attention.
Eye Splashes	Irritant	Irrigate thoroughly with water, if discomfort persists, obtain medical attention.
Skin Contact	Moderate	Wash thoroughly with soap and water.
Ingestion	Moderate	Wash out mouth thoroughly with water; obtain medical attention.

Other comments:	Chronic effects are usually slight.
Threshold Limit Values:	American Conference of Government and Industrial Hygienists recommend 10 parts per million of air (i.e. 50 mg/m^3 of air)
Fire Hazard:	Moderate when exposed to heat and flame.
Explosion Hazard:	Moderate, in the form of dust. Can react vigorously with oxidising materials.

Protective Measures

To Fight Fire:	Water, Carbon-dioxide, dry powder or vaporising liquids.
Personnel Protection:	Rubber or plastic gloves are recommended. Goggles or safety spectacles may be worn. Respirators are not however usually needed (except when handling large quantities at elevated temperatures).

A.1.2 Properties of Inhibisol (Ref.138.)

Description:	Specially treated 111-Trichloroethane, (methyl chloroform) which dries quickly and is non-toxic.
Chemical Formula:	$CH_3.CCL_3$

Physical Properties

Boiling Temperature:	74°C (thus it evaporates fairly rapidly at room temperature)
Molecular Weight:	133.35
Density at 20°C, g/ml:	1.322 to 1.332
Refractive Index at 20°C:	1.4365 to 1.4385
Flash Point:	None
Viscosity at 25°C (Centistokes):	0.61

Threshold Limit Value: 350 ppm

Material Compatibility: Seldom attacks plastics

Precautions in Handling

1. Store in sealed containers in a dry atmosphere away from acids, strong alkalies, naked flames, and welding operations.

2. Avoid prolonged or repeated breathing of vapour.

3. Avoid prolonged or repeated skin contact to avoid defatting.

4. Use with adequate ventilation.

5. Do not smoke whilst using Inhibisol.

First Aid Treatment

Eye Splashes:	Wash the eyes thoroughly with clean water. Obtain medical attention.
Inhalation of vapour:	Remove from exposure. Rest and keep warm. In severe cases, obtain medical attention.
Skin Splashes:	Drench the skin thoroughly with clean water. Wash with soap and water. Apply a good quality Lanolin-based hand cream. Remove contaminated clothing and wash before re-use.
Swallowing:	Wash out the mouth with water and induce vomitting by tickling the back of the throat or by giving luke warm salt water to drink. Obtain medical attention.

DRAWING NO PD 17291

NO.	MODIFICATION
A1	—

ALL DIMENSIONS IN ~~MILLIMETRES~~ INCHES UNLESS OTHERWISE STATED.

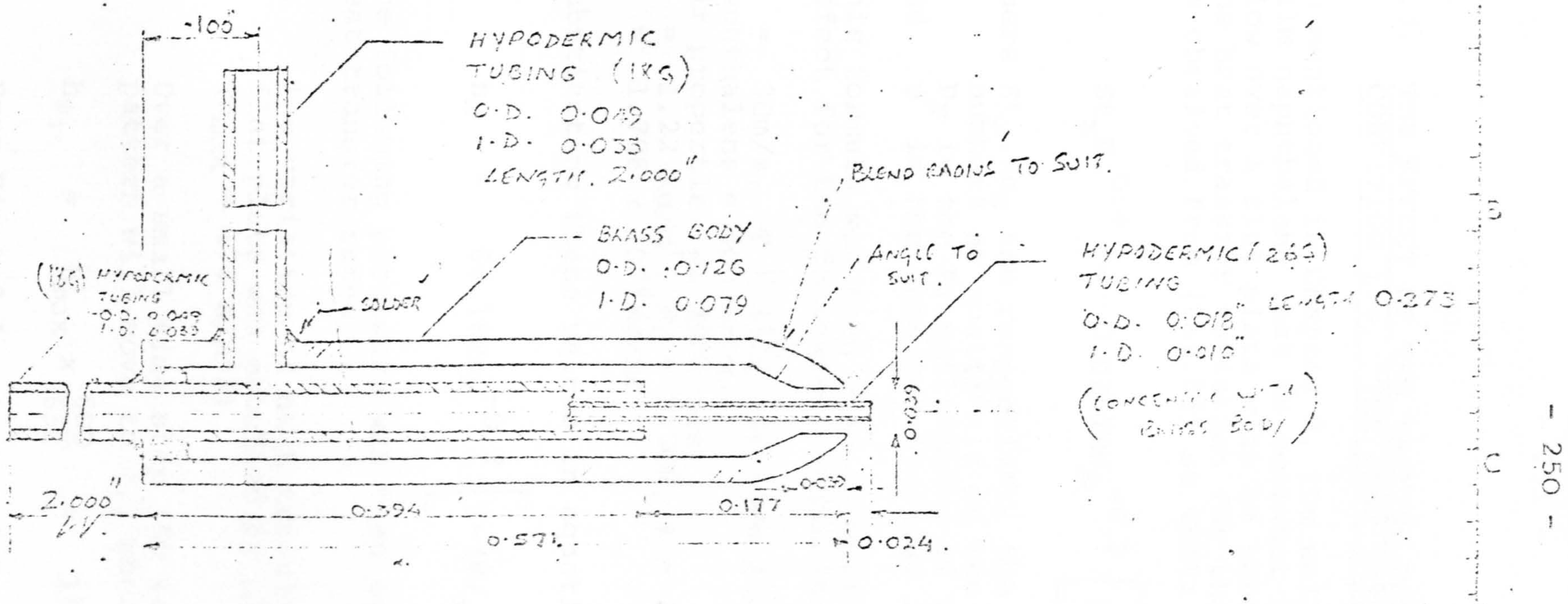

FIG. A.2.1 THE SPRAY NOZZLE

THIRD ANGLE PROJECTION			SHEET SIZE A3	1	PD 17291	SPRAYING NOZZLE	2	EX SME			
				ITEM	PART No.	DESCRIPTION	No. OFF	MATL	SPEC.	REMARKS	
UNLESS OTHERWISE GIVEN DIMENSIONS TO BE IN INCHES TOLERANCES ON DIMENSIONS AS STATED	JOB No	No. OF SHEETS 1	SCALE 10/1	DRAWN M. SHEARWOOD 17-12-76	CHKD	APPVD	ISSUED	TITLE:- SPRAYING NOZZLE			
			FINISH SCF	ISSUED BY SME CRANFIELD INSTITUTE OF TECHNOLOGY CRANFIELD.				DRAWING NO PD 17291			
	USED ON							SHT.	OF	ISSUE	

A.3. THE EFFECT OF THE VARYING NAPHTHALENE BOUNDARY CONDITION i.e. "THE BARE PATCH EFFECT".

As mentioned in Chapter 3, the wall jet flow in this thin-film naphthalene test is somewhat analogous to a parallel flow over a flat plate with an unheated starting length. The heat transfer variation for the latter geometry can be obtained from (Ref.85) so that:

$$St_x Pr^{0.4} = 0.0287 Re_x^{-0.2} \left[1-(\psi/_{x/d})^{0.9}\right]^{-1/9} \quad \text{A.3.1.}$$

where St_x, Re_x are respectively the Stanton and Reynolds numbers at position x on the flat plate
P_r is the Prandtl number of the fluid (air)
and ψ is the unheated starting length.

This formula was then used to estimate the bare patch effect for the following conditions:

u = 30m/s, T = 17°C and time for initial clearance of naphthalene = 600 secs.
Air properties at 290K are:
ρ = 1.22 Kg/m^3, P_r = 0.708, K = 2.546 x 10^{-5}KW/mK
μ = 1.798 x 10^{-5}Kg/ms

Substituting these values in equation A.3.1. gives:

$$h_x = 66.18 Re_x^{-0.2} \left[1-(\psi/_{x/d})^{0.9}\right]^{-1/9} \quad \text{A.3.2}$$

The following procedure was then adopted in estimating the heat transfer rates:

1. The variation of heat transfer on a completely heated flat plate was obtained by putting ψ = 0; see Fig.A.3.1 (h_{max} = 174 W/m^{2}K)

2. Over a small time step (50 secs, say), clearance pattern will move to ψ_1, where

$$h_{\psi_1} = h_{max} \times \frac{600}{650} = 161 \text{ W/m}^2\text{K}$$

From Fig.A.3.1., ψ = 0.8

Thus, the variation of heat transfer rates on the plate was then re-computed using this unheated, ψ_1, in equation A.3.2.

3. Step 2 was repeated until ψ equalled the length of the flat plate. Table A.3.1. presents the values of heat transfer coefficients obtained in this manner for various unheated starting lengths.

4. The 'actual' heat transfer rate at a particular x/d is a time-weighted average of these computed values at this position. For example, the heat transfer at x/d = 2 can be determined by

$$h = \frac{131.9x600+140.6(650-600)+143.6(700-650)+159.4(750-700)}{750}$$

$$= 135.1 \text{ W/m}^2\text{K}$$

5. Table A.3.2.presents these heat transfer coefficients at various positions on the flat plate.

It can be noticed that the results for the completely heated flat plate and those associated with a varying boundary (i.e. the bare patch effect) varied by 2.5% approximately, see Fig.A.3.1.

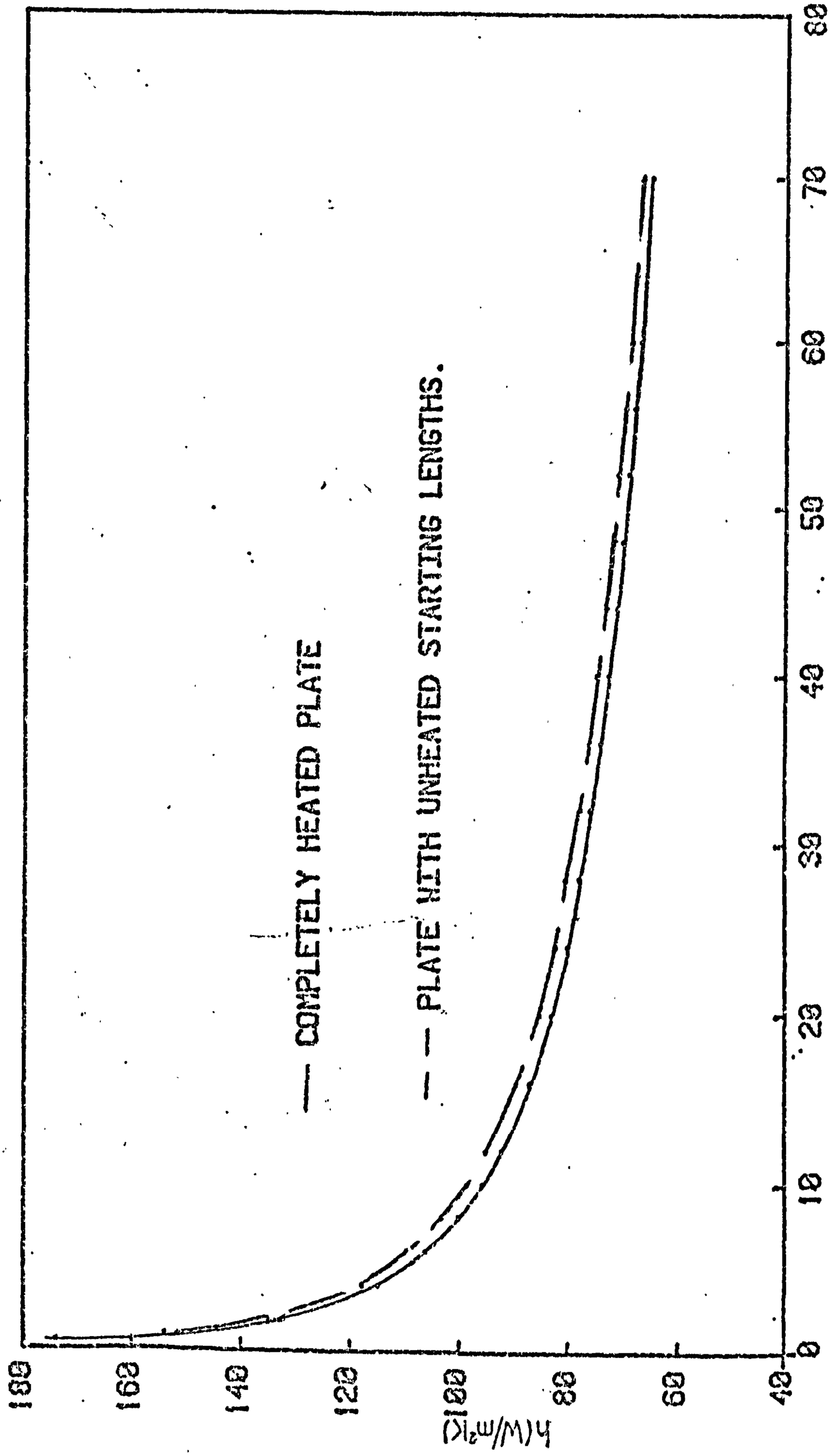

FIG. A.3.1. THE EFFECT OF VARYING NAPHTHALENE BOUNDARY ON HEAT TRANSFER COEFFICIENTS.

TABLE A.3.1.

	t=600	650	700	750	800	850	900	950	1000	1050	1100	1150	1200
x/d	ψ=0	0.8	1.0	1.6	2.2	3.0	4.0	5.2	6.6	8.0	10.0	12.4	16.0
0.5	174	W/m²K											
1.0	151.5	183.1											
2.0	131.9	140.6	143.6	159.4									
4.0	114.8	118.3	119	122.4	126.5	135.3							
6.0	105.6	108	108.5	110.2	112.2	115.3	120.8	133.9					
8.0	100	101.5	102	103	104.2	106.1	109	113.4	122.6				
10.0	95.6	96.8	97	97.9	98.8	100.1	101.9	104.6	108.8	115.5			
12.0	92	92.9	93	93.8	94.5	95.5	96.9	98.7	101.4	104.9	113.5		
14.0	89	90.2	90.3	90.9	91.5	92.3	93.3	94.8	96.7	99.1	103.7	115	
16.0	87	87.7	87.8	88.3	88.8	89.4	90.3	91.5	93	94.7	97.9	103.7	

TABLE A.3.2.

x/d	Heat transfer on a completely heated plate		Value with bare patch effect		% Difference
0.5	174	W/m^2K	174	W/m^2K	0
1.0	151.5		154.2		1.78
2.0	131.3		135.1		2.42
4.0	114.8		117.5		2.35
6.0	105.6		109.4		3.6
8.0	100		103.1		3.1
10.0	95.6		98.1		2.61
12.0	92		94.9		3.1
14.0	89		92.4		3.82
16.0	87		89.4		2.76
				Mean	2.55%

A.4 CALCULATION OF HEAT TRANSFER COEFFICIENTS

The procedure used to obtain local heat transfer coefficients is described in this section. The calculation presented is for a jet in initially stagnant surroundings although a similar calculation is applicable for jets in confined cross flows.

General Data

$z/d = 12$, $Re = 65000$, $\alpha = 60^{o}$

Surface area of slides, A = 64.5 cm^2

Length of plate sprayed = 36 cm

Original weight of slides, w_1 = 1624.5 mg

Weight of slides after spraying, w_2 (1st re-weighing) = 1809.2 mg

Weight of slides at 2nd re-weighing, w_3 = 1792.4 mg

Spray time, t_1 = 3180 secs

Time at commencement of 1st re-weighing, t_2 = 3320 secs

Time at end of 1st re-weighing, t_3 = 3575 secs

Mean of t_2 & t_3, t_{23} = 3447.5 secs

Time at commencement of mass transfer test, t_4 = 3740 secs

Time at commencement of 2nd re-weighing, t_5 = 6500 secs

Time at end of 2nd re-weighing, t_6 = 6800 secs

Mean of t_5 and t_6, t_{56} = 6650 secs

Determination of the Naphthalene Spray Density on the Plate

Weight of naphthalene deposited per unit area of the slides

$$= (w_2 - w_1)/A$$

$$= 2.86 \text{ mg/cm}^2$$

Naphthalene loss rate, $y_1 = \frac{(w_2 - w_3)}{(t_{56} - t_{23})A}$

$= 8.12 \times 10^{-5}$ mg/cm^{2}s

difference in time between 1st re-weighing of the slides and the commencement of the test, $t_7 = (t_4 - t_{23})$

$= 292.5$ secs

Naphthalene loss between 1st re-weighing and the start of the test

$= y_1 \cdot t_7$

$= .0232$ mg/cm^2

$\therefore$ Concentration of naphthalene on the slides when the test began $= \frac{(w_2 - w_1)}{A} - y_1 \cdot t_7$

$= 2.84$ mg/cm^2

The napthalene concentration at any position on the plate can be determined by accounting for the free convective loss. For example, if Δ is the distance between the slides and the centre line of the plate, then

free convective loss $= \Delta \times y_1/y_2$

where y_1 = naphthalene loss rate

y_2 = feed rate of plate

= length of plate sprayed/spray time

= 36/3180 cm/sec

$\therefore$ the loss = 0.109 mg/cm^2

Thus, the concentration of naphthalene along the centre line of plate when the mass transfer test began

$= (2.84 - 0.109)$ mg/cm^2

i.e. 2.73 mg/cm^2
or 27.3×10^{-3} kg/m^2

Calculation of the Heat Transfer Coefficients

Air properties at 290.6 K

$\rho = 1.22\ kg/m^2$ $\quad Pr = .709$ $\quad C_p = 1004.5$

$Sc = 7 \cdot (T_n)^{-0.185} = 2.451$

$(\frac{Sc}{Pr})^{2/3} = 2.286$

Vapour pressure of naphthalene, p_n

$$= 10^{(11.45 - \frac{3729.27}{290.6})} \times 133.31$$

$$= 5.54\ N/m^2$$

By invoking the Chilton-Colburn analogy, the relationship between the heat transfer coefficient, h, and the mass of naphthalene sublimated can be written as :

$$h = \frac{R \cdot T \cdot \rho \cdot C_p}{p_n \cdot t} \cdot \frac{m}{A} \cdot (\frac{Sc}{Pr})^{2/3}$$

$$= \frac{64.7 \times 290.6 \times 1.22 \times 1004.5 \times 27.31 \times 10^{-3} \times 2.286}{5.54 \times t}$$

$$= 259300.00\ /t$$

$t = (t_x - t_4)$ where t_x is the clearance time at position x

The local heat transfer coefficients at various positions are presented in Table A.4.1

Table A.4.1

Position	Clearance time (seconds)		h (w/m^2K)
Stagnation	4410	visual	387
	4418	chart	382
1	4525		330
2	4653		284
3	4915		221
4	5072		195
5	5210		176
6	5590		140
7	5965		116
8	6263		103
9	6535		93
10	7055		78

Figure A.4.1 presents this variation of heat transfer along the line of symmetry.

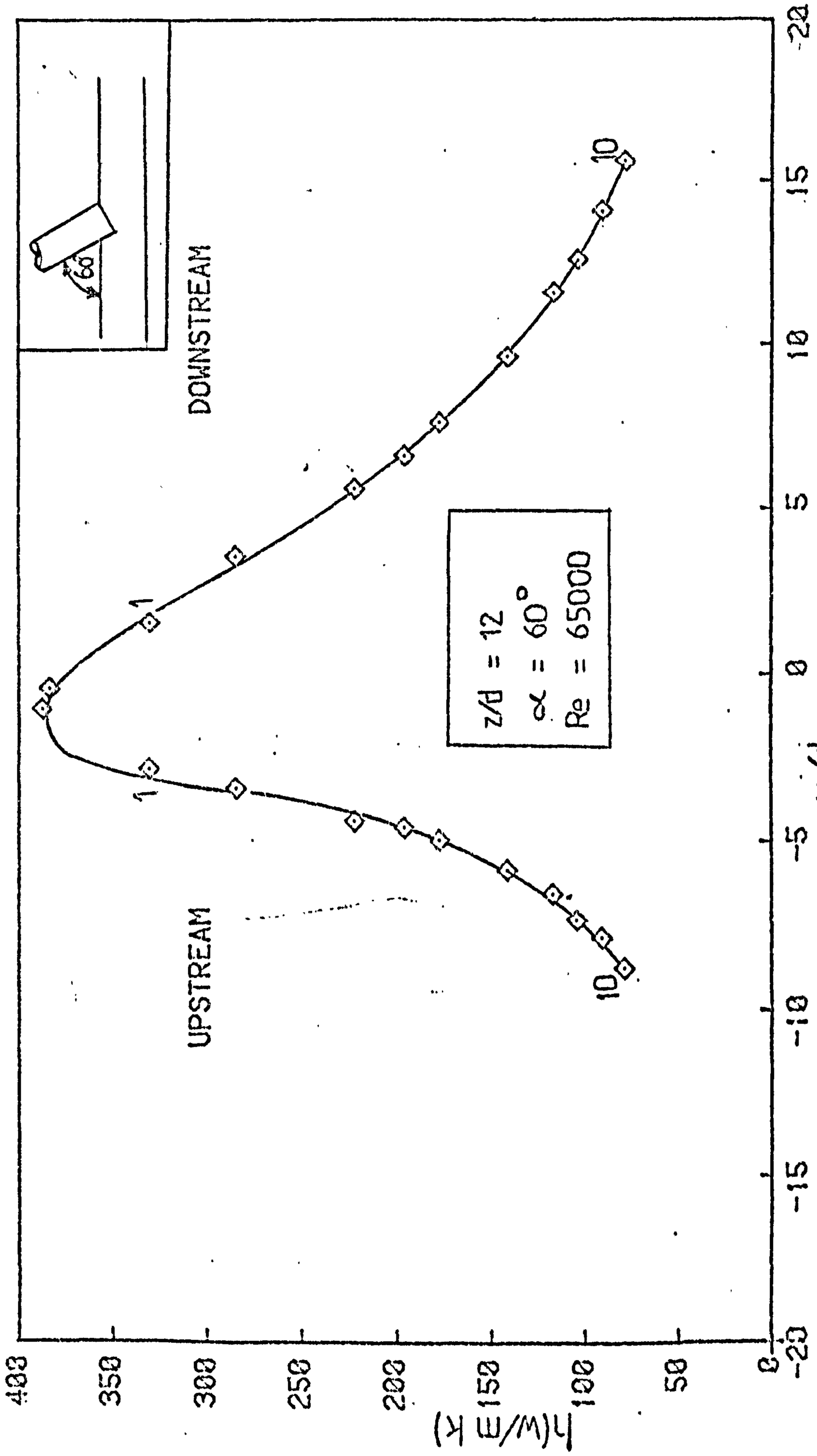

FIG.A.4.1 VARIATION OF HEAT TRANSFER ALONG THE LINE OF SYMMETRY.

A.5. ERROR ANALYSIS

A.5.1 Effect of Misalignment of the Calibration Slides

The naphthalene coating weight should be obtained by weighing a removable plug located in a hole in the test plate so that the surfaces of the plug and plate are flush. In practice, thin slides were mounted on the test plate. Thus, the test surface and the thin slides were not strictly at the same distance from the spray nozzle. Tests were therefore carried out to determine the magnitude of the errors which occurred due to this misalignment.

In normal operation, the test plate was 13mm from the nozzle whilst the corresponding distance for the upper surface of the slides was 12.8mm. To check the errors, three slides were sprayed at separation distances of 12, 14 and 16mm. The results are presented in Table A.5.1. It appears from this table that the naphthalene coating density is practically unaffected by the misalignment of the slides on the test plate. From the graph (Fig.A.5.1) of naphthalene coating density against surface to nozzle spacing, the error is 0.2mg which represents a variation of less than 0.5%. Thus, the effect of misalignment was neglected in this study.

A.5.2 Consistency of the Naphthalene Coating

Ten slides were mounted on the test plate and sprayed under identical conditions (i.e. equal naphthalene concentration and flow rates). The measured weights were 92.2, 92.5, 92.1, 92.8, 93.5, 94.1, 92.3, 93.9, 92.9 and 93.5mg. The mean was found to be 92.98mg and the scatter of these weights was within ±2% of the mean.

Furthermore, forty actual tests were randomly selected and the scatter in the mean of the naphthalene concentration was found to be 2.71mg/cm^2. The standard deviation, σ, was 0.081. It can be seen in Fig.A.5.2. that 98% of this population fall within ±2 deviations of the mean. Thus, it may be concluded that naphthalene density in these tests was very consistent. It therefore appears that the method of spraying produces a 'uniformly' consistent coating.

A.5.3. Estimation of Uncertainties in the Heat/Mass Transfer Experiments.

1. Introduction

Experimental uncertainty in a variable can be defined (Ref. 139) as a possible value the error (in the variable) may have. Errors in experimental data involve factors which contain some amount of uncertainty. There errors may be broadly classified as follows:

Fixed or Systematic Errors can cause readings to be repeatedly in error by roughly the same amount without any apparent reason. These errors can be due either to improper procedures and conditions that are consistent in their effect or to the use of inappropriate measuring apparatus. Careful choice of instrumentation and technique can eliminate this type of error (Ref. 140).

Mistakes such as erroneous reading or instruments.

Random Errors these may be due either to inherent inaccuracy in the instrumentation or to random behaviour of the measuring system. One of the sources of this error is friction in the measuring equipment.

Although care was taken in this investigation to reduce errors, it is essential that the best estimates of the 'true' heat transfer coefficients presented in this thesis include a statement about their probable deviation from the 'true' values.

2. Uncertainty Interval in the Variables

Kline and McClintock (Ref. 139) published a concise method of estimating the uncertainty in experimental data. In this method, uncertainties were specified for the various primary measurements which affected the main variable. For example, a certain temperature reading can be expressed as:

$$T = 270 \pm 0.5^{o}C \text{ (20 to 1)} \qquad \text{A.5.1.}$$

where the plus or minus notation denotes the uncertainty. This equation states that the best value for the temperature is $270^{o}C$ and that the experimenter is willing to bet with 20 to 1 odds that the 'true' value lies within $\pm 0.5^{o}C$ of this best estimate. Uncertainties in the variables are usually specified in this manner.

3. Uncertainty Interval in the Result

Having estimated the uncertainties in each primary variable, it is then necessary to determine how these uncertainties propagate into the calculated result. For example, let the result, R, be a function of n independent variables $(x_1, x_2, x_3 \ldots\ldots x_{n-1}, x_n)$ such that

$$R = R(x_1, x_2, x_3, \ldots\ldots x_{n-1}, x_n) \qquad \text{A.5.2}$$

Let W_R be the uncertainty in the result (dependent variable) and
$W_1, W_2, \ldots\ldots W_n$ the uncertainties in the independent variables.

If these uncertainties are all expressed with the same odds, then the uncertainty in the result is (see Ref. 139):

$$W_R = \left(\frac{\partial R}{\partial x_1}W_1\right)^2 + \left(\frac{\partial R}{\partial x_2}W_2\right)^2 + \ldots + \left(\frac{\partial R}{\partial x_{n-1}}W_{n-1}\right)^2 + \left(\frac{\partial R}{\partial x_n}W_n\right)^2 \quad ^{\frac{1}{2}}$$

A.5.3.

This expression indicates that uncertainties in individual variables contribute to the uncertainty in the dependent variable by a square law.

4. Sample Analysis

As mentioned in Chapter 3, the heat transfer coefficient can be obtained from:

$$h = \frac{R.T.C_p.\rho.m.(SN)^{\frac{2}{3}}}{p.t.} \qquad \text{A.5.4.}$$

where $SN = \frac{Sc}{Pr}$ and $m = \frac{\text{naphthalene weight}}{\text{unit area}}$

The values and uncertainties in the independent variables are:

$R = 64 \pm 0$ JKgK^{-1}

$Cp = 1004.5 \pm 0$

$\rho = 1.22 \pm 0$

$(SN)^{\frac{2}{3}} = 2.286 \pm 0$

$T = 17.6^{o}C \pm 0.3^{o}C$

$m = 2.73 \pm 0.04$ mg/cm^2

$t = (t_x - t_4) \pm 0.5\%$

$p = 5.54 \pm 0.182$ N/m^2

Let W_h = the uncertainty in h

W_R, W_T, W_{Cp}, W_ρ, W_m, W_{SN}, W_p and W_t are respectively the uncertainties in the independent variables.

Combining equations A.5.3. and A.5.4. gives:

$$W_h = \left(\frac{\partial h}{\partial R}W_R\right)^2 + \left(\frac{\partial h}{\partial T}W_T\right)^2 + \left(\frac{\partial h}{\partial Cp}W_{Cp}\right)^2 + \left(\frac{\partial h}{\partial \rho}W_\rho\right)^2 + \left(\frac{\partial h}{\partial m}W_m\right)^2 + \left(\frac{\partial h}{\partial SN}W_{SN}\right)^2 + \left(\frac{\partial h}{\partial p}W_p\right)^2 + \left(\frac{\partial h}{\partial t}W_t\right)^2 \quad ^{\frac{1}{2}}$$

$$= \left[\left(\frac{\partial h}{\partial T}W_T\right)^2 + \left(\frac{\partial h}{\partial m}W_m\right)^2 + \left(\frac{\partial h}{\partial p}W_p\right)^2 + \left(\frac{\partial h}{\partial t}W_t\right)^2\right]^{\frac{1}{2}} \qquad \text{A.5.5.}$$

Partial differentiation of equation A.5.4. gives

$$\frac{\partial h}{\partial T} = \frac{R.m.\rho.C_p.(SN)^{\frac{2}{3}}}{p.t.}$$

$$\frac{\partial h}{\partial m} = \frac{R.T.\rho.Cp.(SN)^{\frac{2}{3}}}{p.t.} \qquad \text{A.5.6.}$$

$$\frac{\partial h}{\partial p} = -\frac{R.T.Cp.\rho.m.(SN)^{\frac{2}{3}}}{p^2.t}$$

$$\frac{\partial h}{\partial t} = -\frac{R.T.Cp.\rho.m.(SN)^{\frac{2}{3}}}{p.t^2.}$$

Substituting equation A.5.6. into A.5.5. and dividing by equation A.5.4. gives:

$$\frac{W_h}{h} = \left[\left(\frac{W_T}{T}\right)^2 + \left(\frac{W_m}{m}\right)^2 + \left(\frac{W_p}{-p}\right)^2 + \left(\frac{W_t}{-t}\right)^2\right]^{\frac{1}{2}} \qquad \text{A.5.7.}$$

Substituting the values and uncertainties of the independent variables into equation A.5.7 gives:

$$\frac{W_h}{h} = \left[\left(\frac{.3}{17.6}\right)^2 + \left(\frac{0.04}{2.73}\right)^2 + \left(\frac{0.182}{5.54}\right)^2 + (.005)^2\right]^{\frac{1}{2}}$$

$$= \left(2.905 + 2.147 + 10.79 + .25\right)x10^{-4}\,^{\frac{1}{2}}$$

$$= 4.01\% \simeq 4\%$$

It can be noticed that the uncertainty in the naphthalene pressure contributed the largest uncertainty to that in the heat transfer result. It must also be mentioned that away from the stagnation point, this uncertainty is increased by an amount (2.5%) due to the varying naphthalene boundary condition.

TABLE A.5.1.

Separation Distance (mm)	Naphthalene Density (mg)
16	152.9
14	153.3
12	154.6

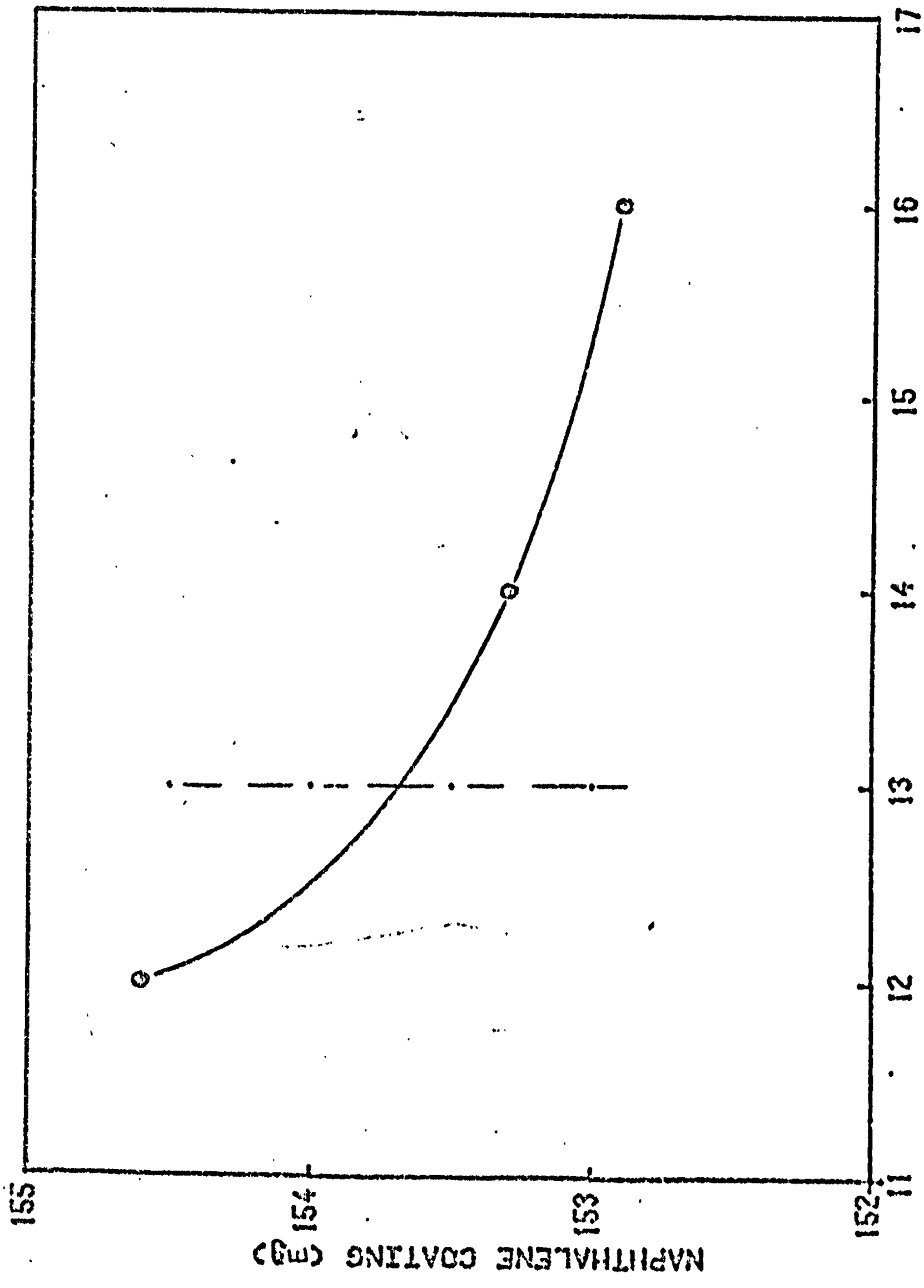
FIG.A.5.1 THE EFFECT OF SEPARATION DISTANCE ON THE NAPHTHALENE COATING DENSITY.
SEPARATION DISTANCE (mm)
NAPHTHALENE COATING (mg)
155
154
153
152
11
12
13
14
15
16
17

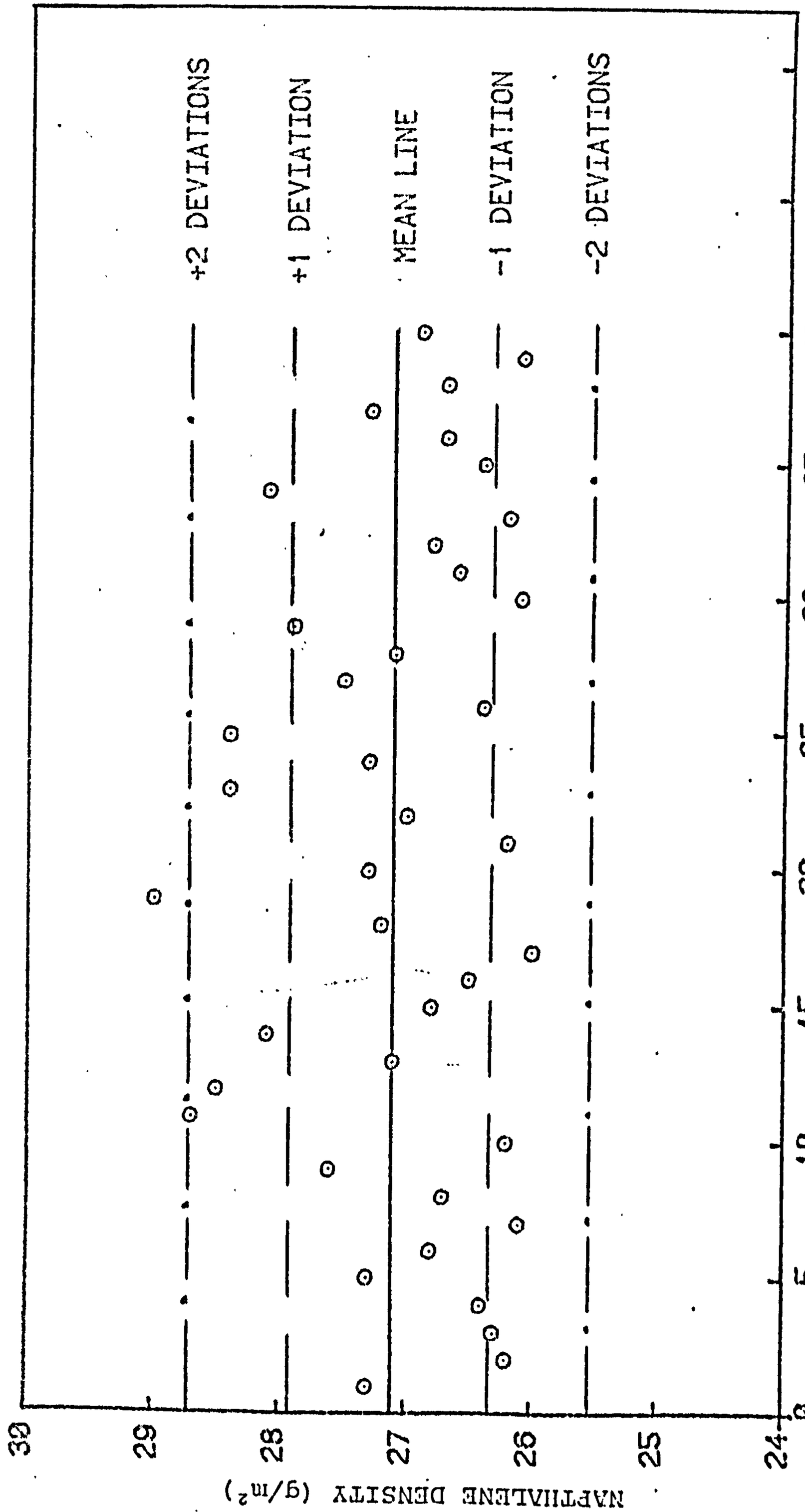

FIG.A.5.2 CONSISTENCY OF NAPHTHALENE COATINGS.

"IN ALL THY WAYS ACKNOWLEDGE HIM, AND HE SHALL DIRECT THY PATHS".

Proverbs 3, Verse 6.

8. A CIRCULAR TURBULENT JET IN A CONFINED CROSS FLOW

8.1 INTRODUCTION

The effect of superimposing a cross flowing stream onto an axisymmetric impinging jet is to produce a more complicated three-dimensional flow field (in which recirculation and separation ensure). A cross flow of even comparatively low velocity when compared with that of the impinging jet can produce considerable changes in both the flow field and the physical structure of the jet (for example, an initially circular jet soon becomes distorted to one of elliptical cross section). Consequently, theoretical information is sparse. Previous workers have used either empirical or semi-analytical approaches to compute the axis of the jet (i.e. the locus of maximum velocity). Furthermore, available experimental impingement heat transfer data is also scanty.

The lateral spread of a single jet in a cross flow is restricted by the presence of the bounding walls which confine the flow in the test section. For a constant nozzle diameter, the degree of confinement is dictated by the duct width, H/d. With multiple jet arrangements, a similar effect occurs since the presence of neighbouring jets inhibits jet spread. The effects of duct width were also studied in the present cross flow investigations.

8.2 FLUID FLOW ASPECTS

A turbulent jet which in the absence of a cross flow would have impinged orthogonally onto the test surface will be referred to as "orthogonal" jet impingement in cross flow in this thesis. For oblique jet situations, acute (i.e. $0 < \alpha < 90$) and obtuse ($90 < \alpha \leq 180$) nozzle inclinations will respectively be termed as 'nozzle inclination into the crossflow' and 'nozzle inclination with the crossflow'.

Figure 8.2.1 is a diagrammatic representation of an orthogonal. axisymmetric impinging jet exiting into a cross flow. The flow field can be divided into three regions, namely: an initial region, a main zone which is then followed by flow over the impingement surface.

Initial Behaviour

As soon as the jet emerges from the nobzle, it is deflected partly by pressure forces exerted by the cross flow and partly